AD NUMBER

AD804728

LIMITATION CHANGES

TO:

Approved for public release; distribution is unlimited.

FROM:

Distribution: Further dissemination only as directed by Federal Aviation Agency, Office of Supersonic Transport Development Program, Washington, DC, 06 SEP 1966, or higher DoD authority.

AUTHORITY

FAA ltr 2 Jul 1973

SUPERSONIC
TRANSPORT
DEVELOPMENT
PROGRAM

PHASE III PROPOSAL
AIRFRAME DESIGN REPORT PART C

DESIGN CRITERIA
LOADS
AERODYNAMICS
HEATING
FLUTTER

BOEING SUPERSONIC TRANSPORT DIVISION

SEPTEMBER 6, 1966

V2-B2707-7

NOTICES

When Government drawings, specifications, o other data are used for any purpose other than in connection w a definitely related Government procurement operation, the United States Government thereby incurs no responsibility nor any obligation whatsoever; and the fact that the Government may have formulated, furnished, or in any way supplied the said drawings, specifications, or other data, is not to be regarded by implication or otherwise as in any manner licensing the holder or any other person or corporation, or conveying any rights or permission to manufacture, use, or sell any patented invention that may in any way be related thereto.

All distribution of this document is controlled. This document may be further distributed by any holder only with specific prior approval of:

Director of Supersonic Transport Development
Federal Aviation Agency
Washington, D. C. 20553

The distribution of this document is limited because it contains technology identifiable with items excluded from export by the Department of State (U. S. Export Control Act of 1949 as amended).

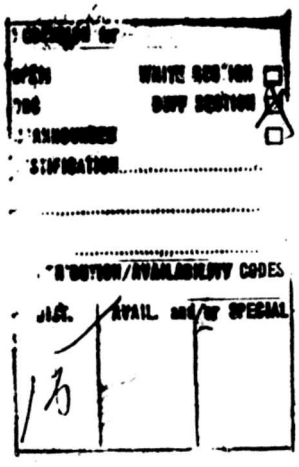

(6) ~~Phase III Proposal~~

Supersonic Transport Development Program •

Phase ~~III~~ 3 proposal.

BOEING MODEL 2707

Volume ~~II~~ 7.

AIRFRAME DESIGN REPORT.
PART C •
DESIGN CRITERIA
LOADS.
AERODYNAMIC HEATING
FLUTTER,

(10) D. R. Donaldson

(14) V2-B2707-7

September 6, 1966

(11) 6 Sep 66 (12) 138 P.

PREPARED BY D R Donaldson APPROVED BY H Wittenberg

(15) ~~Contract~~ FA-SS-66-5

Prepared for

FEDERAL AVIATION AGENCY

Office of Supersonic Transport Development Program

402 097

THE BOEING COMPANY
SUPERSONIC TRANSPORT DIVISION

FAA

ISSUE NO. A 109

2

CONTENTS

B-2707 PHASE III PROPOSAL DOCUMENTATION INDEX

1.0 INTRODUCTION

The Airframe Design Report is one of a series of documents under Volume II, Technical/Airplane, called for by the FAA Request for Proposal for Phase III of the Supersonic Transport Development Program. The Airframe Design Report is bound into five documents: Airframe Design Report – Part A, V2-B2707-6-1; Airframe Design Report – Part B, V2-B2707-6-2; Airframe Design Report – Part D, V2-B2707-8; Airframe Design Report – Part E, V2-B2707-9; and this document, Airframe Design Report – Part C, V2-B2707-7.

The Flight Test Program, V4-B2707-14, includes the accumulation of data for structural evaluation. The Integrated Test Program, V4-B2707-11, describes and integrates all structural tests into a complete program.

This report presents the Boeing proposal for structural design loads and environment on the B-2707 commercial supersonic transport. Information on Phase III planning is included to define an efficient program necessary for first flight of the B-2707 prototype. The proposal also contains planning material directed toward Phase IV activities.

Flight and ground loads criteria, flutter and vibration criteria, and structural design criteria are presented in Sec. 2.0. The prototype and production airplanes will meet these criteria.

The design loads and methods of analysis together with load validation data are presented in Sec. 3.0. The effects of these loads on ride comfort of the passengers and crew are also included.

Structural temperature analyses that define the effects of aerodynamic and engine-induced heating on all major structure are presented in Sec. 4.0.

Flutter prevention is provided to a minimum speed margin of 20 percent above V_D at constant Mach number and constant altitude for all lifting surfaces, control surfaces, and panels. Aeroelastic feedback through the SAS is precluded by electronic filtering. Transonic buzz is prevented by control system stiffness. Fail-safety is provided by systems redundancies.

The external design sound levels are determined for both the GE and P&WA engines; thrust reversers, sound suppressors, and aerodynamic noise are considered.

Critical design conditions for major airframe components are summarized in Table 1-A.

The design gross weight of 635,000 lb for the prototype airplane has been selected to take advantage of the company's airplane growth experience on subsonic jet programs. Analyses, complete component tests, and prototype flight and ground tests, combined with continuing design improvement studies, will provide growth to the production design gross weight of 675,000 lb. In Boeing Document V2-B2707-6-1, Weight and Balance, the weight substantiation of the B-2707 is accomplished through an analysis of the 635,000-lb gross-weight prototype airplane with increments added for the 675,000-lb production airplane. The structural design loads are presented herein for the production airplane with critical design conditions included for the prototype airplane.

Table 1-A. Primary Design Conditions

Cond No.	Condition Description	Critical Component	Λ_{LE} (deg)	n_{CG}	Gross Weight x 10^{-3} (lb)	CG % C_{ROOT}	Mach No.	Alt (ft)	V_e (kn)
9	Flaps-down maneuver	Wing and aftbody	30	2.0	668	59.0	0.295	0	195
					628*				
32	Subsonic V_A maneuver	Wing	42	2.5	650*	59.5	0.85	29,900	307
					609*			31,100	299
25	Supersonic V_A maneuver	Wing	72	2.5	605	60.4	2.7	64,000	433
					570*			65,300	420
17	Dynamic landing	Fwd fuselage	30	---	430	59.0	0.212	0	140
28	Subsonic V_c gust	Fwd fuselage	42	---	380	58.5	0.9	26,600	350
51	Subsonic V_A maneuver	Aftbody	42	2.5	648	59.5	0.9	33,000	303
					608*			34,300	294
50	Supersonic V_A maneuver	Aftbody	72	2.5	605	62.9	2.7	64,000	433
					609*			65,300	420
180	Flaps-down pitch initiation	Horizontal tail	30	1.0	668	59.0	0.295	0	195
					628*				
212	Subsonic rudder maneuver (dynamic overyaw)	Vertical tail	42	1.0	---	---	0.9	26,600	350
203	Ground turn	Main landing gears	30	---	675	---	---	---	---
					635*				
205	Pivot	Main landing gears	30	---	675	---	---	---	---
					635*				

*Prototype airplane

2.0 DESIGN CRITERIA

The structural design criteria complies with the requirements of Federal Aviation Regulations (FAR), Part 25, February 1965, and its amendments. Reference 2-1 is considered for study, trial application, and coordination with the FAA during the detail design phase of the airplane. Some criteria are applied in addition to the FAA requirements. Both flight and ground criteria are presented in this section. The three-view drawing of the airplane, including major dimensions, is shown in Fig. 2-1.

2.1 FLIGHT LOADS CRITERIA

The flight loads criteria are selected to be compatible with the diversified operational environment of the supersonic transport and at the same time meet existing subsonic commercial jet transport criteria. The structural design flight envelope for the maximum-gross-weight airplane is shown in Fig. 2-2.

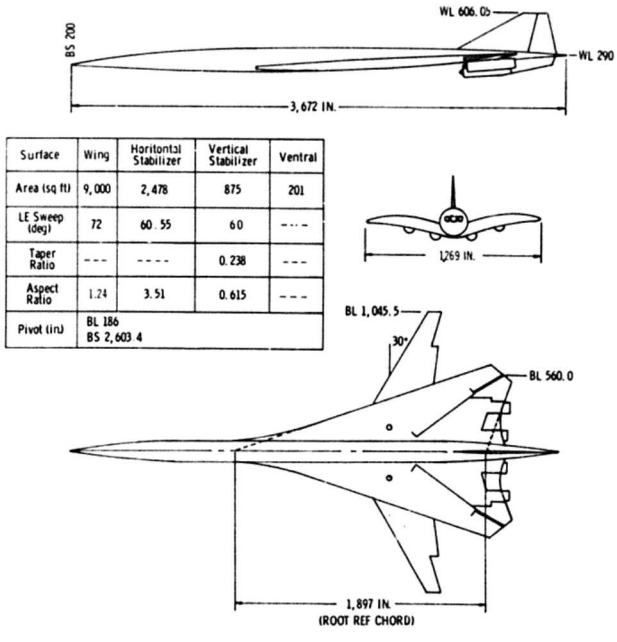

Figure 2-1. B-2707, Three View

2.1.1 Design Gross Weights

The airplane design gross weights used for computing structure design loads are selected to be consistent with each particular flight condition. Where gross weights vary due to the engine differences (GE versus P&WA), the higher of the two is used. The maximum design gross weights consider fuel used during acceleration as well as climb. Structural reserve fuel weight for the minimum flying weight is based on the requirements of FAR, Par. 25.343.

The structural design weights for the production and prototype airplane are as follows:

	Prototype (lb)	Production (lb)
Maximum design taxi weight	635,000	675,000
Minimum design flying weight (FAR 25)	310,000	314,000
Maximum design flight weight at sea level		
Flaps down	628,000	668,000
Flaps up	627,000	666,000
Maximum gross weight with zero outboard wing fuel	440,000	480,000
Maximum design landing weight	425,000	430,000
Beginning of cruise maximum weight	570,000	605,000
Maximum jacking weight	400,000	410,000

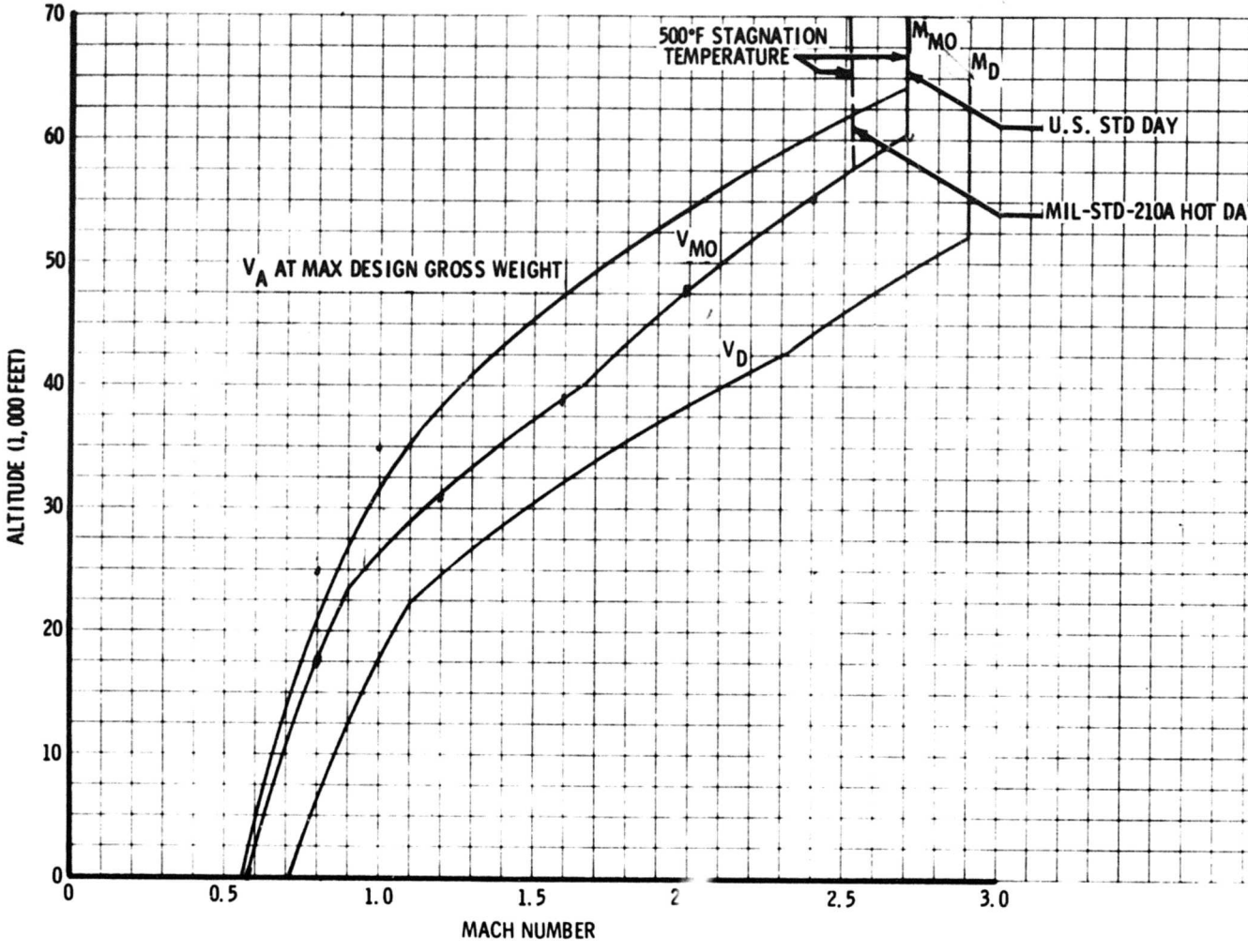

Figure 2-2. Structural Design Speed-Altitude Envelope, 72-Degree Wing Leading-Edge Sweep

The variation of maximum design gross weight with altitude is shown in Fig. 2-3. This is a simplified conservative weight envelope, which covers all climb and acceleration modes. A more detailed breakdown of airplane gross weights is presented in Airframe Design Report – Part A, V2-B2707-6-1.

2.1.2 Design Center-of-Gravity Limits
The design center-of-gravity limits are established as a function of gross weight for various wing sweep positions. The forward and aft limits used for computing structural design loads are presented in percent of root chord in Fig. 2-4. Locations and dimensions of root chord is shown in Fig. 2-1. A tolerance of 0.5 percent of root chord beyond operational limits is used for structural design.

2.1.3 Design Air Speeds and Placards
The structural design limit speeds, including the effects of wing sweep position are shown in Figs. 2-2, 2-5, and 2-6. The high-life and control-surface placards are listed in Table 2-A.

2.1.3.1 Flap Speeds, V_F
Flap placard speeds for takeoff and landing configurations are set to give the recommended margins on the stall speeds as specified in FAR, Par. 25.333(3). The flap placard speeds are functions

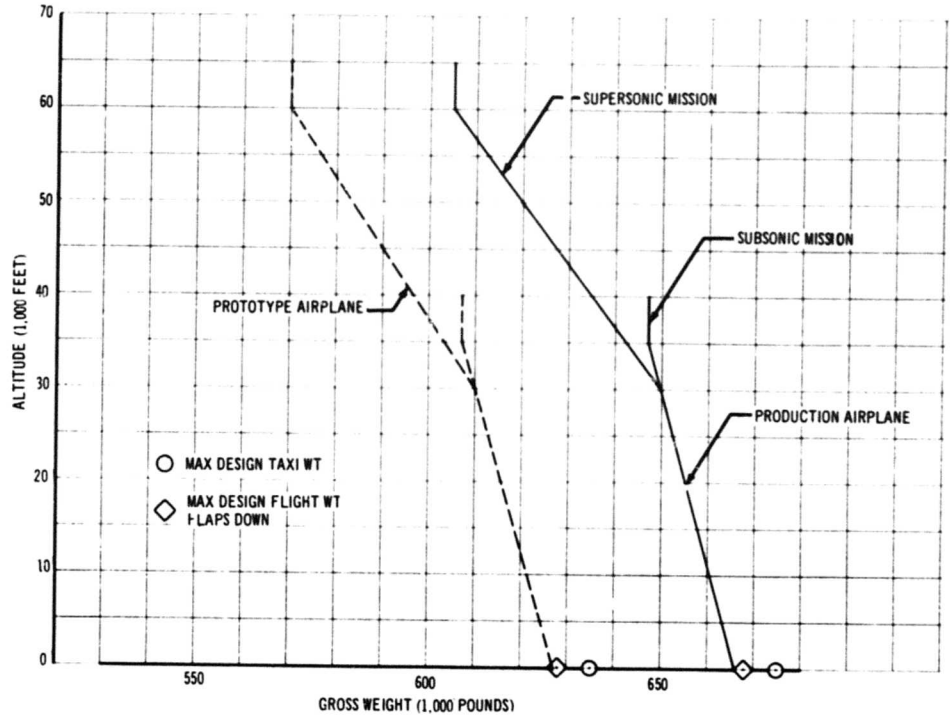

Figure 2-3. Maximum Design Gross Weight

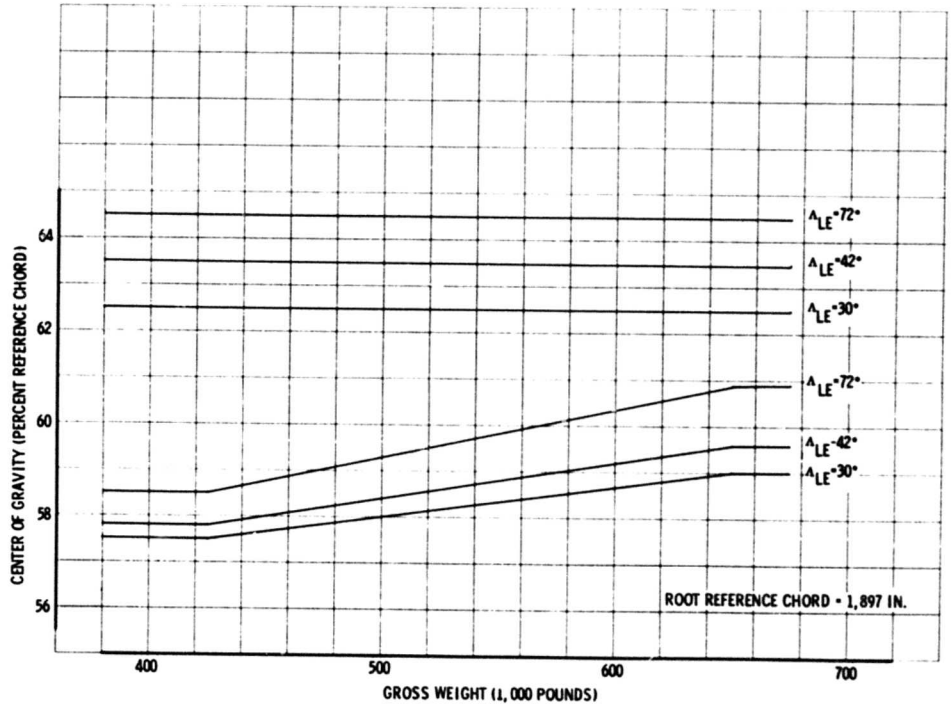

Figure 2-4. Structural Design Center-of-Gravity Limits

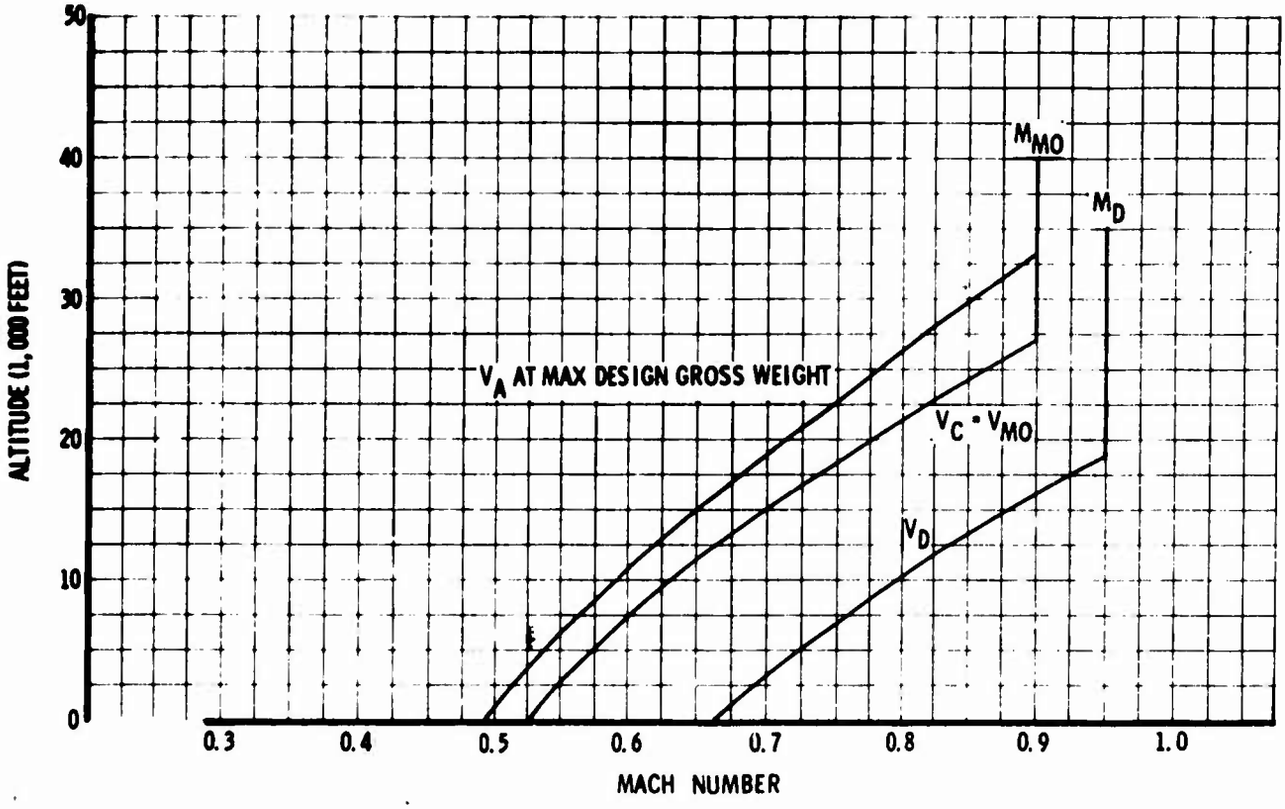

Figure 2-5. Structural Design Speed-Altitude Envelope, 42-Degree Wing Leading-Edge Sweep

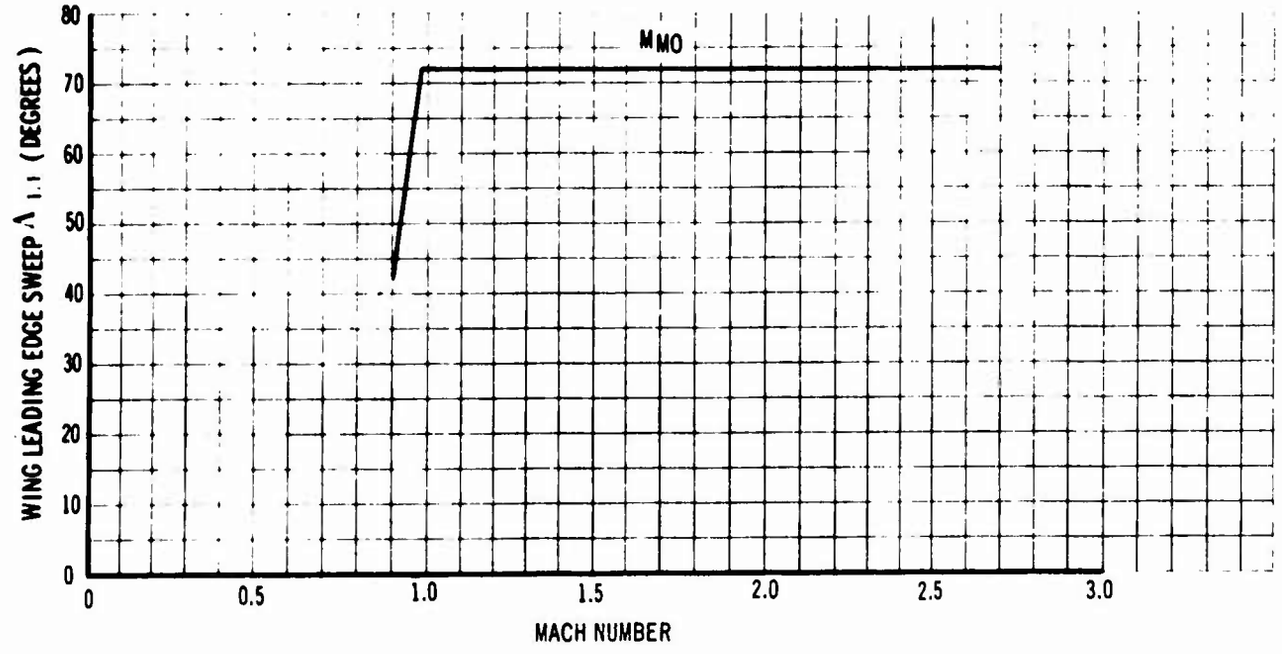

Figure 2-6. Wing Sweep Placard

of wing flap extension as shown in Fig. 2-7 and Table 2-A. Slat, aileron, and spoiler placards are also included in Table 2-A.

2.1.3.2 Landing-Gear Design Speeds
The design landing gear operating and extended equivalent air speeds (EAS) are:

Retract speed . . . . . 250 kn or M 0.83
Extend speed . . . . . 270 kn or M 0.90
Extended speed
(doors closed) . . . . . 320 kn or M 0.90

2.1.3.3 Maneuvering Speeds, V_A
Design maneuvering speeds for all applicable wing sweep positions are selected at the intersection of the C_N maximum curve with the positive maneuver load factor line. In establishing V_A, consideration is given to the maximum lift coefficient based on overshooting the angle-of-attack established by airplane control limits. The V_A speed versus altitude for the maximum gross weight is shown in Figs. 2-2 and 2-5.

2.1.3.4 Speed for Maximum Intensity Gust, V_B
For subsonic flight, the maximum-intensity gust penetration speeds shown in Fig. 2-8 comply with the requirements of FAR, Par. 25.335 and are consistent with airplane slowdown capability. Wing sweep position is considered in establishing the V_B speeds. In accordance with Ref. 2-1, the V_B gust concept is replaced by V_C gust at supersonic speeds.

2.1.3.5 Cruising Speed, V_C
The design cruising speed conforms with FAR, Par. 25.335(a) and is selected to equal V_{MO} (described in the following paragraph).

2.1.3.6 The Maximum Operating Speed Boundary, V_{MO}/M_{MO}
The maximum operating speed boundary, V_{MO}/M_{MO}, is established giving recognition to economic performance, gust environment, control effectiveness, and speed margins on flutter and engine pressure limits. M_{mo} is selected as M 2.7 for wings aft but does not exceed a stagnation temperature of 500°F (Par. 2.1.8). (See Figs. 2-2, 2-5, and 2-6). Justification for these limits is presented in System Engineering Report, V2-B2707-1, Par. 2.1.

2.1.3.7 Dive Speed, V_D/M_D
The dive speed V_D is determined as 1.25 V_{MO} at subsonic speeds and at supersonic speeds by a 7.5-deg nose-down upset with cruise thrust for 20 sec followed by a 1.5g (0.5g-acceleration increment) pullout maneuver. Moreover, in compliance with Ref. 2-1, V_D/M_D is equal to a delta Mach number speed margin of at least 0.05 at all subsonic speeds and a delta Mach speed spread of at least 0.20 at all supersonic speeds. M_D is selected as M 2.9, but does not exceed a stagnation temperature of 585°F (Par. 2.1.8). (See Figs. 2-2 and 2-5.)

2.1.3.8 Wing-Sweep Design Speeds
The operational wing-sweep-versus-speed schedule is selected on the basis of performance. The structural design of the airplane allows for a tolerance on wing sweep position to allow for inadvertent overspeeds. The structural limits on wing sweep position are noted in Figs. 2-2, 2-5, and 2-6.

2.1.3.9 Movable-Nose Placard Speed
Actuation of the movable nose or holding the nose in the down position is limited to either M 0.90 or V_D, whichever is smaller.

2.1.4 Flight Envelopes
Flight conditions that influence the design of major structural components are described in Figs. 2-9 through 2-20 in the form of maneuvering envelopes for flaps-up and high-lift configurations. Critical gross weight, altitude, and wing sweep positions are shown. These envelopes also represent the structural operating limits of the B-2707 airplane.

2.1.5 Maneuvering Conditions
In general, the airplane is designed to the pitching, rolling, and yawing conditions described in FAR, Pars. 25.337, 25.349, and 25.351. The modifications to maneuvering load criteria proposed in Ref. 2-1 are also applied.

Symmetric flaps-up maneuvers to a limit positive load factor of 2.5 are considered between the design maneuvering speeds V_A and V_D/M_D. The limit negative load factor is -1.0 up to V_{MO}/M_{MO} and is reduced linearly to 0.0 at V_D/M_D.

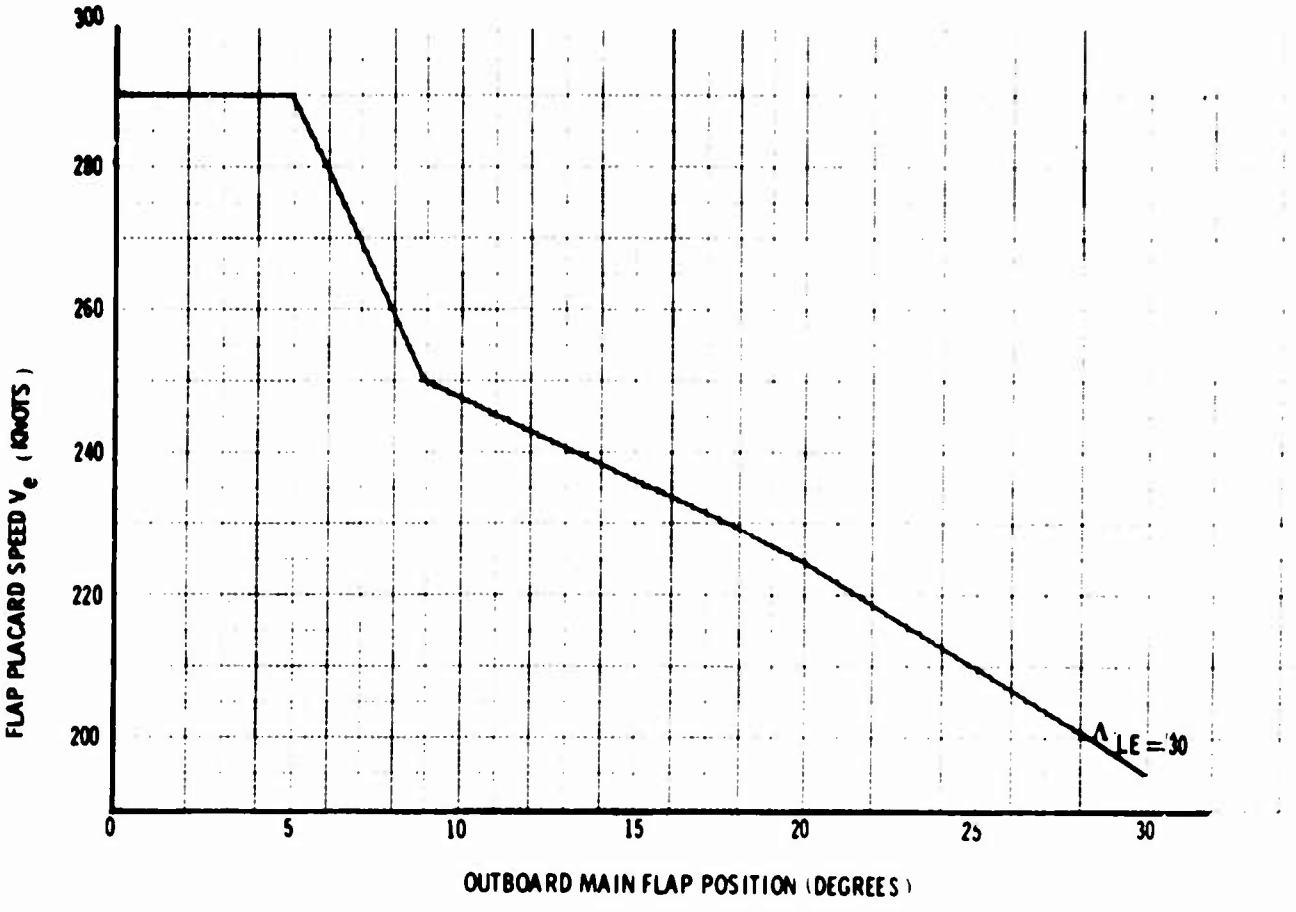

Figure 2-7. Flap Placard Speeds, 30-Degree Wing Leading-Edge Sweep

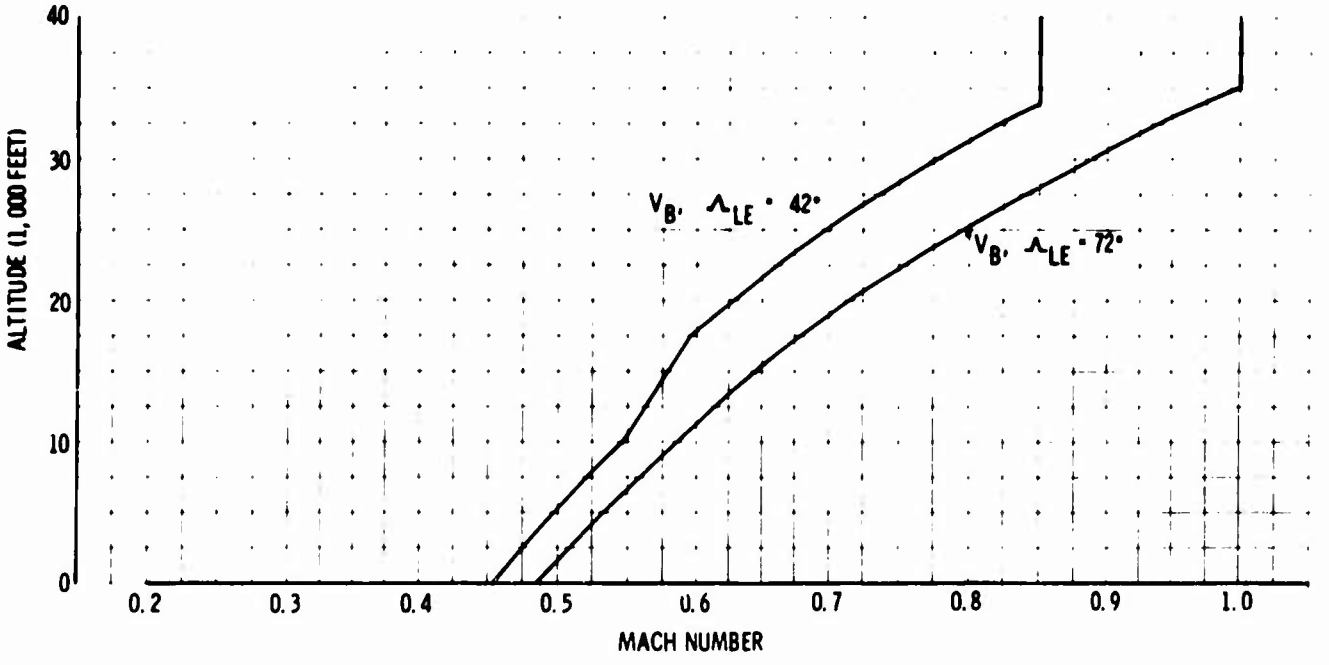

Figure 2-8. Design Speed for Maximum Gust Intensity, V_B

Table 2-A. Configurations and Placards, High Lift and Control Surfaces

Surface	Maximum Deflection (deg)	Initial Blowdown C_{Hq} (psf)	Usage Placards			
			Λ_{LE} (deg)	V_e (kn)	Mach	Flap Setting (deg)
Aileron						
Landing and takeoff	±25	-	30	250	-	(≥ 25%)
Climbout	±25 to 0	-	30	290	-	(25%→0%)
Spoilers						
No. 1	±45	235	All	V_D	M_D	-
No. 2	±45	225	All	V_D	M_D	-
No. 3	±45	280	All	V_D	M_D	-
No. 4	±45	350	All	V_D	M_D	-
No. 5	±45	485	≤42	V_D	M_D	-
No. 6	±45	415	≤42	V_D	M_D	-
Slats	Strake / Wing					
Takeoff	35 / 20	-	30	225	-	20
Landing	35 / 30	-	30	200	-	20
Climbout	25 / 6	-	30	290	0.45	5
Climb	25 / 6	-	42	-	≦ 0.6	0
Holding	25 / 6	-	30	290	≦ 0.6	0
Emergency Descent	25 / 0	-	72	-	≦ 0.6	0
Wing Flaps	Fore / Aft					
Takeoff	20 / 40	-	30	225	-	20
Landing	30 / 50	-	30	195	-	30
Intermediate	9 / 18	-	30	250	-	9
Climbout	5 / 5	-	30	290	0.45	5
Strake Flaps	Fore / Mid / Aft					
Takeoff	26 / 40 / 60	-	30	225	-	20

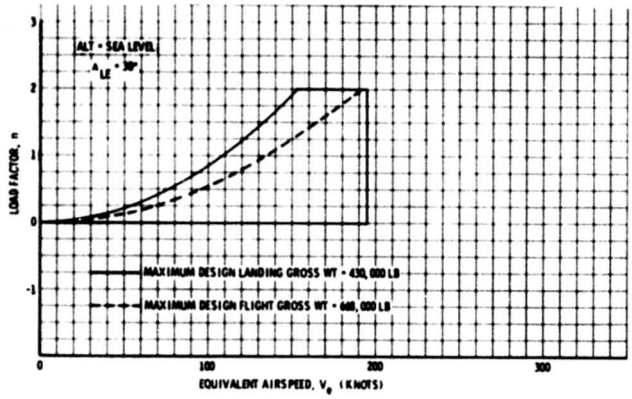

Figure 2-9. V-n Diagram, Landing Flaps

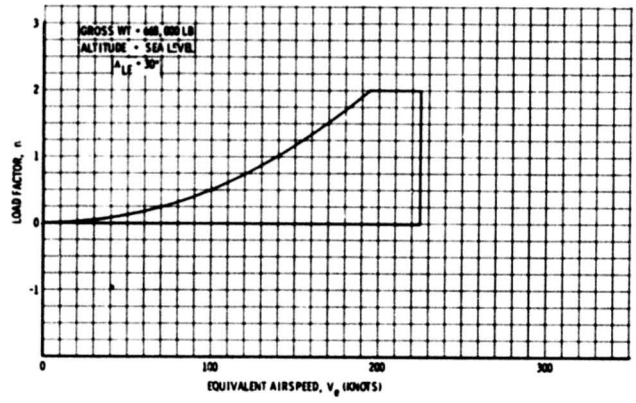

Figure 2-10. V-n Diagram, Takeoff Flaps at Maximum Design Flight Weight

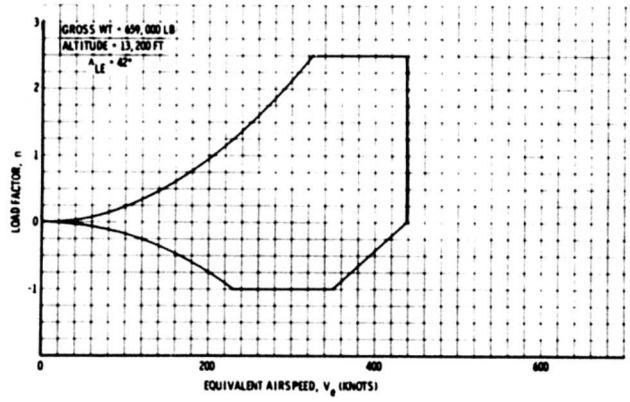

Figure 2-11. V-n Diagram, Subsonic Climb at Maximum Design Gross Weight (13,200 Feet)

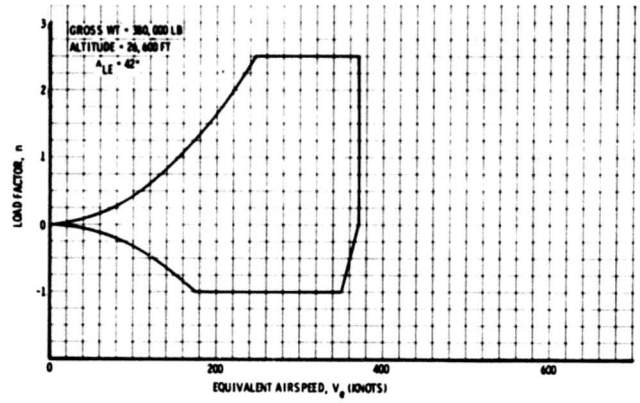

Figure 2-12. V-n Diagram, Minimum Gross Weight With Forward Payload

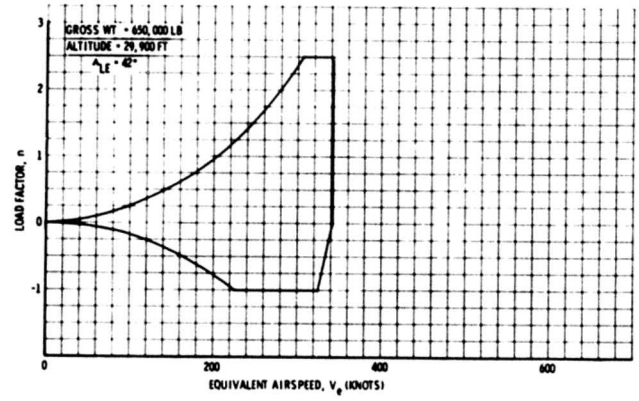

Figure 2-13. V-n Diagram, Subsonic Climb at Maximum Design Gross Weight (29,900 Feet)

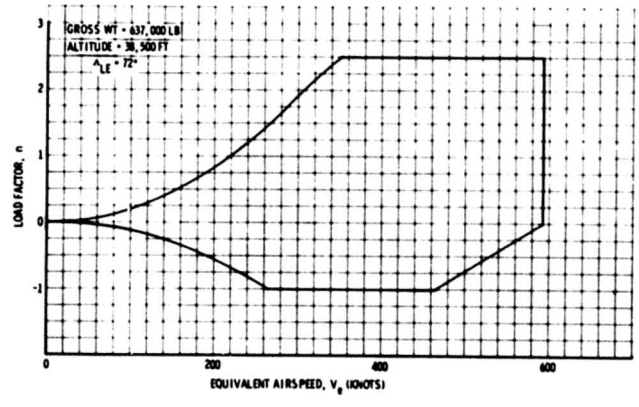

Figure 2-14. V-n Diagram, Transonic Climb at Maximum Design Gross Weight

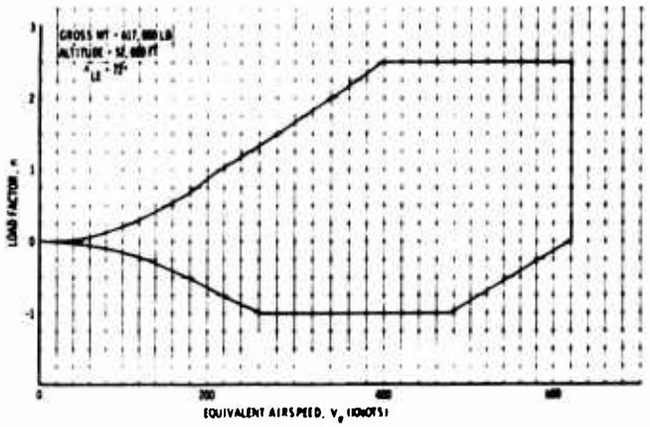

Figure 2-15. V-n Diagram, Supersonic Acceleration at Maximum Design Gross Weight

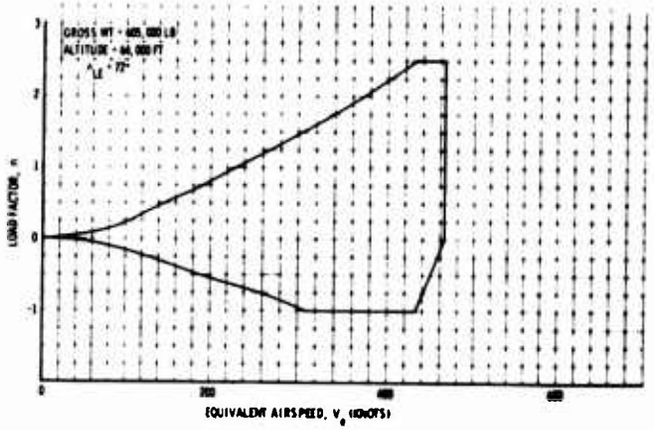

Figure 2-16. V-n Diagram, Maximum Gross Weight at Start of Cruise

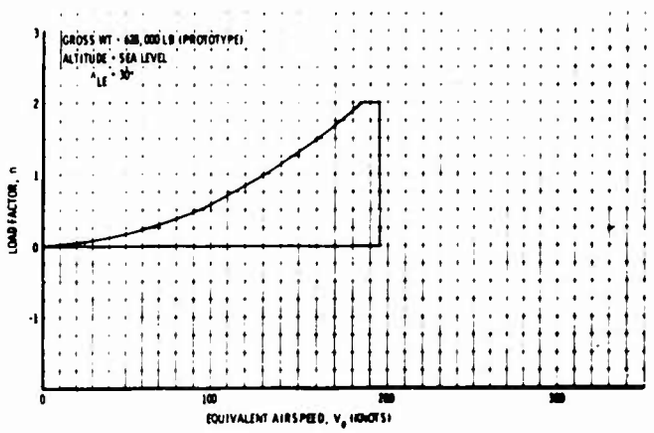

Figure 2-17. V-n Diagram, Landing Flaps at Prototype Maximum Design Flight Weight

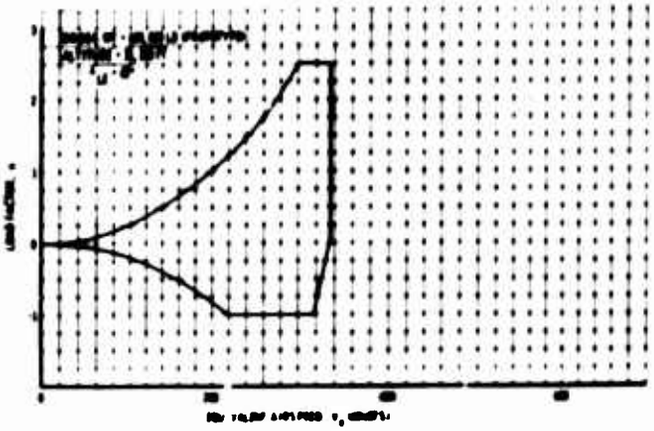

Figure 2-18. V-n Diagram, Subsonic Climb at Prototype Maximum Design Gross Weight

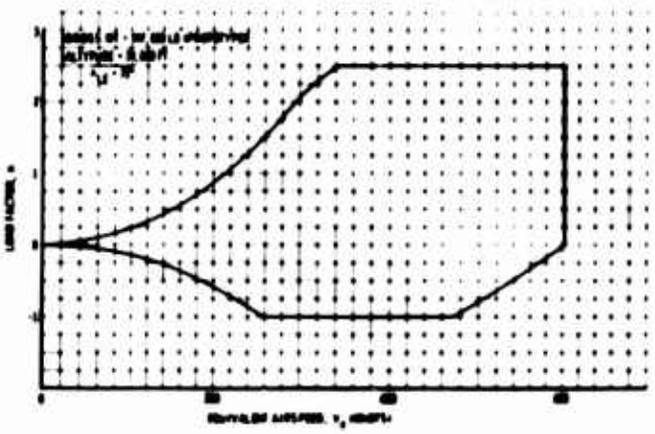

Figure 2-19. V-n Diagram, Transonic Climb at Prototype Maximum Design Gross Weight

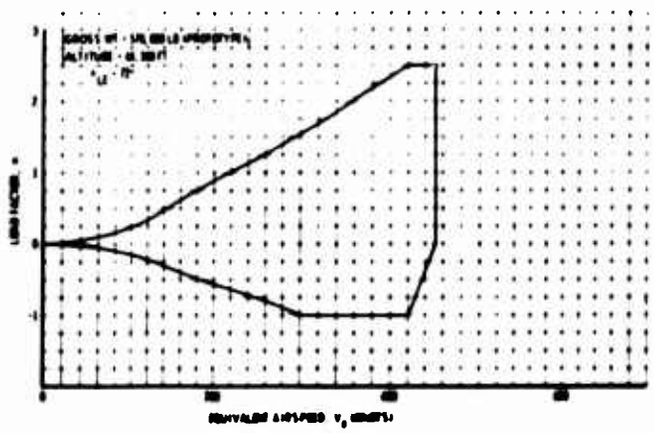

Figure 2-20. V-n Diagram, Maximum Gross Weight at Prototype Start of Cruise

For the takeoff and landing configurations with both leading-edge slats and trailing-edge flaps deflected, the maneuvers are restricted to a positive load factor of 2.0 and a load factor of 0.0.

At the operational empty weight, a maneuver load factor of n = 2.25 is used; whereas, at the minimum flying weight, a maneuver load factor of n = 2.5 is used.

From V_A to V_{MO} the ultimate fail-safe maneuver load factor of 2.0 is combined with a factor of 1.15 to account for the dynamic effects of failure unless a lower factor is substantiated by a rational dynamic analysis.

Investigations are made to determine the critical design flight loads on all parts of the airplane structure. All applicable wing sweep positions and control surface deflections are considered. The methods used to determine the load distribution are described in Par. 3.2.

2.1.6 Gust Design

The airplane is designed to withstand both continuous and discrete forms of atmospheric turbulence to a level of gust protection consistent with proposed operational limits and equivalent to or better than past civil transport practice. Dynamic response of the airplane, including structural flexibility, is accounted for in the design. The triplicated, monitored, fail-operational SAS is considered to be fully effective in evaluating dynamic response for design gust conditions, since full damping augmentation is retained even after two channel failures in pitch and yaw.

Power spectral density (PSD) methods defined in Refs. 2-2 and 2-3 are applied on the basis of both "mission analysis" and "design envelope analysis." The frequency of exceedance for mission analysis is taken as 10^{-5} exceedances per hour. The value of $\sigma_w \eta_D$ at V_C for design envelope analysis is taken as 62 fps at sea level varying to 70 fps at 7,000 ft, to 62 fps at 27,000 ft, and to 20 fps at 80,000 ft. In addition, as determined from analog-computer studies, time history response to random turbulence is considered separately and is correlated with digital-computer PSD results. Discrete gust loads are evaluated on both a (1-cos) dynamic response basis and on a sharp-edged gust formula basis. The discrete gust methods are based on FAR, Par. 25.341 U_{de} requirements except that V_B gusts are not considered at speeds greater than M 1. Further, the design gust velocities are modified as follows:

a. At speeds above M 1, positive and negative gusts of 60 fps at V_C are used at altitudes between sea level and 20,000 ft.

b. At altitudes above 20,000 ft, the gust velocity is reduced by the factor $(\sigma/\sigma_R)^{1/2}$ where σ is the density ratio at any altitude and σ_R is the density ratio at 20,000 ft.

For supersonic flight, a supersonic alleviation factor (K_F) is used in place of the standard subsonic alleviation factor.

Structural margins of safety available for gust loads are determined on the basis of all competing design conditions contributing to final design of the structural elements. Where maneuver or other loads provide margins beyond minimum gust standards, the contributory gust loads, determined by power spectral or discrete gust dynamic analyses, are identified as noncritical for design purposes.

2.1.7 Mission Profiles

The standard flight missions with GE and P&WA engines are shown in Figs. 2-21 and 2-22. These missions are consistent with airplane performance and have been considered in establishing the maximum design gross weights (Fig. 2-3) as well as the structural design speed placards (Figs. 2-2, 2-5, and 2-6). Typical operational 3,500-nmi and 1,700-nmi mission profiles shown in Figs. 2-23 and 2-24 are used for fatigue evaluation. (Refer to Airframe Design Report - Part B, V2-B2707-6-2, Sec. 4.0.) The 3,500-nmi mission, shown in Fig. 2-23, with a more rapid climbout is used for thermal analysis.

2.1.8 Aerodynamic Heating Criteria

The criteria presented here are used for structural temperature analyses. Criteria applicable in the areas of propulsion, air conditioning, hydraulics, and fuel are shown in Propulsion Report - Part B, V2-B2707-13; Systems Report - Part A, V2-B2707-10; and Systems Report - Part B, V2-B2707-11.

In addition to the maximum operating speed (V_{MO}/M_{MO}) and the maximum dive speed (V_D/M_D) limits (defined in Pars. 2.1.3.6 and 2.1.3.7), the following temperature boundaries are established for design purposes.

a. The maximum operating temperature, T_{MO}, is the maximum stagnation temperature associated with the maximum operating speed,

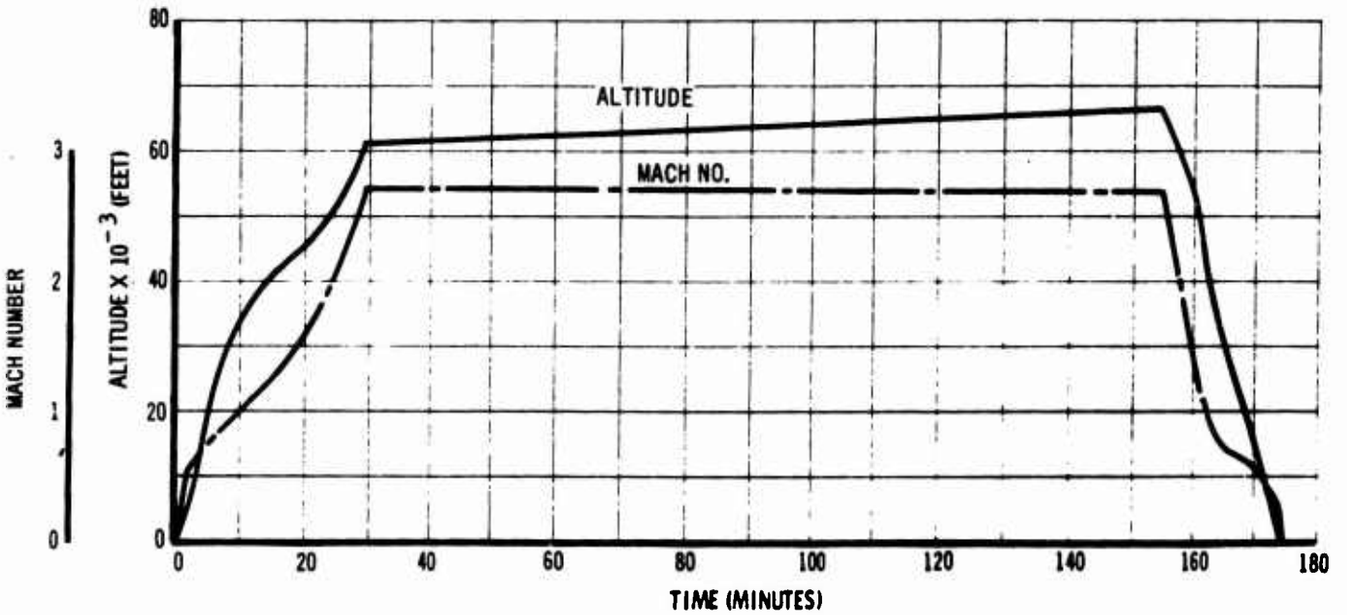

Figure 2-21. Design Flight Profile, GE

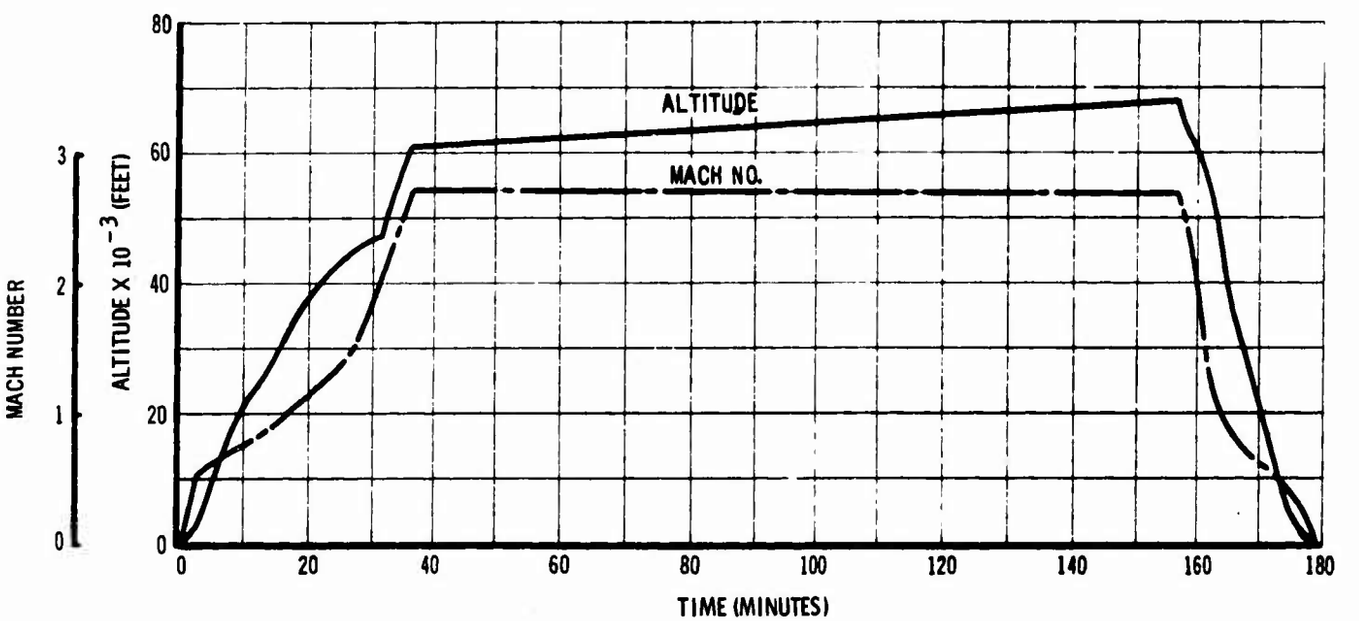

Figure 2-22. Design Flight Profile, P&WA

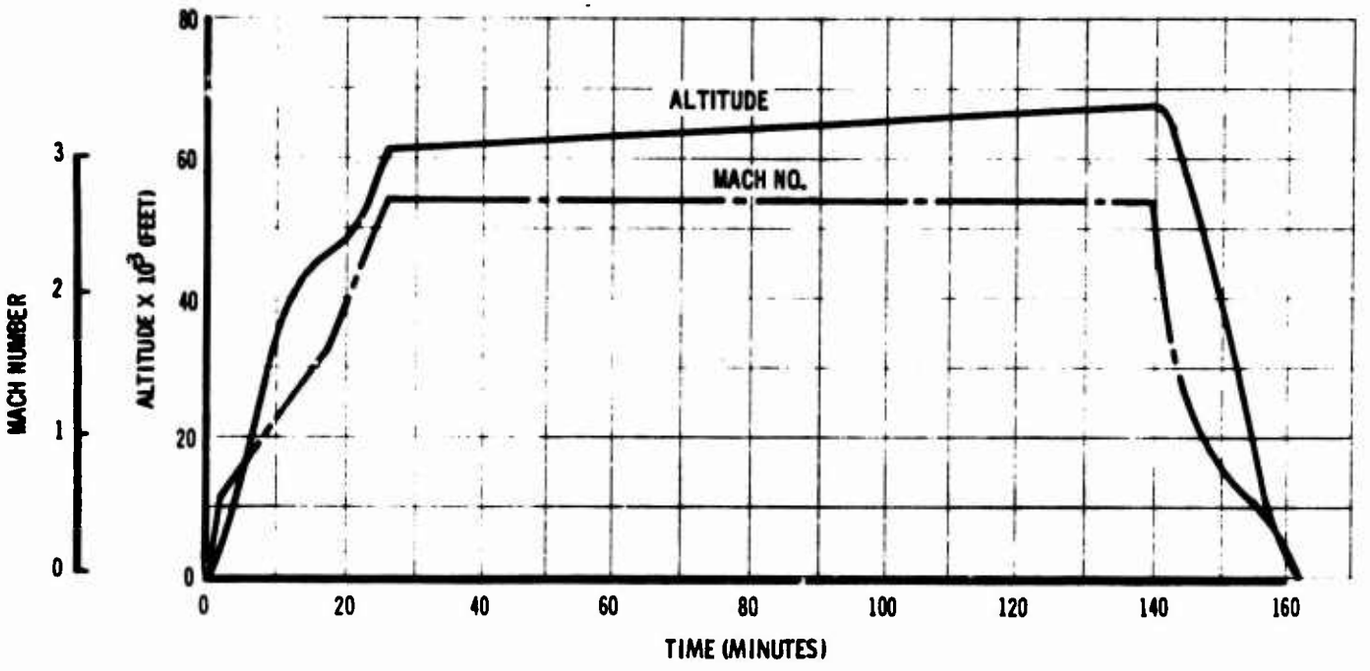

Figure 2-23. Design Flight Profile, 3,500 Nautical Miles

V_{MO}/M_{MO}. The T_{MO} boundary selected for design is 500° F, which is the stagnation temperature at M 2.7 on a U. S. Standard Day.

b. The maximum temperature at dive speed is defined as T_D. For design, T_D is selected as 585° F, which is the stagnation temperature at M 2.9 on a U. S. Standard Day.

Figure 2-25 presents the B-2707 design temperature envelope that results from these limits along with the M_{MO} and M_D boundaries.

The influence of atmospheric temperature variations on cruise Mach number has been studied. For example, the ambient temperatures along North Atlantic routes throughout most of the year are generally higher than U.S. Standard Atmospheres. Using the proposed temperature criteria, the probability curves for cruise speeds on the New York to Paris route are as shown in Fig. 2-26.

For standard thermal analyses of structure, the flight profile shown in Fig. 2-23 is used along with the U.S. Standard Atmosphere (Ref. 2-4) shown in Fig. 2-27. Analyses using this profile provide predictions that are conservative in terms of thermal gradients or stresses. Where structure has large heat-storage capacity (e.g. the wing pivot) and the time between flights is short, temperatures increase with each additional flight. The wing pivot structure is analyzed for this condition using three flights with 30 min of downtime between flights. (See Fig. 2-23.) In addition to using the U.S. Standard Atmosphere for design, both Cold Day and Hot Day conditions from Military Standard MIL-STD-210A are considered. Ambient ground temperatures shown in Fig. 2-27 are assumed to range between -50° and +120°F. The Hot Day Atmosphere is used to determine maximum operating temperatures, while the Cold Day Atmosphere is used primarily in the error analyses evaluation of off-normal conditions.

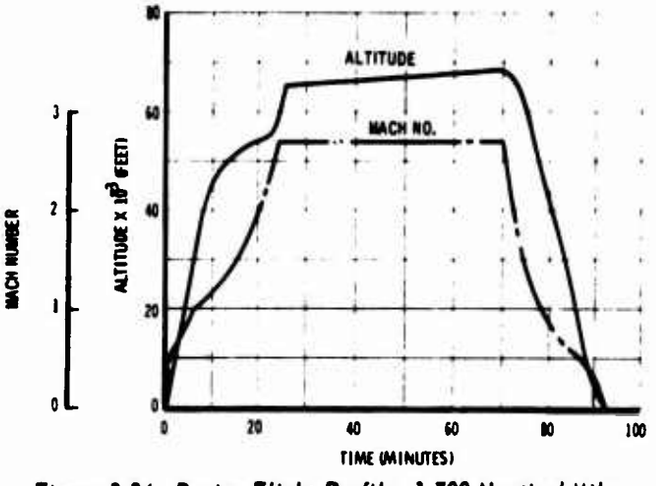

Figure 2-24. Design Flight Profile, 1,700 Nautical Miles

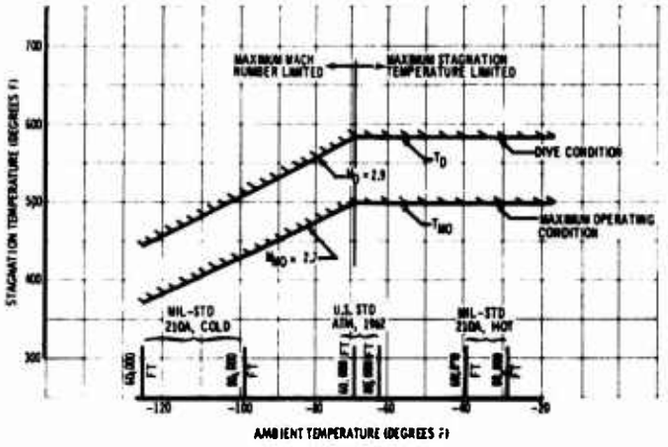

Figure 2-25. Design Temperature Envelope

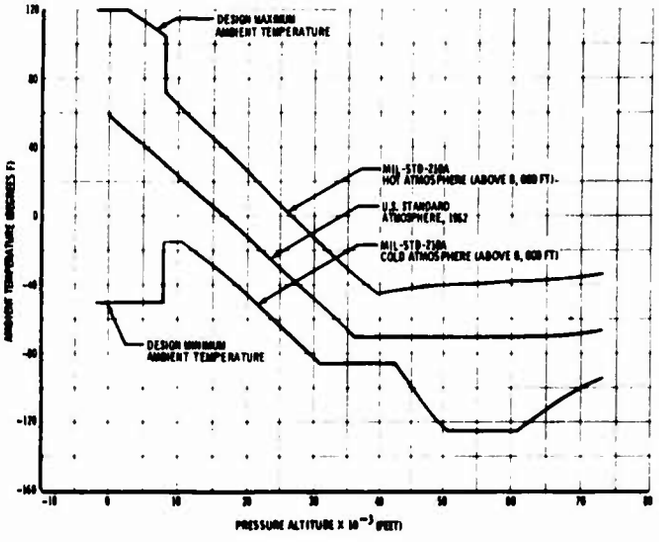

Figure 2-27. Design Atmospheres

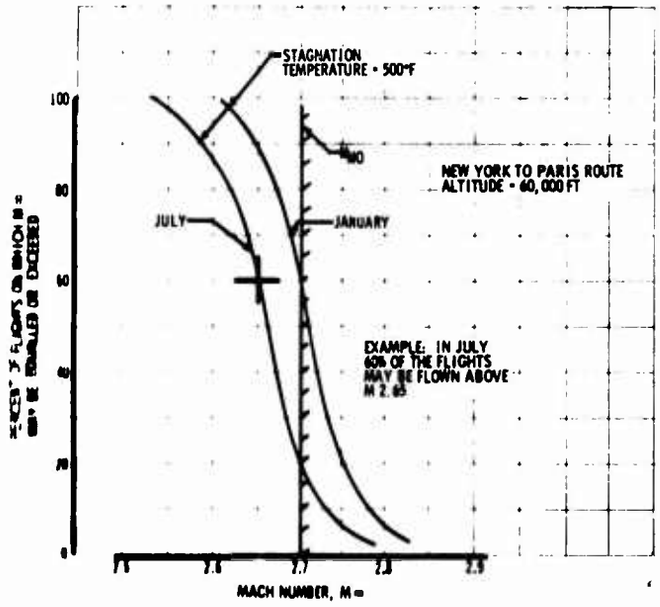

Figure 2-26. Cruise Speed Probability

2.2 GROUND LOADS CRITERIA

Ground handling and landing impact loads are calculated for the rigid airplane in accordance with the general requirements of FAR 25. Dynamic response of the flexible airplane is accounted for by rational dynamic analysis.

Par. 3.1.7 contains the critical ground handling and landing impact loads calculated in accordance with the criteria of Pars. 2.2.1 and 2.2.2. These ground loads are used for landing-gear analysis in Boeing Document V2-B2707-6-2.

2.2.1 Ground Handling

The main- and nose-gear shock struts are assumed to be in the taxi static position for all ground handling loads. The landing gear and airplane structure are investigated for the maximum design takeoff weight with zero wing lift. The aft main gear on one side of the airplane is manifolded to the forward main gear on the same side of the airplane by a hydraulic "evener" system so that the vertical loads are equal.

2.2.1.1 Takeoff Taxi

The airplane is designed for runway and taxiway roughness levels in excess of those anticipated for international-airport operations. Dynamic response of the airframe and landing gear structure is accounted for in the load-estimating methods employed. Direct accounting for dynamics is provided by results of rational dynamic analysis using a 2-in. rms runway roughness profile. Indirect accounting for dynamics is provided by application of the 2.0 limit vertical (N_V = 3.0 ultimate) taxi factor. Although a reduced

taxi factor could be selected in view of the multiple main gear configuration, which inherently averages runway roughness, a factor of 2.0 will be used to provide fail-safe capability in the main gear.

2.2.1.2 Braked Roll
The limit vertical load factor acting at the airplane center of gravity is 1.0 (N_V = 1.50 ultimate). A drag reaction equal to the lesser of either the vertical reaction multiplied by a coefficient of friction of 0.80, or a drag force consistent with available brake torque, is combined with the vertical reaction and applied at the ground contact point of each wheel having brakes.

The airplane is investigated for the following conditions:

a. The airplane is in a level attitude with all wheels contacting the ground. Zero pitching acceleration is assumed.

b. The airplane is in a level attitude with only the main gear contacting the ground. The pitching moment is reacted by angular acceleration of the airplane.

2.2.1.3 Ground Turning
The airplane is assumed to execute a steady turn in such a manner that the limit load factors at the airplane center of gravity are 1.0 vertically (N_V = 1.50 ultimate) and 0.50 laterally (N_S = 0.75 ultimate). The side ground reaction of each wheel is 0.50 of the vertical ground reaction for that wheel. Cornering forces developed on main-gear tires during ground turning are combined with the basic side ground reaction when it is more critical to do so.

2.2.1.4 Pivoting
The airplane is assumed to pivot about the centerline of one main gear with the brakes on that gear locked. The limit vertical factor at the airplane center of gravity is 1.0 (N_V = 1.50 ultimate), and the ground coefficient of friction is 0.80.

2.2.1.5 Nose Gear Yawing, Static
A limit vertical load factor of 1.0 (N_V = 1.50 ultimate) at the airplane center of gravity is combined with a side component at the ground contact point of the nose gear of 0.80 of the vertical reaction.

2.2.1.6 Nose-Gear Yawing, Unsymmetrical Braking
The nose gear and supporting structure are investigated for the loads resulting from application of brakes on one pair of main gear. The limit vertical load factor at the airplane center of gravity is 1.0 (N_V = 1.50 ultimate). The forward-acting load at the center of gravity is assumed to be 0.80 of the vertical reaction on one main gear unit. The side and vertical forces at the nose-gear ground contact point are those necessary for static equilibrium. The side load factor is assumed zero.

2.2.1.7 Towing
The limit load for towing, F_{TOW} (forward and aft) = 0.150 W_T (design maximum takeoff weight), or F_{TOW} (side) = 0.053 W_T, is applied at the nose-gear tow lugs. A towing load equal to 0.75 F_{TOW} acting in any horizontal direction is applied to each main-gear tow lug.

2.2.1.8 Reverse Braking
The airplane is assumed to be in three-point static ground attitude. The limit vertical load factor at the airplane center of gravity is 1.0 (N_V = 1.50 ultimate). A forward-acting drag load equal to the lesser of either 0.55 of the vertical reaction or a drag force consistent with available brake torque, is combined with the vertical reaction and applied at the ground contact point of each wheel having brakes. The airplane pitching moment is balanced by airplane rotational inertia.

2.2.1.9 Jacking Conditions
Landing-gear jack pads, located at either end of each main-gear truck beam and on the nose-gear centerline, enable the airplane to be jacked at all weights up to the maximum taxi weight. The limit vertical load factor of 1.33 (N_V = 2.0 ultimate) is combined with a side, forward, or aft factor of 0.40 (0.60 ultimate).

Tail and body jack pads enable the airplane to be jacked at all weights up to the jacking weight. The maximum jacking weight is 400,000 lb for the prototype and 410,000 lb for the production airplane. The vertical limit load factor of 1.67 (N_V = 2.50 ultimate) is combined with a side, forward, or aft factor equal to 25 percent of the vertical load factor.

2.2.2 Landing Impact Loads
The airframe and landing gear structure are designed to withstand the following landing conditions:

a. Two-point level landing

b. Tail-down landing

c. One-gear landing

d. Drift landing

e. Special conditions

Loads for these conditions are determined from rational dynamic analysis. Airplane dynamic response is included due to both main-gear and nose-gear impact. All landing-gear loads are conservatively assumed to be applied with the main or nose-gear shock struts (or both) 20-percent compressed from full extension. A wing lift equal to the weight of the airplane is assumed to be acting at the airplane center of gravity throughout the landing impact phase. The entire center-of-gravity range is investigated for the normal design landing weight at 10-fps descent velocity and for the design takeoff weight at 6-fps descent velocity in determining the critical design loads for each landing-gear element. The vertical reactions of the spin-up and spring-back conditions are calculated in a rational manner based on the energy absorption characteristics of the shock strut. The drag loads are determined by multiplying the vertical impact reaction by a factor of 0.70 for spin-up and a factor of 0.50 for spring-back. These spin-up and spring-back factors were used for structural design on the 707 airplanes and have been substantiated by test. These factors include consideration for dynamic magnification due to adverse phasing of the spin-up (or spring-back) loads from the forward and aft set of wheels on each of the main gears. The same factors are conservatively applied to the nose gear calculations. The maximum spin-up or spring-back load is conservatively combined with the maximum vertical impact reaction. The spin-up and spring-back drag loads are applied at the axle centerline. The side loads are applied at the ground contact point.

2.2.2.1 Two-Point Level Landing
The airplane is assumed to contact the runway in a level attitude with the nose gear clear of the runway and carrying no load. All landing impact is assumed reacted by the aft main-gear units, which have longer shock-strut strokes and extend further downward than the forward main-gear units. Unbalanced pitching moments are balanced by airplane inertia. The main-gear hydraulic interconnect is conservatively assumed ineffective.

2.2.2.2 Tail-Down Landing
The airplane is assumed to contact the runway in a tail-down attitude. All landing impact is assumed reacted by the aft main-gear units. Ground reactions are resolved into components parallel and perpendicular to the shock strut. Unbalanced pitching moments are balanced by airplane inertia. The main-gear hydraulic interconnect is conservatively assumed ineffective.

2.2.2.3 One-Gear Landing
The airplane is assumed to contact the runway in a level attitude on one rear main-gear unit with the same ground loads and assumptions as for the two-point level condition. Unbalanced moments are reacted by airplane inertia.

2.2.2.4 Drift Landing
The airplane is assumed to be in a level attitude with only the main gear contacting the ground. The vertical impact reactions are taken as 0.50 of the reactions obtained for the two-point level landing case. Side loads equal to 0.80 of the vertical reaction (on one side) acting outward are assumed acting at the ground contact points. The side loads are assumed to occur immediately after wheel spin-up and to persist through the gear spring-back cycle. The spring-back loads are calculated in the normal manner and combined with the side and vertical reactions with the spin-up drag load assumed as zero. The external loads are balanced by airplane inertia.

2.2.2.5 Maximum Strut Reaction
The rate-of-descent energy is apportioned to the gear units in accordance with the static reactions resulting from application of 1.0 load factor vertical and 0.25 forward load factor acting through the airplane center of gravity. An aft-acting drag load equal to 0.25 of the maximum vertical reaction is combined with the maximum vertical reaction.

2.2.2.6 Boeing Condition
Effects of nose-gear touchdown on airframe loads are investigated for both wings-forward and wings-aft landing conditions. The nose gear and supporting structure is investigated for the effect of

rotating the airplane in pitch with the elevator from an initial tail-down attitude. The main gear units are assumed to be in the taxi static position (the vertical translational energy having been absorbed and the vertical translational velocity at zero). The nose gear absorbs the rotational energy. Full spin-up and spring-back drag loads are combined with the vertical reaction.

2.2.2.7 Landing Rebound
The landing-gear shock strut is assumed to be in the fully extended position and not in contact with the ground. Two conditions are considered:

a. A limit load factor of 20 is assumed acting on the landing gear upsprung weight; its line of action is along the shock-strut centerline tending to extend the shock strut.

b. A limit load factor of 2 is assumed acting on the shock-strut internal pressure.

2.2.3 Unsymmetrical Load Distribution
Limit ground loads are distributed among the wheels of a gear unit in accordance with the requirements of FAR 25. In determining the total load on a gear unit, the shift in load centroid (due to unsymmetrical load distribution on the wheels) is neglected.

Due to the truck-type main gear with its center pivot (allowing pitch rotation of the truck), the total vertical load on the forward two wheels must equal the total vertical load on the aft two wheels. The brake equalizer linkage assures equal braking between forward and aft wheels.

Limit ground loads are distributed between laterally adjacent wheels of a gear unit as described in the following paragraphs.

2.2.3.1 All Tires Inflated
Sixty percent of the total ground loads acting on a gear unit is applied to either side of the gear unit with 40 percent applied to the other side. This distribution is conservative (for the critical design conditions) with respect to the distribution obtained by consideration of the factors outlined in FAR 25 (runway crown, tire wear and growth, structural deflections, etc.) and will be substantiated in the final stress analysis. The 60-percent load need not be applied to the inboard wheel with an inward-acting side load, nor to the outboard wheel with an outward-acting side load, since the structural deflections resulting from the side loads increase the vertical load on the noncritical wheel. Hence, a symmetrical distribution is most critical for this load condition. For braking conditions the maximum drag load applied to any wheel need not exceed a drag force consistent with available brake torque.

2.2.3.2 Deflated Tires
For the case of one tire flat on the nose gear or any one or two tires flat on the main gear, the loads specified in the following paragraphs are applied to the inflated tires.

In case of one or two deflated tires, the applied load to each gear unit is assumed to be 60 percent or 50 percent, respectively, of the limit load applied to each gear for each of the prescribed landing conditions. However, for the drift landing condition, 100 percent of the vertical load must be applied.

A limit vertical load factor of 1.0 is assumed acting at the airplane center of gravity for all flat-tire ground handling conditions; however, a factor of 1.33 is used for one flat tire in the taxi condition. For one flat tire, the side or drag load factor at the airplane center of gravity is assumed to be 50 percent of the condition with no flat tires. Forty percent of nonflat tire drag or side load factor is used for the case of two flat tires on a main gear unit. For braked roll conditions (with one or two flat tires) the drag load acting on each inflated tire is assumed equal to the drag load acting on each tire in the nonflat condition. Flat tires are not considered for the pivot condition.

2.2.4 Emergency Landing Conditions
The airplane structure is designed to the general emergency landing requirements of FAR, Par. 25.561, as amended by Ref. 2-1. The airplane structure will sustain, without damage, the impact loads resulting from a 3-fps descent velocity under the following conditions:

a. Any one main-gear unit assumed inoperative

b. Any two main-gear units assumed inoperative, one on either side of the airplane

The structural design is sufficient to withstand the loads resulting from a nose-gear-up landing so that the fuselage fuel cells and passenger compartments are not ruptured. The forebody structure is designed as a skid surface. For inordinately severe landing impact loads, the main gear units are designed to separate cleanly from the

basic support structure with no damage to either the basic structure or the fuel cells. (Also refer to Par. 2.4.15.4)

Ditching considerations are in accordance with the requirements of FAR, Par. 25.563. Fuselage pressure loads are based on Military Specification MIL-A-8865.

2.3 FLUTTER AND VIBRATION CRITERIA

2.3.1 Flutter

Flutter prevention is provided to a minimum speed margin of 20 percent above V_D for constant Mach number and constant altitude for all lifting surfaces, control surfaces, and panels. Aeroelastic feedback through the SAS is precluded by electronic filtering. Transonic buzz is prevented by control system stiffness. Fail-safety is provided by systems redundancies. Free-play is maintained within acceptable standards.

Control surface and spoiler flutter is prevented by providing rotational frequencies sufficiently high, compared with those of the primary surface, so that no detrimental coupling exists. A preliminary minimum criterion for frequency separation is as specified in Military Specification MIL-A-8870. If a control surface extends outboard of the 75-percent span station of the main surface, the rotational frequency of the control surface will be at least 1.5 times the uncoupled torsional natural frequency of the main surface. This criterion is applied subject to later confirming analysis.

High frequencies result from the minimum stiffness required for the prevention of transonic control-surface buzz. The criterion used for buzz prevention (in terms of minimum frequency, and, thereby, the minimum stiffness) is

$$C = \frac{1.05\,a}{b\,\omega_\beta}$$

where:

- a = speed of sound (fps)
- b = control-surface semi-chord (ft)
- ω_β = control-surface rotational frequency (rad/sec)

Based on a survey made of several different types of high-performance airplanes, it was found that for C-values of from 0 to 5.0, no buzz existed. When C was greater than 5.0 but no larger than 8.0, buzz existed for some configurations, and when C was larger than 8.0, buzz occurred, except in rare cases. Based on C = 5.0, a minimum frequency is then established:

$$\omega_\beta \geq \frac{0.21a}{b} \text{ radians/sec}$$

Design tolerances for free play of control surfaces are given by the following, as stated in Military Specification MIL-A-8870:

a. If a trailing-edge control surface extends outboard of the 75-percent span station of the main surface, the total free-play does not exceed 0.22 percent of the distance perpendicular to the hinge line from the hinge line to the trailing edge of the control surface.

b. If a trailing-edge control surface extends outboard of the 50-percent span station but inboard of the 75-percent span station of the main surface, the total free-play does not exceed one-percent of the distance perpendicular to the hinge line from the hinge line to the trailing edge of the control surface.

c. If a trailing-edge control surface is inboard of the 50-percent span station of the main surface, the total free-play does not exceed 2 percent of the distance perpendicular to the hinge line from the hinge line to the trailing edge of the control surface.

d. The total free-play of all movable control surfaces does not exceed 0.06 percent of the distance perpendicular to the axis of rotation from the axis of rotation to the trailing edge of the control surface.

The requirement for the wing pivot is the same as for all movable control surfaces; however, the 0.06-percent requirement is restated as an 0.0344-deg (0.0006 radian) angular requirement.

2.3.2 Vibration

Interior vibration levels are well below minimum acceptable levels for passengers, crew, and equipment. Aft mounting of the engines on the horizontal tail provides effective attenuation of the vibration due to acoustic noise pressures. In addition, the engine manufacturer has agreed to meet a vibration limit of 5.0 mils double amplitude at selected points. Structural vibrations due

to engine rotary frequencies that might be transmitted into the airframe through the engine mount structure are attenuated by the low-frequency engine mount design. In addition, engine vibration isolators will be used at the inboard engine location (as in the 727 subsonic jets) due to the short structural path to the fuselage.

2.4 STRUCTURAL DESIGN CRITERIA

The airplane structure will be designed to the requirements of FAR 25 and criteria presented herein.

2.4.1 Fail-Safe and Safe-Life Design

The structure will be designed so that failure of individual elements (fatigue or damage from foreign objects) will not cause catastrophic failure or loss of the airplane. In general, fail-safety will be accomplished through redundancy in structural design so that failure of any single element will not reduce the airframe strength below 80-percent design limit load. Safe-life structure may be used where fail-safe design is impractical.

2.4.2 Fatigue Criteria

2.4.2.1 Design Life

The design structural fatigue service life of the airplane will be 50,000 flight hours of typical usage.

2.4.2.2 Scatter Factor

The structure will be designed and analyzed for the design service life multiplied by a scatter factor. The scatter factor will be 4 except for the following situation. Parts that can be readily inspected and replaced, (and where sufficient redundancy exists so that safety is not compromised) may be designed to a scatter factor of 2.

2.4.2.3 Airplane Usage

The airplane usage for fatigue design and analysis will include operational, training, and check flights as predicted for airline operations. Details are shown in Airframe Design Report - Part B, V2-B2707-6-2.

2.4.2.4 Load Spectra

Fatigue loading spectra will be based on the airplane usage of Par. 2.4.2.3. Thermal stress excursions will be included in the flight stresses.

2.4.2.5 Cumulative Fatigue-Damage Method

The linear cumulative fatigue-damage theory will be used as an analytical tool.

2.4.3 Allowables

Basic material properties will be taken from the Boeing Design Manual (Ref. 2-5) and Military Handbook MIL-HDBK-5. The effects of reduced allowables resulting from heat exposure will be taken into account. The design allowables will be as follows:

a. The following basic relationship will apply in the design of tension structure:

$$f_t + 1.25\, f_{th} \leq F_{tu}$$

$$f_t + 2.0\, f_p + 1.25\, f_{th} \leq F_{tu}$$

$$2.5\, f_p \leq F_{tu}$$

$$3.0\, f_p \leq F_{tu} \text{ in areas of stress concentration}$$

where:

f_t = tension stress

f_{th} = tension stress due to temperature (thermal)

f_p = tension stress due to cabin pressure differential

F_{tu} = ultimate tension allowable

The stress due to limit flight loads plus fuselage operating pressure plus thermal stress will not exceed the yield of the material.

b. The ultimate allowable compression stress will be based on either the column allowable or the section crippling stress. The combined axial compression stress (f_c) plus thermal compressive stress (f_{th}) will not exceed the crippling allowable of any segment. The equation relationship is

$$f_c + 1.25\, f_{th} \leq F_{cc}$$

c. A fitting factor will be used for joints between major structural components. In general, all joints and reinforcements will be designed by a fitting factor in accordance with FAR 25.

2.4.4 Buckling Criteria

To minimize aerodynamic drag, skin surfaces are designed to remain unbuckled for normal cruise flight conditions. In addition, integral fuel tank walls are designed so as to prevent buckling at limit load that could cause leakage.

2.4.5 Sonic Criteria

Sonic fatigue resistance will be provided throughout the airframe design for the sonic noise environment shown in Figs. 2-28 through 2-31. The detail design criteria shown in Fig. 2-32 will be used to establish minimum structural requirements. Sonic tests and detail design data are presented in Airframe Design Report - Part E, V2-B2707-9, Par. 3.7.

2.4.6 Wing-Tail Connection Criteria

The wing and horizontal tail interconnect structure will be designed to withstand holding loads incurred within the load-factor speed envelope of the airplane. During the engaging operation, relative wing horizontal-tail deflections will be considered for all airplane design gross weights, fuel loadings, centers of gravity, and control-surface deflections. The interconnect probes will be designed to allow for positive latching during wing sweep cycle actuation with perturbations of $\Delta n = \pm 0.5$ from the nominal $n = 1.0$ position. The design will provide satisfactory engagement during the occurrence of gusts up to 25 fps in any direction.

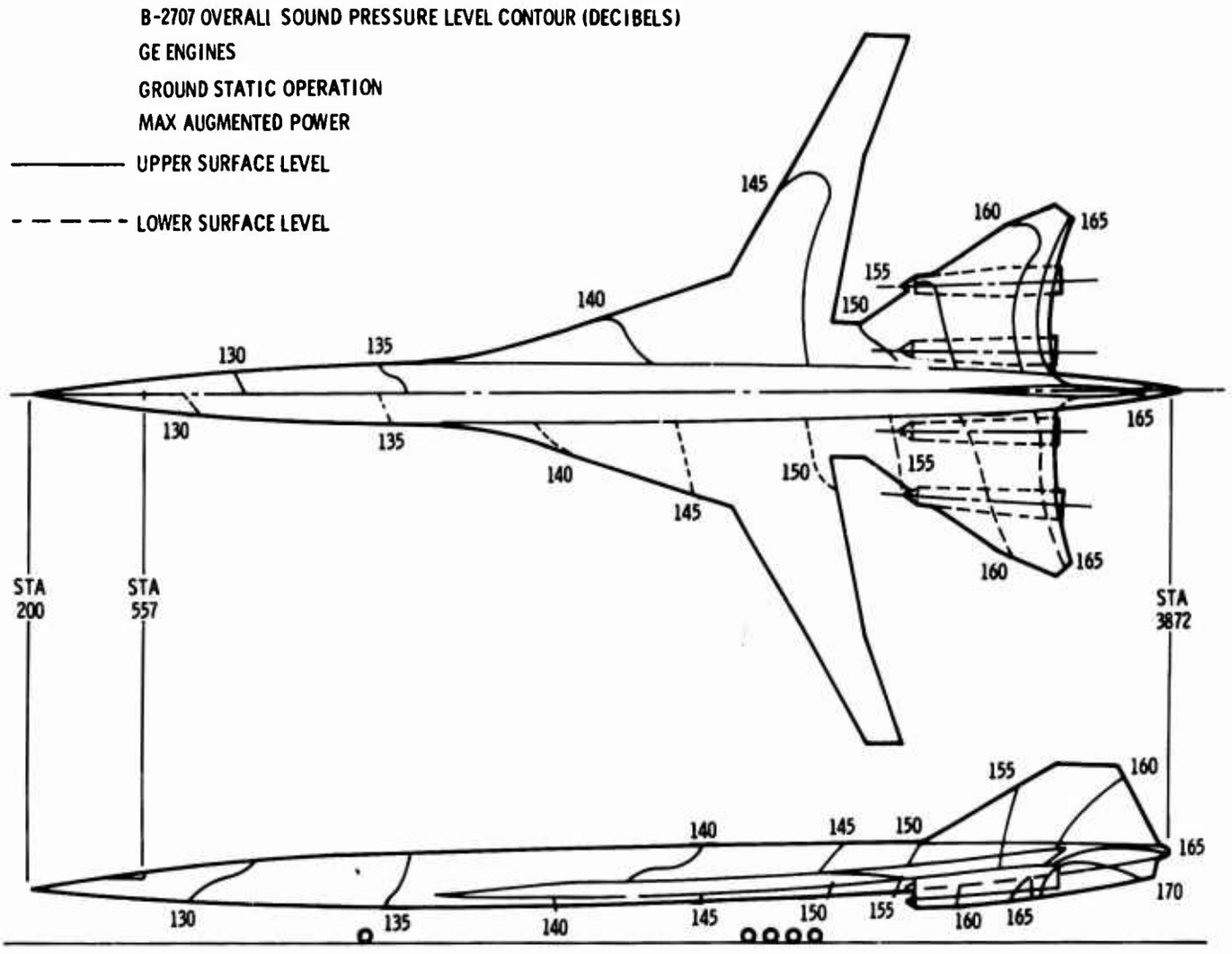

Figure 2-28. Takeoff Sound Levels, GE Engines

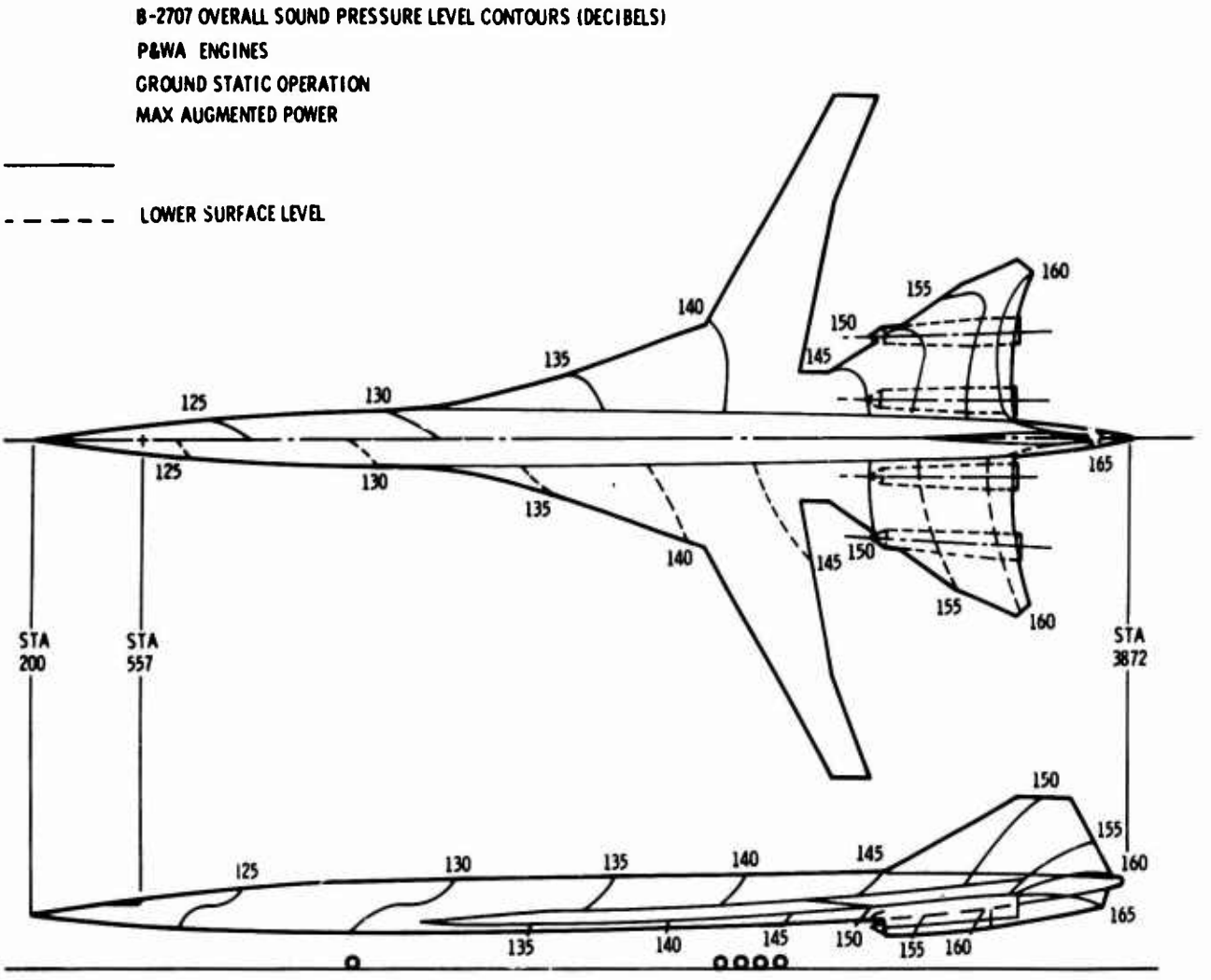

Figure 2-29. Takeoff Sound Level, P&WA Engines

2.4.7 Hail Damage

The structure will be designed to provide maximum resistance to hail impingement. Particular attention will be given to the design of the empennage, wing leading edge, engine inlet, and body nose structure to prevent loss of aerodynamic characteristics from hail damage during flight. Resistance to damage from hail will be at least equivalent to contemporary commercial airplanes.

2.4.8 Fuel Tanks

The fuel tank structure will be designed to withstand the effects of pressure fueling, fuel dead weight, pressure head, and the effects of a maximum airplane roll rate of 1 radian per second with fuel tanks full. The forward end of the fuselage tail compartment will be designed to withstand crash loading without rupturing with a full fuel tank. With the wings swept forward, the pressure for side acceleration will be based on a head equal to the distance between tank baffles. Typical ribs will be designed to withstand a slosh load equal to 2 factors ultimate with the head equal to the rib spacing. Fuel tanks will be designed to withstand loads imposed by maximum fuel-vent pressure combined with flight loads. Fuel weight will be assumed to be 6.7 lb/gal for these conditions.

For the crash landing condition, fuel cells outside of the fuselage will be designed to withstand an ultimate forward acceleration of 3.0 factors with a head equal to the maximum streamwise distance in the cell.

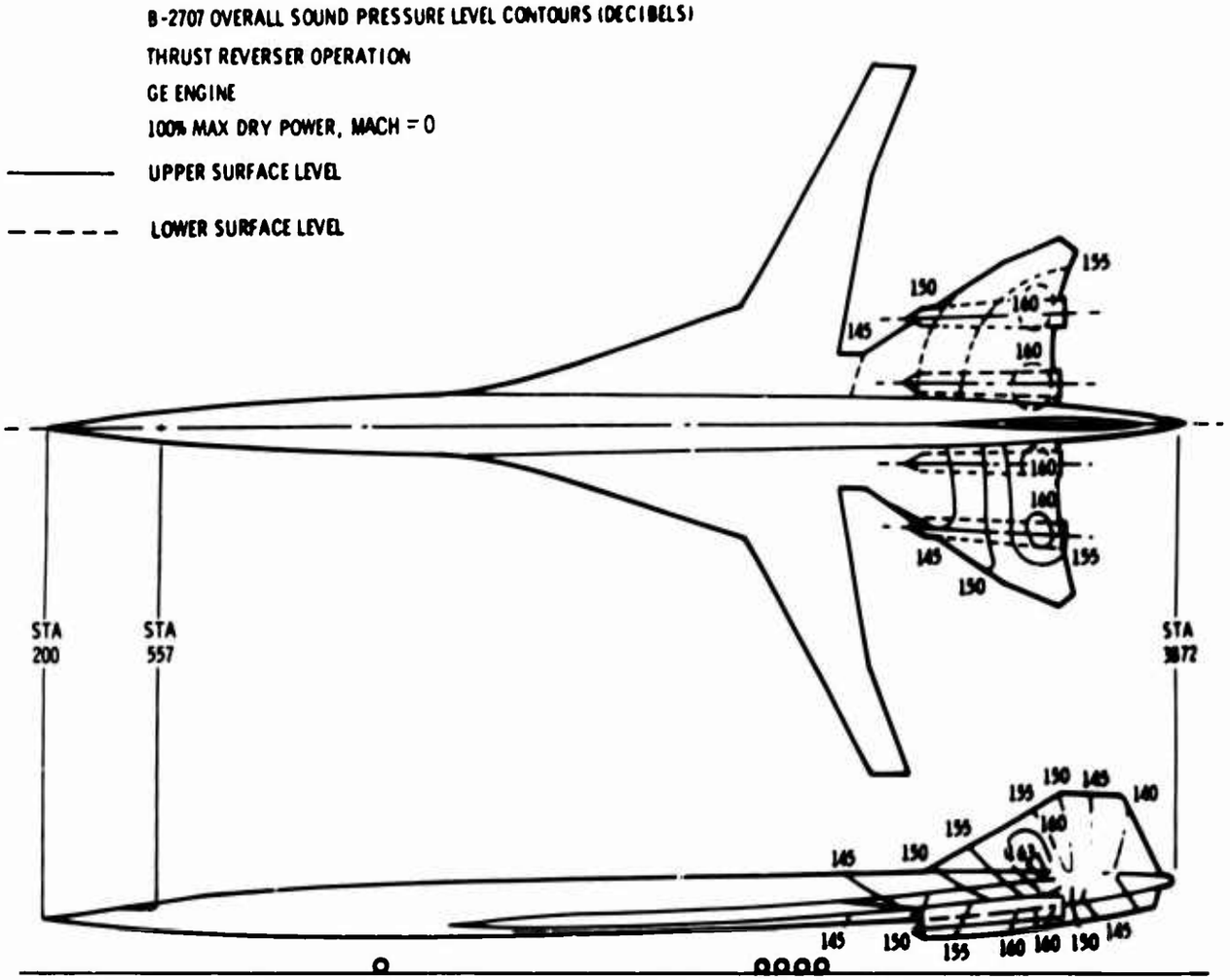

Figure 2-30. Reverse-Thrust Sound Levels, GE Engines

For crash landing conditions, fuel cells inside the body cavity will be designed to withstand the following ultimate factors acting singularly:

Below the passenger floor	Above the passenger floor
9.0g forward	12.0g forward
4.5g downward	4.5g downward
2.0g upward	2.0g upward
2.5g sideward	2.5g sideward

2.4.9 Passenger Windows

Passenger windows will be designed with three elements; two of the elements will be load carrying panes designed for fail-safety, and the third element will be an inner protective pane.

a. The primary pressure pane (middle) will be capable of carrying a minimum of 3 factors on maximum operating pressure at a temperature of 250°F. It will also be capable of withstanding the maximum relief-valve pressure setting for a period of 3 hr at a temperature of 450°F.

b. The secondary fail-safe pane (outer) will be capable of withstanding, at 450°F, the dynamic pressures resulting from an instantaneous failure of the primary (middle) pane at the maximum relief-valve setting.

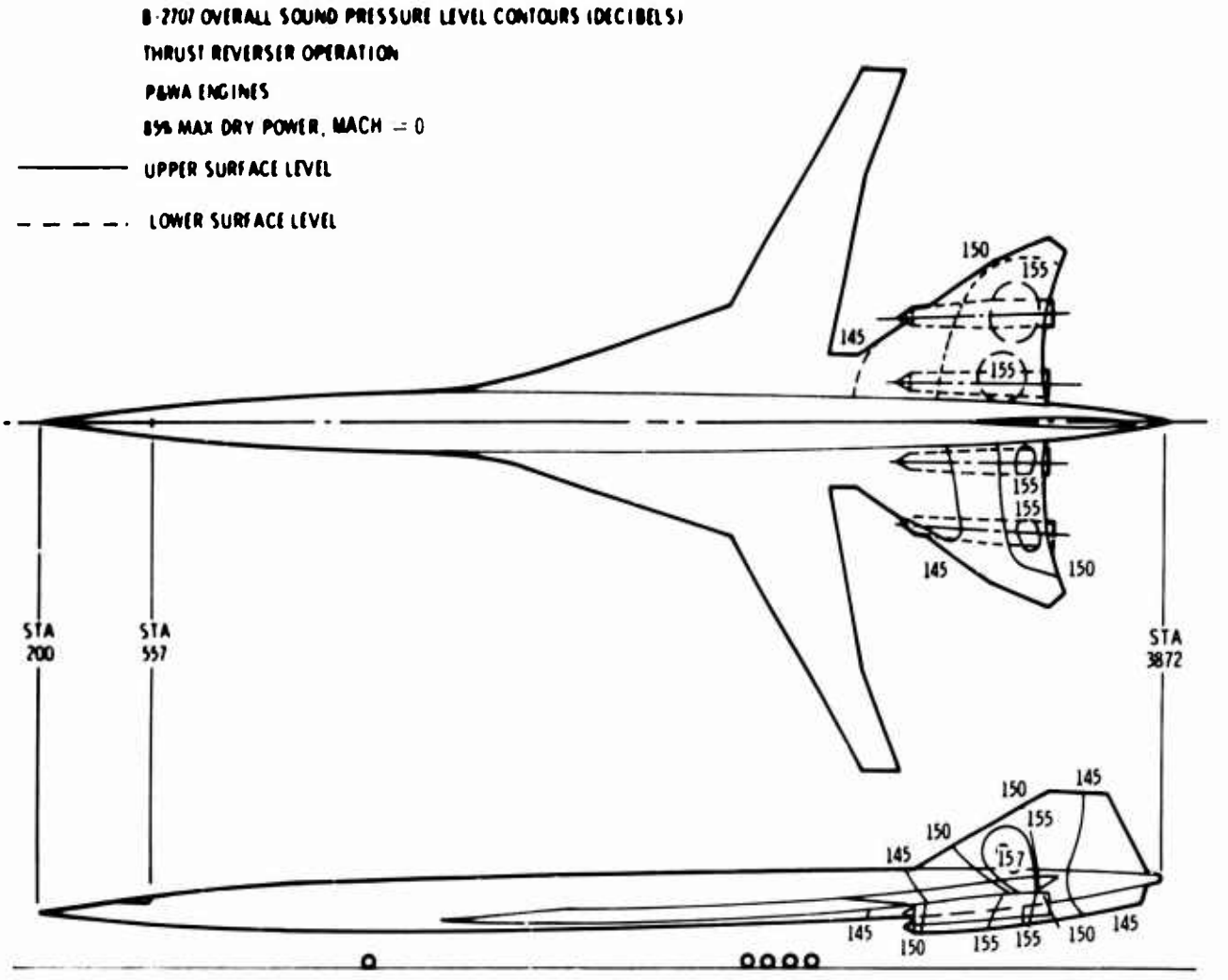

Figure 2-31. Reverse-Thrust Sound Levels, P&WA Engines

2.4.10 Crew Compartment Windows

Crew compartment windows must withstand three times the maximum pressure differential when subjected to the most adverse temperature condition. Dual fail-safe load paths will be provided through the use of three load-carrying panes. Each pane will withstand a maximum pressure differential of 1.5, accounting for the resulting temperature effects after the failure of adjacent panes.

The crew compartment windshield will withstand bird strikes in accordance with FAR, Par. 25.775.

2.4.11 Floor Structure

The floor in the passenger cabin will be designed for 100 psf locally. The total load in pounds in any area and load per running inch will be based on maximum-density seating.

The floors in the galley, main entry, and main aisle areas will be capable of withstanding a concentrated load of 300 lb applied with a 3/4-in.-diameter steel ball at any point on the top surface without failure or permanent indentation greater than 0.050 in. The remainder of the floors will be capable of withstanding a concentrated load of 200 lb applied in a similar manner without failure or permanent indentation greater than 0.050 in.

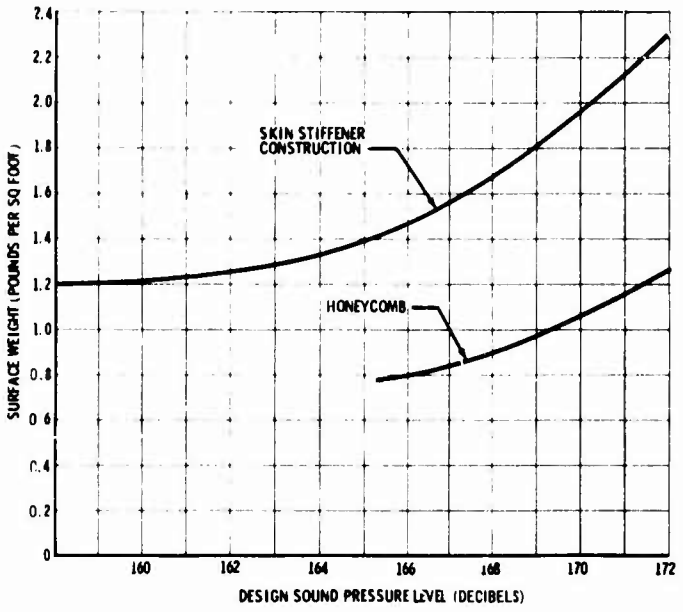

Figure 2-32. Sonic Resistance Design Criteria

The floor in the cargo compartment will be designed for 150 psf locally and 50 lb per running inch maximum. All cargo compartment floors will be capable of withstanding a concentrated load of 400 lb and applied with a 3/4-in.-diameter steel ball at any point on the top surface without failure or permanent indentation greater than 0.050 in.

2.4.12 Seat Loads
Loads will be based on man-weight of 170 lb plus seat weight. All seats in the crew compartment will be designed for the following ultimate crash load factors acting singularly:

a. Forward: 16 (acting within a 20-deg angle to either side of forward)

b. Vertical: 13 down and 7.5 up

Nonflight-deck crew seats and other passenger seats will be designed to withstand maximum design load factors, or for the following ultimate crash load factors acting singularly, whichever is greater:

a. Forward: 9.0

b. Downward: 7.5

c. Upward: 4.5

d. Sideward: 3.0

These load values will be multiplied by 1.33 for seat design and safety-belt local attachment.

2.4.13 Attachment of Equipment
All items of equipment that would injure passengers or crew in case of installation failure will be designed for the following singular ultimate load factors:

Crew compartment	Ultimate load factor
Forward	20.0
Vertical	8.5 down, 5.5 up
Sideward	4.0
Passenger Compartment	
Forward	16.0
Vertical	7.5 down, 4.5 up
Sideward	3.0

2.4.14 Pressure
The maximum operating cabin pressure differential will be 11.12 psi. This is equivalent to 6,000-ft cabin altitude at 70,000 ft. In the event of failure of the pressure regulator, the pressure relief valve will limit the differential pressure 12.34 psi maximum.

2.4.14.1 Design Factors for Pressure Only
The following pressure ultimates are not combined with flight loads:

a. An ultimate factor of 3.0 on maximum operating pressure will be used.

(1) Tension material adjacent to cutouts or areas of high-stress concentration

(2) Bolts in tension

(3) Door latches

b. An ultimate factor of 2.5 on maximum operating pressure will be used.

(1) Basic monocoque tension material

(2) Monocoque frames tension material, excepting adjacent to cutouts or stress concentrations

(3) Pressure floor beams tension material

(4) Pressure bulkheads tension material

(5) Shear material adjacent to cutouts

(6) Plug doors

(7) Shear connections

c. An ultimate factor of 2.0 on maximum relief vaive pressure will be used.

Members critical in compression or shear, except shear members adjacent to cutouts.

2.4.14.2 Pressure Combined With Flight Loads
An ultimate factor of 2.0 times the maximum operating pressure differential will be used in combination with the critical flight conditions. An ultimate factor of 1.5 on maximum relief valve pressure differential may be permitted in cases that are not fatigue critical.

2.4.14.3 Pressure Combined With Landing Loads
A pressure differential of 2.0 psi ultimate combined with landing loads will be used.

2.4.14.4 Negative Pressure
A negative pressure of 1.5 psi ultimate acting singularly will be used.

2.4.14.5 Fuselage Decompression Criteria
The structure between compartments must withstand the effect of a sudden pressure release resulting from an opening in the fuselage shell. The magnitude of the pressure differential between fuselage compartments depends on the size of the opening and the intercompartment venting. FAR, Pars. 25.365(e) and 25.365(f), state that the opening may result from failure of doors or windows or penetration of the fuselage and that the fail-safe features of the design may be considered when selecting the opening.

For some subsonic airplanes, the opening has been based on the loss of a skin panel bounded by stringers and crack stoppers. The tests on the titanium fuselage structure indicate that only local failures occur. (Refer to V2-B2707-9, Par. 3.3.4.) The maximum opening in a series of fail-safe tests is about 1 in. wide by 13 in. long. In spite of passenger-window fail-safe features, it appears reasonable to use the 6.5-in. diameter, 33-sq-in. opening for design purposes. Portions of the analysis have conservatively used a 42-sq-in. opening, which was established before the fail-safe pressure testing was completed.

2.4.15 Propulsion Pod Criteria

2.4.15.1 Engine Attachment
The engine attachment structure will be designed to criteria that is based on previous subsonic commercial-transport programs and supplemented by additional aerothermodynamic conditions encountered in the operating environment of supersonic flight. The design conditions are defined in Sec. 3.0 and include maneuver and landing load factors, gyroscopic loadings, aerodynamic loadings, normal and reverse thrust loadings, and sudden engine stoppage. Thermal effects on the attachment structure have been considered.

2.4.15.2 Engine Inlet
Additional criteria similar to the engine design conditions have been established for those conditions peculiar to the variable-geometry engine inlet. Engine thrust considerations have been replaced by conditions involving inlet internal pressures. The interior portions of the inlet are designed for an ultimate factor of 1.5 on the maximum pressures attainable during an upset condition at dive speed. An ultimate factor of 2.5 is applied to the normal operating pressures; a factor of 2.0 is applied to pressures sustained in conditions of external compression. Inlet skins are designed to withstand 1.5 times the maximum negative pressure differential without buckling.

2.4.15.3 Cowling
An ultimate factor of 2.0 is used on the combined maximum internal plus external pressure. The effects of yaw and pitch angles consistent with airplane maneuvers are also included.

All latches are designed for 3.0 factors ultimate on the maximum combined pressures. The structure is capable of supporting limit load with any one latch unlatched. The cowling is designed for an ultimate factor of 1.5 on the maximum pressure resulting from any duct failure combined with normal flight loads. Thermal effects on cowling structure are included.

2.4.15.4 Emergency Landing and Ditching Provisions will be made that will allow the propulsion pods to be torn free of the stabilizer structure without rupturing any fuel cell if a wheels-up or ditching condition is encountered.

2.4.16 Hydraulic Actuators
The following design conditions will apply to hydraulic actuators:

a. Pressure vessel: 3.0 factors ultimate on normal system pressure

b. Column (fully extended):

(1) 1.5 factor ultimate on limit inertia and airload

(2) 1.5 factor ultimate on load available from system maximum relief-valve pressure

c. Local attachment of actuator to structure: 2.5 factors ultimate on power available from normal system pressure

d. Tension:

(1) 3.0 factor ultimate on normal system pressure

(2) 1.5 factor ultimate on limit inertia and airload

BLANK PAGE

3.0 LOADS

Methods of analysis and validation procedures to be used for establishing structural design loads on the prototype and production B-2707 airplanes are based on technology within the current state of the art. The general approach to the steady and dynamic loads problem is consistent with past experience on the Boeing subsonic commercial airplane series. The philosophy of this approach is summarized in the following general description of three levels of loads technology.

a. Level 1: Preliminary design loads are established for a prototype airplane to provide a basis for structural layouts and to substantiate airplane weight estimates. Load distributions are based primarily on theoretical methods combined with wind tunnel data obtained on similar configurations. During this time period, the wind-tunnel test program is underway but not complete. Loads are not supported by completely sufficient test data and result in conservative values.

b. Level 2: Final design loads use detail wind-tunnel pressure data to establish final prototype design loads for support of engineering drawing release.

c. Level 3: Verification loads use complete wind-tunnel and structural test deflection data, as well as the flight load survey, to define design verification loads and to establish growth potential for production airplanes.

The historical progression of the wing design bending moment for the Boeing 367-80 subsonic jet transport prototype through these three levels of technology is shown in Fig. 3-1. The net reduction in bending moment from Level 1 to Level 3 is approximately 15 percent. It is expected through the use of present loads prediction technology that this percentage will be reduced.

The structural design loads shown in this document are considered to be at technology Level 1 and are appropriate for defining the preliminary design of the prototype airplane. The maximum design taxi gross weight for the preproduction prototype B-2707 airplane is 635,000 lb For comparison purposes, preliminary design loads are included for the production airplane at 675,000-lb maximum design taxi weight. It is emphasized that structural design loads at technology Level 3 for the production airplane are expected to be below the currently justifiable Level 1 values. Summarized descriptions of the planned verification tests as well as methods of analysis leading to the production B-2707 are included in this section.

3.1 DESIGN LOADS

The speed altitude diagram, Fig. 3-2, shows the flight regime for determination of structural design loads for the B-2707. Data defining airplane design speeds, wing sweep placards, center-of-gravity limits, and gross weights, as well as other design criteria, appear in Sec. 2.0. The B-2707 design loads, including all critical static-elastic and dynamic conditions, are summarized in the paragraphs that follow. Preliminary design loads are shown for a prototype and a production airplane at 635,000 and 675,000 lb, respectively. Methods of analysis are discussed in Par. 3.2. Sign conventions used to define all external loads are shown in Fig. 3-3.

Airplane 6-deg-of-freedom maneuver time histories have been calculated for critical and near critical transient maneuver conditions to evaluate airplane response characteristics. Typical

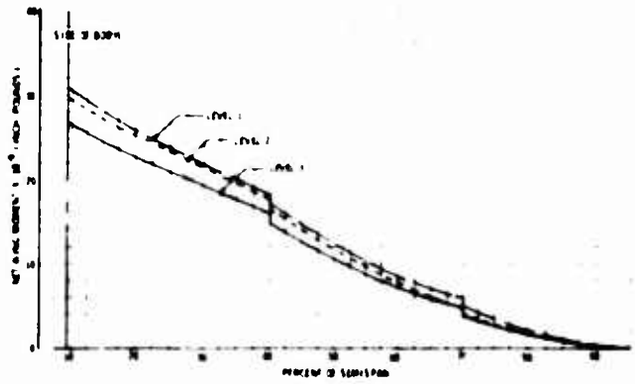

Figure 3-1. Wing Load History Model 367-80

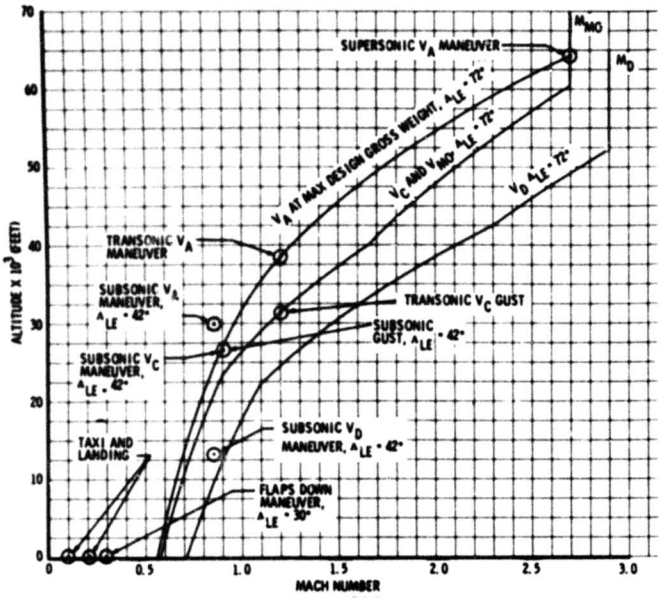

Figure 3-2. Structural Design Conditions

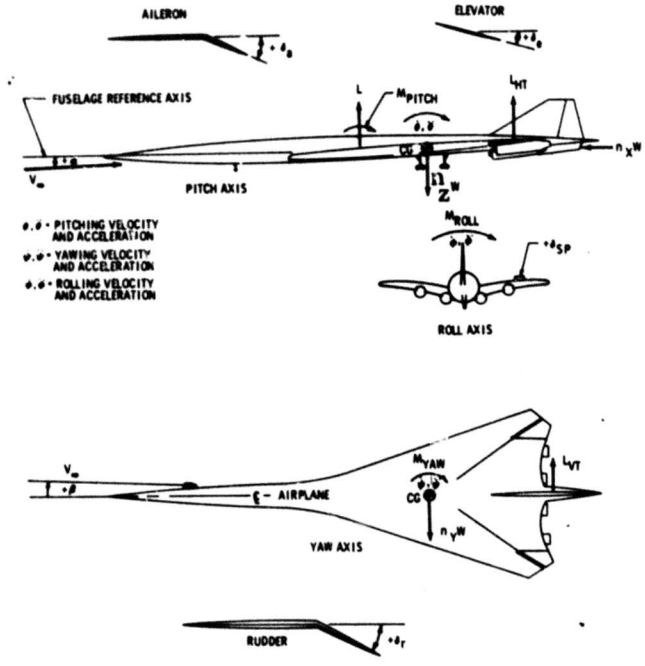

Figure 3-3. Loads Sign Convention

solutions for airplane pitch, yaw, and rolling pullout maneuvers are shown in Par. 3.2.2. Preliminary design maneuver loads shown in this document are all conservatively based on instantaneous surface deflections with no relief due to airplane response.

The airplane load distribution for all steady-state design conditions are based on the aerodynamic influence coefficient method described in Par. 3.2.1. Loads are computed using the flexible wing, body, tail, and their associated aerodynamic forces in a single simultaneous solution. This method is designated as a unified simultaneous solution.

3.1.1 Wing Loads

Critical load conditions for wing structural design are summarized in Table 3-A. The critical center-of-gravity limits are conservatively assumed for all wing conditions. Symmetric, balanced maneuver conditions at limit maneuver load factor are critical for wing design. Unsymmetric loading due to roll is maximum with the airplane in the high-lift configuration at maximum design gross weight. With the wing sweep placards established for the B-2707, the wing is not critical for dynamic gust conditions. Wing-span load distributions and centers of pressure for five design conditions are shown in Figs. 3-4 through 3-8.

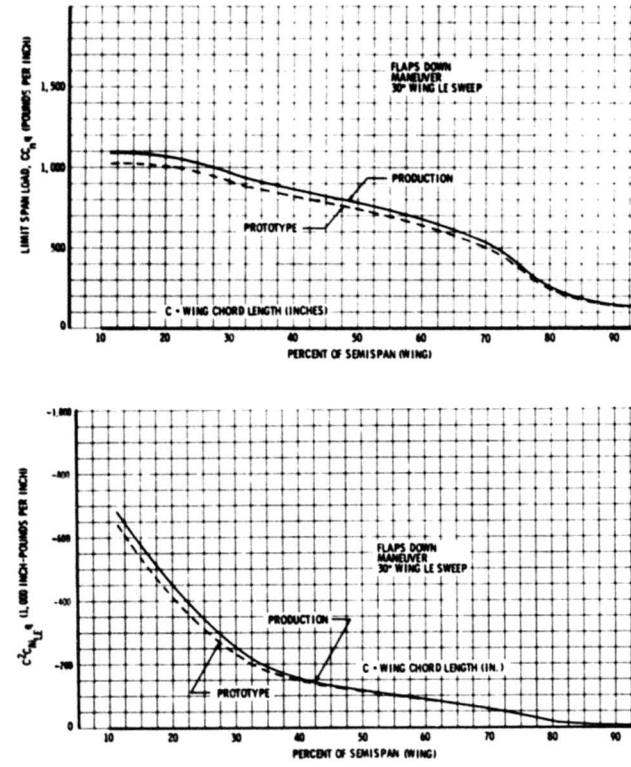

Figure 3-4. Wing Airload Distribution, Condition 9

Table 3-A. Wing Design Conditions

Condition No.	Condition Description	Wing LE Sweep (deg)	Mach No.	Altitude x 10^{-3} (ft)	V_e (kn)	Gross Weight x 10^{-3} (lb)	CG % C_{root}	Outbd Wing (% max fuel)	n_{CG} (Limit)
9	Flaps-down maneuver	30	0.295	0	195	668	59.0	96.5	2.0
32	Subsonic V_A maneuver	42	0.85	29.9	307	650	59.5	87.6	2.5
22	Transonic V_A maneuver	72	1.2	38.5	354	637	60.8	81.2	2.5
25	Supersonic V_A maneuver	72	2.7	64	433	605	60.4	65.3	2.5
402	Flaps-down steady roll	30	0.295	0	195	668	59.0	96.5	1.33
24	Supersonic negative maneuver	72	2.7	64	433	605	60.4	65.3	-1.0
204	Takeoff taxi	30	---	---	---	675	---	100	---
9*	Flaps-down maneuver	30	0.295	0	195	628	59.0	96.5	2.0
32*	Subsonic V_A maneuver	42	0.85	31.1	299	609	59.5	87.1	2.5
22*	Transonic V_A maneuver	72	1.2	39.8	344	597	60.8	81.2	2.5
25*	Supersonic V_A maneuver	72	2.7	65.3	420	570	60.4	67.8	2.5
402*	Flaps-down steady roll	30	0.295	0	195	628	59.0	96.5	1.33

*Prototype airplane

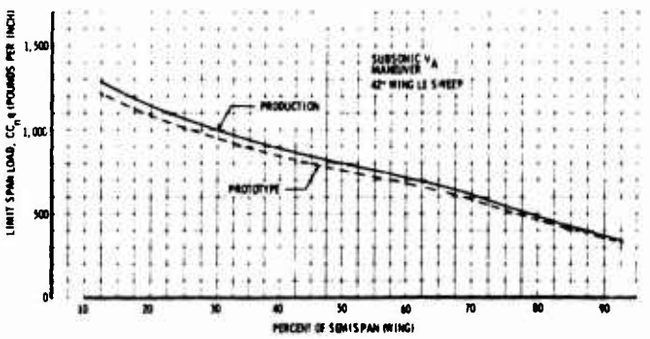

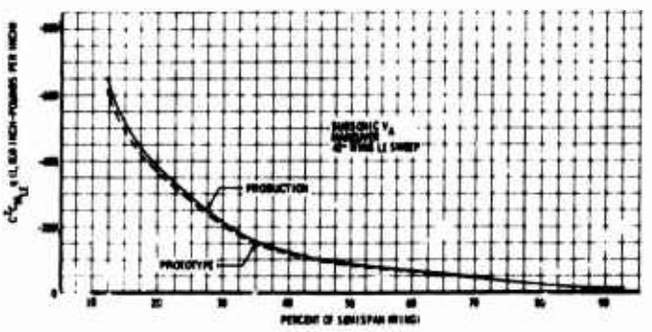

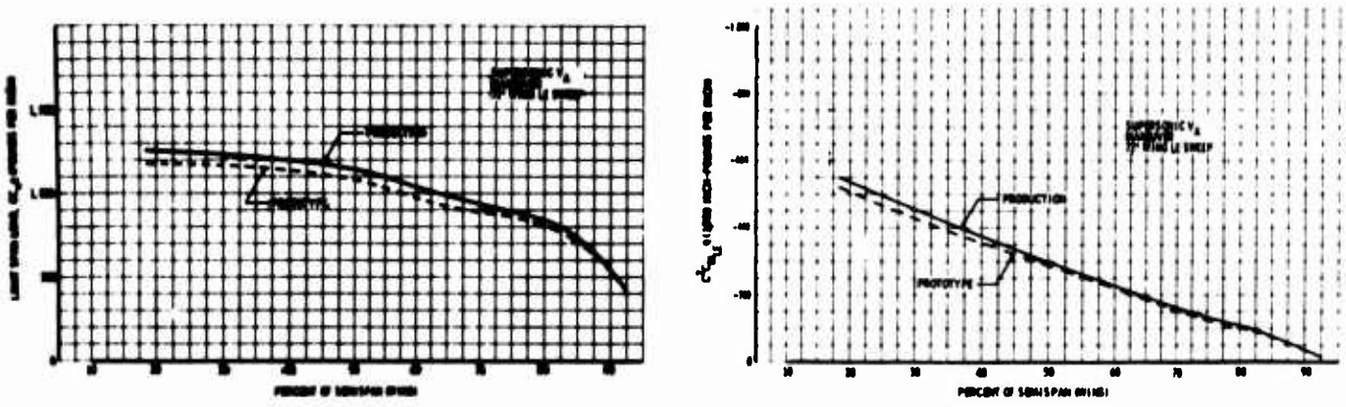

Figure 3-6. Wing Airload Distribution, Condition 25

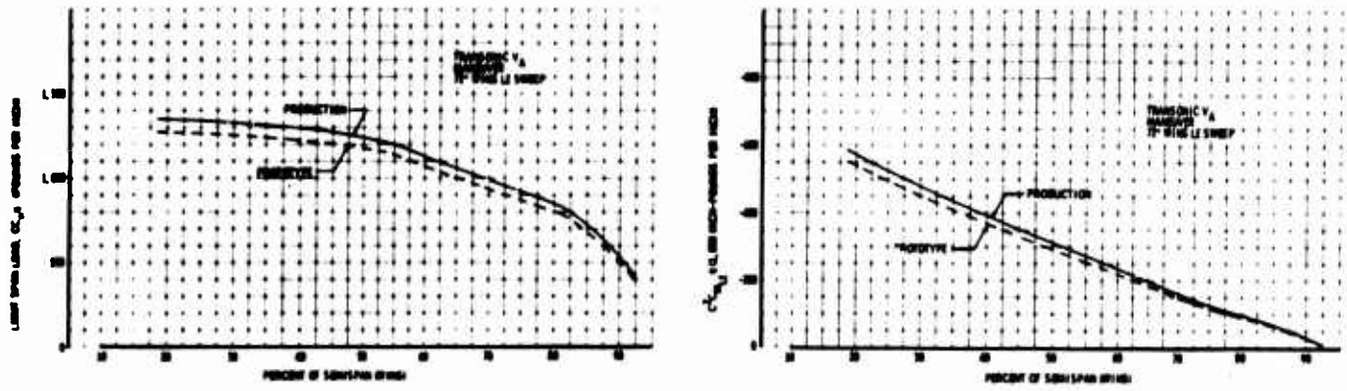

Figure 3-7. Wing Airload Distribution, Condition 22

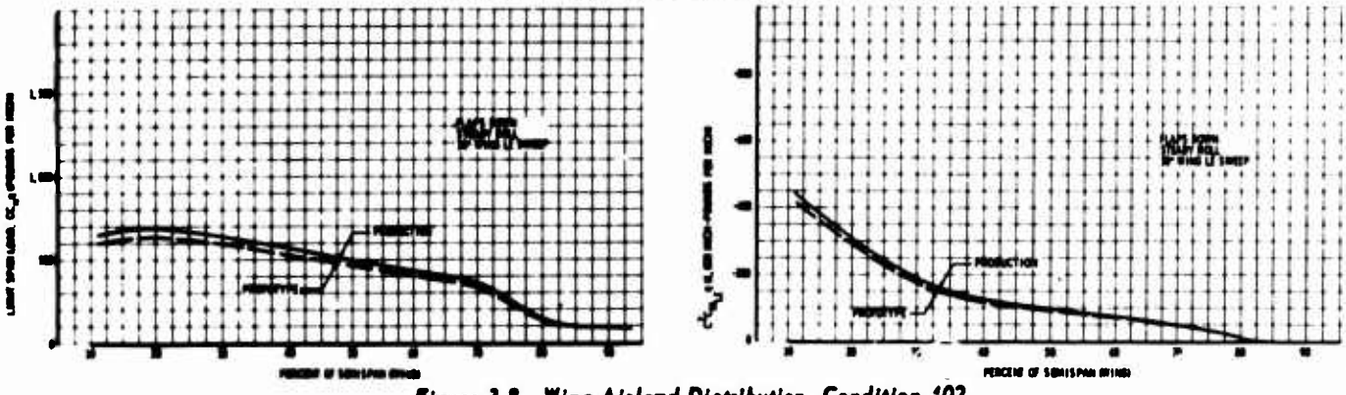

Figure 3-8. Wing Airload Distribution, Condition 402

Design net shear moments and torsions are shown in Airframe Design Report – Part B, V2-B2707-6-2, Par. 3.2, for the 675,000-lb production airplane and in Airframe Design Report – Part A, V2-B2707-6-1, Par. 8.1, for the 635,000-lb prototype airplane.

Wing pivot design holding and actuating loads for the B-2707 airplane are shown in Fig. 3-9. Wing sweep actuation requirements are limited to $n = 1.0 \pm 0.25$. The system stalls without failure if the applied actuator load exceeds the system actuation capability. Integrated pressure data obtained from Phase II wind tunnel tests are utilized in defining the flaps-up chord moments. The in-plane components of wing slats, flaps, and roll control surfaces, used to calculate flaps-down chord moments, have been estimated from wind-tunnel force tests of the B-2707 and from pressure tests of related configurations. The effects of inertia, when relieving, are conservatively ignored.

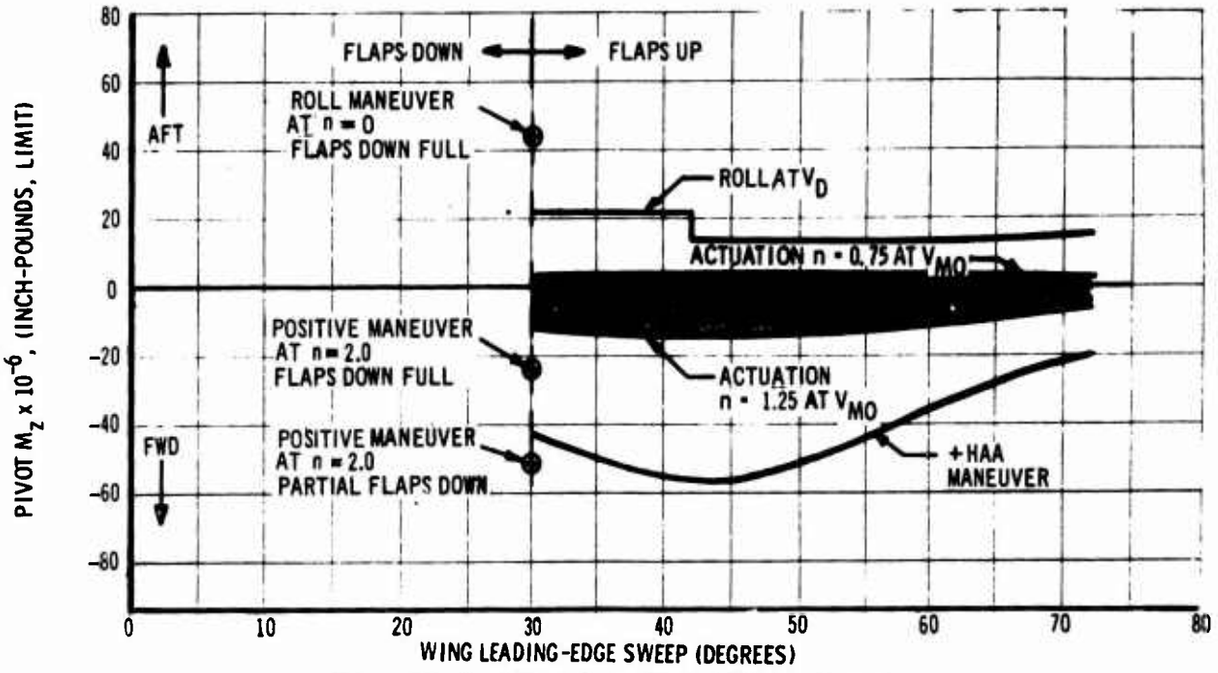

Figure 3-9. Wing Pivot Actuating and Holding Moment

3.1.2 High-Lift and Control-Surface Loads
The design high-lift and control-surface loads for the B-2707 are shown in Table 3-B. These loads have been calculated using information from tests of Boeing commercial transports and SST pressure models. Allowance has been included for a 25-fps head-on gust during flaps-down, level flight. The high-lift and control-surface speed placards are listed in Table 2-A. Movable surface loads on the empennage are shown in Airframe Design Report – Part B, V2-B2707-6-2, Par. 3.4.

Table 3-B. Design Loads, High Lift and Control Surfaces

Flight Condition				Surface Deflection (deg)			Limit Surface Loading			Positive Load Direction
Description	Λ_{LE} (deg)	Mach No.	Alt x10-3 (ft)				$C_N q$ (psf)		Center of Pressure, Fraction of Chord from LE	
Wing Flaps				Fore	Aft		Fore	Aft		
Positive maneuver, landing	30	0.30	0	30	50		570	360	0.40	Up
Positive maneuver, takeoff	30	0.34	0	20	40		600	380	0.40	Up
Positive maneuver, climbout	30	0.44	1.0	5	5		480	480	0.40	Up
Strake Flaps				Fore	Mid	Aft	Fore	Mid	Aft	
Positive maneuver, landing	30	0.30	0	26	40	60	420	260	140	0.40	Up
Positive maneuver, takeoff	30	0.34	0	26	40	60	530	330	170	0.40	Up

Table 3-B. (Concluded)

Flight Condition				Surface Deflection (deg)	Limit Surface Loading		Positive Load Direction
Description	Λ_{LE} (deg)	Mach No.	Alt x 10^{-3} (ft)		C_{Nq} (psf)	Center of Pressure, Fraction of Chord from LE	
Wing Slats							
Positive maneuver, subsonic cruise	42	0.67	1.0	0 holddown	770	0.30	Up
Positive maneuver, climb	42	0.50	1.5	6	950	0.30	Up
Positive maneuver, climbout	30	0.45	1.0	6	860	0.30	Up
Negative maneuver, climbout	30	0.45	1.0	6	-540	0.40	Up
Negative maneuver, climb	42	0.50	1.5	6	-880	0.40	Up
Strake Slats							
Positive maneuver, emergency descent	72	0.72	1.0	0 holddown	750	0.30	Up
Positive maneuver, climb	42	0.50	1.5	25	880	0.30	Up
Negative maneuver, climb	42	0.50	1.5	25	-880	0.40	Up
Negative maneuver, emergency descent	72	0.50	1.5	25	-1550	0.40	Up
Spoilers							
Negative manuever, roll	42	0.70	3.0	45	520	0.45	Down
Negative maneuver, roll	72	2.30	42.5	45	520	0.45	Down
Positive maneuver, emergency descent	72	0.72	1.0	0 holddown	-970 (outbd)	0.50	Down
Positive maneuver, emergency descent	72	0.72	1.0	0 holddown	-300 (inbd)	0.50	
Ailerons							
Positive maneuver, climbout	30	0.44	1.0	25	400	0.35	Up
Positive maneuver, emergency descent	72	0.72	1.0	0 holddown	900	0.50	Up

3.1.3 Fuselage Loads

The airloads on the fuselage and fixed-wing strake regions used to define fuselage net loads in Airframe Design Report - Part A, V2-B2707-6-1, Par. 8.5, and Airframe Design Report - Part B, V2-B2707-6-2, Par. 3.3, are obtained from a unified simultaneous solution. A summary of the design conditions for the fuselage is presented in Table 3-C. Airload distribution for critical flight maneuver conditions are shown in Figs. 3-10 and

Table 3-C. Fuselage Design Conditions

Condition No.	Condition Description	Wing LE Sweep (deg)	Mach No.	Altitude x 10^{-3} (ft)	V_e (kn)	Gross Weight x 10^{-3} (lb)	CG % C_{root}	n_{CG} (Limit)
9	Flaps-down maneuver	30	0.295	0	195	668	59.0	2.0
17a	Dynamic landing negative bending	30	0.212	0	140	430	59.0	---
17b	Dynamic landing positive bending							
25	Supersonic V_A maneuver	72	2.7	64	433	605	60.4	2.5
50	Supersonic V_A maneuver	72	2.7	64	433	605	62.9	2.5
28	V_C gust at forward CG	42	0.9	26.6	350	380	58.5	---
51	Subsonic V_A maneuver	42	0.9	33	303	648	59.5	2.5
52	Subsonic negative maneuver	42	0.9	33	303	648	59.5	-1.0
202	Nose gear yaw	30	---	---	---	675	---	---
203	Ground turn	30	---	---	---	675	---	---
204	Takeoff taxi	30	---	---	---	675	---	---
101	Lateral gust	72	1.21	31.5	423	380	58.5	---
9*	Flaps-down maneuver	30	0.295	0	195	628	59.0	2.0
50*	Supersonic V_A maneuver	72	2.7	65.3	420	570	62.8	2.5
51*	Subsonic V_A maneuver	42	0.9	34.3	294	608	59.5	2.5
202*	Nose gear yaw	30	---	---	---	635	---	---
203*	Ground turn	30	---	---	---	635	---	---
204*	Takeoff taxi	30	---	---	---	635	---	---

*Prototype airplane

3-11. Airloads on the fixed wing strake, which are reacted directly in the fuselage, are included. The aerodynamic loads acting on the fuselage during dynamic landing are shown in Fig. 3-12. The dynamic landing condition is described in Par. 3.2.4. The critical dynamic gust condition occurs at $M_C = 0.9$ for a minimum structural reserve-fuel, maximum payload condition with the wings in the intermediate, $\Lambda_{LE} = 42$ deg, position. Details of the analyses used for gust design are presented in Par. 3.2.3.

The movable-nose airloads listed in Table 3-D have been calculated using slender-fuselage theory plus crossflow. The design conditions for movable-nose up and locked and for the nose drooped 21 deg are presented.

3.1.4 Horizontal-Tail Loads

Conditions influencing the design of the B-2707 horizontal tail are shown in Table 3-E. Airload distributions for two flight conditions are shown in Figs. 3-13 and 3-14. Pitch initiation by abrupt control-surface deflection yields maximum flight loads for the horizontal tail. Time histories of these maneuvers, indicating the conservatism of the design loads, are presented in Par. 3.2.2. It is noted that the design of major portions of the horizontal tail are dictated by stiffness requirements for flutter prevention and for elevon and elevator aeroelastic effectiveness. The maximum net design loads for the horizontal tail on the 675,000-lb production airplane are shown in Airframe Design Report – Part B, V2-B2707-6-2, Par. 3.4.

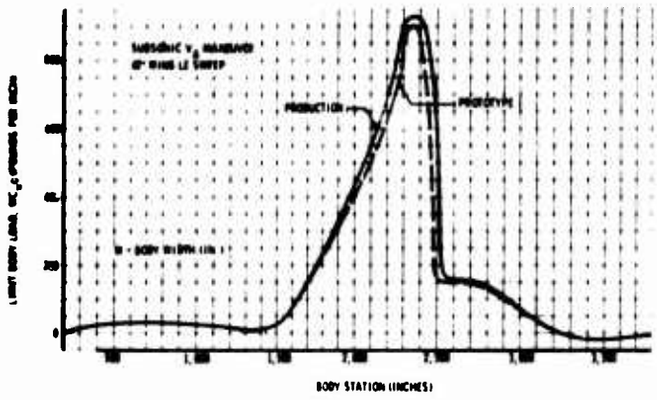

Figure 3-10. Fuselage Airload Distribution, Condition 9

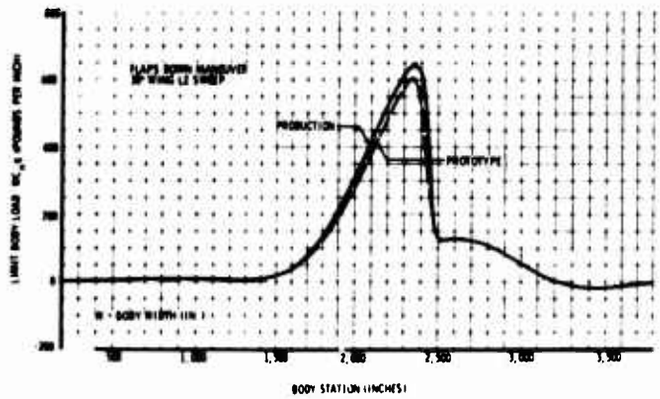

Figure 3-11. Fuselage Airload Distribution, Condition 51

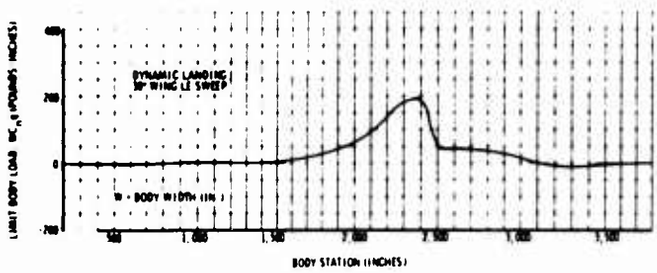

Figure 3-12. Fuselage Airload Distribution, Condition 17

Table 3-D. Movable-Nose Design Airloads

Nose Configuration	Wing LE Sweep (deg)	Flight Condition			Limit Airload	
		Mach No.	Limit Load Factor	Altitude (ft)	Shear at BS 611 (lb)	Center of Pressure BS
Nose up and locked	72	2.70	2.5	60,200	15,300	420
		2.90	2.5	52,000	12,400	420
		2.31	2.5	42,500	12,800	420
Nose droop of 21°	72	0.90	-1.0	23,500	-25,300	461
		0.71	0	0	-24,900	475

Table 3-E. Horizontal-Tail Design Conditions

Condition No.	Condition Description	Wing LE Sweep (deg)	Mach No.	Altitude x 10^{-3} (ft)	V_e (kn)	Gross Weight x 10^{-3} (lb)	CG % C_{root}	n_{CG} (Limit)
20	Flaps-down pitch initiation	30	0.34	0	225	668	59.0	1.0
180	Flaps-down pitch initiation	30	0.295	0	195	668	59.0	1.0
141	Transonic pitch initiation	72	1.2	38.5	354	637	60.8	1.0
140	Supersonic pitch initiation	72	2.7	64	433	605	60.4	1.0
341	Subsonic roll initiation	42	0.85	13.2	438	659	59.6	1.67
9	Flaps-down maneuver	30	0.295	0	195	668	59.0	2.0
17a	Dynamic landing	30	0.212	0	140	430	59.0	---
270	Maximum jacking load	30	---	---	---	410	---	---
180*	Flaps-down pitch initiation	30	0.295	0	195	628	59.1	1.0
141*	Transonic pitch initiation	72	1.2	39.8	344	597	60.8	1.0
270*	Maximum jacking load	30	---	---	---	400	---	---

*Prototype airplane

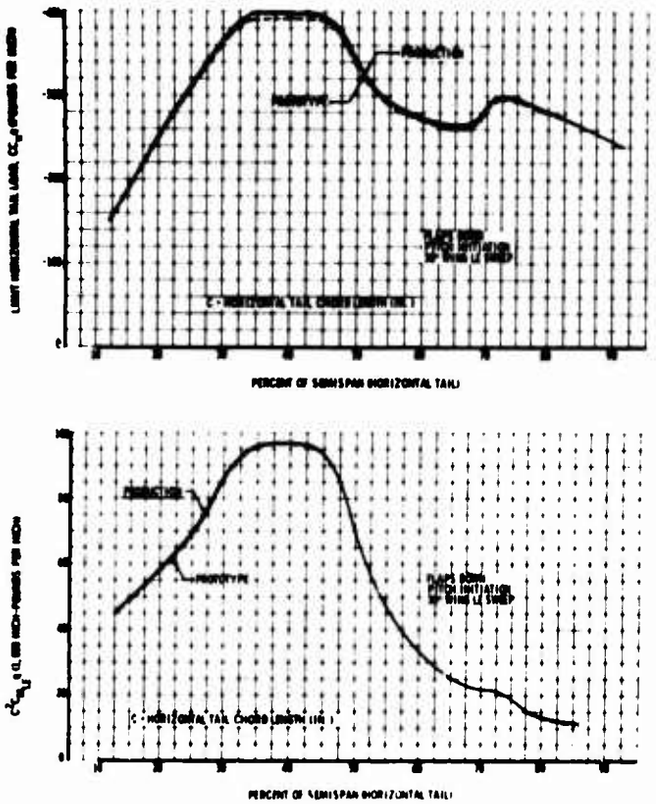

Figure 3-13. Horizontal-Tail Airload Distribution Condition 180

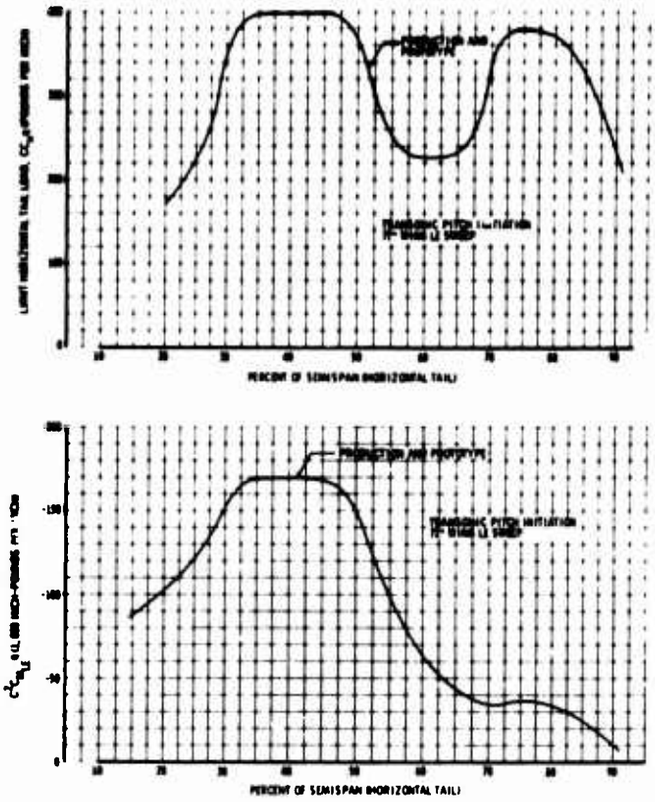

Figure 3-14. Horizontal-Tail Airload Distribution, Condition 141

3.1.5 Vertical-Tail Loads

Vertical-tail design loads are summarized in Table 3-F. Solutions for elastic vertical-tail loads are obtained by the aerodynamic influence coefficient method for the isolated surface as explained in Par. 3.2.1. Normal force and pitching moment distributions for the vertical-tail design conditions are shown in Figs. 3-15 through 3-17. These rudder-induced maneuver loads are based on an instantaneously deflected rudder. Dynamic overyaw to 1.7 times the steady side-slip angle is assumed for design load calculations. Rational rudder deflection rates have been used in the rudder maneuver time histories presented in Par. 3.2.2. These time histories show the airplane yaw response characteristics with and without stability augmentation.

The maximum lateral-gust load results from the formula of FAR, Par. 25.351, assuming a rigid vertical-tail lift curve slope and Kg = 1.0. Results of dynamic lateral-gust studies of the

Table 3-F. Vertical-Tail Design Conditions

Condition No.	Condition Description	Mach No.	Altitude $\times 10^{-3}$ (ft)	V_e (kn)	Limit Load Due to Rudder $\times 10^{-3}$ (lb)	Limit Load Due to Sideslip $\times 10^{-3}$ (lb)	Total Exposed Vertical Tail Load $\times 10^{-3}$ (lb)
101	Lateral gust	1.21	31.5	423	0	92	92
211	Subsonic rudder maneuver, yaw initiation	0.9	26.6	350	72	0	72
212	Subsonic rudder maneuver, dynamic overyaw	0.9	26.6	350	72	-181	-109
213	Subsonic rudder maneuver, checkback to $\delta_r = 0$ from steady sideslip	0.9	26.6	350	0	-106.4	-106.4
217	Transonic rudder maneuver, yaw initiation	1.2	31.2	421	41.3	0	41.3
226	Supersonic rudder maneuver, yaw initiation	2.7	60.2	475	23	0	23

NOTE: Vertical-tail design loads are the same for the production and prototype airplanes.

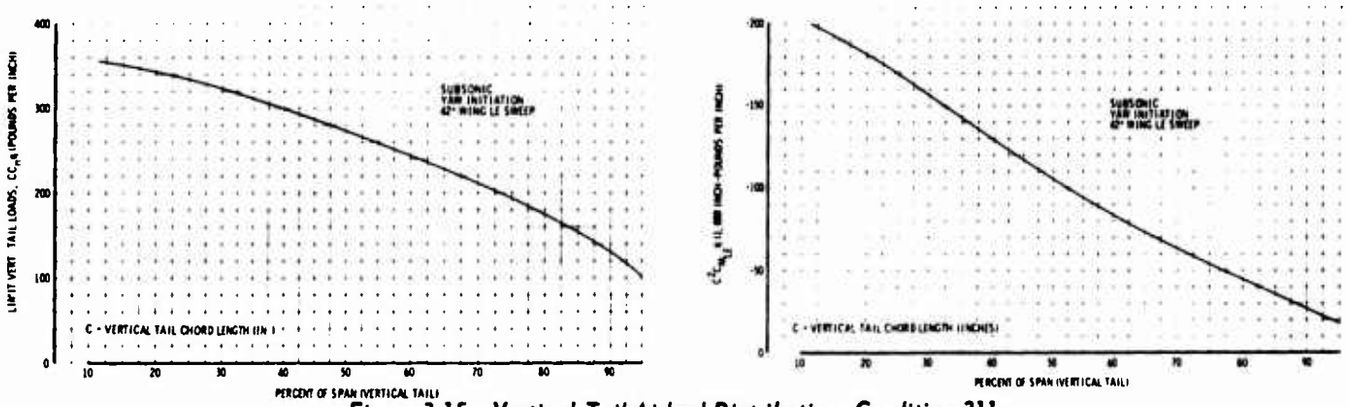

Figure 3-15. Vertical-Tail Airload Distribution, Condition 211

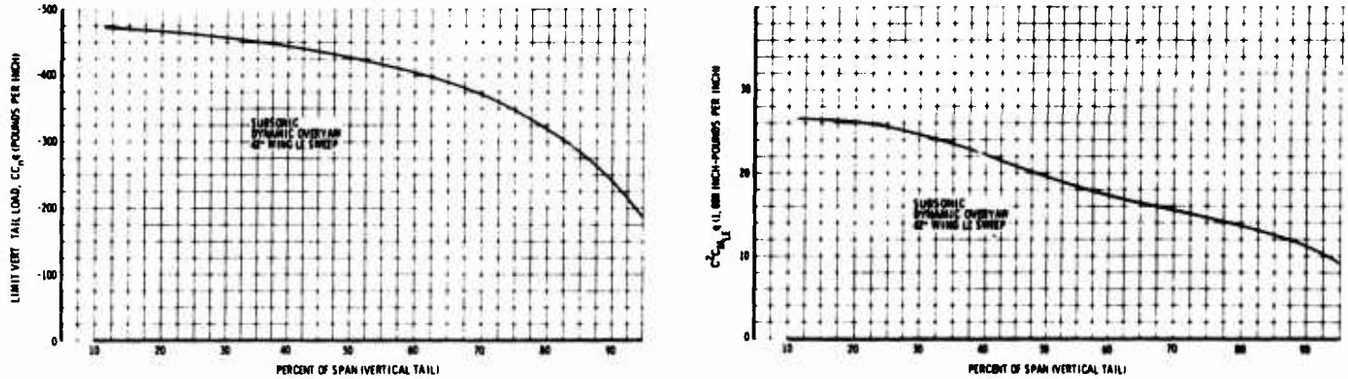

Figure 3-16. Vertical-Tail Airload Distribution, Condition 212

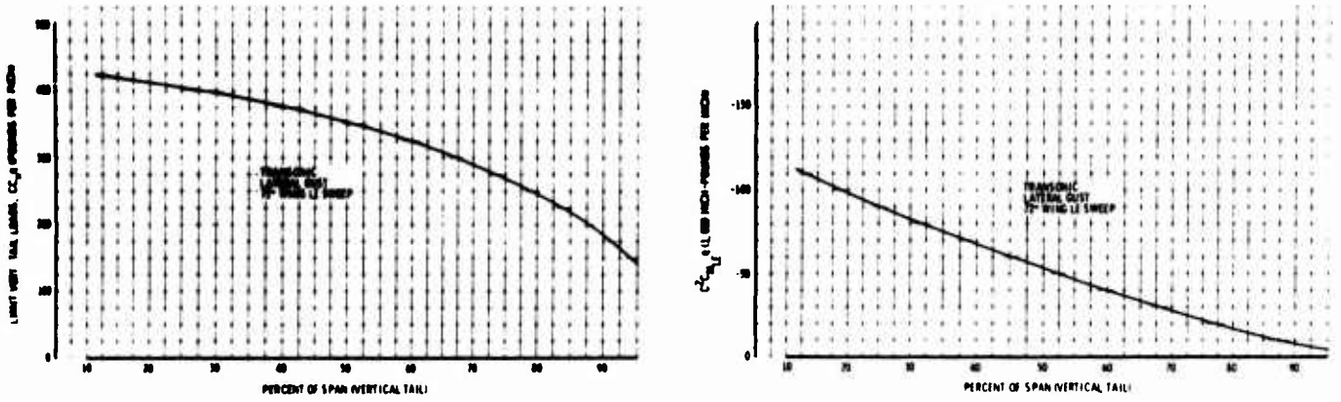

Figure 3-17. Vertical-Tail Airload Distribution, Condition 101

B-2707 are presented in Par. 3.2.3. Design loads for the vertical tail are shown in Airframe Design Report – Part B, V2-B2707-6-2, Par. 3.7.

3.1.6 Propulsion-Pod Design Loads
The propulsion-pod design conditions for both inboard and outboard nacelles as outlined in Table 3-G satisfy the criteria of Par. 2.4.15. A separate set of conditions are defined for inlet design in Table 3-H. The aerodynamic loading shown in Fig. 3-18 for the outboard pod is applied to all four engines. Maximum pressures during inlet unstart, which have been considered for local design of the propulsion pod, wing, and horizontal tail, are shown in Fig. 3-19.

External design loads for the propulsion pod are shown in Airframe Design Report - Part B, V2-B2707-6-2, Par. 3.7.

3.1.7 Design Ultimate Ground Loads
The ultimate ground loads are calculated in accordance with the criteria of Sec. 2.2 and are used for landing-gear stress analysis in Sec. 3.6. Loads for the 675,000- and 635,000-lb takeoff weights are listed in Tables 3-I and 3-J.

3.2 LOAD ANALYSIS
Methods of analysis used to calculate B-2707 design loads and those proposed for final Phase III design are described for the steady-static elastic flight conditions as well as dynamic ground and flight conditions. In general, the approach relies heavily on proven techniques except for modifications dictated by configuration details and the operating regime of the B-2707 airplane.

3.2.1 Steady-State Aeroelastic Analysis
The fuselage, wing, and horizontal-tail airload distribution for all steady-state flight conditions is analyzed by a panel aerodynamic influence solution. The elastic properties of the entire airplane, including the fuselage, are represented by

Table 3-G. Propulsion-Pod Design Conditions

Condition No.	Condition (ultimate)	
1	Landing	6.0V
2	Landing	-4.0V
3	Supersonic maneuver	6.0V + 1.5 Tm
4	Supersonic maneuver	-4.0V + 1.5 Tm
5	Fatigue	3.0V + 3.0 Tm
6	Fatigue	3.0 Tm
7	Maneuver	2.5S
8	Maneuver	-2.5S
9	Gyroscopic	1.5V + 1.5 Tm + My
10	Gyroscopic	1.5V + 1.5 Tm - My
11	Gyroscopic	3.75V + 1.5 Tm + Mp
12	Gyroscopic	3.75V + 1.5 Tm - Mp
13	Supersonic maneuver	1.5 Tm + Aero (S)
14	Supersonic maneuver	1.5 Tm - Aero (S)
15	Transonic maneuver	1.5 Tm + Aero (T)
16	Transonic maneuver	1.5 Tm - Aero (T)
17	Wheels-up landing	9.0D
18	Ditching	-6.0D
19	Reverse thrust	3.0V + 3.0 Tr
20	Engine seizure	Mr

V = weight of propulsion pod acting vertically
D = weight of propulsion pod acting forward
S = weight of propulsion pod acting laterally
Tm = maximum engine thrust
Tr = maximum engine reverse thrust
Aero (S) = total aerodynamic load acting on propulsion pod (supersonic)
Aero (T) = total aerodynamic load acting on propulsion pod (transonic)
My = gyroscopic yawing moment
Mp = gyroscopic pitching moment
Mr = engine rolling moment induced by stoppage of critical rotating mass in 0.3 sec

Table 3-H. Engine-Inlet Design Conditions

Condition No.	Condition (ultimate)	
1	Landing	6.0V
2	Landing	-4.0V
3	Supersonic maneuver	6.0V + 1.5 T_D
4	Supersonic maneuver	-4.0V + 1.5 T_D
5	Supersonic maneuver	3.75V + 2.5 T_{s-u}
6	Supersonic maneuver	3.75V + 2.0 T_{u-u}
7	Maneuver	2.5S
8	Maneuver	-2.5S
9	Emergency landing	9.0D
10	Ditching	-6.0D
11	Supersonic maneuver	1.5 T_D + Σ Aero (S)
12	Supersonic maneuver	1.5 T_D - Σ Aero (S)
13	Transonic maneuver	1.5 T_t + Σ Aero (T)
14	Transonic maneuver	1.5 T_t - Σ Aero (T)

V = Weight of inlet acting vertically downward
D = Weight of inlet acting forward
S = Weight of inlet acting laterally
Aero (S) = total aerodynamic load acting on inlet (supersonic)
Aero (T) = total aerodynamic load acting on inlet (transonic)
T_D = Inlet internal-pressure net thrust load at M 2.90
T_{s-u} = Inlet internal-pressure net thrust load at M 2.70 (normal operation) or at M 2.35 (normal operation); whichever is greater
T_{u-u} = Inlet internal pressure net thrust load at M 2.70 or M 2.35 (unstarted, centerbody expanded), whichever is greater
T_t = Inlet internal-pressure net thrust load at M 1.40

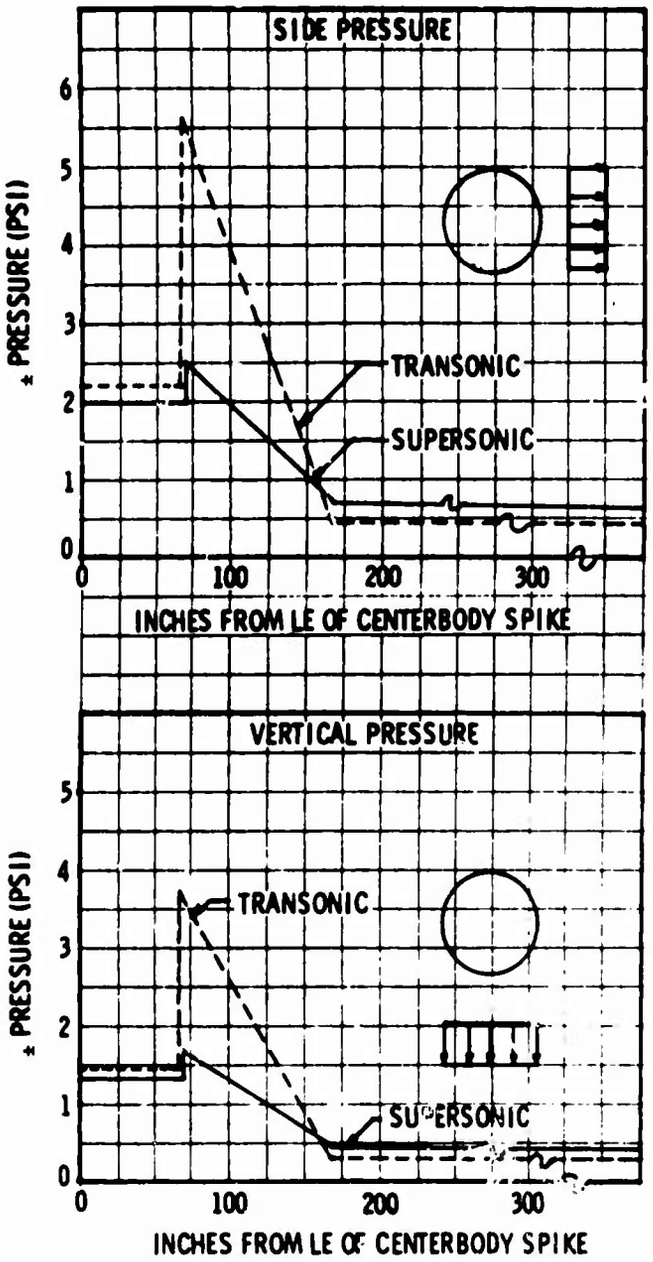

Figure 3-18. Design Aerodynamic Pressures, Propulsion Pod

a structural flexibility matrix defining angle-of-attack changes at each analysis panel due to applied loads in the system. The analysis grids for the airplane in the subsonic and supersonic cruise configurations are shown in Fig. 3-20.

The vertical-tail analysis grid is shown in Fig. 3-21. Effects of fuselage flexibility in the vertical tail solution are included as a boundary condition.

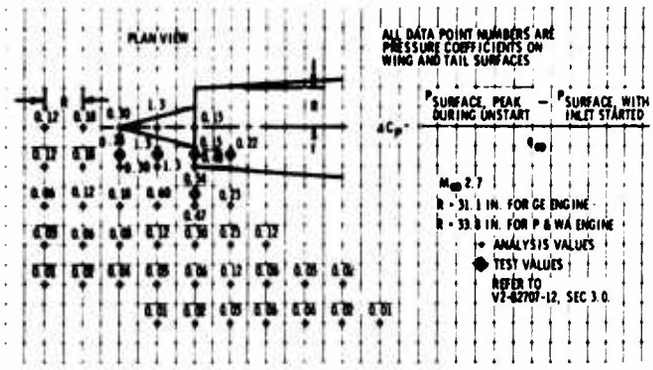

Figure 3-19. Inlet Unstart Pressure Coefficients

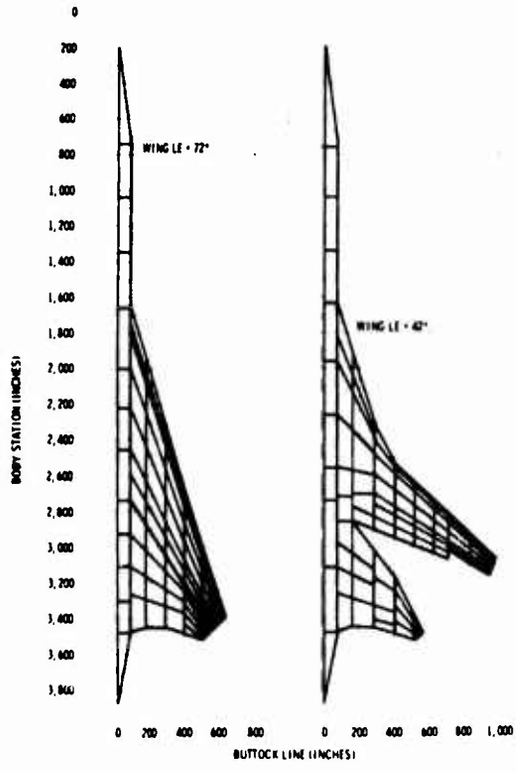

Figure 3-20. Panel Layout, Wing and Horizontal Tail

The aerodynamic matrix used in the solution is based on the method of Ref. 3-1, which obtains a solution to the linearized potential flow equation for subsonic, sonic, and supersonic flow by numerical means. This influence matrix has been used in the development of a static, aeroelastic, airload distribution solution.

Table 3-I. Production-Airplane Design Ground Loads

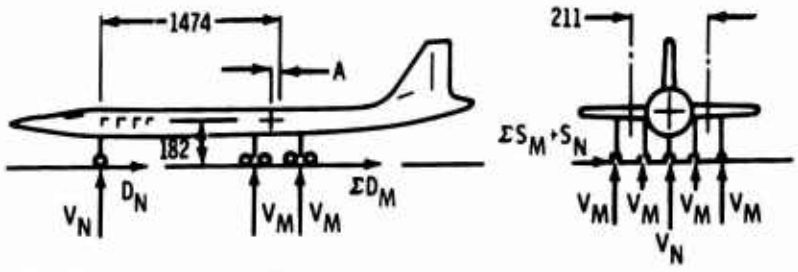

Limit Static Vertical Loads Per Gear						
Gross Weight (lb)	Forward CG			Aft CG		
	A (in.)	V_{Main}	V_{Nose}	A (in.)	V_{Main}	V_{Nose}
675,000	105	157	48	47	163	22
430,000	124	98	37	47	104	14

Design Ultimate Ground Loads												
	Condition	Nose Gear			Aft Main Gear				Forward Main Gear			
		V	D	S	V	D	S	TQ	V	D	S	TQ
Ground Handling	2-point braked roll	---	---	---	253	176	0	0	293	176	0	0
	3-point braked roll	157	0	0	222	176	0	0	222	176	0	0
	With flat tire	116	0	0	233	88	0	0	233	88	0	0
	Yaw, unsymmetrical braking	117	0	26	233	176	0	0	233	176	0	0
	With flat tire	95	0	14	238	88	0	0	238	88	0	0
	Yaw, static	72	0	58	---	---	---	---	---	---	---	---
	With flat tire	72	0	29	---	---	---	---	---	---	---	---
	Ground turn	72	0	36	475	0	238	2,620	479	0	238	2,620
	With 1 flat tire	72	0	18	359	0	90	2,080	359	0	90	2,080
	With 2 flat tires	-	-	-	336	0	67	1,340	336	0	67	1,340
	Takeoff taxi	144	0	0	486	0	0	0	486	0	0	0
	Pivoting	-	-	-	244	0	0	±6,580	244	0	0	±6,580
	Forward towing	72	-152	0	244	-114	0	0	244	-114	0	0
	Aft towing	72	152	0	244	114	0	0	244	114	0	0
	Side towing	72	0	54	244	0	±114	0	244	0	±114	0
	Reverse braking	-	-	-	244	-134	0	0	244	-134	0	0

Table 3-I. (Concluded)

Design Ultimate Ground Loads												
	Condition	Nose Gear			Aft Main Gear				Forward Main Gear			
		V	D	S	V	D	S	TQ	V	D	S	TQ
Landing Impact	2-point level with spin-up	-	-	-	255	182	0	0	-	-	-	-
	2-point level with spring-back	-	-	-	255	-126	0	0	-	-	-	-
	Tail down with spin-up	-	-	-	276	122	0	0	-	-	-	-
	Tail down with spring-back	-	-	-	251	-170	0	0	-	-	-	-
	Right drift	-	-	-	128	-63	102	0	-	-	-	-
	Left drift	-	-	-	128	-63	-77	0	-	-	-	-
	Boeing condition											
	With spin-up	151	106	0	-	-	-		-	-	-	-
	With spring-back	151	-75	0	-	-	-	-	-	-	-	-
	Max strut reaction	140	35	0	-	-	-	-	-	-	-	-

V = vertical load per gear in kips (positive up)
D = drag load per gear in kips (positive aft)
S = side load per gear in kips (positive inboard)
TQ = moment about main-gear vertical centerline in inch-kips (positive counterclockwise in plan view)
All nose-gear side loads are reversible.
All dimensions are in inches.

Table 3-J. Prototype-Airplane Design Ground Loads

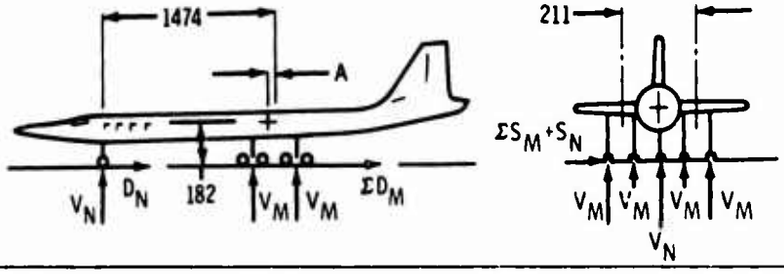

Limit Static Vertical Loads Per Gear						
Airplane Gross Weight (lb)	Forward CG			Aft CG		
	A (in.)	V_{main}	V_{nose}	A (in.)	V_{main}	V_{nose}
635,000	105	148	46	47	153	21
425,000	124	97	36	47	98	13

Table 3-J. (Concluded)

Design Ultimate Ground Loads												
		Nose Gear			Aft Main Gear				Forward Main Gear			
	Condition	V	D	S	V	D	S	TQ	V	D	S	TQ
Ground Handling	2-point braked roll	---	---	---	239	176	0	0	239	176	0	0
	3-point braked roll	148	0	0	209	167	0	0	209	167	0	0
	With flat tire	110	0	0	219	88	0	0	219	88	0	0
	Yaw unsymmetrical braking	110	0	24	219	176	0	0	219	176	0	0
	With flat tire	90	0	13	224	88	0	0	224	88	0	0
	Yaw, static	68	0	55	---	---	---	---	---	---	---	---
	With flat tire	68	0	28	---	---	---	---	---	---	---	---
	Ground turn	68	0	34	435	0	218	2,465	435	0	218	2,465
	With 1 flat tire	68	0	17	332	0	83	1,960	332	0	83	1,960
	With 2 flat tires	---	---	---	312	0	63	1,260	312	0	63	1,260
	Takeoff taxi	136	0	0	459	0	0	0	459	0	0	0
	Pivoting	---	---	---	230	0	0	±6,190	230	0	0	±6,190
	Forward towing	68	-143	0	230	-108	0	0	230	-108	0	0
	Aft towing	68	143	0	230	108	0	0	230	108	0	0
	Side towing	68	0	51	230	0	±108	0	230	0	±108	0
	Reverse braking	---	---	---	230	-127	0	0	230	-127	0	0
Landing Impact	2-point level with spin-up	---	---	---	255	182	0	0	---	---	---	---
	2-point level with spring-back	---	---	---	255	-126	0	0	---	---	---	---
	Tail down with spin-up	---	---	---	276	122	0	0	---	---	---	---
	Tail down with spring-back	---	---	---	251	-170	0	0	---	---	---	---
	Right drift	---	---	---	128	-63	102	0	---	---	---	---
	Left drift	---	---	---	128	-63	77	0	---	---	---	---
	Boeing condition											
	With spin-up	151	106	0	---	---	---	---	---	---	---	---
	With spring-back	151	-75	0	---	---	---	---	---	---	---	---
	Max strut reaction	140	35	0	---	---	---	---	---	---	---	---

V = vertical load per gear in kips (positive up)
D = drag load per gear in kips (positive aft)
S = side load per gear in kips (positive inboard)
TQ = moment about main-gear vertical centerline in inch-kips (positive counterclockwise in plan view)
All nose-gear side loads are reversible.
All dimensions are in inches.

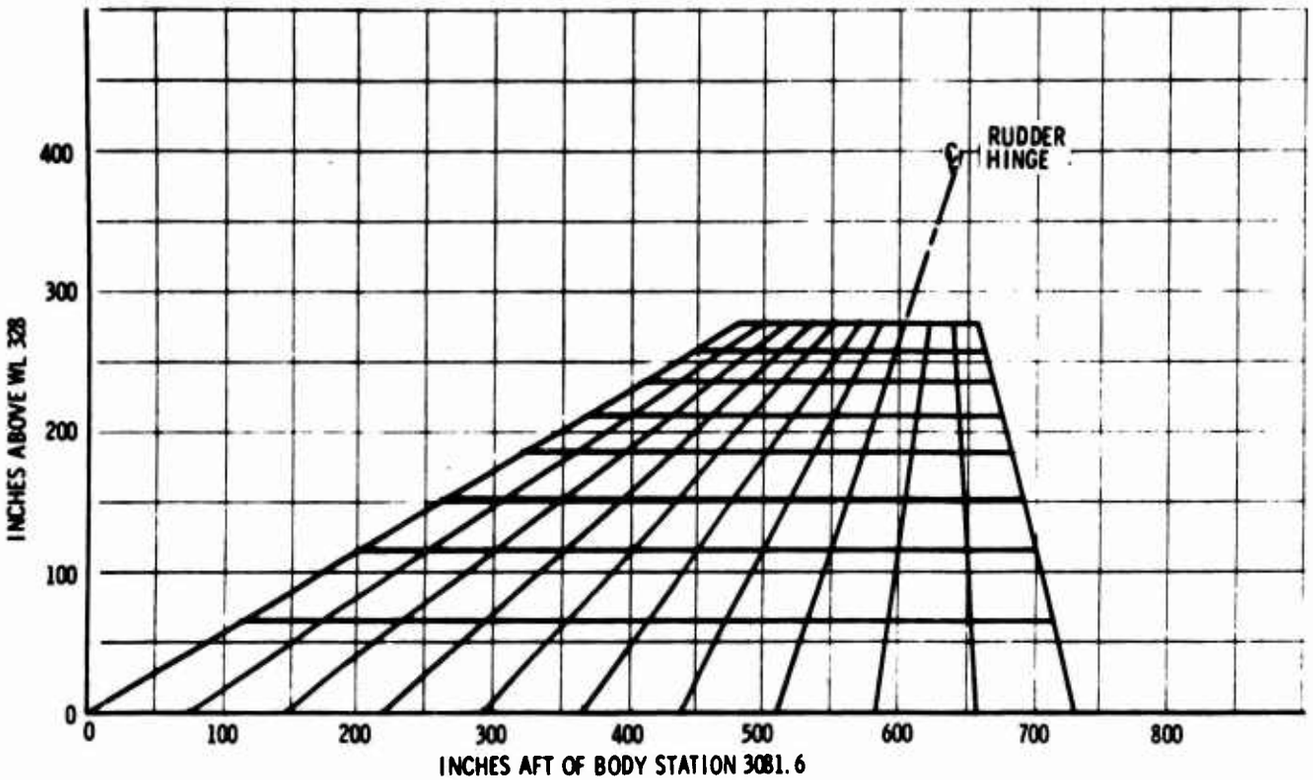

Figure 3-21. Panel Layout, Vertical Tail

The basic distribution equation of the airload solution is, in matrix form:

$$\{\Delta P_{AP}\} = (q_\infty)(S_w)[A]\left[k^{o}_{EXP}\right]\{\alpha\}$$

where:

$\{\Delta P_{AP}\}$ = net panel airload (lb)

$[A]$ = aerodynamic influence matrix (1/radian)

$\left[k^{o}_{EXP}\right]$ = experimentally derived corrective slope factor (nondimensional)

$\{\alpha_{EXP}\}$ = experimentally derived corrective angle of attack (radians)

$\{\alpha\}$ = net panel angle of attack (radians)
$= (\alpha_R)\{1\} + \{\alpha_s\} + \{\alpha_g\} + \{\alpha_{EXP}\}$

$\{\alpha_s\}$ = panel angle of attack change due to external loads (radians)
$= [S]\{\Delta P_{AP}\} + (P_E)\{\alpha_{sE}/P_E\}$

$\{\alpha_g\}$ = collection of angle of attack increments due to built-in twist, engine thrust, pitch velocity, and inertia loads (radians)

P_E = pitch balance load

$[S]$ = structural influence matrix (radians/lb)

$\{\alpha_{sE}/P_E\}$ = structural influence matrix, radians/unit pitch balance load (lb)

q_∞ = free-stream dynamic pressure (psf)

S_w = wing area (sq ft per side)

α_R = airplane reference angle of attack (radians)

Two additional equations are included to supply equilibrium of normal force (controlled by load factor) and of pitching moment (controlled by elevon-elevator load). Pitching velocity, pitching acceleration, and engine thrust are incorporated into the detail equations. The entire set of equations is then solved simultaneously for net panel airload, reference angle of attack, and pitch

balance load. Allowance is made to correct the theory for the panel normal-force curve slopes and intercepts using wind-tunnel-model pressure data. The corrective factors, k_{EXP} and α_{EXP}, are calculated by a reversed solution that utilizes measured test data.

The steady-state loads presented in this document are based on the theoretical aerodynamic matrix with modifications made only in the lift and moment balance equations to match data obtained from B-2707 wind-tunnel force tests. The comparative wing-load distributions shown in Par. 3.3.3.2 give a measure of the results obtained from this procedure.

3.2.2 Maneuver Time Histories

Preliminary design loads for symmetric and unsymmetric transient maneuver conditions presented in Par. 3.1 are based on instantaneous control surface deflections. In order to study airplane response characteristics, time histories of critical design flight conditions have been calculated. The analysis consists of expanding a numerical solution to the 6-deg-of-freedom stability equations to compute time histories of selected loads using the methods described in Ref. 3-2. In order to compute the specified maneuver in terms of load factor, internal loops are provided that iterate the control movements until the required load factor is obtained. Aeroelastic derivatives, compatible with the airplane flight condition are used as inputs. The conditions investigated are consistent with the maneuvering criteria presented in Par. 2.1.5.

Symmetric pitch maneuver with the airplane in the high-lift configuration is shown in Fig. 3-22. Pitch, yaw, and rolling pullout maneuver with the airplane in the subsonic cruise configuration and the supersonic wings-aft configuration are illustrated in Figs. 3-23 through 3-28. Design empennage loads are identified on these plots.

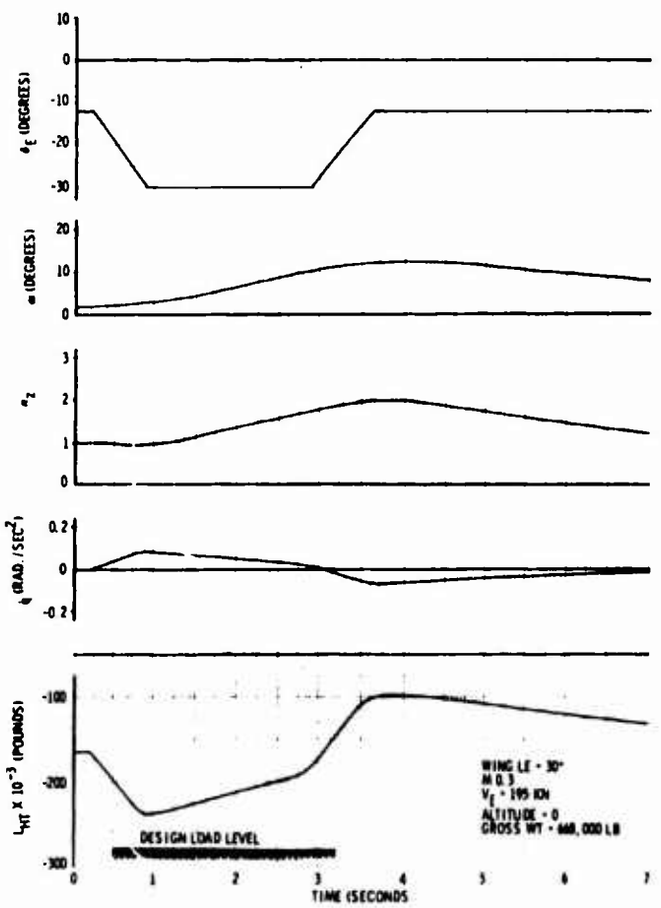

Figure 3-22. Flaps Down Pitch Maneuver

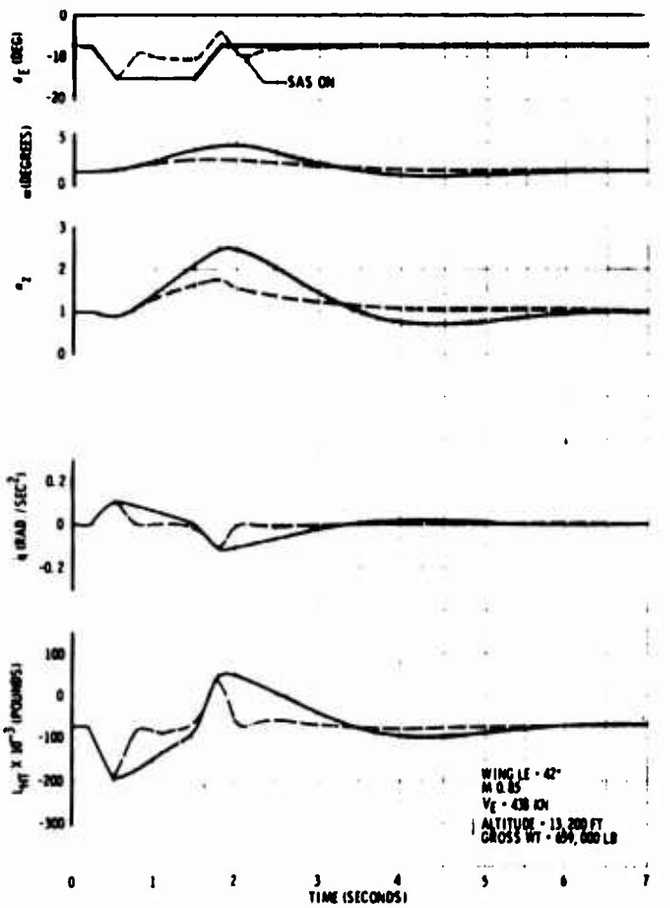

Figure 3-23. Subsonic Pitch Maneuver

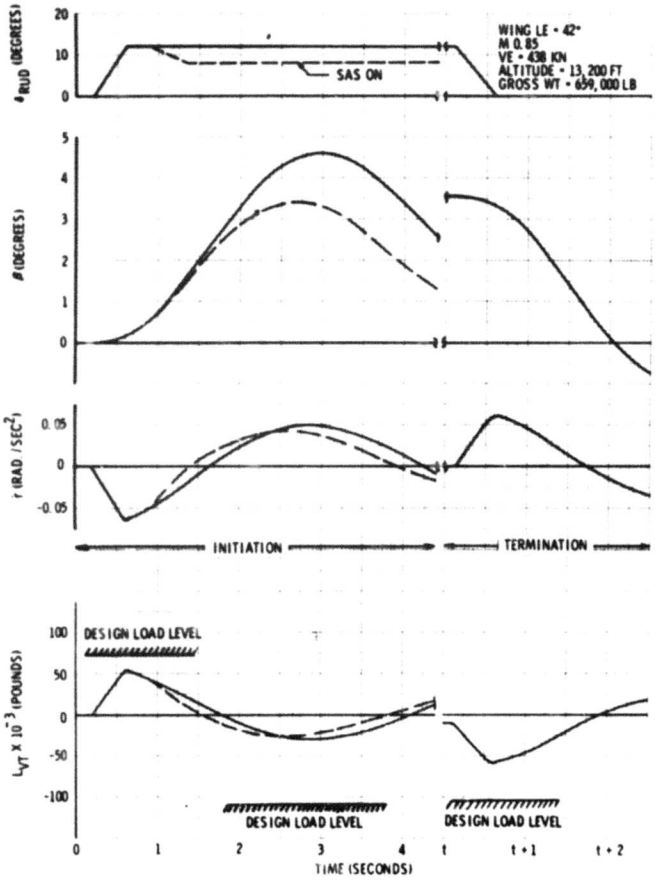

Figure 3-24. Subsonic Yaw Maneuver

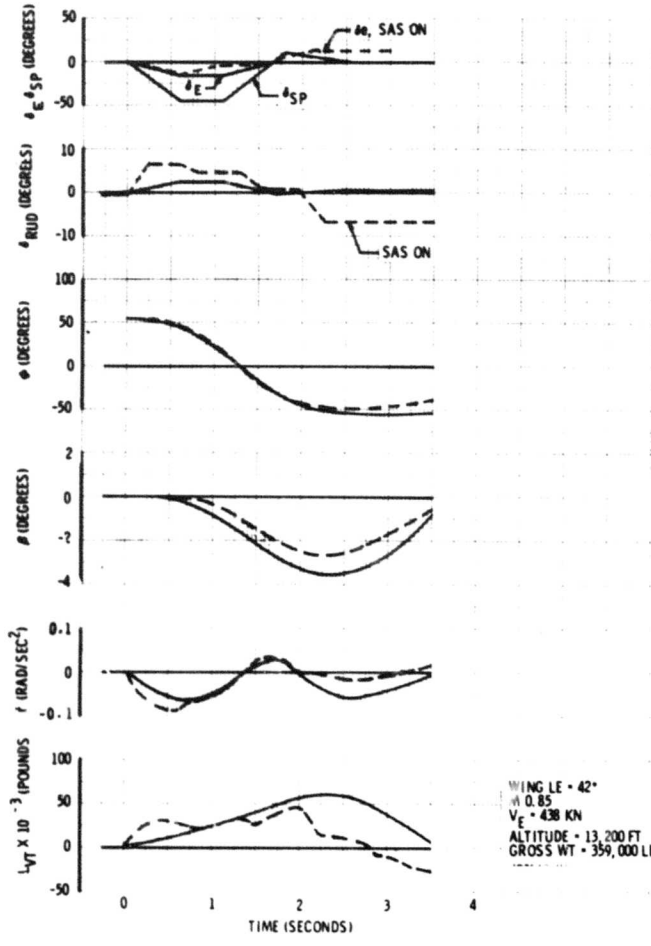

Figure 3-25. Subsonic Rolling-Pullout Maneuver

Supersonic upset and overspeed maneuvers have been investigated to determine maximum, transient, aerodynamic heating cycles to be combined with maneuver loads at cruise Mach number. The upset time history shown in Fig. 3-29 represents a design condition of upset to dive Mach number with power-on followed by power-off recovery at n = 1.5, then climb to initial conditions. Airframe aerodynamic heating during this condition is discussed in Sec. 4.0.

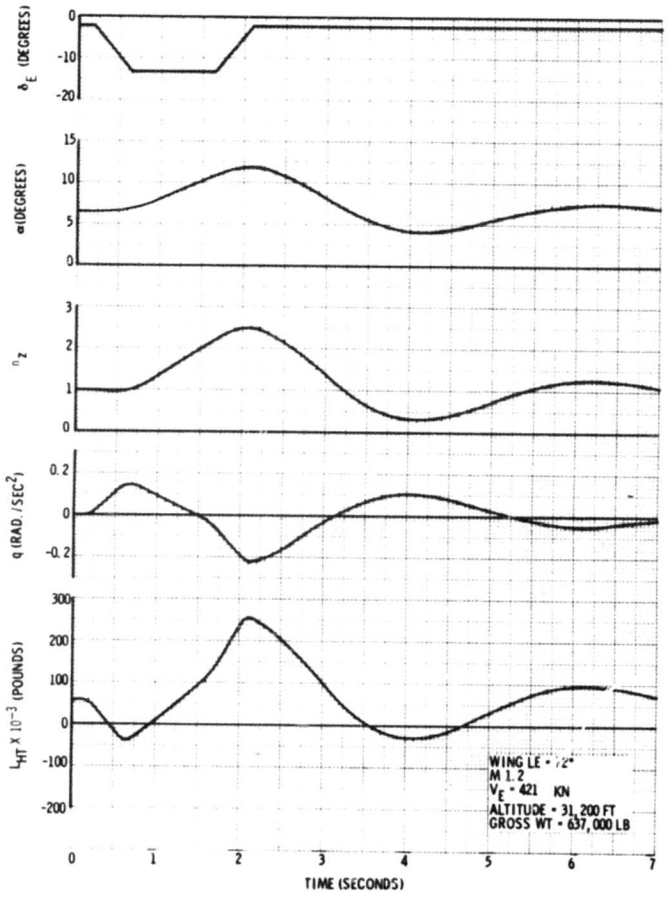

Figure 3-26. Transonic Pitch Maneuver

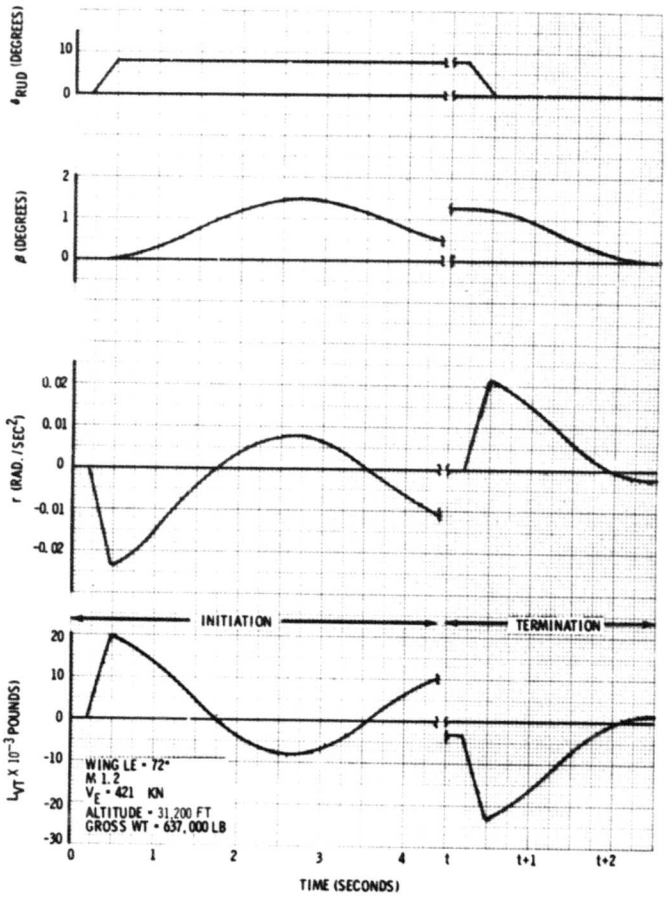

Figure 3-27. Transonic Yaw Maneuver

3.2.3 Dynamic Gust

The gust load results and approaches presented herein are consistent with the design criteria specified in Par. 2.1.6. Considerable emphasis is placed on the analytical approaches used since the rational dynamic gust analysis employed involves newly developing technologies. The established methods of discrete gust analysis are retained to complement the statistical power spectral density (PSD) approaches.

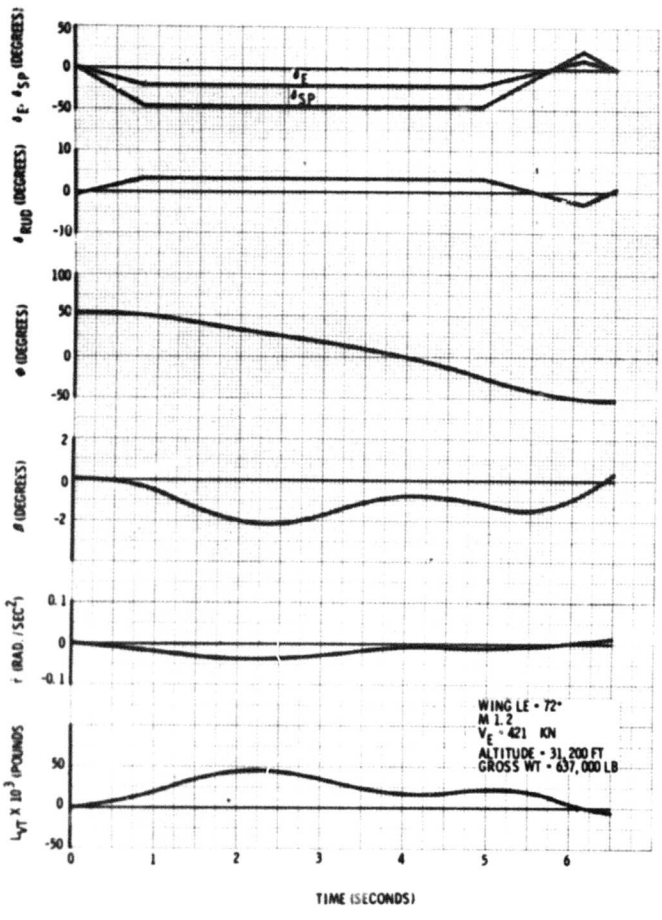

Figure 3-28. Transonic Rolling-Pullout Maneuver

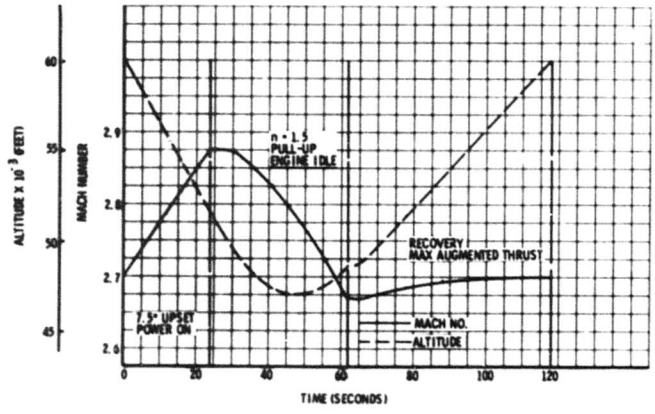

Figure 3-29. Upset Maneuver

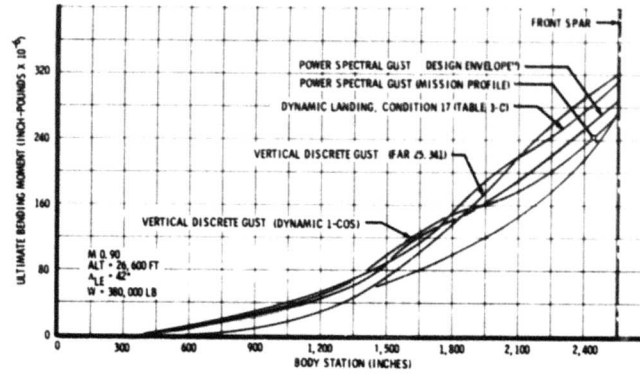

Figure 3-30. Forward-Fuselage Bending Moment Distribution

3.2.3.1 Results of Analysis

The results of the vertical, dynamic gust analyses are summarized in Figs. 3-30 through 3-34. These curves compare four separate sets of ultimate, dynamic gust loads on the forward fuselage, wing, and horizontal tail with the maximum values from other loading conditions. The comparison indicates that only a portion of the forward fuselage is vertical-gust critical. Results from lateral, dynamic gust analyses are given in Figs. 3-35 and 3-36 for the fin. The lateral gust loads are less than those obtained by other load conditions.

Additional effort during Phase III will continually refine all of the dynamic gust analyses to include

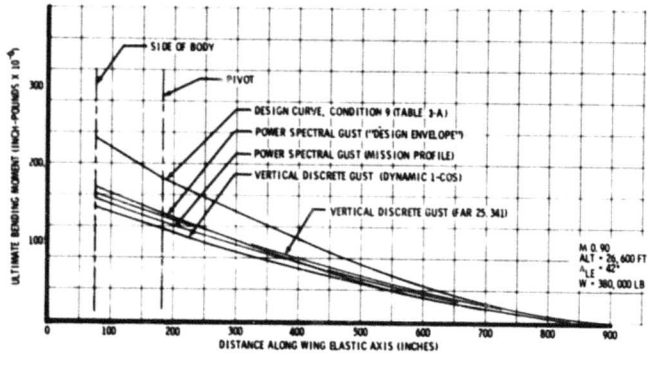

Figure 3-31. Wing Bending Moment Distribution

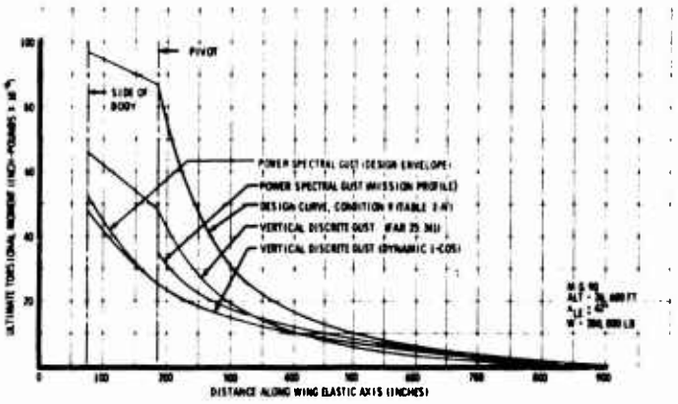

Figure 3-32. Wing Torsional Moment Distribution

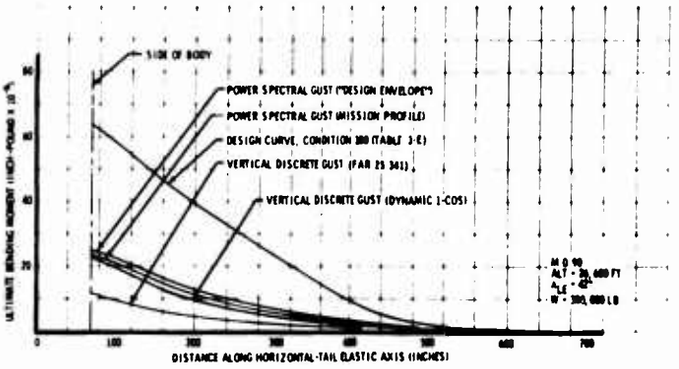

Figure 3-33. Horizontal-Tail Bending Moment Distribution

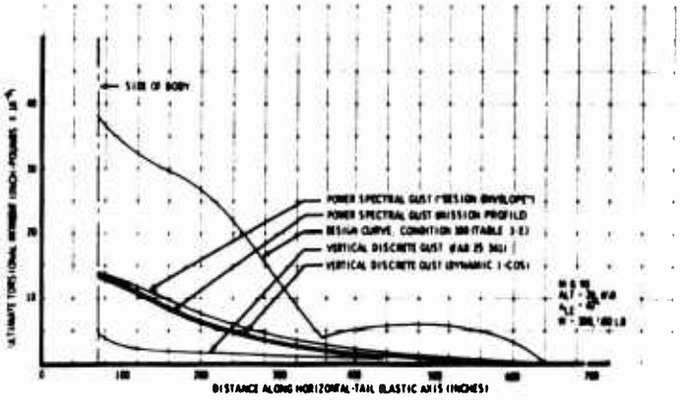

Figure 3-34. Horizontal-Tail Torsional Moment Distribution

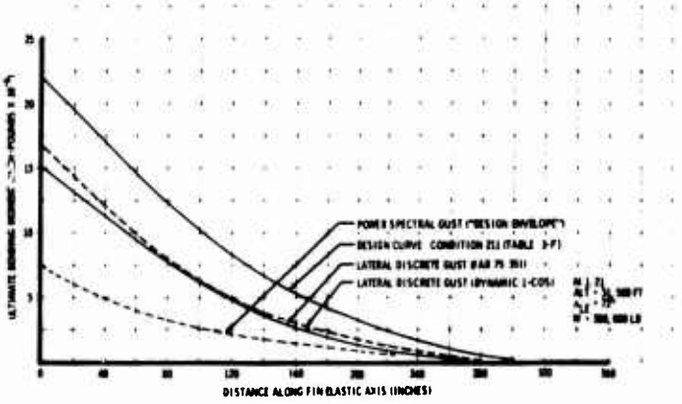

Figure 3-35. Fin Bending Moment Distribution

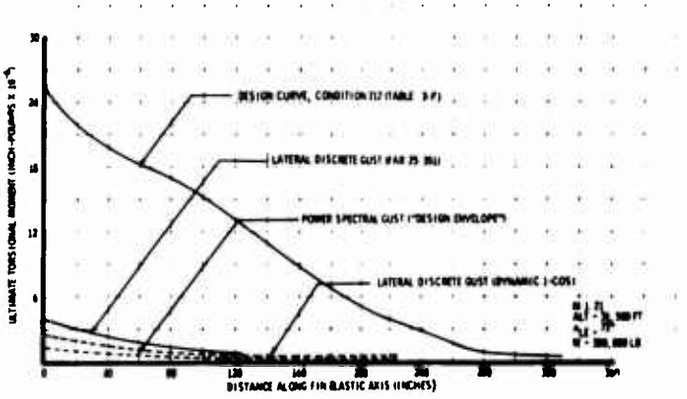

Figure 3-36. Fin Torsional Moment Distribution

any influential structural changes that arise as a result of design iteration. In the continuous turbulence studies, other mission profiles will be analyzed. A full review of airplane weight, speed, and altitude combinations will also be made to ascertain critical conditions. Finally, the inclusion of the SAS will be expanded to a closed-loop analysis, which includes the effects of flexible as well as rigid airplane motion.

3.2.3.2 Methods of Analysis

Two of the four sets of dynamic gust loads (Par. 3.2.3.1) are obtained from the statistical analysis of flight through continuous random turbulence. The third group is obtained by dynamic analysis based on a discrete gust input. The fourth group is obtained by application of the gust formula of FAR, Par. 25.341.

3.2.3.2.1 Continuous Turbulence Studies
The two statistical methods are termed the mission profile analysis and the "design envelope" analysis and assume that the airplane is forced by a continuous gust input that is random in nature but has a specific statistical description. Airplane flexibility is described in terms of bending and torsional stiffness distributions along separate elastic axes of the structural components. The associated airplane vibratory effects are incorporated into the study in terms of natural vibration mode shapes expressed as surface distributions of vertical deflection over the entire airplane, as shown in Par. 3.4. Aerodynamic forces due to both airplane motion and gust encounter are determined by lifting-surface theories that provide aerodynamic influence coefficients over the body, wing, and tail for the complete range of flight Mach number. Unsteady aerodynamic effects are accounted for by the introduction of appropriate exponential lift growth functions. These aerodynamic forces enter the equations of motion as generalized forces obtained by integrating pressures over the entire airplane with the significant (first five) vibration mode shapes used as weighting functions. The equations of motion, when once formulated, are solved by both digital and analog computers. These solutions provide both the forced airplane response and the related structural loadings.

The basic power spectral relationships employed in the statistical analyses are illustrated in Fig. 3-37. The power spectral density of the gust input shown is a frequency-sensitive function that describes the harmonic gust content of the atmosphere. The input PSD used is the Van Karman turbulence spectrum denoted in Fig. 3-37. The combination of this gust input and any airplane frequency response function of interest yields an output PSD function, which, in turn, provides two basic, statistical parameters. These are $\overline{A}$, the rms value of the output due to a unit rms gust input and N_0, the expected number of output zero crossings per unit of distance traveled. Different usage of these parameters results in the two aforementioned analysis methods.

The mission profile approach sums the individual load contributions on a time-weighted basis from all of the composite segments of the selected mission profile. The reference midpoints of the flight segments selected for the present analysis are shown in Fig. 3-38. The application of this method produces the N_0 and $\overline{A}$ values for all responses and loads of interest. Within each segment the frequency of exceedance at some incremental load (y) can be calculated (Ref. 3-3) from the equation:

$$N(y) = N_0 \left[P_1 e^{-y/b_1\overline{A}} + P_2 e^{-y/b_2\overline{A}} \right]$$

where P_1, P_2, b_1, and b_2 (Ref. 2-2) are constants that define exposure times and gust intensities in nonstorm and storm turbulence. The separate exceedances are then weighted by the fraction of total mission time spent in each segment to establish exceedance-level loading curves. The final and crucial interpretive step in the application of this analysis method is the establishment of a definite relationship between exceedance load levels and design load values. In the present study the limit incremental gust load is designated to be that value that is associated with a probability level of 10^{-5} exceedances per hr. Vertical-gust exceedance curves for bending moments on the forward-fuselage and horizontal tail are plotted in Figs. 3-39 and 3-40.

The "design envelope" approach provides limit design gust loads by multiplying the rms load, $\overline{A}$, determined at the most critical gust condition by a factor, U_σ, giving limit load = $U_\sigma \overline{A}$. The largest gust loads occur at velocity V_C on the design envelope. The flight conditions are as follows:

	Vertical gust	Lateral gust
Mach No.	0.9	1.21
Altitude (ft)	26,600	31,500
Wing sweep (deg)	42	72
Airplane weight (lb)	380,000	380,000
U_σ (true), (fps)	62.2	58.4

The values of U_σ are obtained from Fig. 3-41. All of the limit, incremental, dynamic gust loads have been added to the net 1g loads and multiplied by 1.5 to obtain the final results indicated in Par. 3.2.3.1.

Another method of studying airplane response to random turbulence is to obtain actual time histories from an analog computer. This approach provides additional understanding of the composition of both the gust input and the statistical output of the digital study. The random gust input is obtained by shaping the output of a white-noise generator to fit the selected mathematical form of the

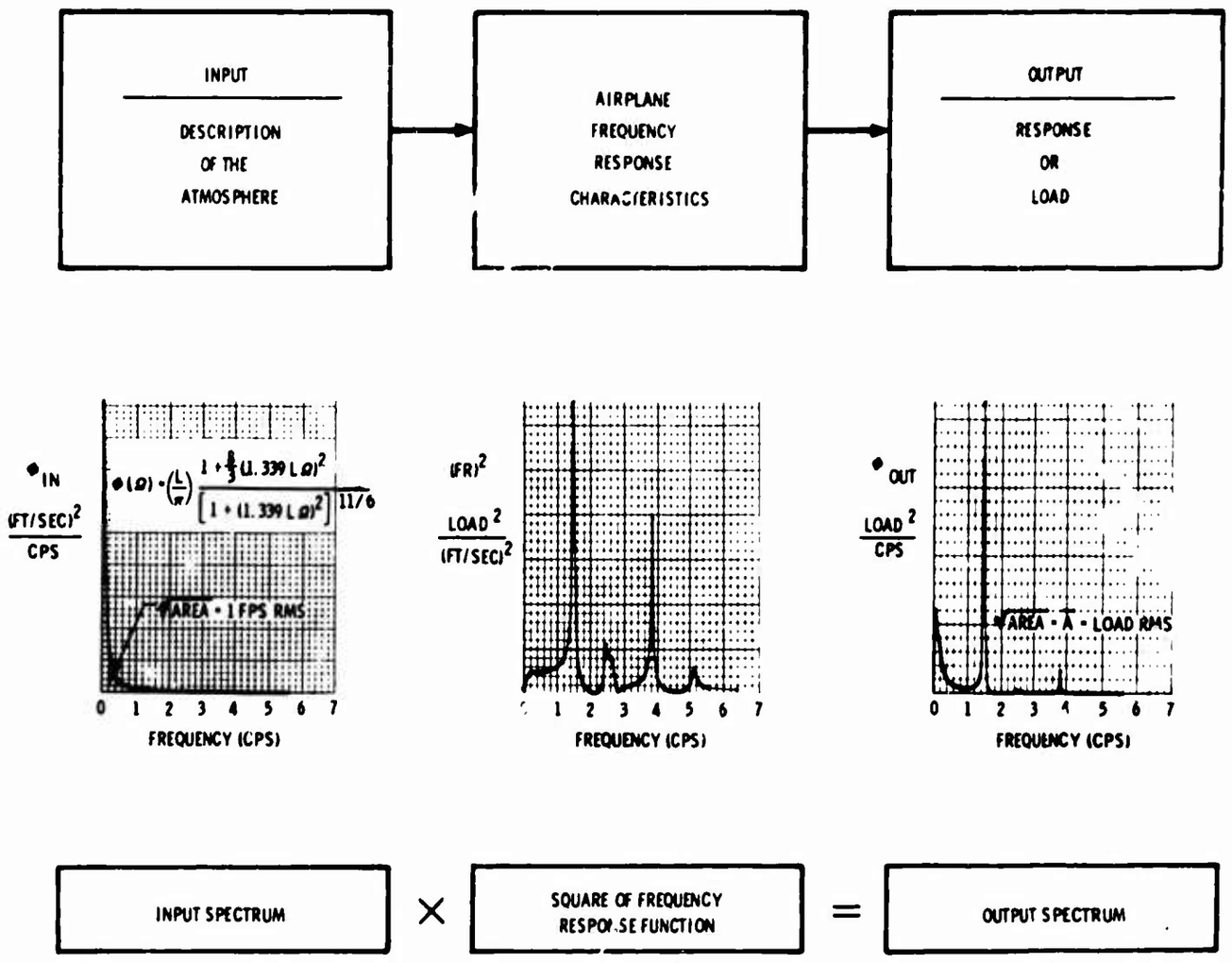

Figure 3-37. Basic Power Spectral Relationships

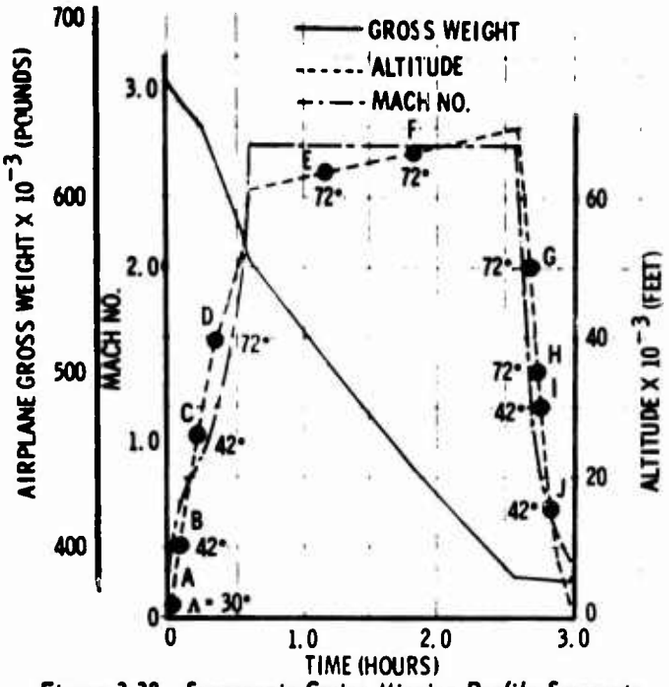

Figure 3-38. Supersonic-Cruise Mission Profile Segments

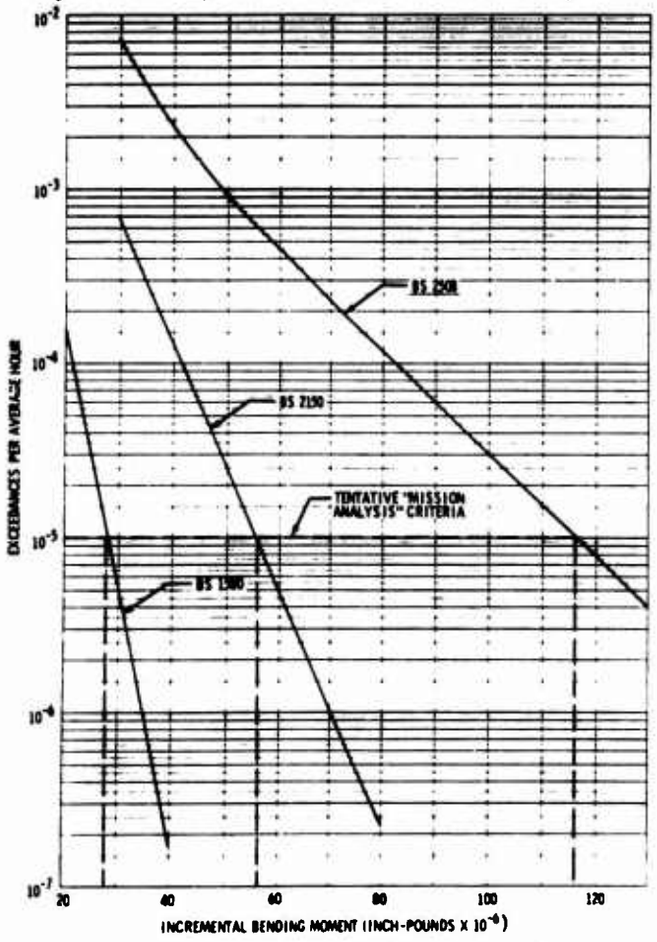

Figure 3-39. Forward-Fuselage Exceedance Curves, Vertical PSD Gust Study

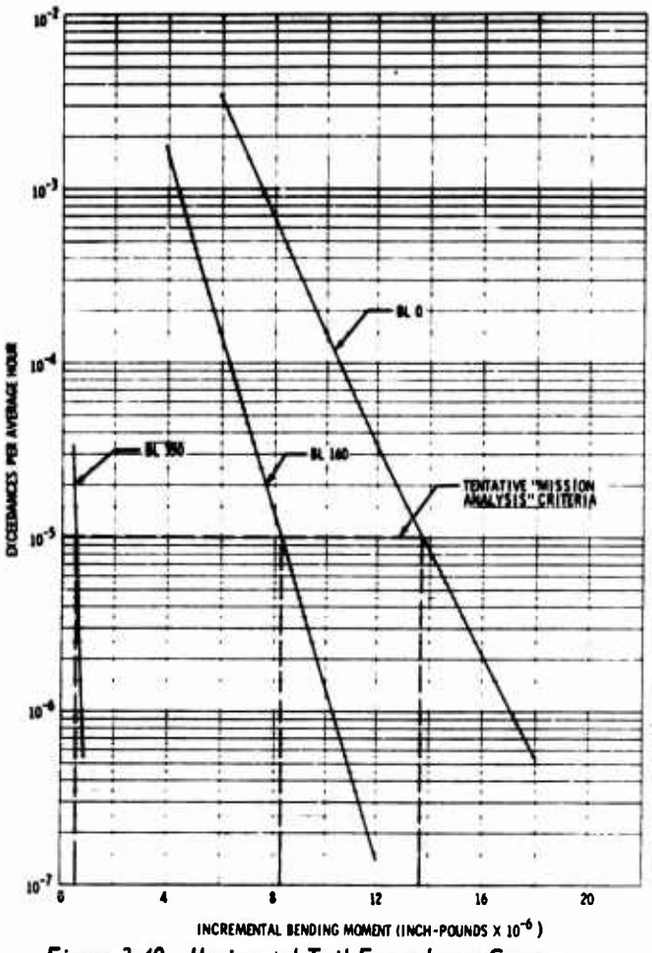

Figure 3-40. Horizontal-Tail Exceedance Curves, Vertical PSD Gust Study

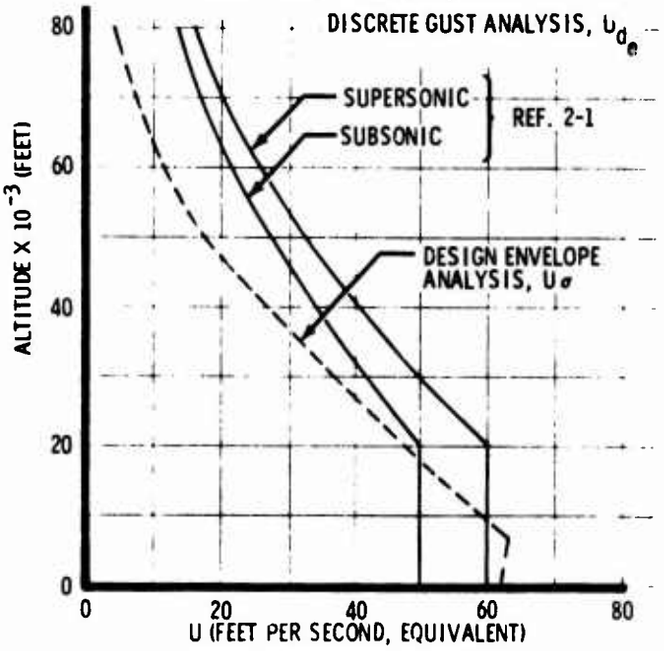

Figure 3-41. Gust Input Velocities

atmospheric power spectrum. In addition to exceedance levels and rms intensities, the critical peak-load values are also available by this method. Another advantage of the time history approach is that proper phasing of combined loadings is inherently included in the analysis. A sample analog record from the vertical gust study is shown in Fig. 3-42. Although the various responses occasionally show a tendency to grow, the gust input irregularity constrains any serious resonance buildup. Comparable analog and digital rms values of vertical acceleration are tabulated as follows:

	RMS g per unit rms gust	
	Digital	Analog
Pilot station	0.0347	0.0327
Airplane center of gravity	0.0144	0.0122
Horizontal tail root	0.0170	0.0143

3.2.3.2.2 Discrete Gust Analysis

This method uses the same descriptions of airplane structure and aerodynamic forces as outlined for the power spectral gust analysis. In this case, however, the entire input spectrum of atmospheric turbulence is represented by discrete one-minus-cosine-shaped gusts of constant intensity, which are then critically phased to produce the maximum structural loading in the component under investigation. The maximum design gust magnitude U_{de}, is selected by accumulated speed-load-factor-altitude (VGH) to ensure that a new airplane will possess sufficient structural strength to withstand limit gust loading throughout its service. Appropriate values of U_{de} are indicated in Par. 2.1.6 and shown in Fig. 3-41. The discrete gust approach includes detailed airplane dynamics and yields absolute load values for use in design. The flight conditions used in the discrete gust analysis are those for the design envelope analysis. Airplane responses and load outputs are obtained from a step-by-step digital solution of the equations of motion and are displayed by an automated plotting routine. Complete time history summaries of both vertical and lateral discrete gust analyses are displayed in Figs. 3-43 and 3-44. The resulting envelopes of maximum incremental gust loads are also presented as ultimate loadings in Par. 3.2.3.1.

3.2.4 Dynamic Landing

The load results and approaches presented herein are consistent with the design criteria specified in Par. 2.2.2. The results shown reflect specialized usage of a California Engineering Associates (CEA) computer that simulates the stiffness and mass properties of the real airplane structure by

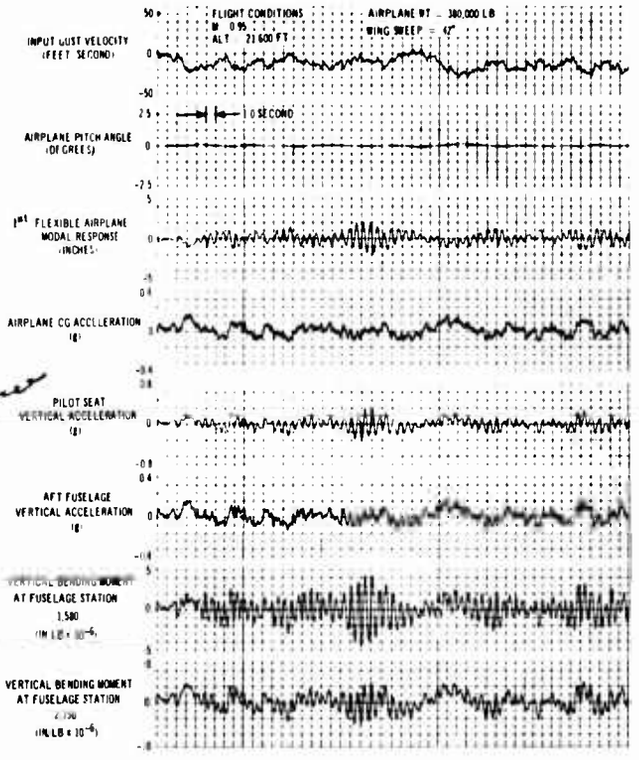

Figure 3-42. Sample Analog Record, Vertical PSD Gust Study

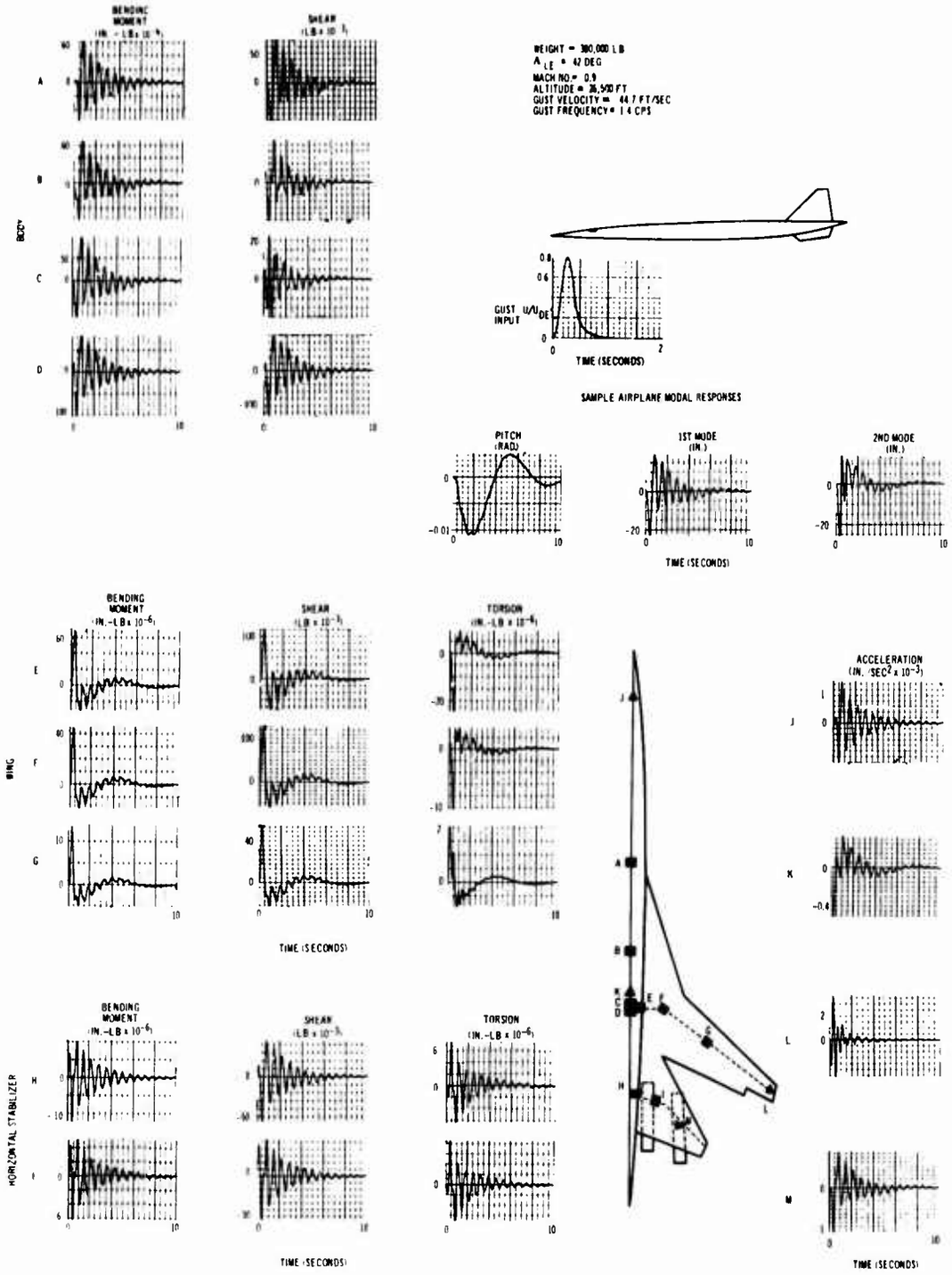

Figure 3-43. Vertical Discrete-Gust Analysis Time Histories

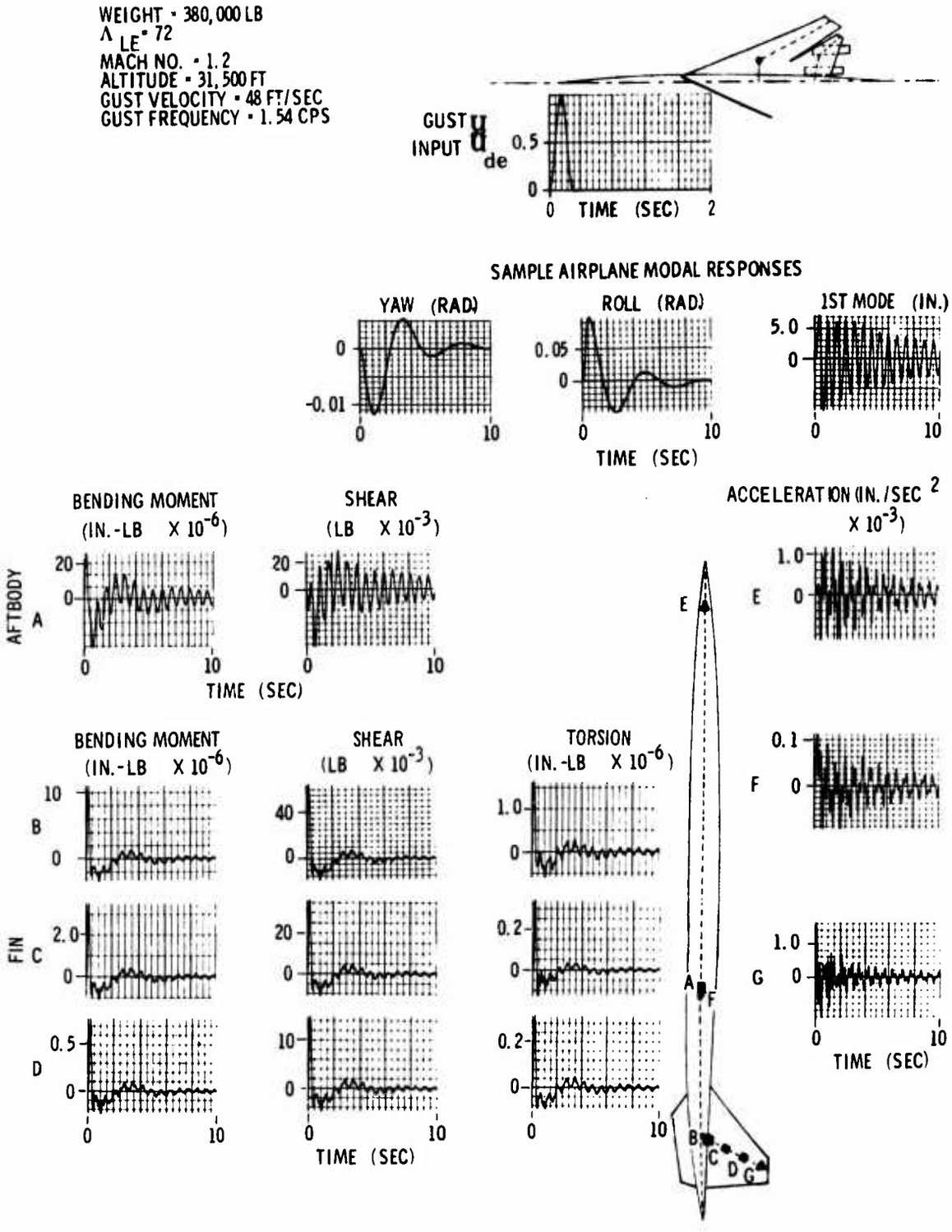

Figure 3-44. Lateral Discrete-Gust Analysis Time Histories

equivalent electrical elements. Attention is paid to both main-gear and nose-gear impact.

3.2.4.1 Landing Analysis Results

Envelope distributions of maximum incremental bending moments and shears along the forward-fuselage due to landing impact are shown in Figs. 3-45 and 3-46. These results are also presented in magnification factor form in Figs. 3-47 and 3-48. These factors are obtained by dividing the dynamic analysis loads by the corresponding static loads, which are based on a $\Delta n = 0.8$ load factor due to vertical translation only. The magnification factors, therefore, reflect the combined

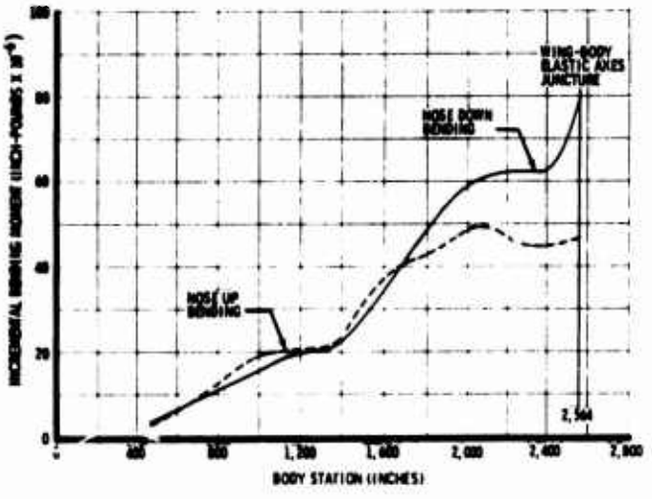

Figure 3-45. Envelope of Forward-Fuselage Bending Moments Due to Landing Impact

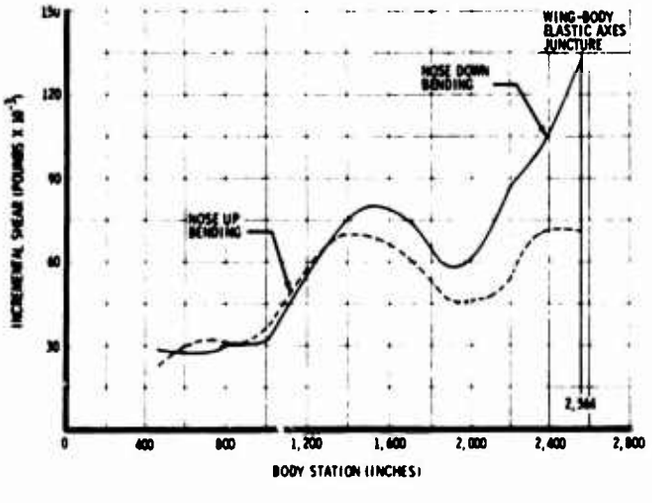

Figure 3-46. Envelope of Forward-Fuselage Shears Due to Landing Impact

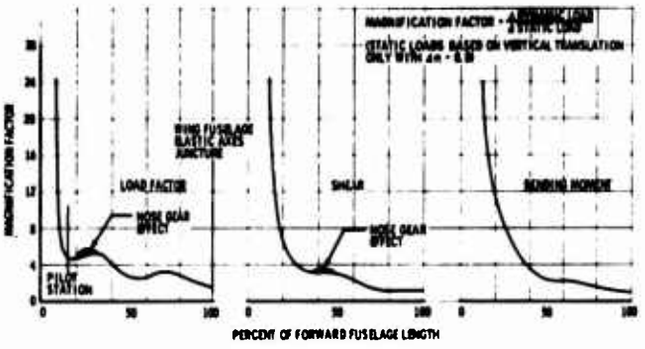

Figure 3-47. Dynamic Magnification Factors, Nose Down Bending

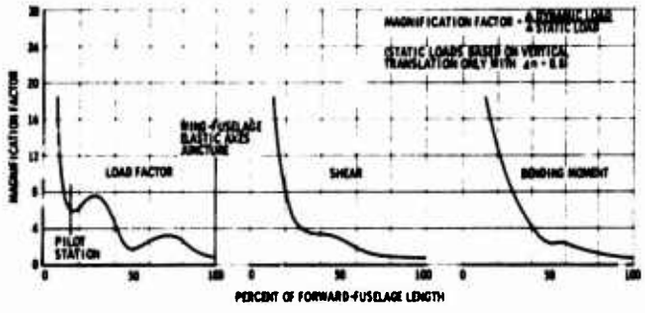

Figure 3-48. Dynamic Magnification Factors, Nose Up Bending

effects of rigid airplane pitch, vertical-force time history, spin-up drag moment, and airplane flexibility. The shaded area in Fig. 3-47 shows the minor load increase due to nose-gear impact. As shown in Fig. 3-30, the landing impact loads are critical and are accounted for in the design of the major portion of the airplane forward fuselage.

Summary arrays of load time histories are presented for seven separate landing studies in Figs. 3-49 through 3-55. The first four cases consider impact on the main gears only, while the last three cases also include the nose gear. The latter set permits time delays of 0.1, 0.5, and 3.3 sec between the instants of main and nose gear contacts. For the most critical landing condition with the airplane sink speed, V_S = 10 fps, only the 3.3-sec delay case is regarded as reasonable. This is based on a study of nose-gear sink speed, which assumes that there is no pilot action, and that after main gear contact, the lift diminishes in proportion to airplane pitch attitude from L = W to L = 0.2W at nose gear contact. The resulting time history of nose-gear descent rate for this extreme condition is shown in Fig. 3-56.

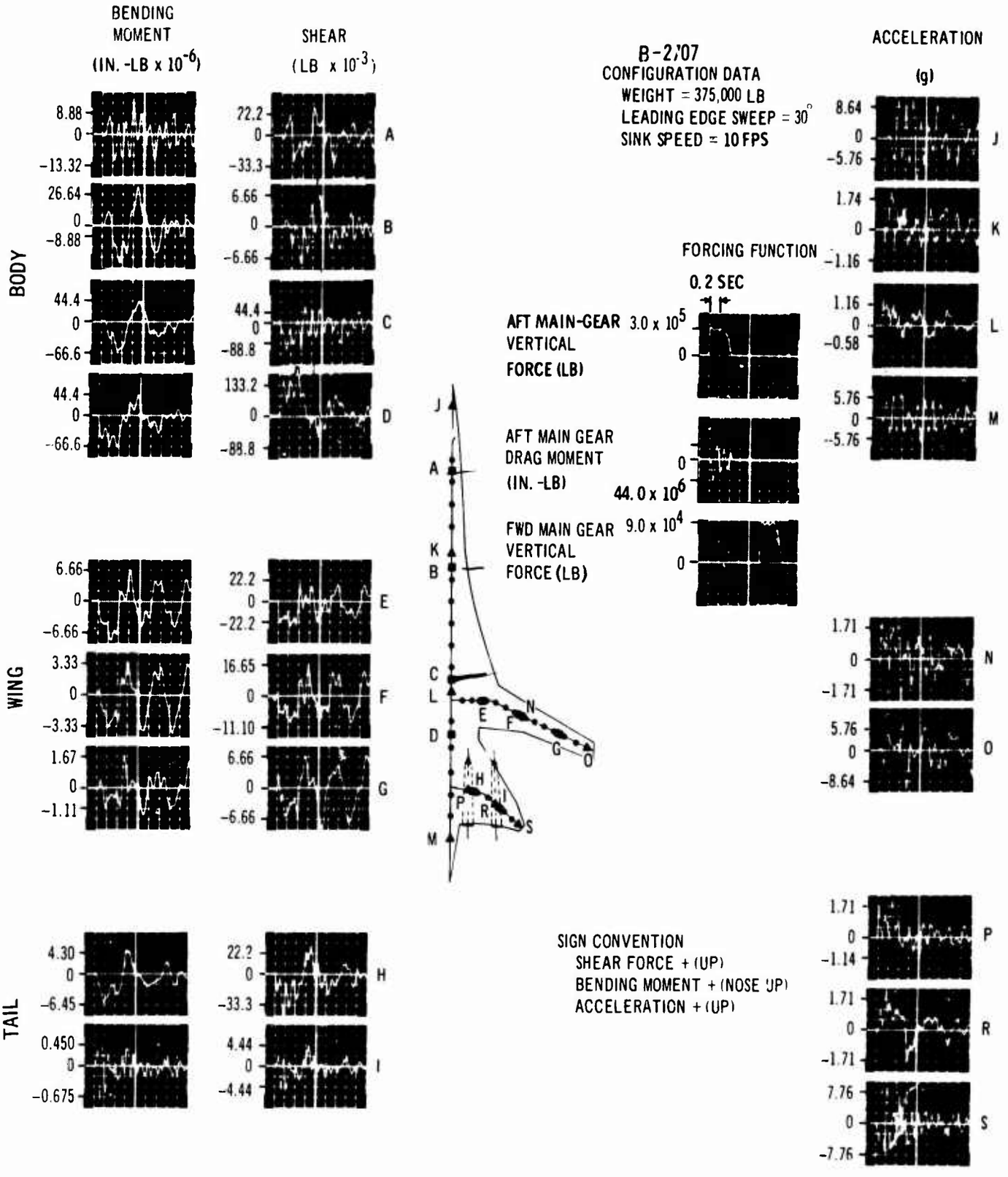

Figure 3-49. Landing Impact Study, Nominal Configuration

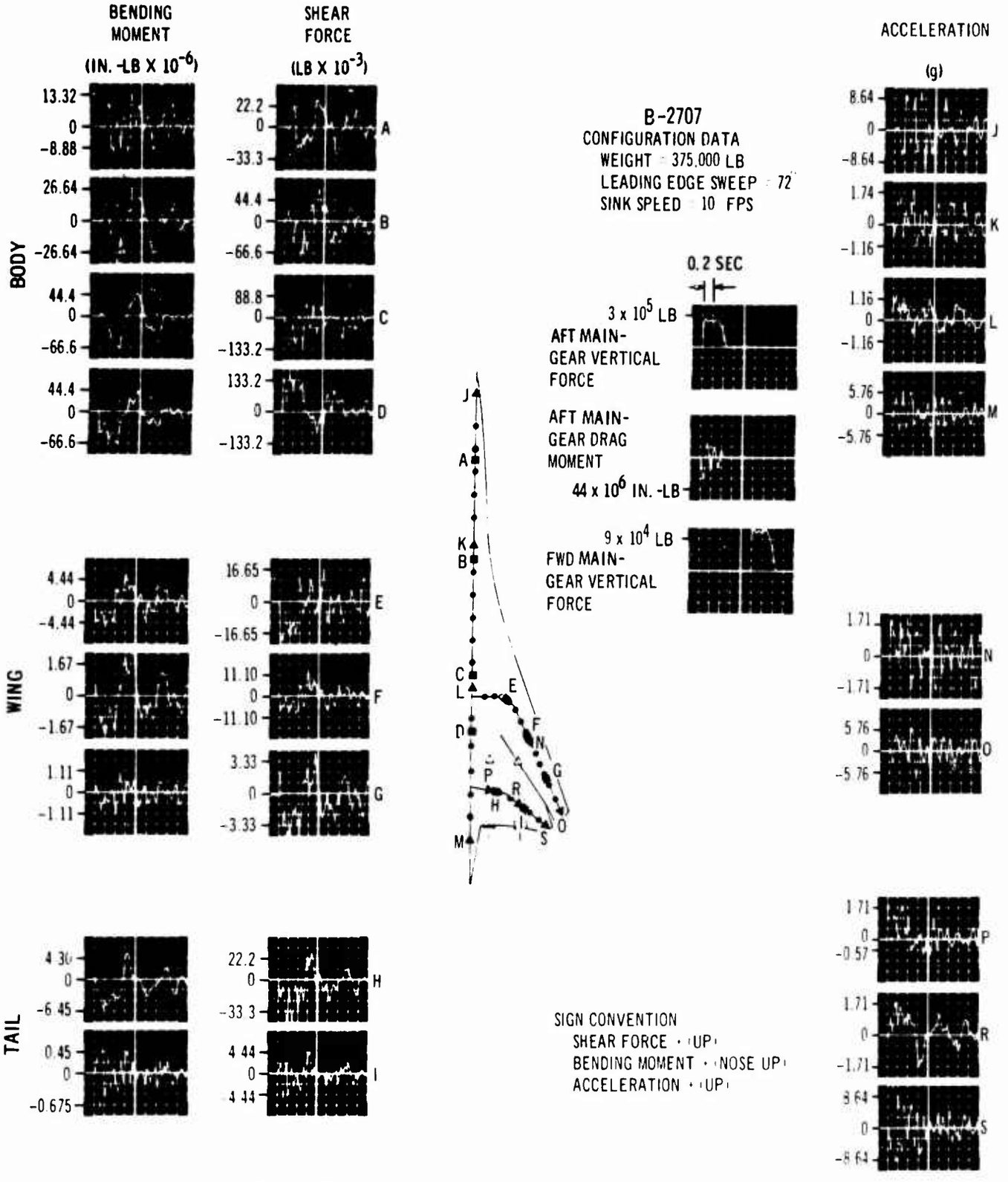

Figure 3-50. Landing Impact Study, Nominal Weight, Wings Aft

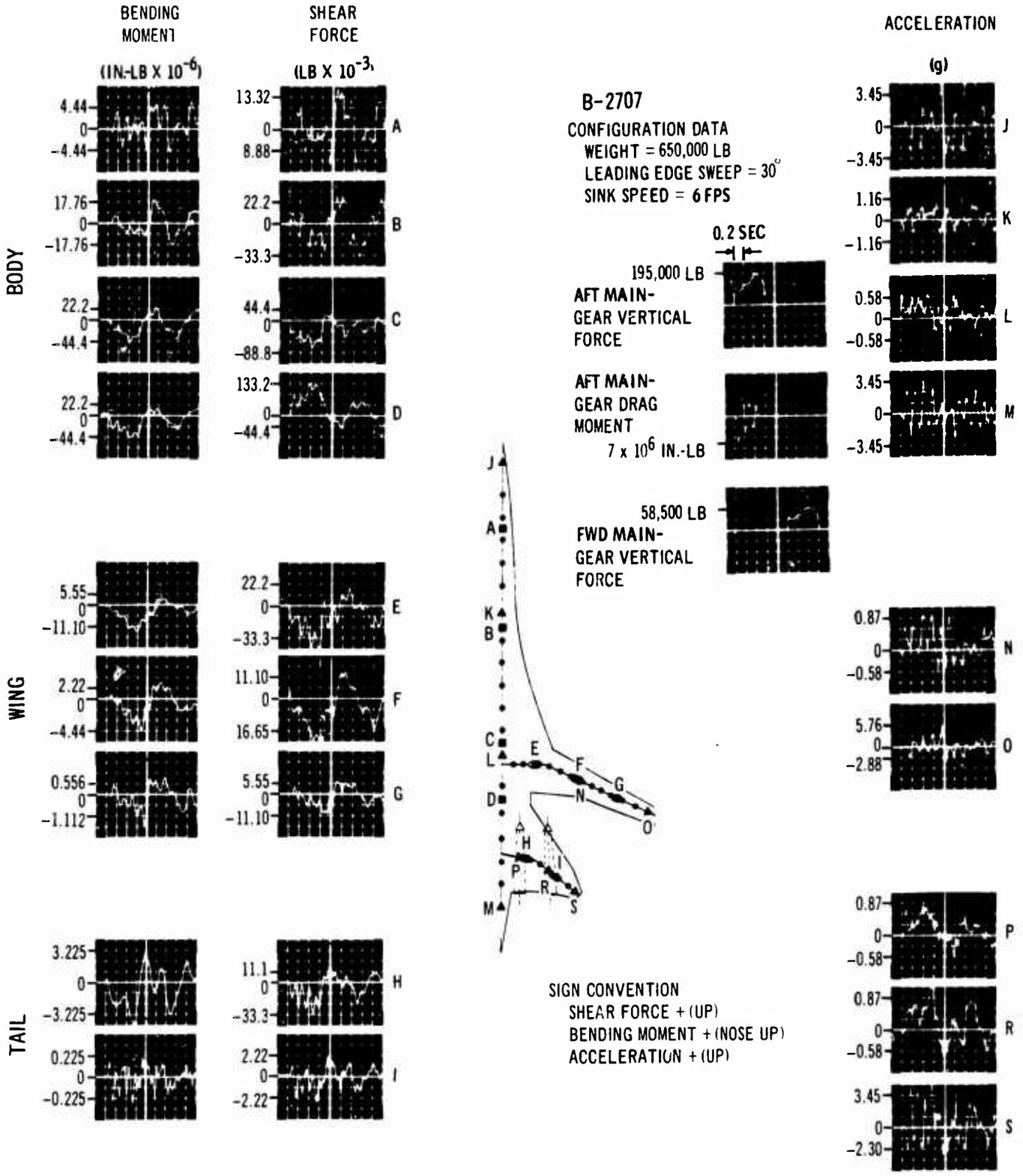

Figure 3-51. Landing Impact Study, Heavy Weight Configuration

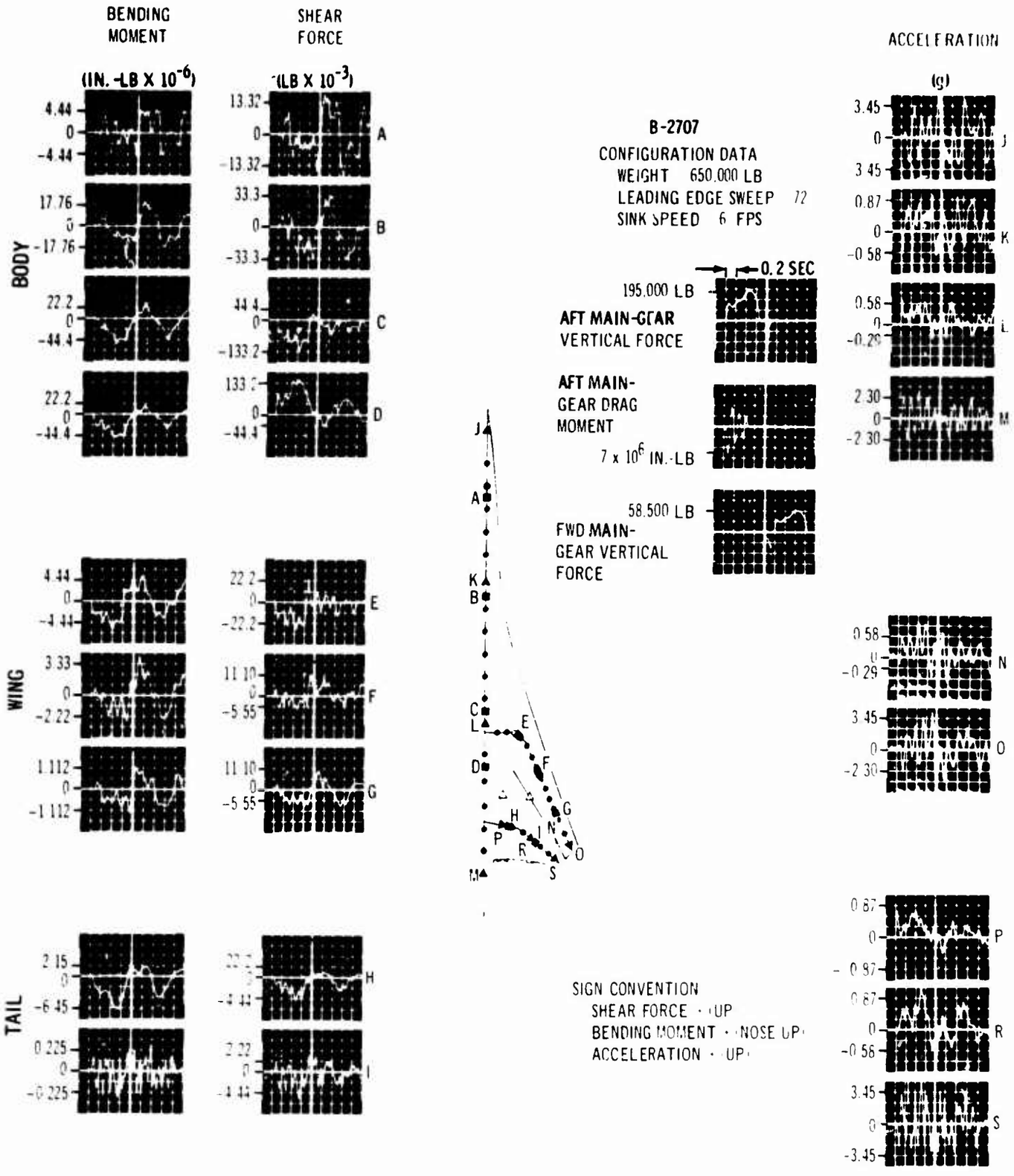

Figure 3-52. Landing Impact Study, Heavy Weight, Wings Aft

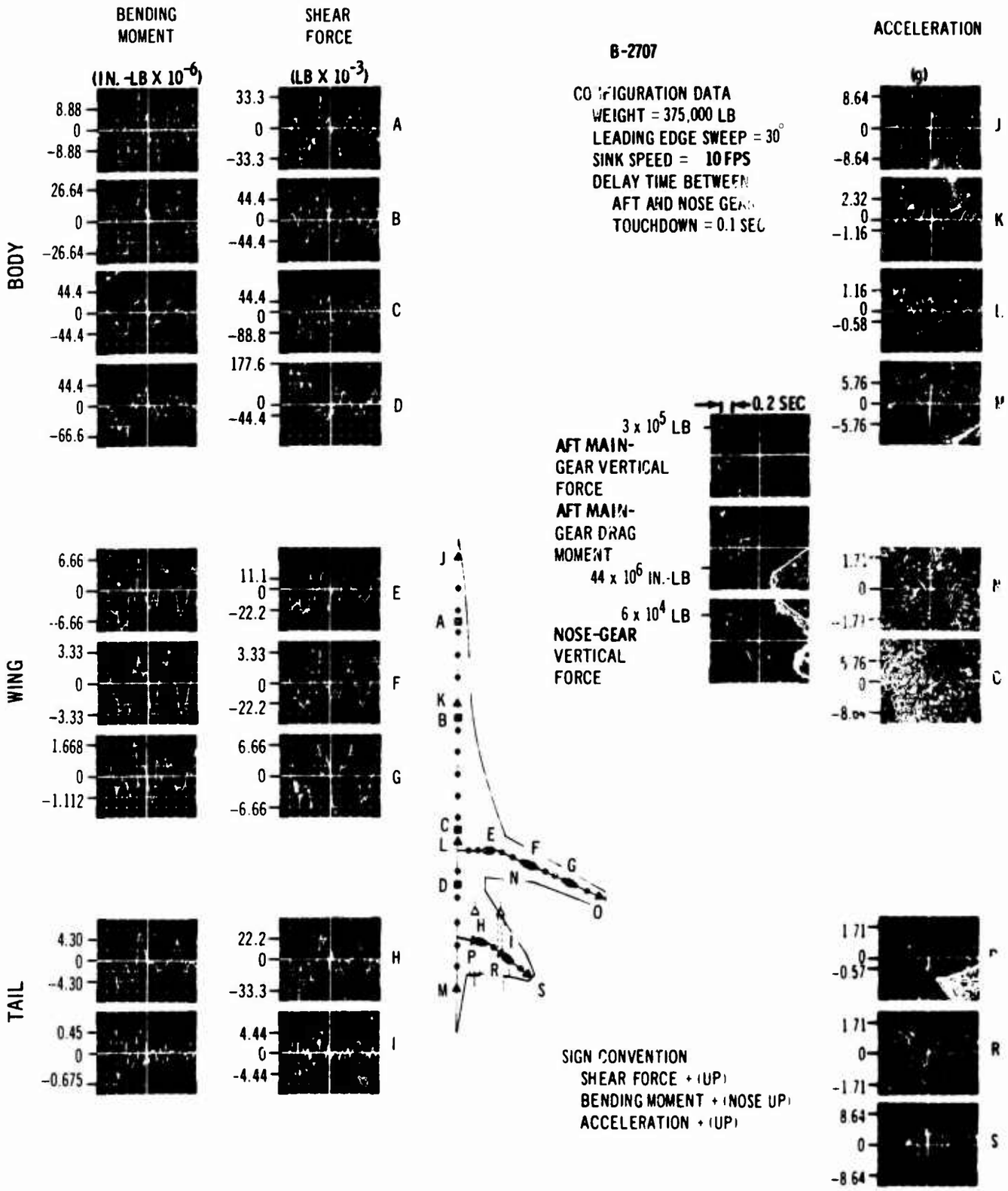

Figure 3-53. Landing Impact, 0.1-Second Nose Gear Delay

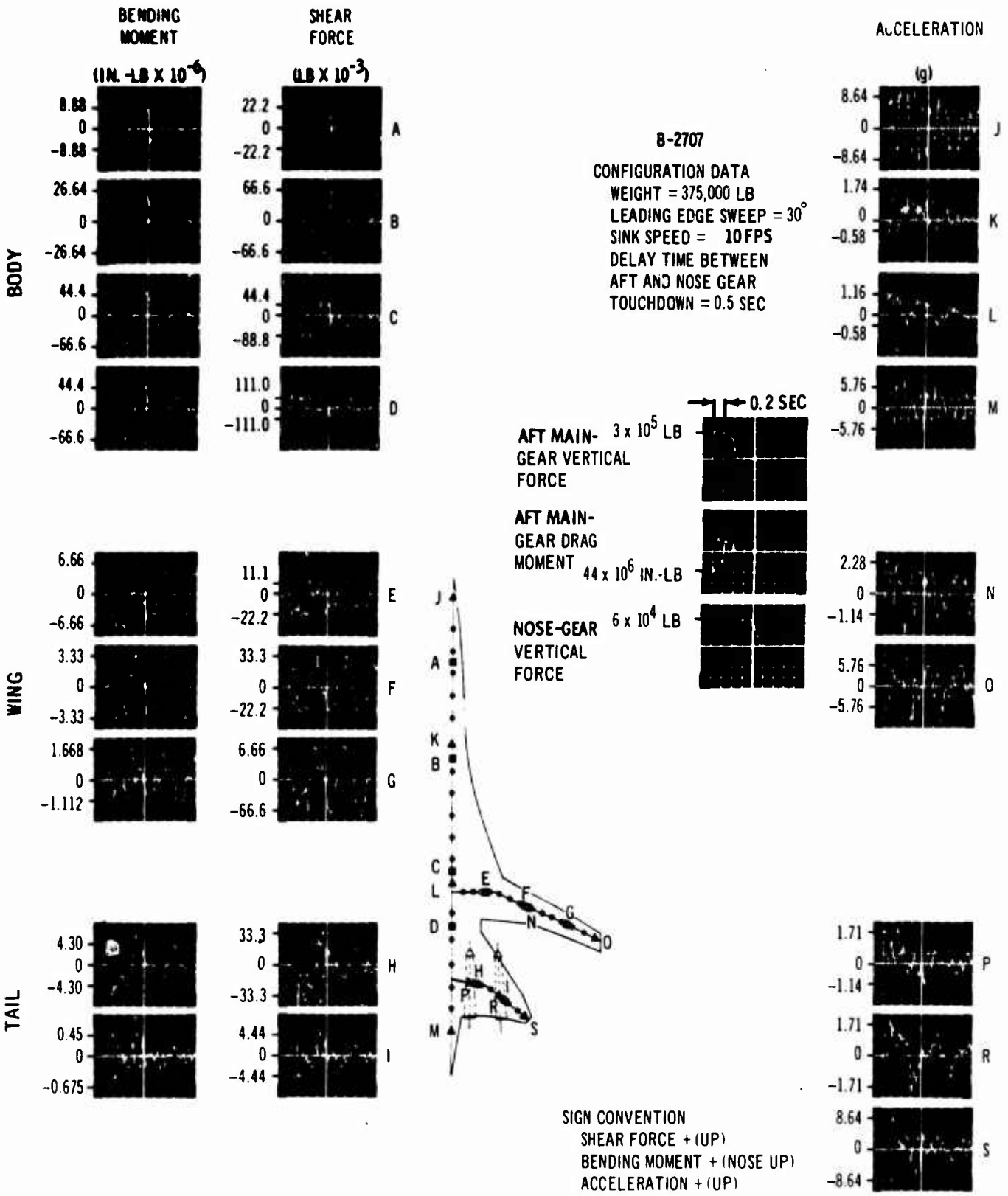

Figure 3-54. Landing Impact, 0.5-Second Nose Gear Delay

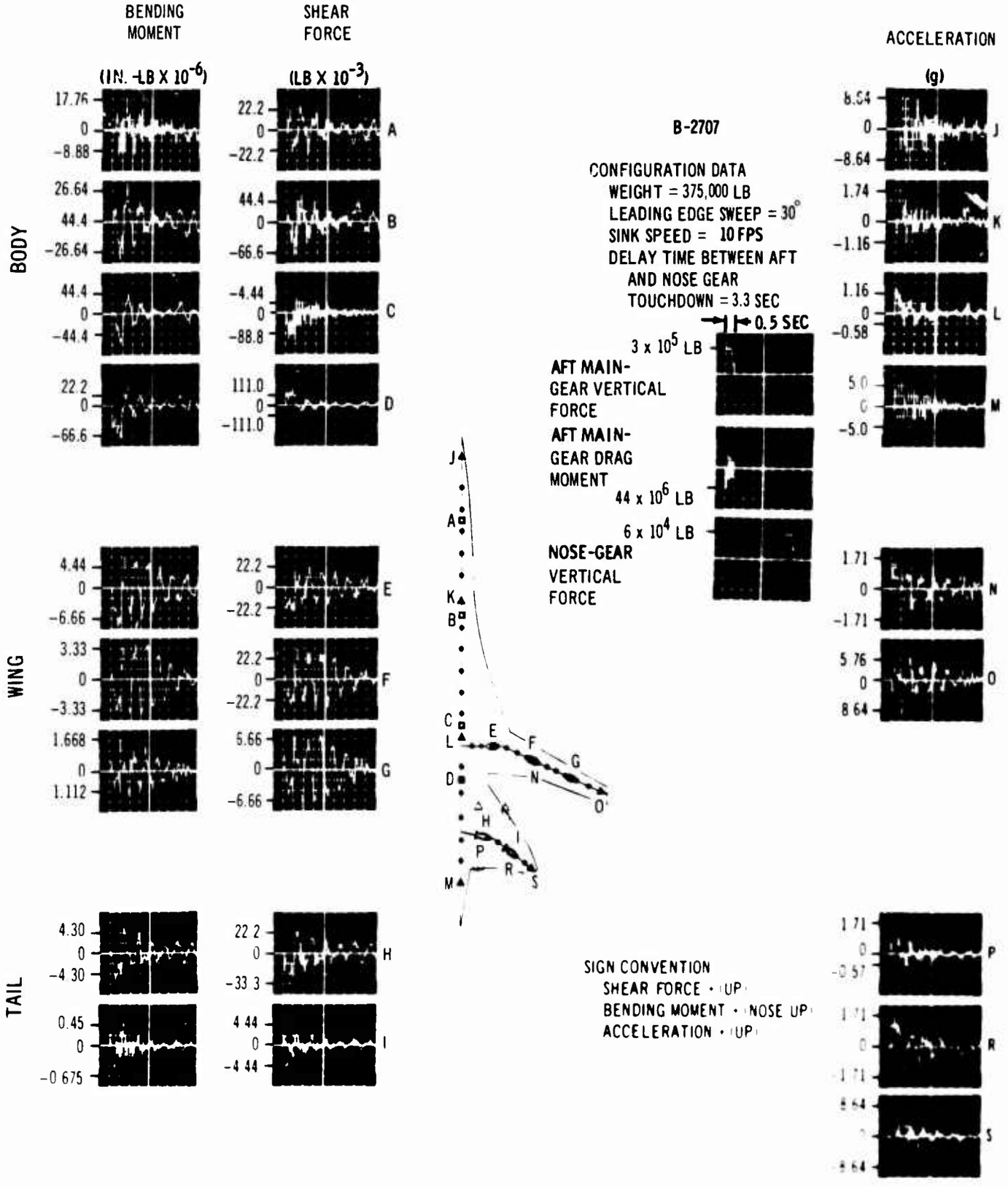

Figure 3-55. Landing Impact, 3.3-Second Nose Gear Delay

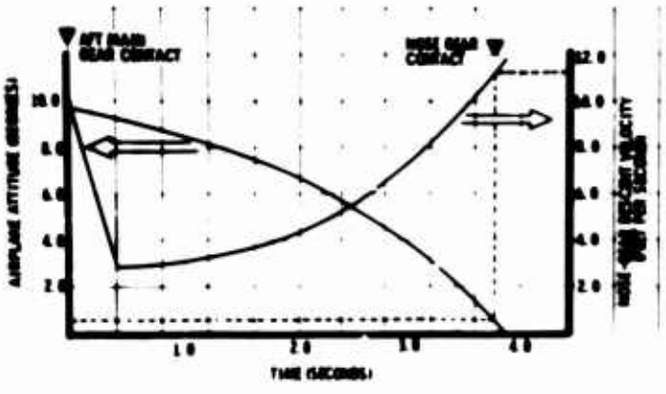

Figure 3-56. Nose-Gear Sink Speed Time History

3.2.4.2 Analysis Method

CEA computer utilization provides an airplane simulation that responds to external electric force application just as the actual airplane responds to the corresponding mechanical force excitation. This simulation incorporates accurate descriptions of mass and stiffness distributions and enables dynamic studies to be made without the use of analytical equations. Loads are monitored at any desired point on the airplane, displayed individually on an oscilloscope, and photographed. Manual arrangement of the load pictures results in the final summary array.

The prior determination of input gear reaction forces and spin-up drag moments is accomplished by nonlinear computer analyses. The shape of the gear-force time histories used in the present study was obtained from a study on a previous SST configuration. This separate study accounts for tire behavior, oleo damping characteristics related to metering pin contour, airspring compression, Coulomb friction, vibratory response of the wheel, and airplane flexibility.

Expanded analysis effort in Phase III will continue to optimize the landing gear design to provide excellent airplane landing characteristics and minimize landing impact loads. The CEA computer simulation will be continued to assure accurate prediction of structural loads during landing.

3.2.5 Taxi

The taxi load results and approaches discussed in the following paragraphs are consistent with the design criteria described in Par. 2.2.1. These studies include takeoff runs and landing rollouts on a specific runway as well as constant speed runs over runways of different roughness levels. Only representative data is included due to the large volume of data generated by modern computer analyses.

3.2.5.1 Results of Analysis

Results of taxi runs at various speeds over a very rough (2-in. rms) runway are presented in Figs. 3-57 through 3-59. Figure 3-57 indicates the incremental vertical acceleration environment at various airplane locations. The most severe incremental accelerations shown are at the pilot station, where the rms values are less than 1g. Figures 3-58 and 3-59 show the low level of incremental rms structural loading experienced during taxi. The analog record in Fig. 3-60 shows a portion of the response time histories taken during the 150-fps taxi run. Nose tire deflection and aft main-gear force are included in this display. Figure 3-61 contains a summary of time history responses that occur during a constant velocity (150-fps) run over the old San Francisco International runway, which was surveyed just prior to repair. Peak pilot-station vertical

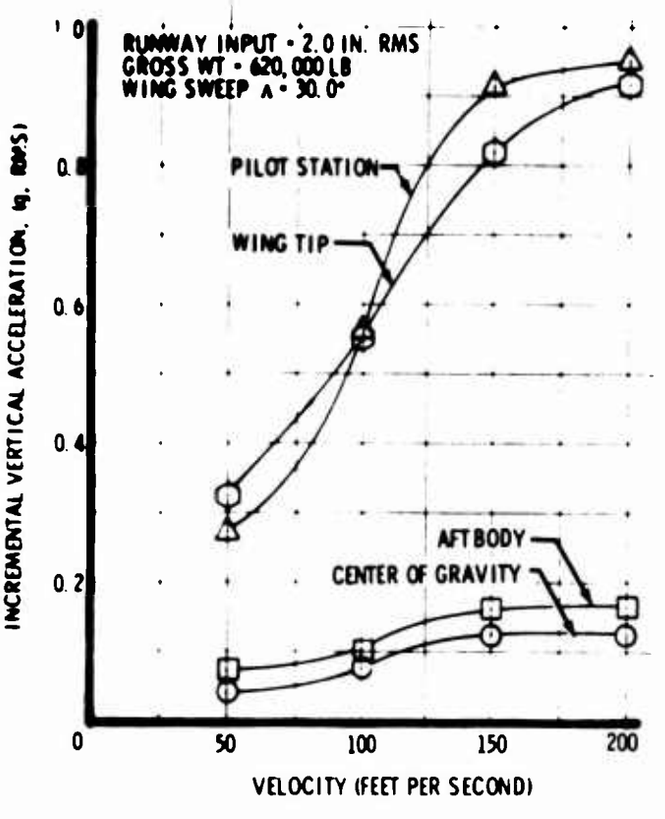

Figure 3-57. Effect of Taxi Speed on Vertical Acceleration

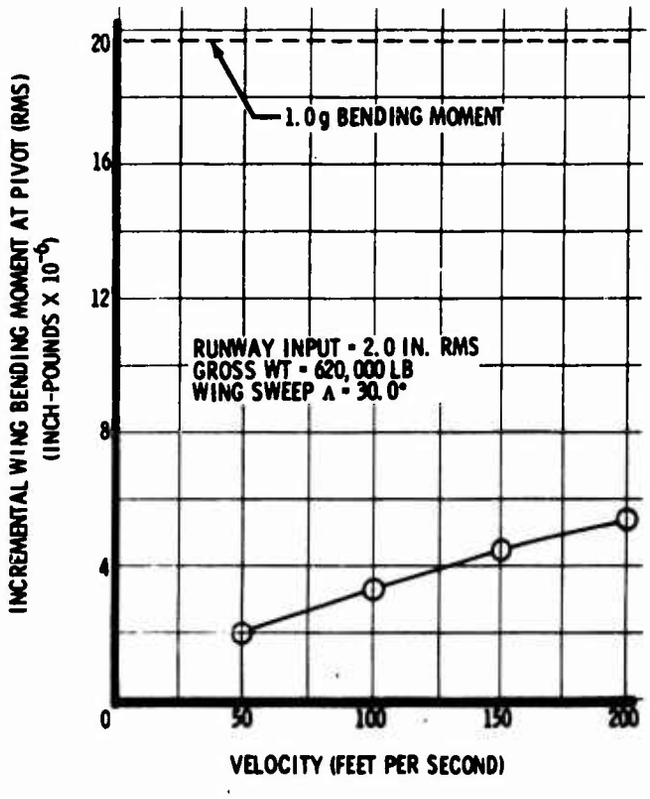

Figure 3-58. Effect of Taxi Speed on Wing Bending Moment

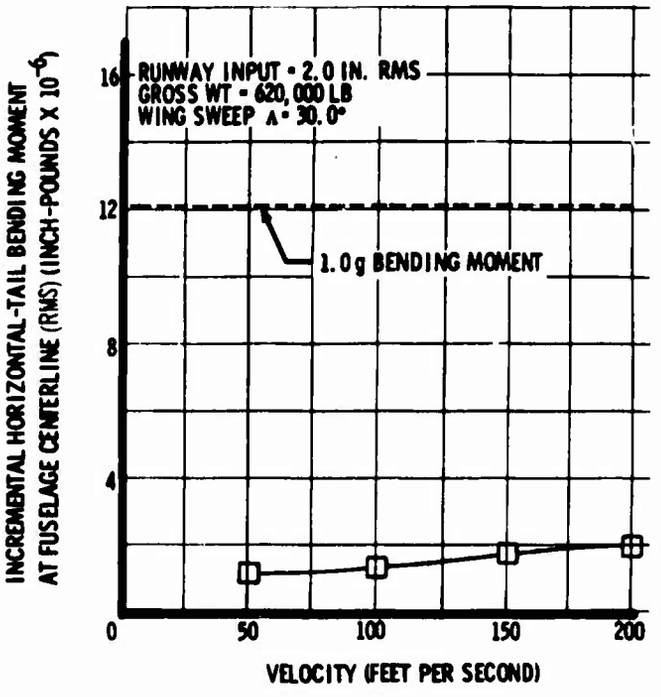

Figure 3-59. Effect of Taxi Speed on Horizontal-Tail Bending Moment

accelerations in excess of 2g occur at the relatively sharp bumps associated with runway intersections.

Continuing effort in Phase III will further investigate the effects of landing gear characteristics and locations on taxi responses. Additional actual runways (e.g. J. F. Kennedy International) will be introduced into the studies to fully define the structural loads and handling qualities of the B-2707 airplane during taxi.

3.2.5.2 Methods of Analysis

Two methods of taxi loads analysis are employed. One method (Ref. 3-4) utilizes digital computing equipment and allows investigation of taxi loads induced by a specific, measured runway. The other technique uses an analog computer and subjects the airplane to a random-roughness runway of variable rms intensity having a specified power spectral density. Both methods account for airplane flexibility in terms of vibration modes and incorporate the nonlinear damping and stiffness characteristics of the landing gears. No aerodynamic forces are included.

The power spectral density description of runway roughness is obtained from Ref. 3-5. To determine an appropriate level of runway roughness that will encompass all taxiways that the SST might use, the rms roughness levels of numerous existing NATO runways are plotted in Fig. 3-62. Based on this information a roughness level of 2 in. rms was selected as an extreme condition for the analog study.

3.2.6 Engine Unbalance

Estimates of structural design margins provided for possible incidents of engine unbalance in normal service are presented in Figs. 3-63 through 3-66. Figure 3-63 shows that effective engine frequencies in the normal operating range are well above the airframe structural frequencies of greatest concern. Figure 3-64 shows estimated airframe flexibility based on preliminary analyses of presently proposed structure. Figure 3-65 shows amplitude-frequency relationships for an unsupported engine package floating in free space but subject to an oscillatory force input; that is, centrifugal load due to engine unbalance. Figure 3-66 relates centrifugal force and engine unbalance for several values of engine rpm. Use of these figures in combination allows evaluation of

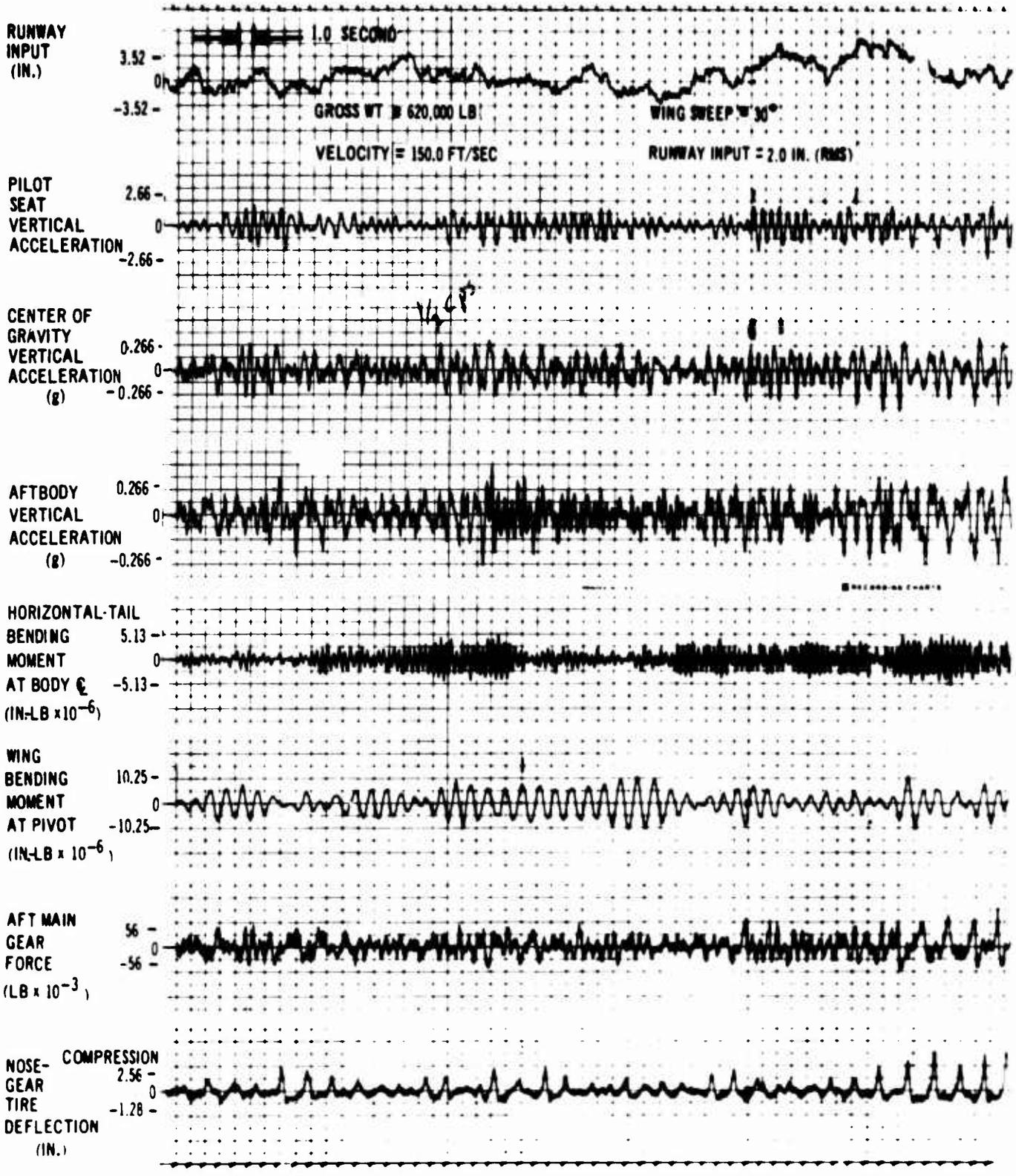

Figure 3-60. Sample Analog Record, Taxi Study

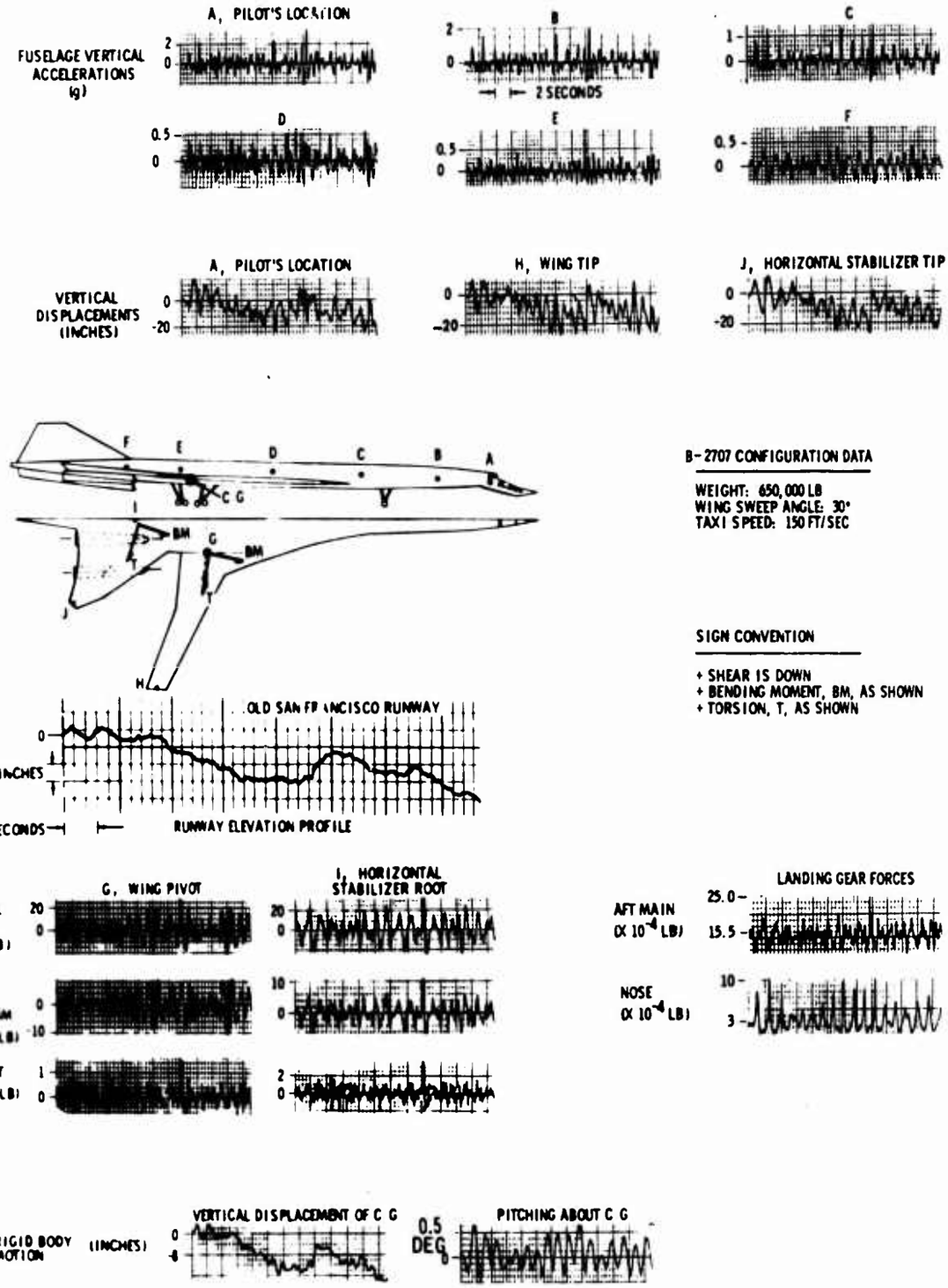

Figure 3-61. Digital Time Histories, Constant-Velocity Taxi Run

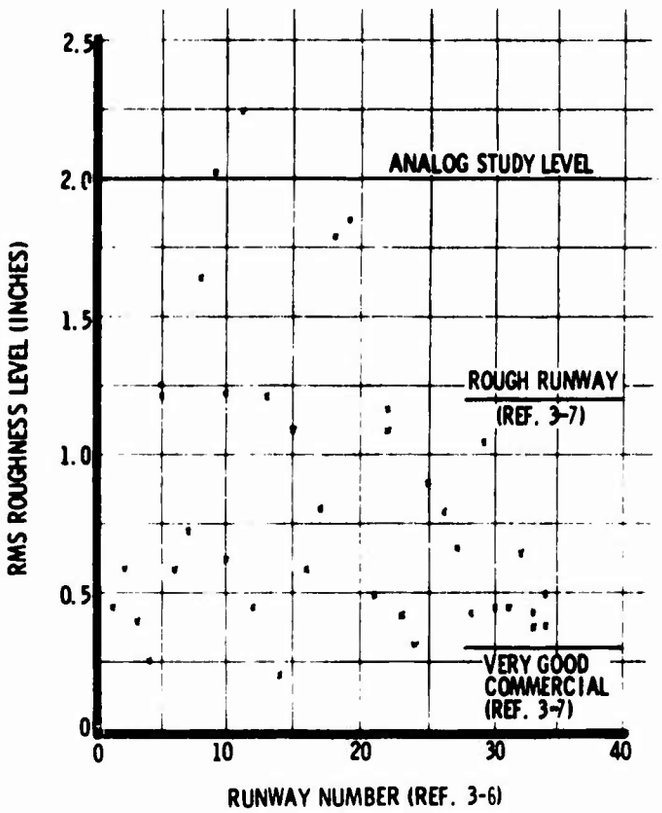

Figure 3-62. Roughness Intensity of Existing Runways

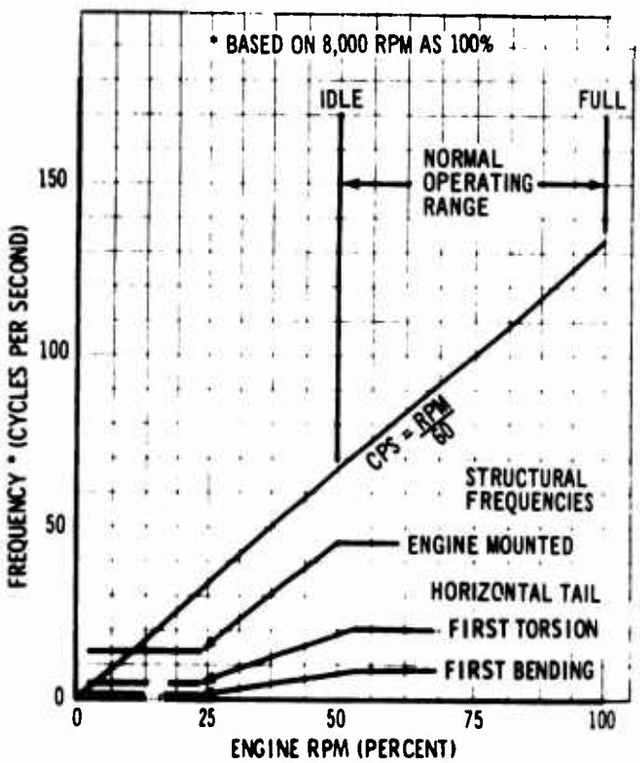

Figure 3-63. Structural and Engine Frequency Relationships

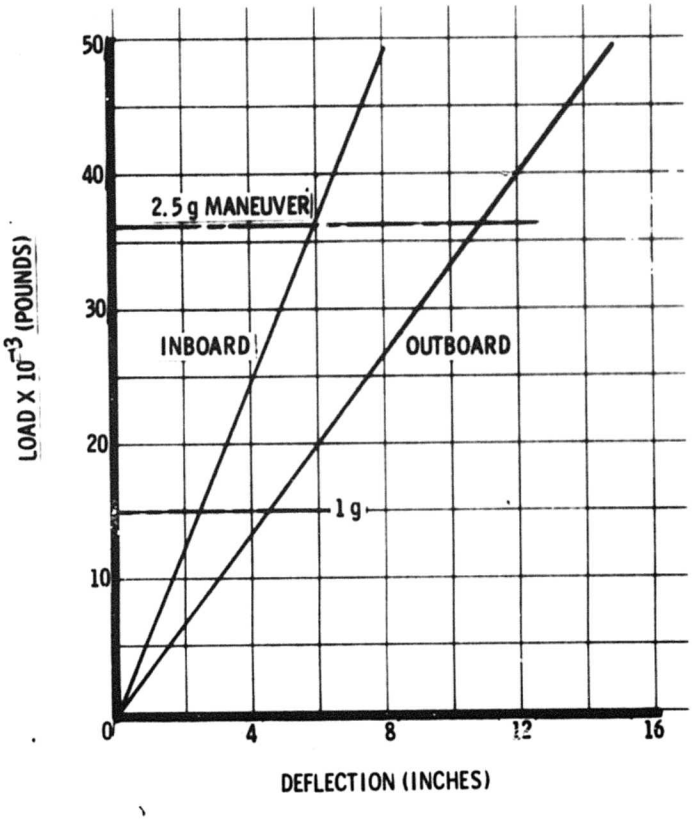

Figure 3-64. Airframe Flexibility (Estimated)

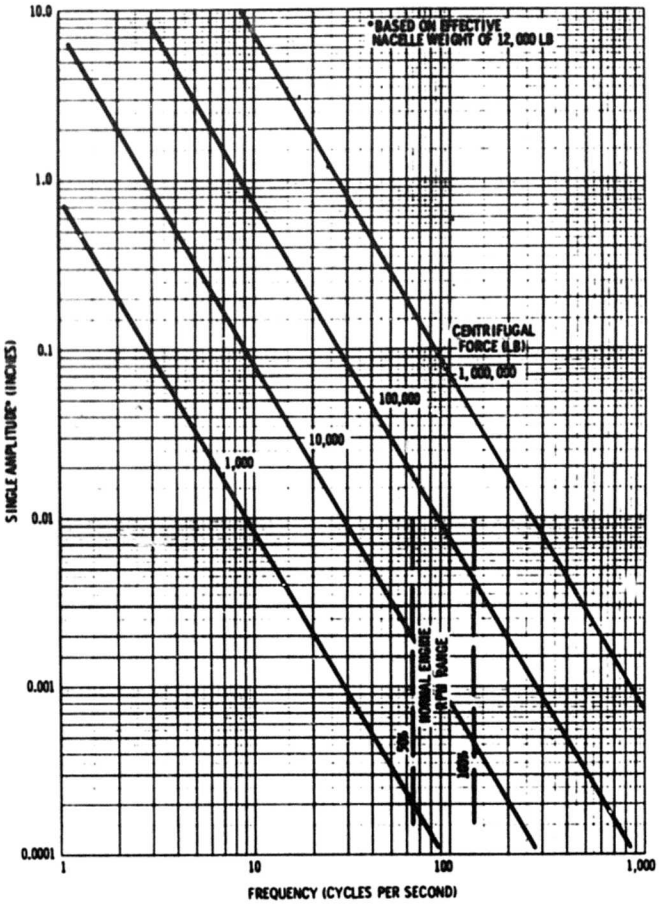

Figure 3-65. Relationship of Engine Amplitude, Frequency, and Centrifugal Force

damage potentials associated with any desired amount of engine unbalance.

It can readily be seen that structural design margins are available for substantial levels of engine unbalance, that is, well in excess of that associated with blade loss. For example, consider an extreme unbalance of 1,000 in.-lb. From Fig. 3-66, the centrifugal force for 1,000 in.-lb at 100 percent rpm is given as 200,000 lb. From Fig. 3-65, the single-amplitude of vibration at 100 percent rpm with a centrifugal force of 200,000 lb is given as 0.007 in. Figure 3-63 shows that 100 percent rpm corresponds to a frequency of 133 cps, which is well above the primary frequencies of the horizontal tail and engine-mount installations. Figure 3-64 shows that a single-amplitude vibration of 0.007 in. will impose negligible loads on the airframe and engine mount structure.

To provide another example (involving critical phasing), consider an unbalance of 1,000 in.-lb at an engine rpm well below idle, for instance, 4 percent. In Fig. 3-66, the centrifugal force is 500 lb. In Fig. 3-63, the frequency for 4-percent rpm is about 5 cps, which is close to the horizontal-tail first-torsion frequency. Referring to Fig. 3-65 using the value of 5 cps and a centrifugal force of 500 lb indicates a single-amplitude of about 0.016 in. Assuming a low-damped structure with a conservative magnification factor of 40 results in a possible critically-phased vibration amplitude of 0.64 in. Figure 3-64 indicates negligible airframe loads for a 0.64-in. nacelle motion.

This will be confirmed by model test during Phase III. The use of a wind-tunnel flutter model for this purpose has been well established as part of the 707 and 727 programs. Such models provide inherent dynamic similarity to the full-scale airplane.

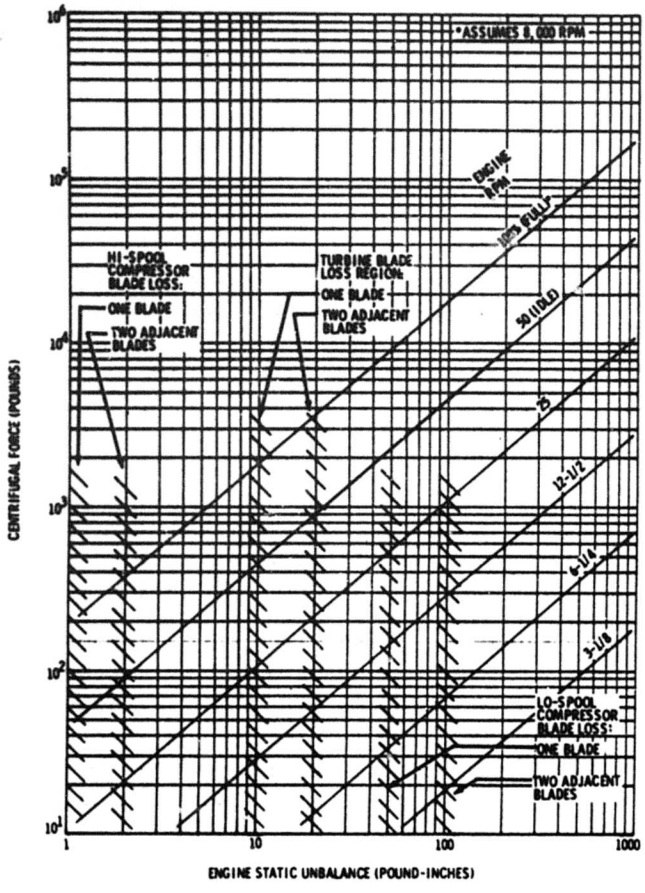

Figure 3-66. Relationship Between Engine Centrifugal Force and Unbalanced Moment

3.3 LOAD VALIDATION

Past, current, and future planned tests and analyses to validate structural design loads for the B-2707 are presented in this section. Load distribution comparisons of wind-tunnel pressure data and basic theory are shown in summary form.

3.3.1 Pressure Models

Wind tunnel tests of pressure models are required to supply data to support the design approach described in Sec. 3.0. The following paragraphs describe the models, instrumentation, and schedules for Phase III and Phase IV tests. Phase III models will be designed during Phase IIC.

3.3.1.1 Model Descriptions

The models will be 0.032 scale and will be built for sting mounting. The outboard wings will be adjustable to three sweep positions. The nacelles will be designed to allow simulation of the complete flow field by use of exit plugs, bypass doors, inlet spikes, and shrouds. The Phase III models will be of the prototype and the Phase IV models will be of the production configuration.

3.3.1.2 Instrumentation

The models will be instrumented primarily with pressure orifices: 600 on the high-speed models and 700 on the low-speed models. These orifices will be distributed over the outboard wing, strake, horizontal and vertical tail, nacelles, and fuselage on one side of the models. The nacelles on the other side of the model, the drooping nose, and the model sting will be instrumented with four component balances that read normal and side loads and pitch and yaw moments. During the unsymmetric tests, the vertical tail will be mounted on a three-component balance reading side force and roll and pitch moments.

Internal scanivalves will sample the orifice pressures, and transducer outputs will be read by the Boeing portable pressure data system. The force balance output will be read by the test facility instruments.

3.3.1.3 Data Handling and Presentation

The Boeing portable pressure data system will be used to take and record the pressure data. The force data will be taken and recorded using the test facility instrumentation. All final data will be available on magnetic tape for documentation tabulation and for use with structures analysis programs.

3.3.1.4 Schedules

The testing schedules for Phase III and Phase IV tests are presented in Table 3-K. Tentative test dates have been arranged with NASA-Ames at a preliminary scheduling meeting. Tentative test time has been allocated for the Convair low-speed tunnel in 1967; test time beyond 1967 will be arranged as required.

3.3.2 Structural Loads and Temperature Survey

Safe operational structural limits will be established in Phase III during the first 100 hr of flight. These data will be sampled in parallel with other planned testing. (Refer to Flight Test Program, V4-B2707-14, Sec. 4.0.) Strain gage and thermocouple data will be monitored at a sufficient number of locations on the airplane to verify general applicability of design loads and stress analysis. Thermal-sensitive paint will also be used

Table 3-K. Pressure Model Test Schedule

Phase III, Two Models, Four Tests				
Test	Tunnel	Model	Occupancy hr	Test Date
Symmetrical, high speed	Ames Unitary	A	240	1 June 1967
Symmetrical, low speed	Convair	B	120	1 Sept 1967
Unsymmetrical, high speed	Ames Unitary	A	270	1 April 1968
Unsymmetrical, low speed	Convair	B	80	1 July 1968
Phase IV, Two Models, Two Tests				
Test	Tunnel	Model	Occupancy hr	Test Date
High speed	Ames Unitary	C	420	1 July 1971
Low speed	Convair	D	120	15 Sept 1971
Phase V, No Tests				

on local areas of the structure to determine the heat influx.

A flight test program will be conducted during Phase IV on a prototype airplane to verify and refine the load and temperature distributions used in design. Such a program is required to provide the design optimization and permit development of the total airplane capability. Boeing experience gained from similar programs conducted on several military and commercial airplanes will contribute greatly to this program. New techniques made available by advanced instrumentation as made necessary by expanded flight envelopes will be used. A schedule of the program appears in Fig. 3-67. The phase relationship to other structural testing is shown in Airframe Design Report – Part E, V2-B2707-9.

The loads to be measured include both flight and ground loads. The flight loads are to include

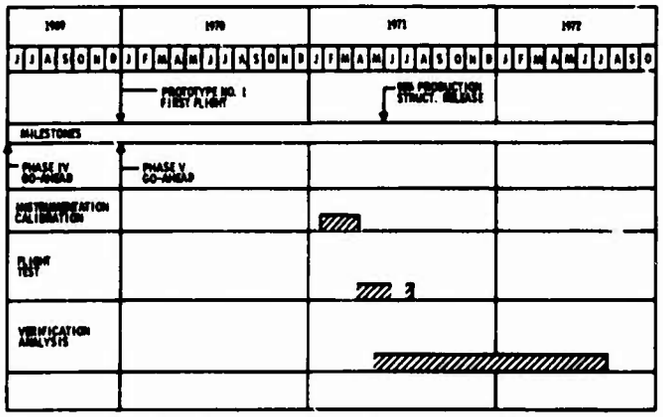

Figure 3-67. Flight Loads, Ground Loads, and Temperature Survey Schedule

those caused by maneuver and those caused by gusts. The ground loads will include both taxi and landing loads. Both steady-state and dynamic loads and sonic pressure levels are included in the general category of loads. The temperatures to be measured include internal distributions as well as skin temperatures.

3.3.2.1 Test Conditions

The flight program will consist of maneuver and gust flight programs. Flight conditions in all regions of the design V-n envelope will be investigated. Temperatures will be continuously recorded during supersonic test runs. A schedule of flight test conditions is shown in Table 3-L. Special test conditions will be flown to check sound levels at critical locations on the airplane.

Maneuver load survey test conditions are listed in Table 3-L. The test maneuvers are described as follows:

a. Roller Coaster Maneuvers

These maneuvers will be initiated from level, unaccelerated flight. A symmetrical pullup to 80 percent of design positive limit load factor will be followed by a pushover-to-zero load factor, then recovery to the initial condition. In addition to recording basic flight loads data, strain gage zero reference points will be obtained from these maneuvers. Rate of change of load factor will be approximately 0.3g per sec.

b. Windup Turns

Loads for steady maneuvers without pitch acceleration from n = 1.0 to 80 percent of the limit positive load factor will be obtained by performing steadily decreasing radius turns.

c. Symmetric Pitch Maneuvers

Beginning from level trimmed flight, abrupt pullups and pushovers will be initiated with maximum available control-surface deflection followed by checkback to neutral. In no case will this maneuver exceed 80 percent of the design limit positive or negative load factor. Horizontal stabilizer, elevator, and aftbody loads as well as airplane response characteristics will be substantiated by these maneuvers.

d. Rolling Pullouts

Loads for unsymmetric conditions will be obtained from rolling pullout conditions. The maneuver begins with a steady turn at 80 percent of the limit positive load factor for rolling conditions followed by a roll to an opposite bank angle not greater than the initial bank angle. Load factor will be maintained nearly constant. Left and right turns will be performed.

e. Yaw Maneuvers

Yaw maneuvers will be performed at n = 1.0 with lateral control surfaces deflected as necessary to prevent roll. The rudder will be initially deflected to the maximum available. After steady sideslip is obtained, the rudder will be abruptly returned to neutral. Vertical tail, rudder, and aftbody loads will be obtained.

f. Unsymmetric Thrust Conditions

Various unsymmetric thrust conditions, including critical engine at idle power, will be performed to verify calculated empennage loads and airplane response characteristics.

g. Wing-Sweep Transition Conditions

Actuator and wing loads will be measured during steady unaccelerated flight at specified airplane airspeeds and angles of attack while the wings are being swept through the entire range.

h. Transient-Temperature Check Conditions

Conditions simulating typical mission climb, cruise, and descent from cruise as well as various upset maneuvers from cruise Mach number will be performed to check transient temperature effects.

Gust load survey flight conditions are listed in Table 3-L. Test conditions will be run with the autopilot on and off. During autopilot-off tests, only slow corrections for major flight-path variations will be made. Temperatures will be continuously recorded during supersonic test runs. Sustained turbulence records will be sought wherever possible; however discrete gust encounters will be sought as well. The data obtained relating to continuous turbulence will provide material for comparison with theoretical power spectral results. Data gathered from flight through discrete turbulence will enable correlation with results from discrete gust analysis.

The dynamic ground loads program will include landing impact tests at sink speeds up to 7 fps with no appreciable crosswind. Crosswind landings will be made at reduced sink speeds. Accelerations and structural loads will be measured for correlation with predicted values. Wings-aft landing capability will be demonstrated initially at a remote base (Edwards AFB) and later at an

Table 3-L Flight Survey Test Conditions

Test Description	Configuration	Wing LE Sweep (deg)	Altitude x 10^{-3} (ft)	Speed Range	Limit Load Factor Range
Maneuver Load and Temperature Survey					
Pressure distributions on flaps and slats and basic load distribution	Takeoff, climb, approach, and landing	30	10	To 0.9 x flap placards	0.4 to 1.6
	Climb and maneuver	42	10	$M \leq 0.45$	0.4 to 2.0
	Holding	30	10	$M \leq 0.45$	0.4 to 2.0
	Emergency descent and landing	72	10	$M \leq 0.45$	0.4 to 2.0
Basic load and temperature distributions	Wing-sweep transition	30 to 42	10	$V_e \leq 290$ kn	1.0
		42 to 72	10	$V_e \leq 350$ kn	1.0
		72 to 42	10	$V_e \leq 350$ kn	1.0
		42 to 30	10	$V_e \leq 290$ kn	1.0
	Clean	42	10	$V_e \leq 438$ kn	0 to 2.0
		42	25	$M \leq 0.95$	0 to 2.0
		72	10	$V_e \leq 469$ kn	0 to 2.0
		72	25	$V_e \leq 492$ kn	0 to 2.0
		72	42.5	$V_e \leq 620$ kn	0 to 2.0
		72	61	$M \leq 2.90$	
Gust Load Survey					
Gust load response	Clean	42	10	$V_e \leq 350$ kn	$1.0 \pm \Delta n_g$
		42	25	$M \leq 0.90$	$1.0 \pm \Delta n_g$
		72	10	$V_e \leq 375$ kn	$1.0 \pm \Delta n_g$
		72	25	$V_e \leq 383$ kn	$1.0 \pm \Delta n_g$
		72	42.5	$V_e \leq 475$ kn	$1.0 \pm \Delta n_g$
		72	61	$M \leq 2.70$	$1.0 \pm \Delta n_g$
Acoustic Level Survey					
Noise levels	Takeoff	30	0	$V_e = 200$ kn	1.0
	Clean	42	10 to 18	$V_e = V_D$	1.0
		72	12.5 to 25	$V_e = V_D$	1.0
		72	42.5	$V_e = 620$ kn	1.0

international airport. Otherwise, all landing tests will be in the normal landing configuration. In addition, taxi, takeoff, and landing rollout runs at various airplane weights and speeds will be made. These particular tests will verify that the airplane has satisfactory ride and steering qualities.

A noise level survey test with various symmetric thrust settings will be flown to check noise levels. These conditions are listed in Table 3-L.

3.3.2.2 Data Requirements
The raw data measured in flight test will be consistent in quality with the objectives of the program. The final reduced data that are required for loads and temperature verification are outlined as follows:

a. General

- Airspeed
- Mach number
- Pressure altitude
- Outside air temperature
- Stagnation temperature
- Gust velocity and direction
- Angles of attack, sideslip, and bank
- Pitch, roll, and yaw rates
- Control forces (pilot's)
- High-lift and control-surface positions
- Throttle settings
- Accelerations at several body, wing, tail stations, and engine locations
- Gear position
- Droop nose position
- Gross weight, fuel distribution, and center of gravity
- Wing sweep position
- Time correlation and event marker

b. Loads

(1) Wing

- Beam shear, moment, and torsion at several stations on the left wing and one station on the right wing
- Left-wing pivot beam and chord loads during holding and actuation
- Left-wing actuator loads
- Control-surface actuator loads
- Flap and slat pressure distribution
- Flap and slat attachment and actuator loads
- Left wing strake to fuselage-junction vertical shear and moment distributions
- Some wing and strake surface pressures

(2) Horizontal Tail

- Vertical shear, moment, and torsion at several stations on left side and one station on right side
- Elevator and elevon actuator and attachment loads

(3) Vertical Tail

- Beam shear, moment, and torsion at several spanwise stations
- Rudder actuator and attachment loads

(4) Fuselage

- Vertical and lateral shear and moment at several stations on forward fuselage
- Vertical shear, lateral shear, vertical moment, lateral moment, and torsion at several stations on aftbody
- Nose-boom gust angle of attack

(5) Propulsion Pod

- Vertical and lateral load, pitching moment, and yawing moment on each left side pod

- Internal and external pressures on inlet and pod
- Variable inlet actuator load and position

(6) Miscellaneous

- Wing-tail interconnect loads
- Airspace cavity pressures
- Landing gear and actuator loads
- Landing-gear door pressures

c. Temperatures

Structural temperature requirements for supersonic test conditions during the maneuver and gust load surveys in general coincide with the foregoing load requirements. Thermosensitive paint will be used to survey potentially critical areas. Sufficient thermocouple recordings will be provided to verify the design temperatures. Temperature measurements will be obtained for the long-cruise, steady-state conditions, as well as for climb and descent gradient conditions. Airspace cavities throughout the airplane will be instrumented with thermocouples.

d. Noise Levels

Sound measurements will be made with sufficient density of instrumentation so that acoustic pressure contour maps can be substantiated. Sound generated aerodynamically and by the engines are of interest.

3.3.2.3 Instrumentation

Flight loads will be measured using a combination of pressure transducers and fully calibrated strain gages.

Temperature measurements will be made with thermocouples and temperature indicating paints, which will be placed at each load measurement station and at other locations of interest.

Sound measurements will be obtained by remote pickups through orifices drilled through the outer skin.

3.3.2.4 Calibration

Load measuring strain gages will be calibrated by determining responses to applied calibration loads. The technique outlined in Ref. 3-8 will be used. Maximum calibration loads will correspond to loads expected to occur during flight load survey. Pressure transducers will be calibrated by applying a known pressure and reading the response. All instrumentation will be temperature compensated.

Concurrent with the strain gage calibration, a check on structural flexibility influence coefficients will be made. The results will be compared with theoretically determined coefficients used in design. This effort will require a very accurate method of determining structural slopes and deflections and very accurate measurement of the applied loads.

3.3.2.5 Data Reduction and Presentation

In general, flight recordings will be made of basic instrument responses, and conversion to time-correlated load data by digital computer processing will be performed at the ground station. Ground station equipment will be capable of producing strip charts to allow on-the-spot monitoring of the data.

Load data for gust load survey conditions will be presented as peak count and cycle count summaries.

3.3.3 Airload Distribution

A measure of the accuracy of the theoretical load distribution method described in Par. 3.2.1 is illustrated by comparing theoretical-versus-experimental wing-span load distribution for wind-tunnel pressure model tests conducted during Phase II. The two model tests are described in Par. 3.3.3.1, and the comparison with theory is presented in Par. 3.3.3.2.

3.3.3.1 Pressure Model and Test Description

The TA 569P-1 model, shown in Fig. 3-68, was tested in the Boeing Transonic Wind Tunnel (BTWT 871) in November 1964. The variable-sweep model is 0.038 scale and contains 218 pressure taps, 152 on the wing and 66 on the strake. The test included Mach numbers from 0.4 to 0.93, angles of attack between -7 to +19 deg, and wing sweep positions of 15 through 74 deg. The configurations tested included upper- and lower-surface spoilers fully deflected. Model pressure distributions and total model force data were taken.

The TA 885P-1 model shown in Fig. 3-69 was tested in the Ames Unitary Wind Tunnel in August 1965. The fixed wing (Λ_{LE} = 72 deg), 0.032-scale model of the 733-290 proposal configuration contains 335 pressure taps: 172 on the wing, 103

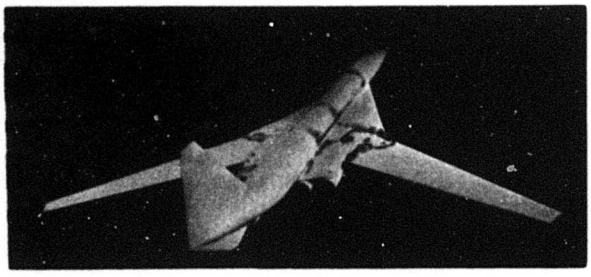

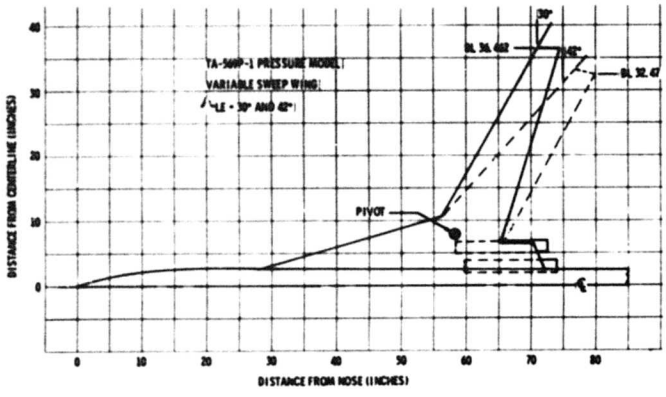

Figure 3-68. TA-569P-1 Pressure Model

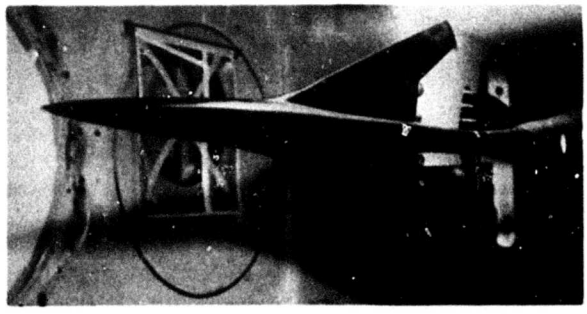

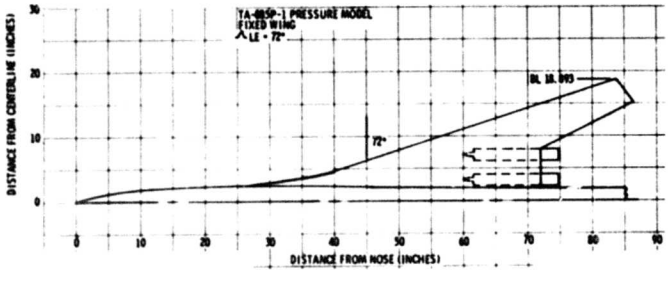

Figure 3-69. TA-885P-1 Pressure Model

on the strake, and 60 on the body. The test covered the Mach number range of 0.60 to 3.2 in the three legs of the Ames Unitary Wind Tunnel. The symmetric flight angle-of-attack range was -9 to +19 deg; side-slip angles of +5 and -5 deg were tested for an angle-of-attack range of -1 to +15 deg. Spoiler deflections of one half and full were tested over a reduced Mach number series. Model pressure distributions, as well as tail and nacelle force data, were recorded.

3.3.3.2 Comparison of Theory and Experiment Comparisons of theoretical and experimental normal force distribution (CC_N) and pitching moment distribution ($C^2C_{M_{LE}}$) along the wing semispan are shown in Figs. 3-70 through 3-77. The wing forward (30-deg sweep) and wing-intermediate (42-deg sweep) configurations are analyzed at subsonic Mach numbers using the TA-569P1

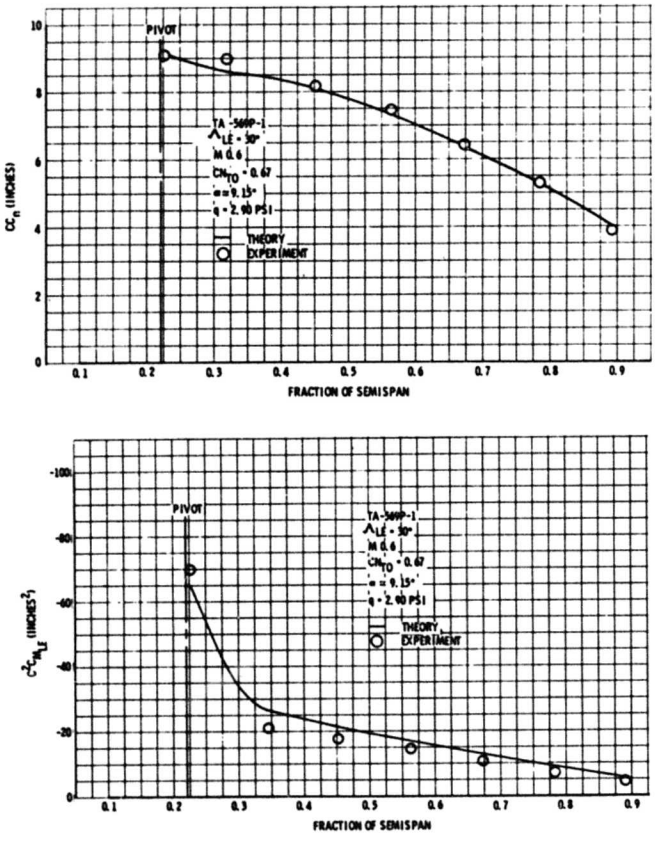

Figure 3-70. Model TA-569P-1, Airload Distribution, 30-Degree Wing Leading-Edge Sweep

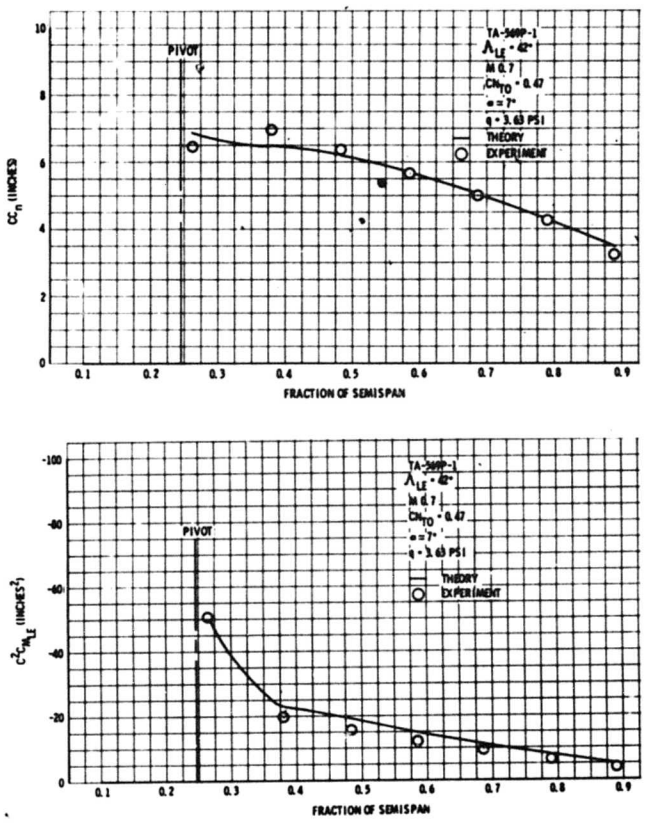

Figure 3-71. Model TA-569P-1, Airload Distribution, 42-Degree Wing Leading-Edge Sweep

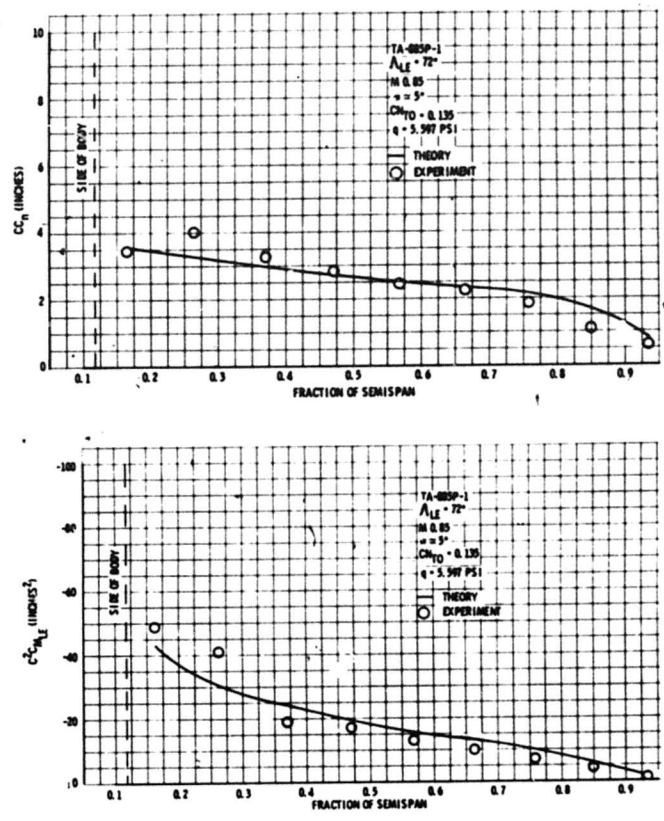

Figure 3-72. Model TA-885P-1, Airload Distribution Subsonic Low Angle

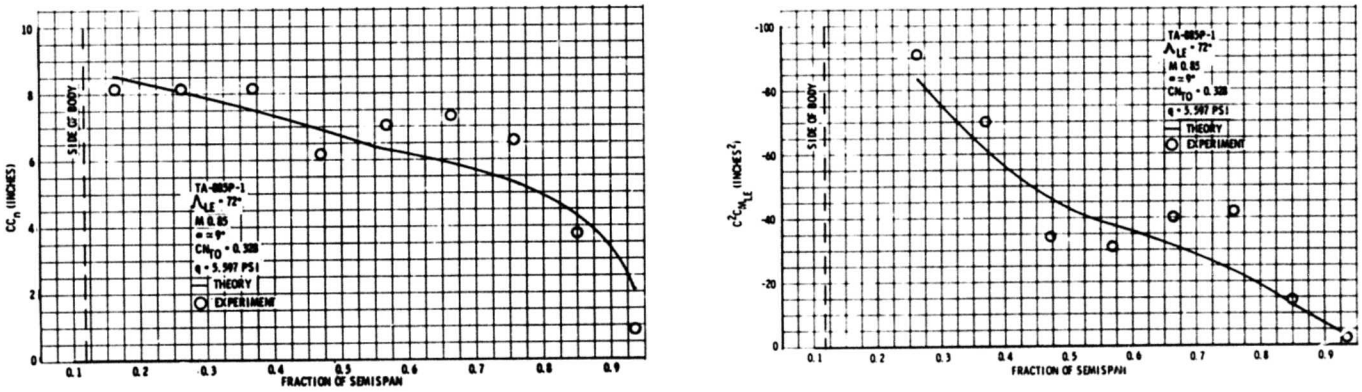

Figure 3-73. Model TA-885P-1, Airload Distribution Subsonic High Angle

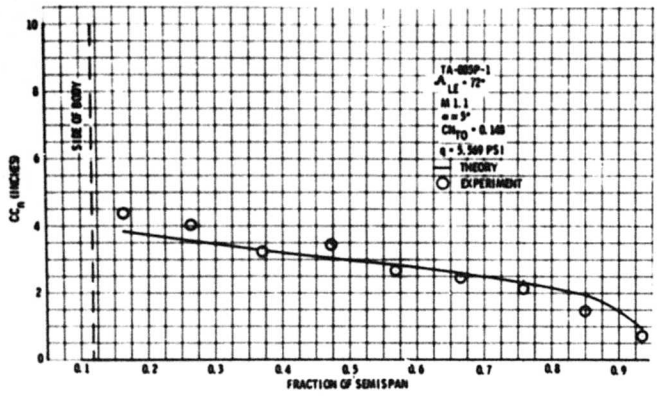

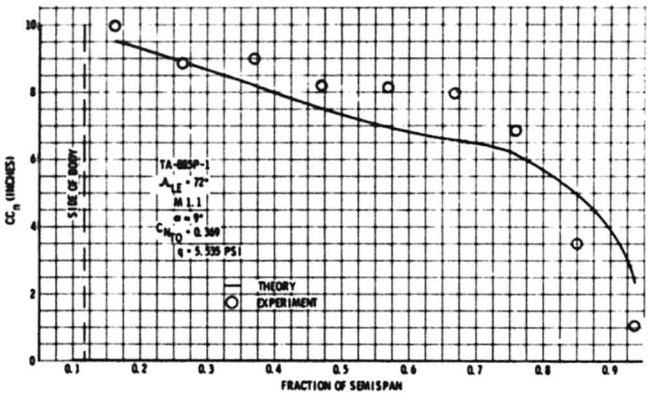

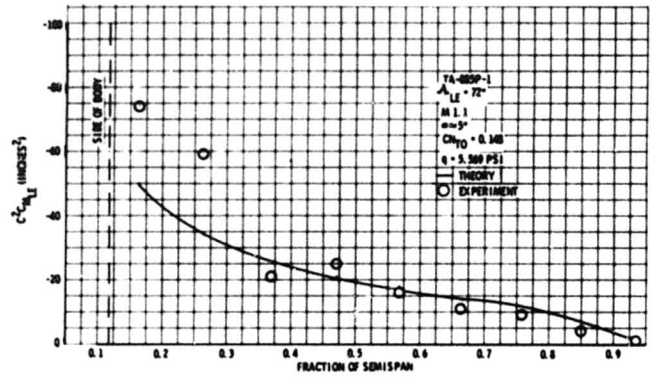

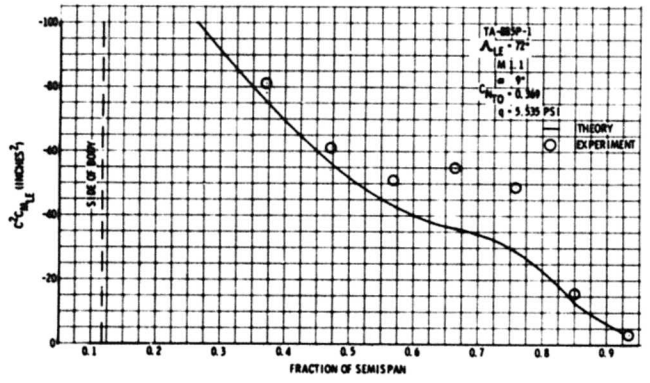

Figure 3-74. Model TA-885P-1, Airload Distribution Transonic Low Angle

Figure 3-75. Model TA-885P-1, Airload Distribution, Transonic High Angle

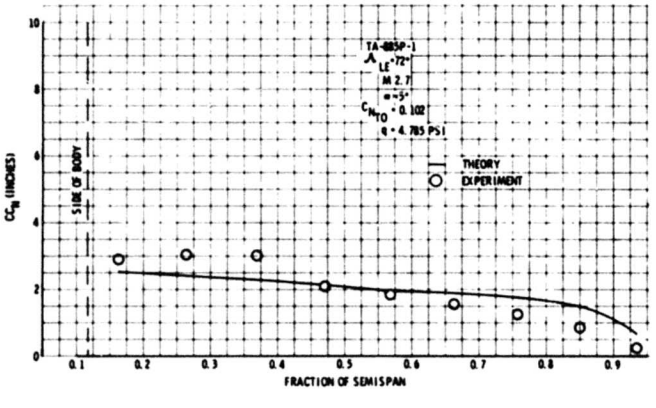

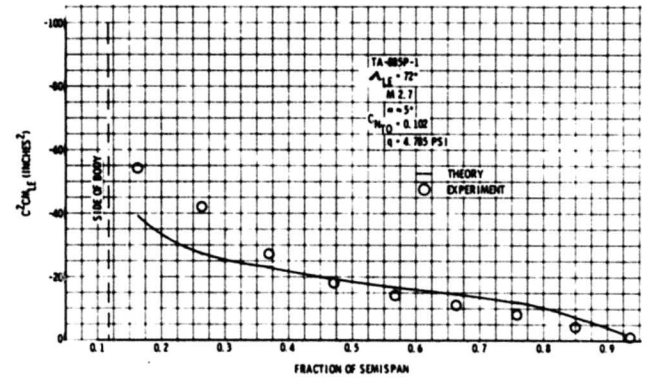

Figure 3-76. Model TA-885P-1, Airload Distribution, Supersonic Low Angle

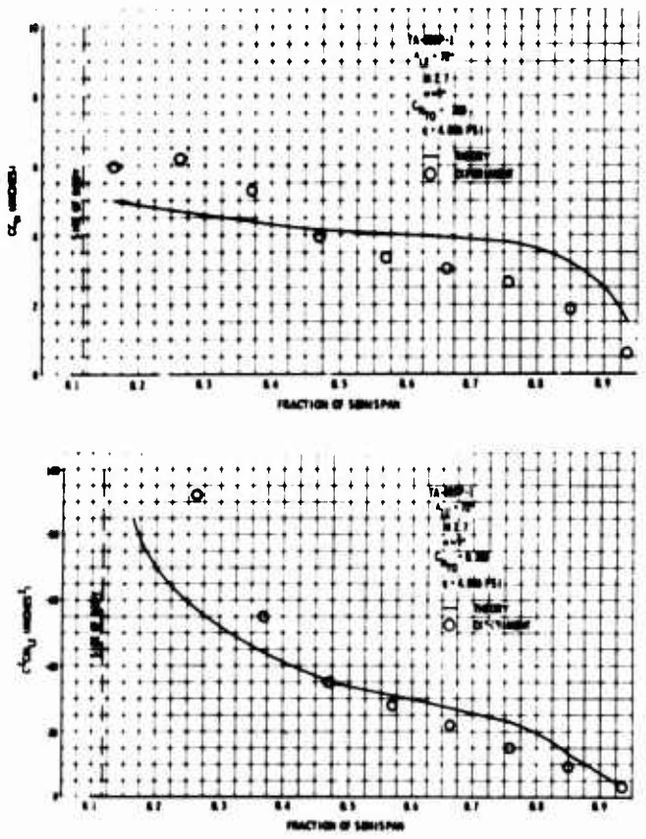

Figure 3-77. Model TA-885P-1, Airload Distribution, Supersonic High Angle

variable-sweep pressure model for comparison. The wing-aft (72-deg sweep) configuration is analyzed at subsonic, transonic, and high-supersonic Mach numbers, using the TA-885P1 fixed-wing pressure model for comparison. In each case the theoretical and experimental total tail-off lift coefficients ($C_{N_{to}}$) are equalized.

The comparisons indicate that the theoretical method matches the experimental data in the low-angle-of-attack range. Where these comparisons show disagreement, theoretical results produce conservative loadings. Deviations are attributed to nonlinear flow.

3.4 RIDE COMFORT

The effect of the loads (outlined in Par. 3.3.2.2) on passenger ride comfort and on the ability of the crew to perform the assigned mission is discussed in the following paragraphs under the separate but related topics of turbulence-induced acceleration environment and the resulting subjective response to this environment.

3.4.1 Acceleration Environment

Figure 3-78 compares estimated acceleration levels for the B-2707 relative to the B-70 and B-58 airplanes. The B-70 and B-58 data shown are for side-by-side gust exposure at the same airspeed and clearly support the rough-ride experience reported for the B-70. By comparison, the B-2707 estimates are shown to be more favorable for the 72-deg wing sweep position than for even the smooth-riding B-58. In the 42-deg wing position, the B-2707 estimate is shown to approach (but remain less than) the Model 707 estimate, although exceeding the B-58 ride level. Partial confirmation of the foregoing comparisons

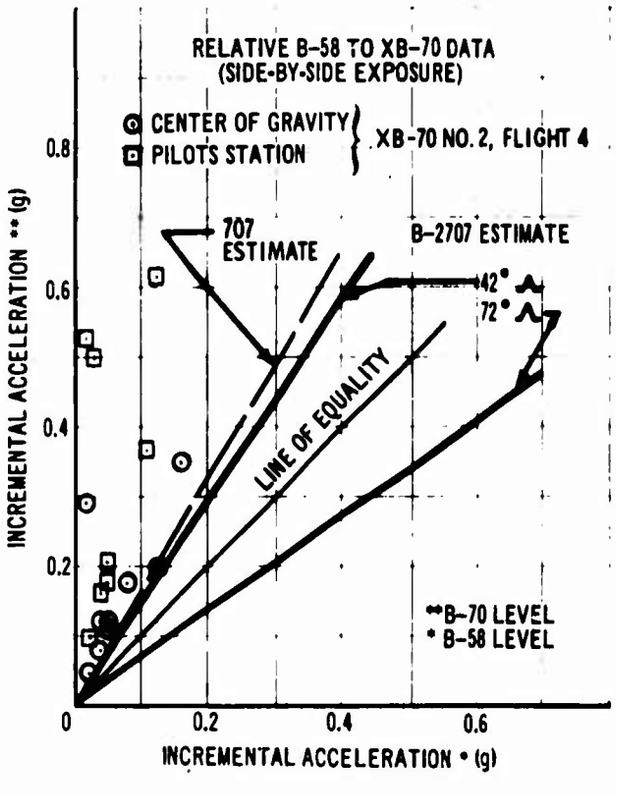

Figure 3-78. Relative Response to Turbulence of B-2707

are offered by Fig. 3-79, which shows the product of lift curve slope (C_{L_α}) and reference area (S_{REF}) for the B-2707 and a typical delta SST configuration. This sort of comparison assumes a common airspeed but does illustrate the greater advantage of increased wing sweep.

In view of the greater B-70 fuselage flexibility relative to previous airplanes and the even greater fuselage flexibility for the B-2707, an understanding of the higher incremental gust accelerations recorded for the B-70 is desirable. Coordination with FAA, NASA, and NAA is presently underway in order to develop a full understanding of the B-70 ride. Continuation of the B-70 program is expected to provide the necessary understanding; however a reasonable explanation would appear to lie in structural excitation by the canard lifting surface in response to direct gust inputs to the canard. Such excitation feeds forward to the crew compartment very readily but also feeds rearward to the airplane center of gravity due to the somewhat aft canard location. This explanation is consistent with the B-70 acceleration data shown in Fig. 3-78 for both pilot's station and center of gravity.

Low damping in the third elastic mode may well contribute to the higher B-70 accelerations. As shown in Fig. 3-80, the B-70 third elastic mode consists of a forebody nodding motion and hardly any lifting surface motion (i.e. aerodynamic damping). In contrast, it is of interest to note that the B-2707 modes (Fig. 3-81) all show substantial amounts of lifting surface motion, and thus, all possess favorable damping levels. It is also of interest to note that increased flexibility alone would not be expected to increase the acceleration environment since the increased fuselage deflection associated with greater flexibility is offset heavily by reduction in body-bending frequency. Additional B-70 testing is expected to support this overall view. It should be noted from the specific data shown in Fig. 3-78 that only mild turbulence encounters are involved in the B-70 and B-58 data shown; that is, the B-58 level is under 0.2g incremental.

Airframe flexibility effects on acceleration environment are provided by Figs. 3-82 and 3-83.

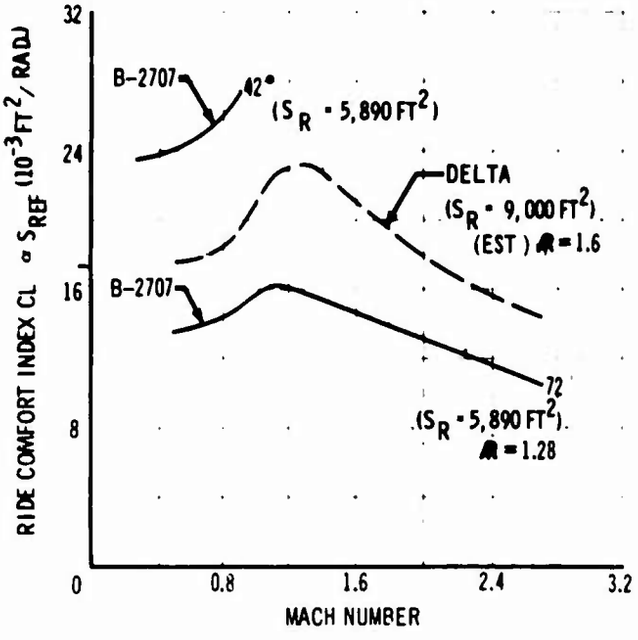

Figure 3-79. Relative Ride Qualities of B-2707 and Typical Delta Configuration

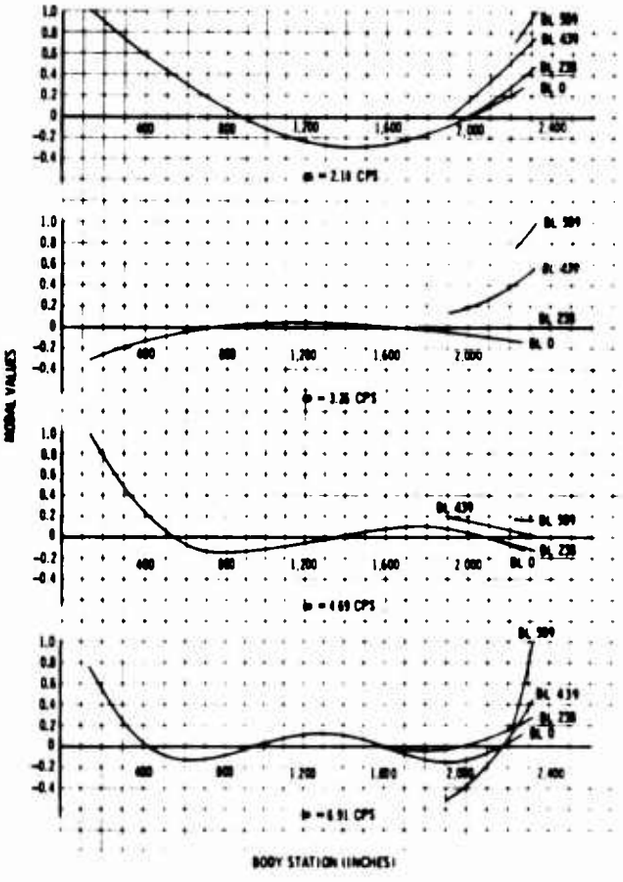

Figure 3-80. Natural Vibration Characteristics, XB-70 (Light Weight Condition)

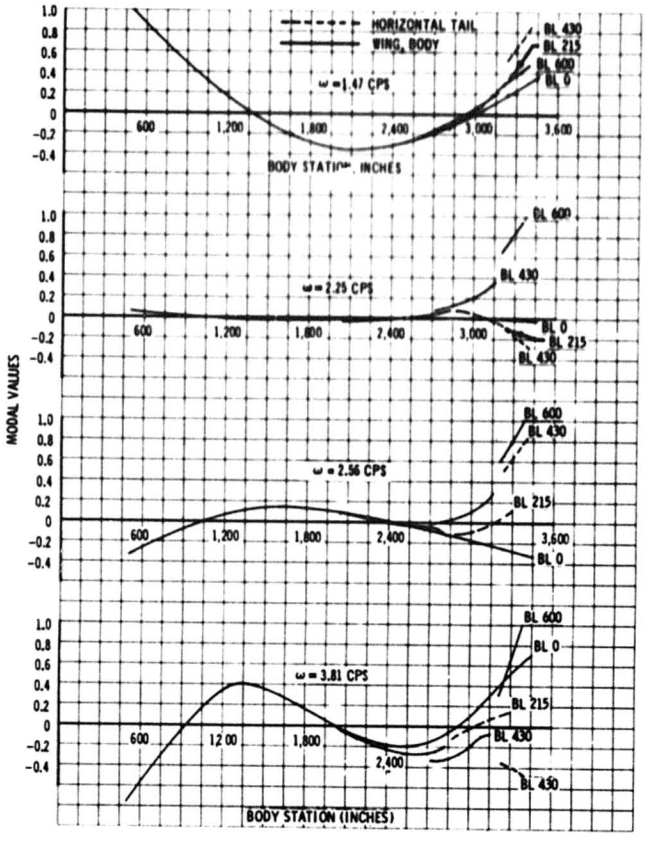

Figure 3-81. Natural Vibration Characteristics, B-2707 (Light Weight Condition)

Figure 3-82 shows the variation in acceleration level along the fuselage from nose to tail based on power spectral analyses along the representative trip profile shown in Fig. 3-84. Flexibility is shown to increase acceleration levels primarily in the forward fuselage; much of the passenger area shows a relatively similar environment. The climb and descent environments approach the 707 environment but a very much improved environment is indicated for supersonic cruise due to the favorable effect of wing sweep on lift sensitivity and the reduction in basic gust environment at high altitudes. Figure 3-83 compares total trip exposure for the B-2707 and 707 airplanes. The B-2707 is shown to have a significantly lower acceleration environment on this overall statistical basis as well.

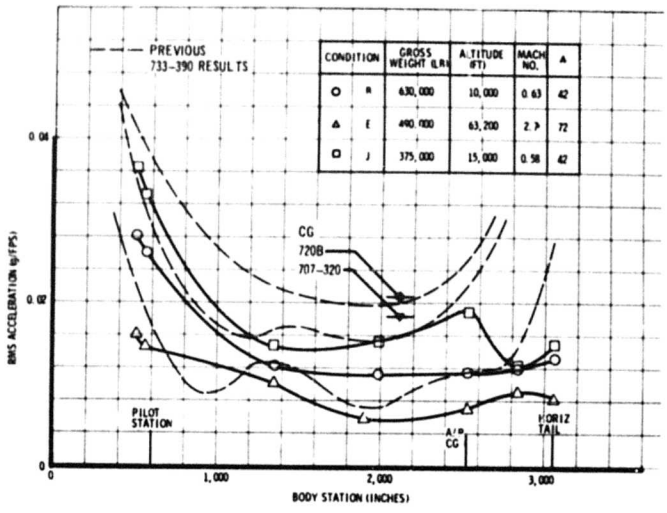

Figure 3-82. Relative Acceleration Environment Along the Fuselage (B-2707)

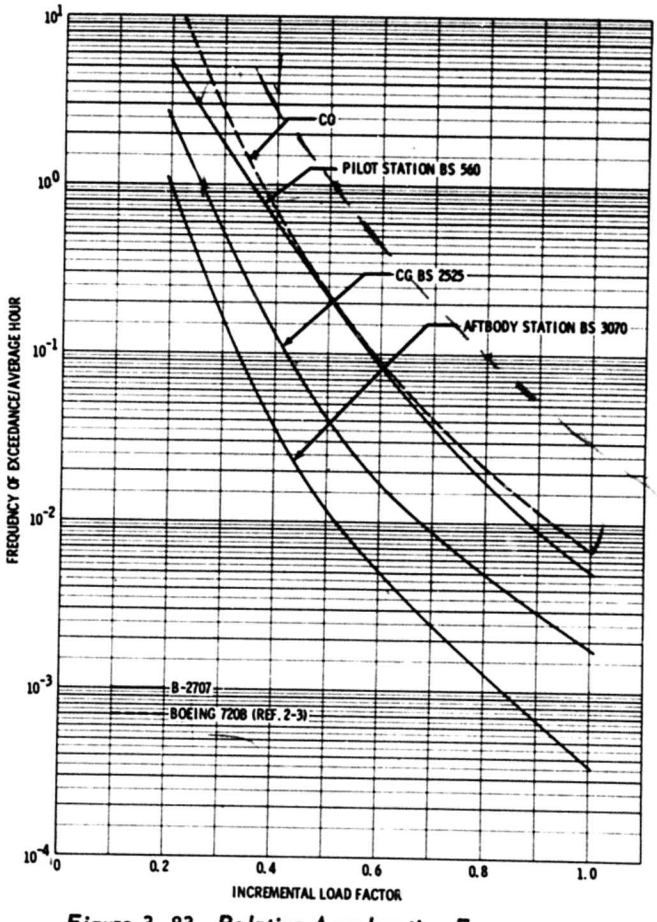

Figure 3-83. Relative Acceleration Exposure, Entire Trip

Representative transfer functions at the pilot's station, airplane center of gravity, and most rearward passenger station are shown in Fig. 3-85 for wings aft with SAS fully effective. Corresponding output spectrum for the same conditions is shown in Fig. 3-86. This display more clearly emphasizes the relative role played by airplane pitching and airframe elasticity on the acceleration environment at the various fuselage stations. Elasticity is shown to have a relatively greater effect in the forward fuselage than in the aftbody.

3.4.2 Subjective Response

The increased airframe flexibility of the B-2707 will provide a considerably improved ride for both flight crew and passengers when compared to present subsonic jet transports subjected to the same gust environment. This appraisal is well supported by the comparative simulator study conducted in January 1965 on the NASA-Ames Height Control Apparatus (Fig. 3-87). Experienced pilots (Boeing, NASA, and FAA) were subjected to both a representative SST simulation and a typical subsonic jet simulation and asked to comment on the relative disturbance associated with the elastic frequencies. The opinion was unanimous in favor of the SST because of the less disturbing influence of the lower SST fuselage frequency. While elastic motions were larger for the SST, the motions remained small enough so that acceleration environment was the predominant factor; the motion-sickness level was not approached.

The foregoing simulator findings are also supported by Fig. 3-88, which shows human reaction to sinusoidal accelerations at varying frequency as obtained from laboratory testing. As shown, tolerance of acceleration exposure is greater for 1 cps (the approximate lowest B-2707 fuselage bending frequency) than for 4 cps (a typical subsonic jet fuselage bending frequency). The simulator evaluation was based on a gust environment having randomness shaped to power spectral form rather than based on sinusoidal gusts of varying

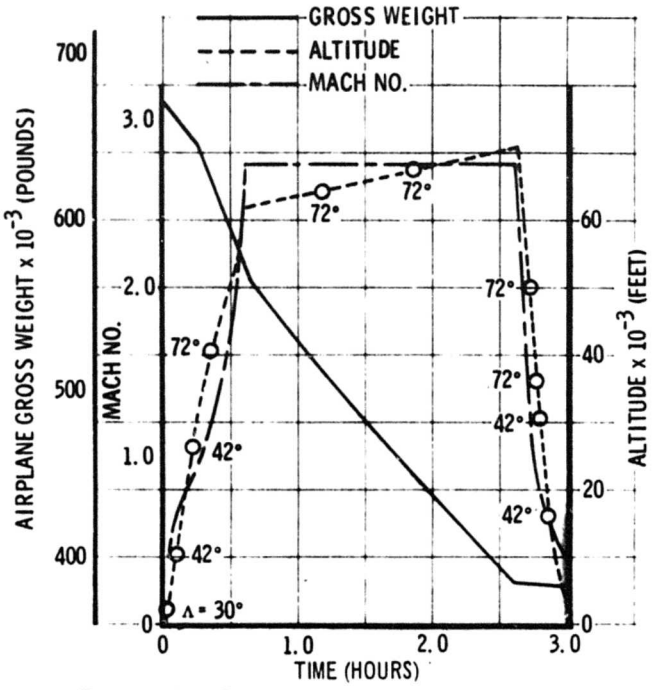

Figure 3-84. Representative Trip Profile (B-2707)

frequencies. It is interesting to note that the simulator evaluation displayed the same trend of structural frequency change in the 1- to 4-cps region as exhibited by the sinusoidal data presented in Fig. 3-88.

Additional moving-base simulator studies are planned for Phase III to further investigate elastic frequency effects. These additional studies will investigate the possible effects of low damping in elastic modes and possible methods to improve damping if significant effects prove to exist. Wichita flight test programs presently being performed on the B-52 under Air Force Contracts AF 34(615)-3753, Load Alleviation and Mode Stabilization Program, and AF 34(601)-25146, Stability Augmentation System for Improved B-52 Structural Life, are expected to provide early information on the feasibility of structural damping augmentation.

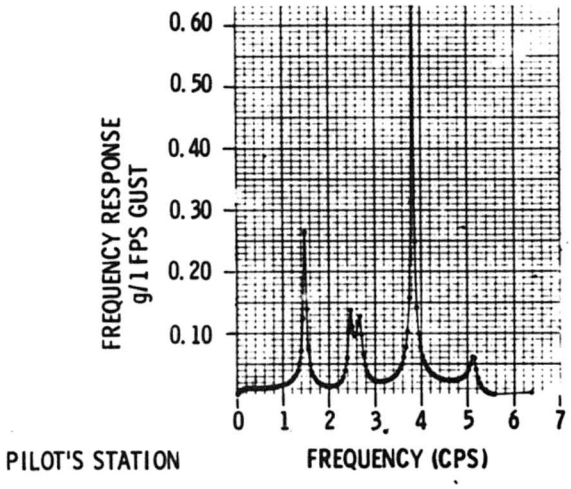

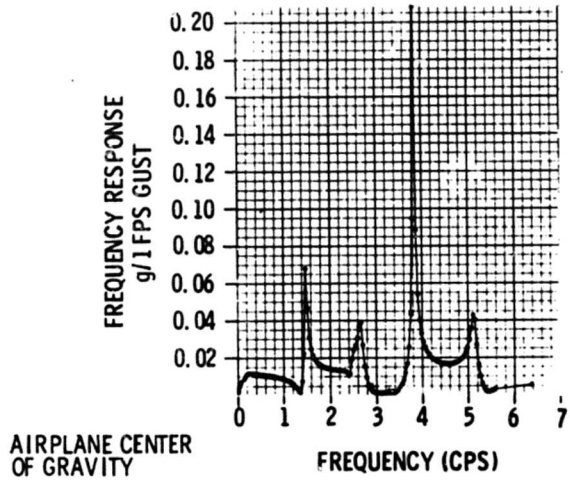

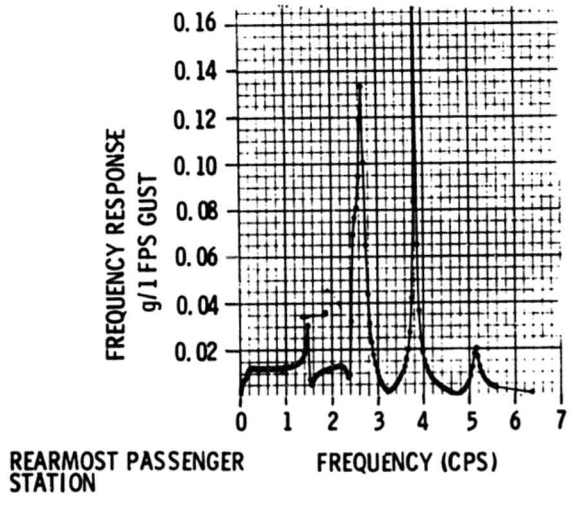

Figure 3-85. Representative Acceleration Transfer Functions

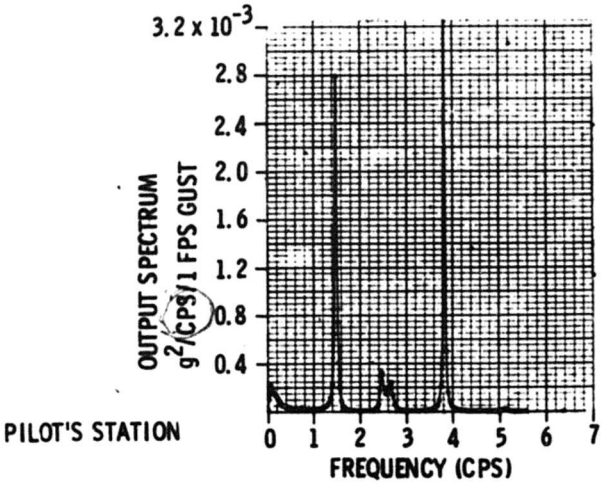

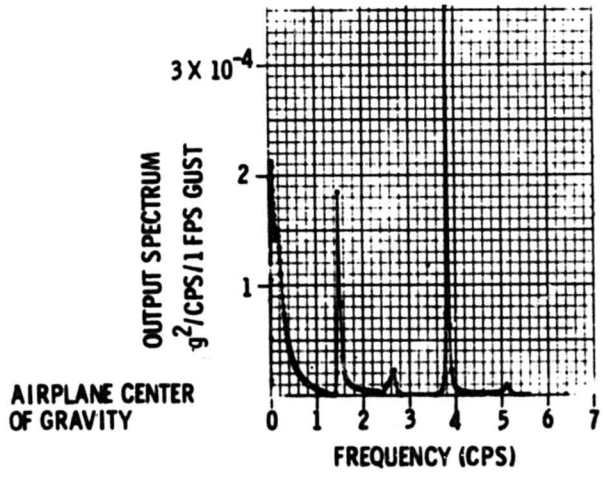

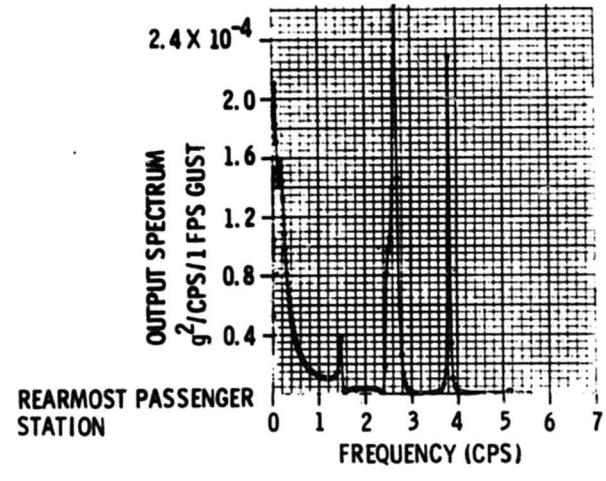

Figure 3-86. Representative Acceleration Output Spectra

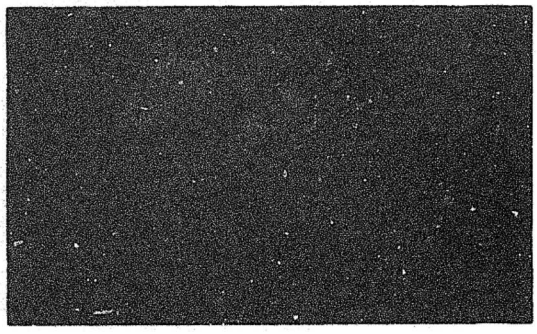

EXTERIOR VIEW

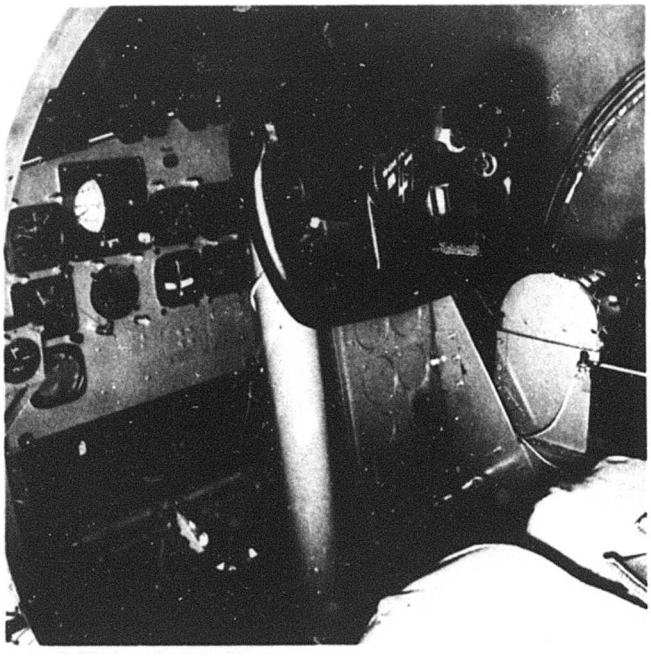

INTERIOR VIEW

Figure 3-87. NASA-Ames Height Control Apparatus

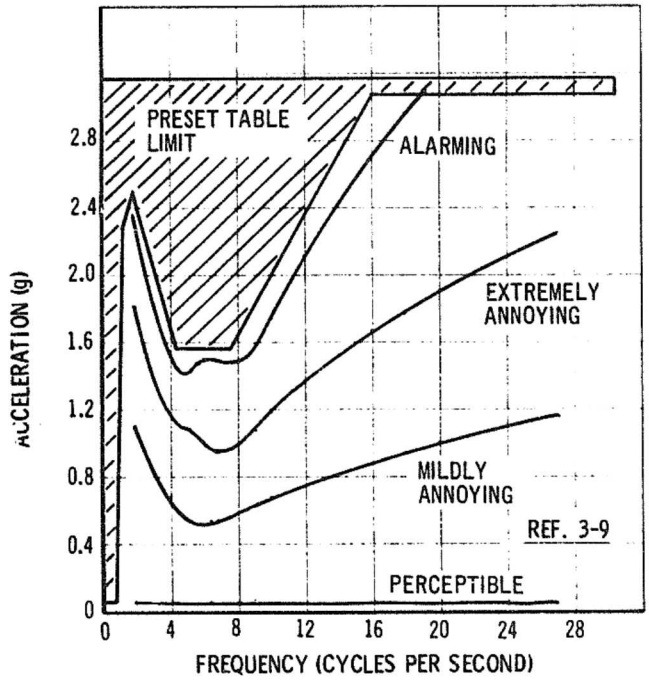

Figure 3-88. Subjective Human Vibration Response Curves (Medians)

Removed from Vol 8

5.0 FLUTTER

Subsonic and supersonic flutter analyses and subsonic wind-tunnel flutter tests of the complete airplane have been accomplished. These investigations have been supported by extensive parametric flutter studies of major components. Figures 5-1 and 5-2 present airplane flutter boundaries for the 42-deg and 72-deg wing sweep positions based on minimum envelopes developed from a composite of complete-airplane and parametric study data. The B-2707 airplane meets the 1.2 V_D design goal for flutter at 42 deg and with the wing locked at 72 deg. During the interval of sweeping the wing from 42 deg to 72 deg, and until the wing and horizontal tail are locked, the speed envelope of 42 deg should be observed.

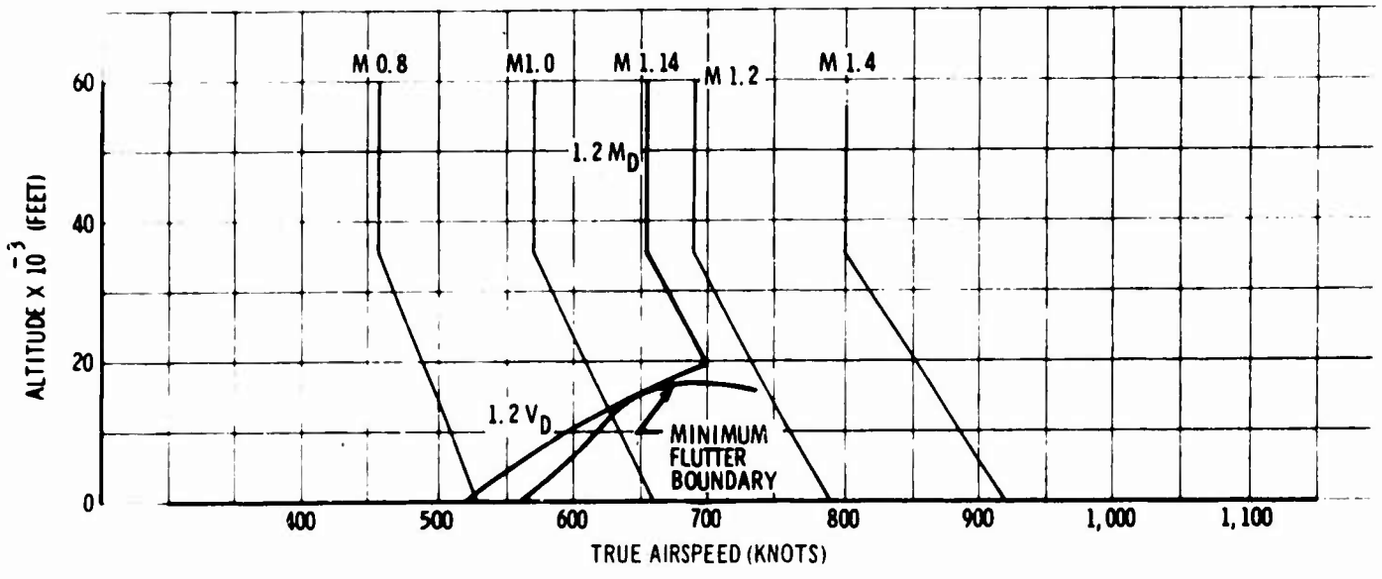

Figure 5-1. Minimum Flutter Boundary, Complete Airplane, 42-Degree Wing Leading-Edge Sweep

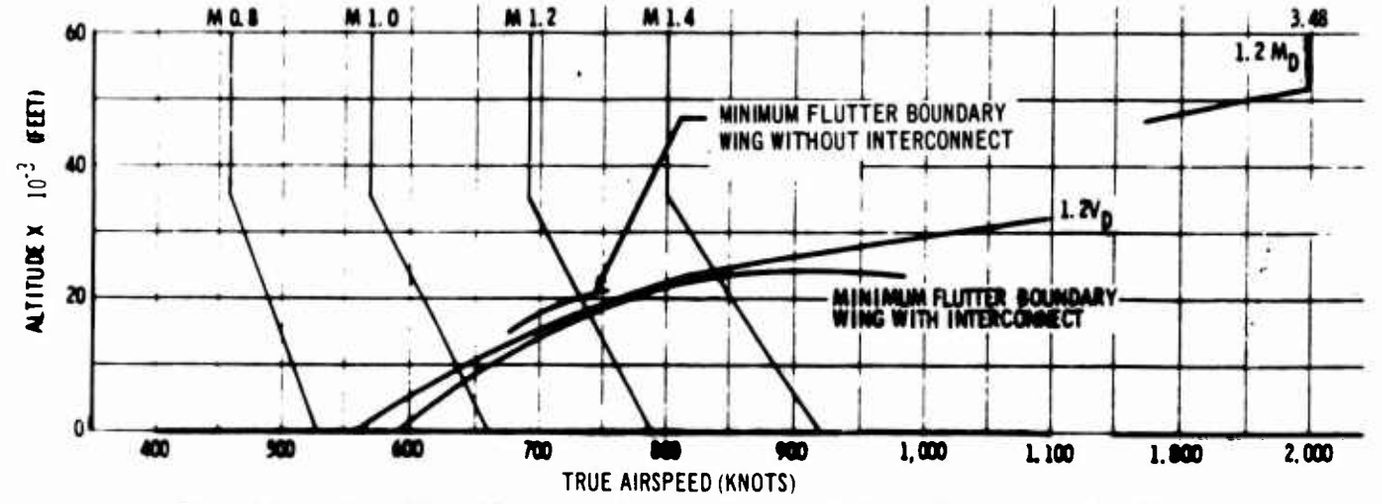

Figure 5-2. Minimum Flutter Boundaries, Complete Airplane, 72-Degree Wing Leading-Edge Sweep

5.1 COMPLETE AIRPLANE

Flutter analyses and wind-tunnel tests of the complete airplane were conducted for the subsonic speed regime. In addition, flutter analyses have been made for the supersonic case. Summary results are shown in Figs. 5-3 and 5-4. Analytical results are indicated by continuous lines; test points are scaled to airplane values from the wind-tunnel model data. Satisfactory speed margins are indicated throughout the operational altitude range.

5.1.1 Computer Analysis

The analyses were conducted for the operating-empty-weight condition since previous wing analyses and wind tunnel tests have shown it to be the most critical condition. Symmetrical and antisymmetrical flutter conditions were analyzed for 42-deg wing sweep subsonically and both 42- and 72-deg wing sweep supersonically. Analyses are of the modal type. The symmetric cases contain 19 deg of freedom: 4 fuselage vertical bending, 4 wing bending, 3 wing torsion, 3 stabilizer bending, 3 stabilizer torsion, and rigid-airplane vertical translation and pitch modes. The antisymmetric cases contain 28 deg of freedom: 5 fuselage side bending, 3 fuselage torsion, 4 wing bending, 3 wing torsion, 3 stabilizer bending 3 stabilizer torsion, 2 fin bending, 2 fin torsion, and rigid-airplane side translation, yaw, and roll modes. In determining the degrees of freedom to be included in the analyses, a cutoff frequency of 13 cps was chosen above which little or no participation could be expected in any potentially serious flutter mode. All modes having frequencies below this value were then included. The elastic

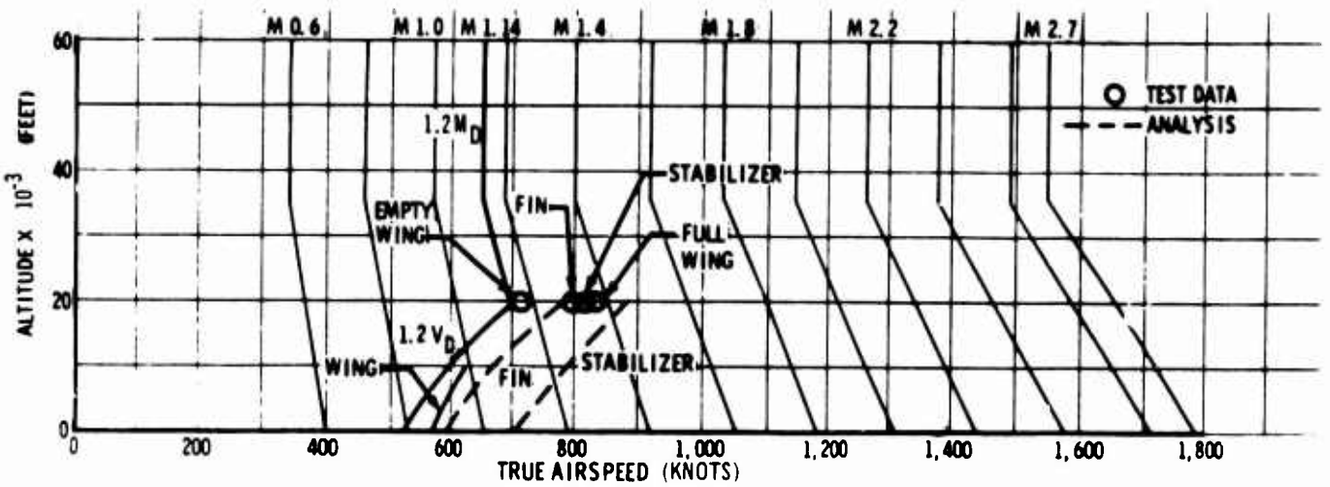

Figure 5-3. Flutter Speed Summary, 42-Degree Wing Leading-Edge Sweep

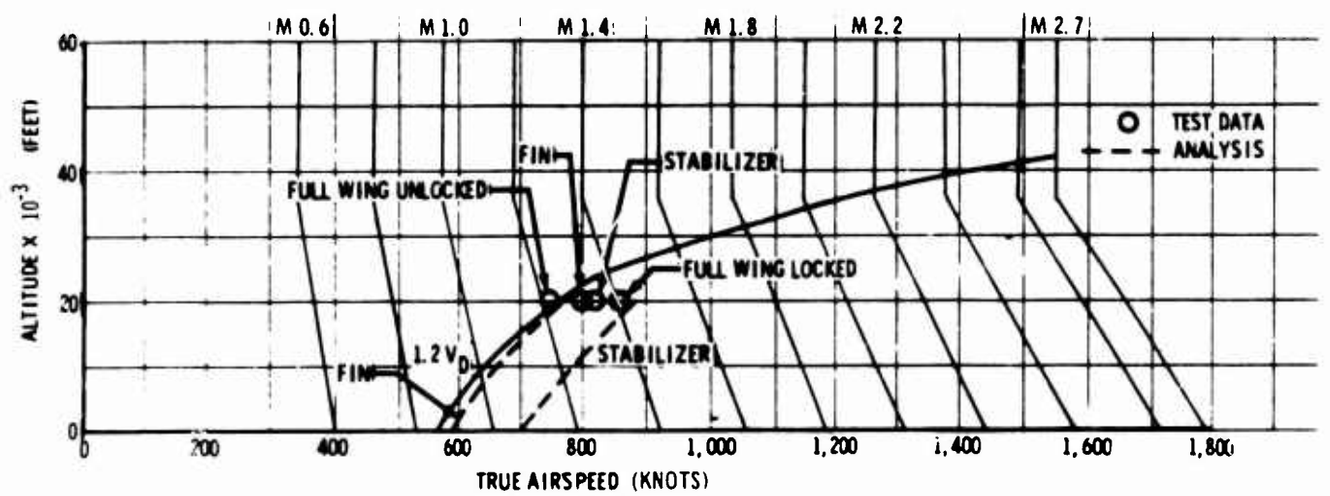

Figure 5-4. Flutter Speed Summary, 72-Degree Wing Leading Edge Sweep

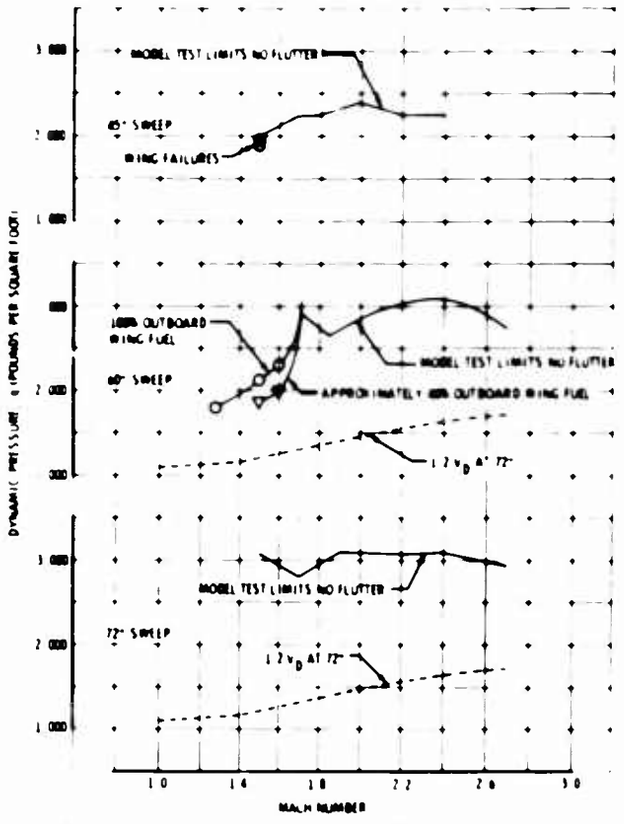

Figure 5-32. Supersonic Wing Flutter Test Data November 1965

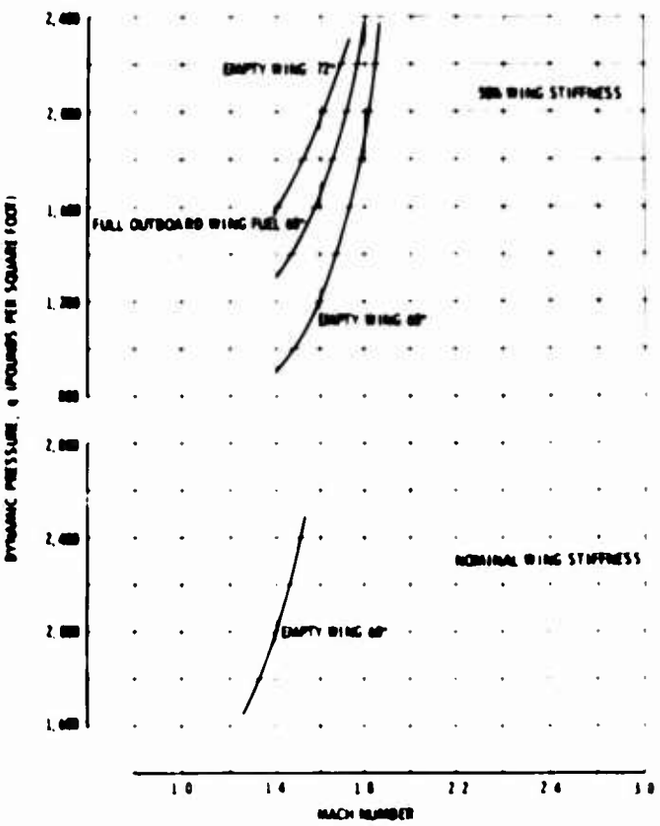

Figure 5-33. Supersonic Wing Flutter Test Data April 1966

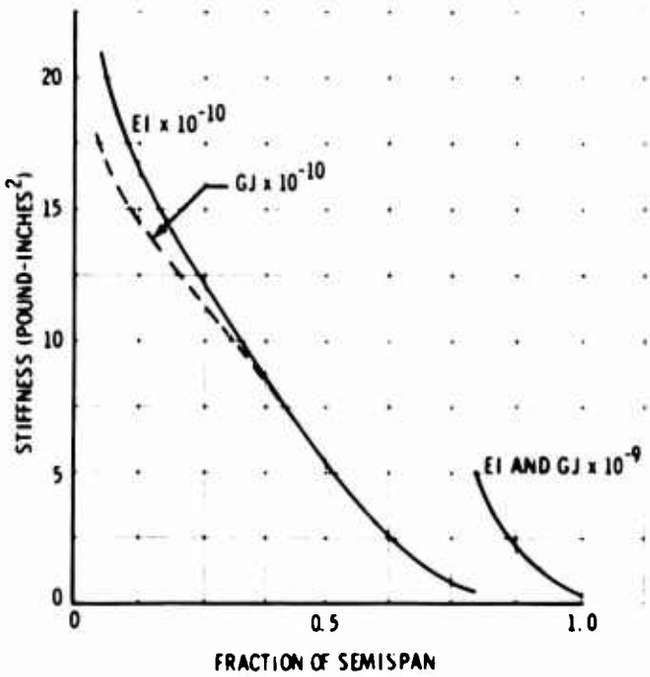

Figure 5-34. B-2707 Horizontal-Tail Stiffness

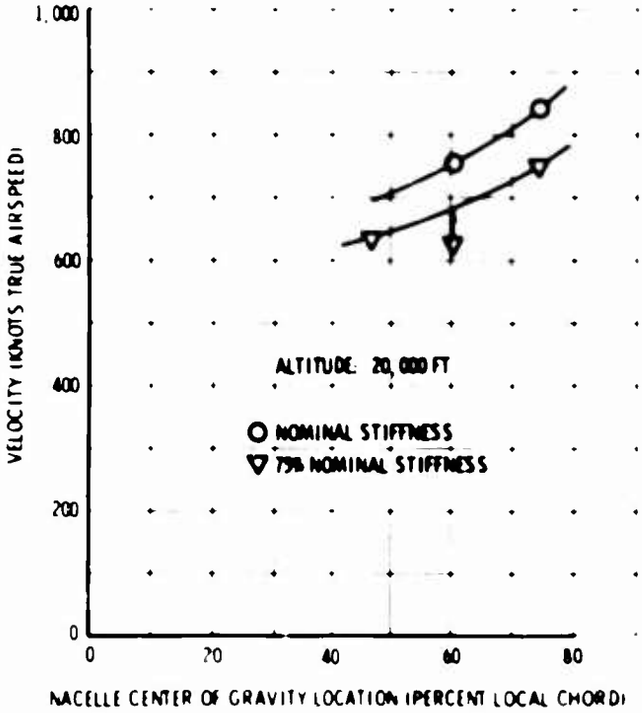

Figure 5-35. Semispan Horizontal-Tail Test Speeds

Table 5-A. Engine-Mounted Horizontal-Tail Configuration Comparison

Configuration	LE Sweep (deg)	Aspect Ratio	Area (sq ft)	Taper Ratio	Outboard Engine CG Location	
					% Local Chord	% Span
-461C	60	1.92	2,478	0.224	49.2	64.3
-467D	60	2.11	2,356	0.173	68.2	59.1
B-2707	55 inbd and 60 outbd	2.60	3,125	0.136	68.3 (P&WA)	56.0 (P&WA)
					53.6 (GE)	55.6 (GE)

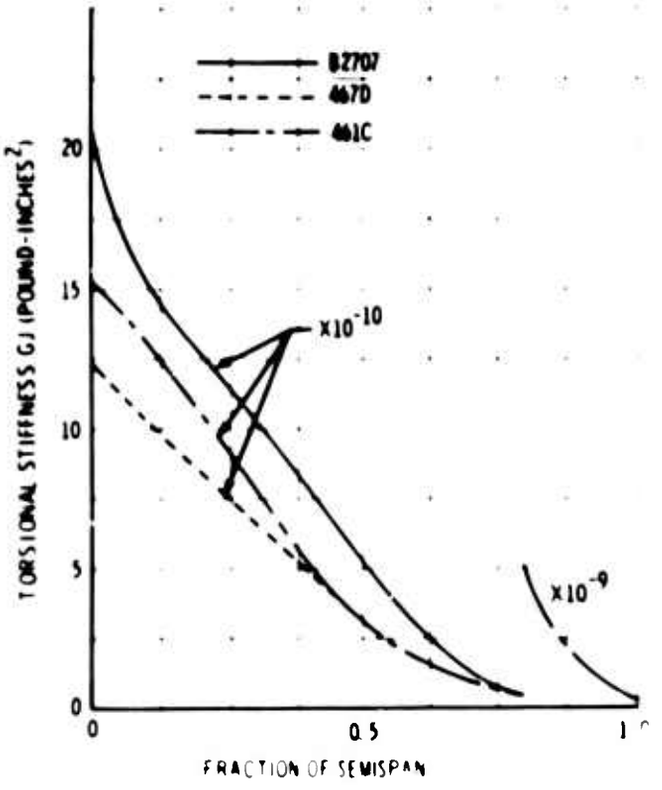

Figure 5-36 Horizontal-Tail Stiffness Comparison

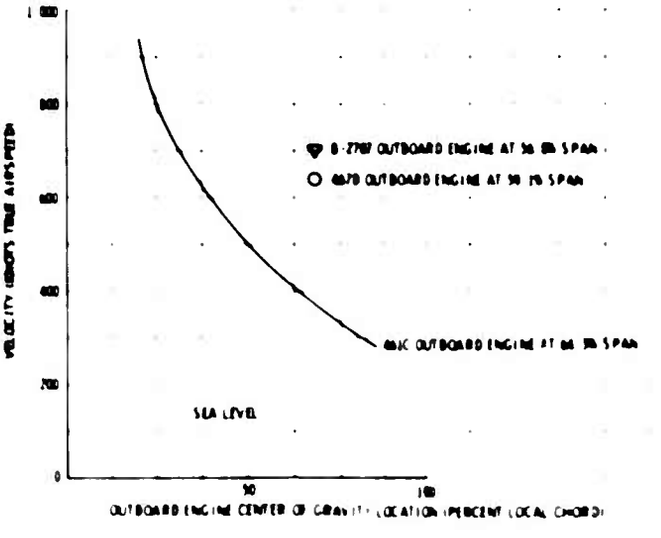

Figure 5-37 Effect of Outboard-Engine Chordwise Location on Flutter Speeds

Table 5-B. Comparison of Flutter Speeds

Surface				Flutter Speeds (knots)		
Configuration	Aspect Ratio	LE Sweep Angle (deg)	Taper Ratio	Ref. 5-1 Aero Theory	Ref. 5-3 Aero Theory	Model Test Data
-362, Fin No. 1	1.12	55	0.254	375	485	475 500
-362, Fin No. 2	1.04	50	0.202	335	525	505 530
-362 horiz plus aftbody (rot. freq = 10 cps)	0.98 (0.5 span)	50	0.210	365	530	570
-362 horiz plus aftbody (no rot. freedom)	0.98	50	0.210	355	555	570

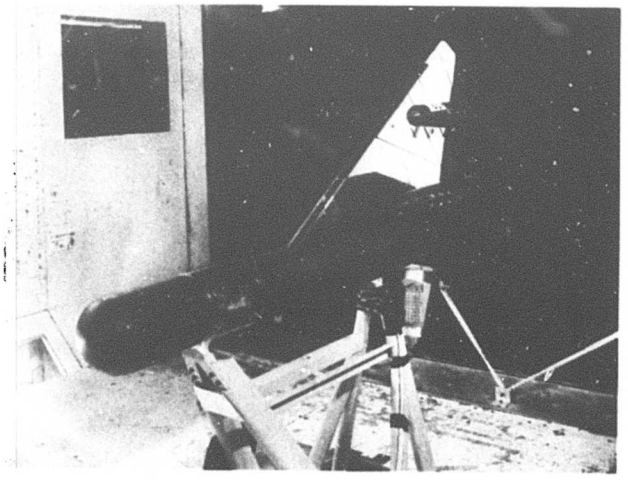

Figure 5-38. Semispan Subsonic Horizontal-Tail Model

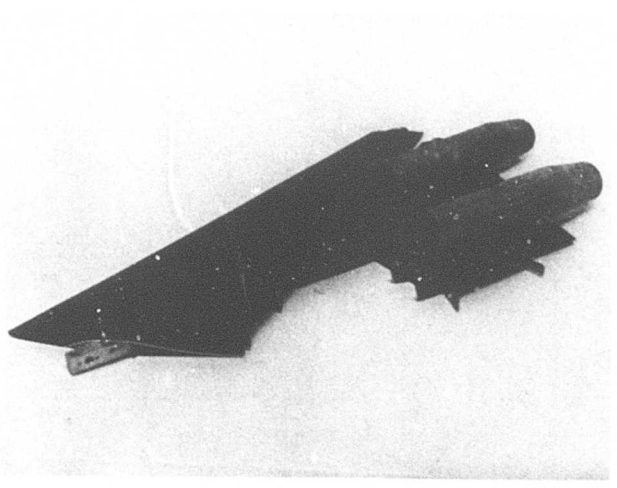

Figure 5–39. Supersonic Wing and Horizontal-Tail Flutter Model

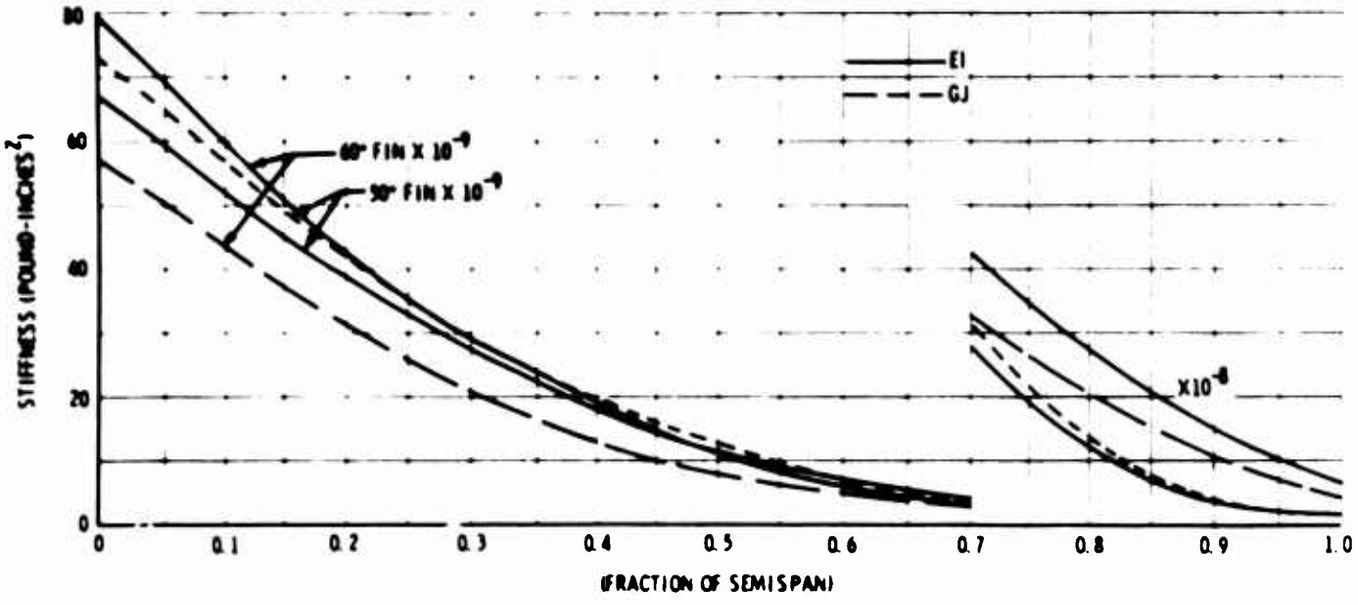

Figure 5-40. Fin Stiffness Distribution

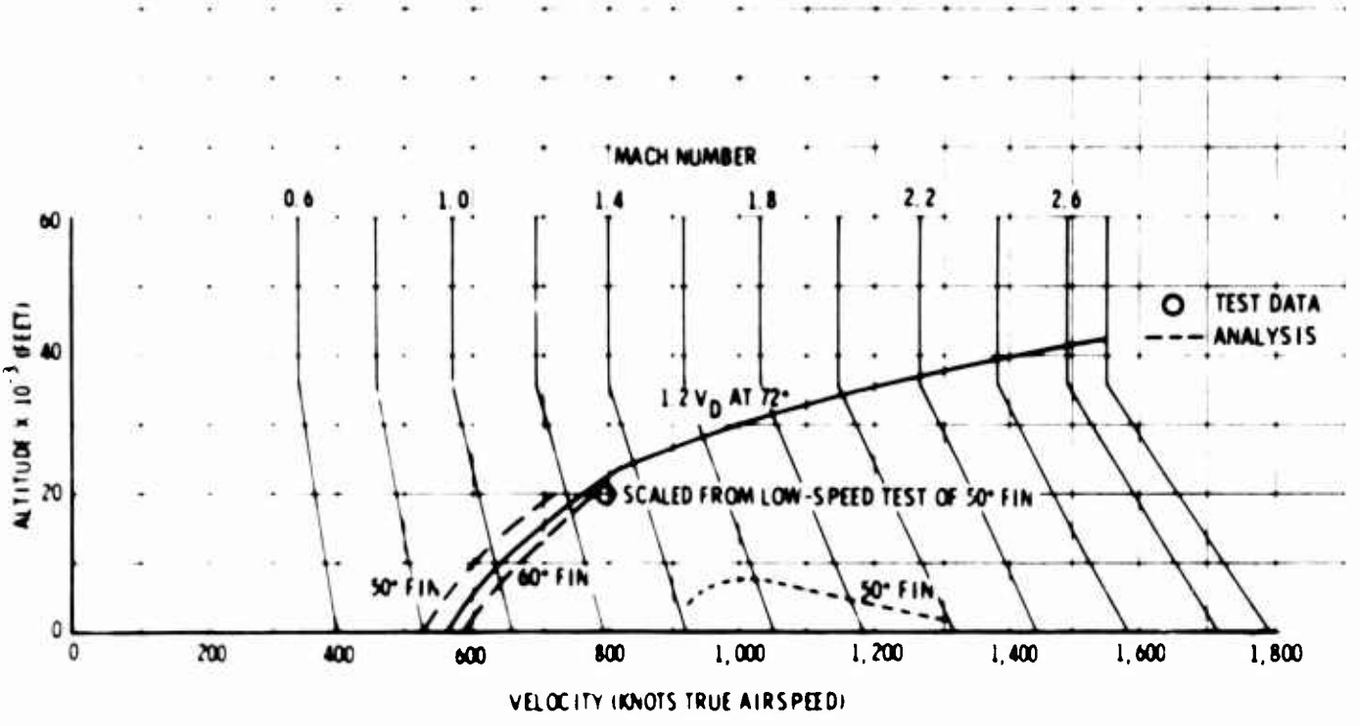

Figure 5-41 Fin Flutter Speed Summary

axis concept was used in determining the flexible mode shapes and frequencies; however, the effect of the shape of the elastic axis was taken into account (that is, the mode shapes reflect the effects of a bent elastic axis in each component in which it occurs).

The two-dimensional strip theory (Ref. 5-1) was used to represent the oscillatory subsonic airforces for the 42-deg wing sweep angle. Some compromise in the airforce representation of the forward strake area results from limitations of this theory; however, this has proven to be of little significance in flutter studies of previous configurations for which comparisons of theoretical and test results have been excellent. Piston theory airforces of Ref 5-2 were used to represent the oscillatory supersonic airforces for both the 42- and 72-deg wing sweep angles.

The solutions to the flutter equations were obtained using an IBM 7094 computer. Figure 5-5 presents results of the supersonic analysis of the 42-deg wing sweep condition in terms of flutter dynamic pressure variation with Mach number for the symmetric and antisymmetric cases. Figure 5-6 presents results for the 72-deg wing sweep condition. These results are valid down to M 1.6, which is a reasonable lower limit of application for piston theory aerodynamics.

Figure 5-7 presents the results of the subsonic analysis of the 42-deg wing sweep configuration in terms of variation of flutter speed with altitude for the symmetric and antisymmetric conditions. These results include modifications to account for aspect ratio and compressibility effects. (The curves are extrapolated beyond M 1.0 only to show trends.)

Typical plots of critical velocity versus damping (V-g) are shown in Figs. 5-8 through 5-11 for selected conditions to illustrate the slope of the V-g lines at crossover and to show the number and relationship of the more critical flutter modes.

5.1.2 Subsonic Tests

Wind-tunnel flutter tests were conducted during August 1966 on a 0.05-scale complete airplane model of the B-2707 configuration in the Convair 8- by 12-ft low-speed tunnel. Test results for

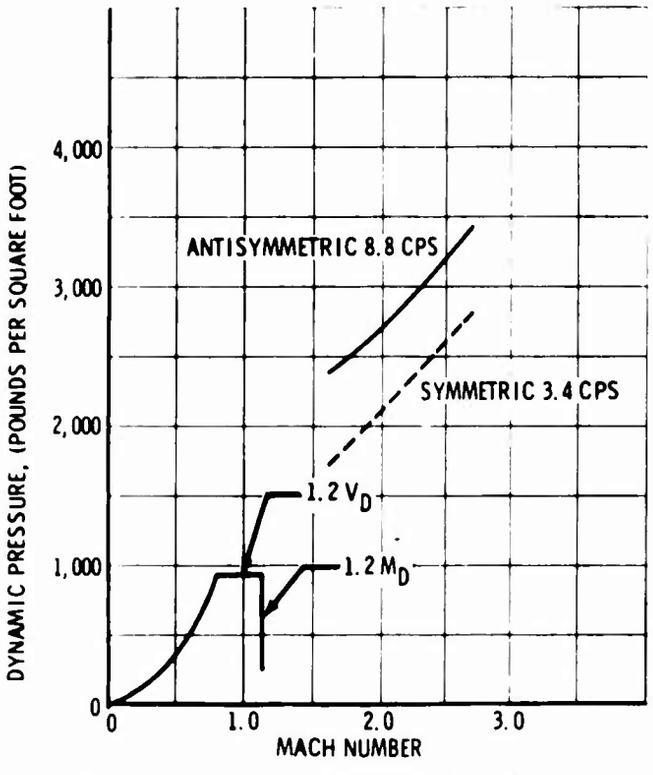

Figure 5-5. Supersonic Flutter Analysis Results, 42-Degree Wing Leading-Edge Sweep

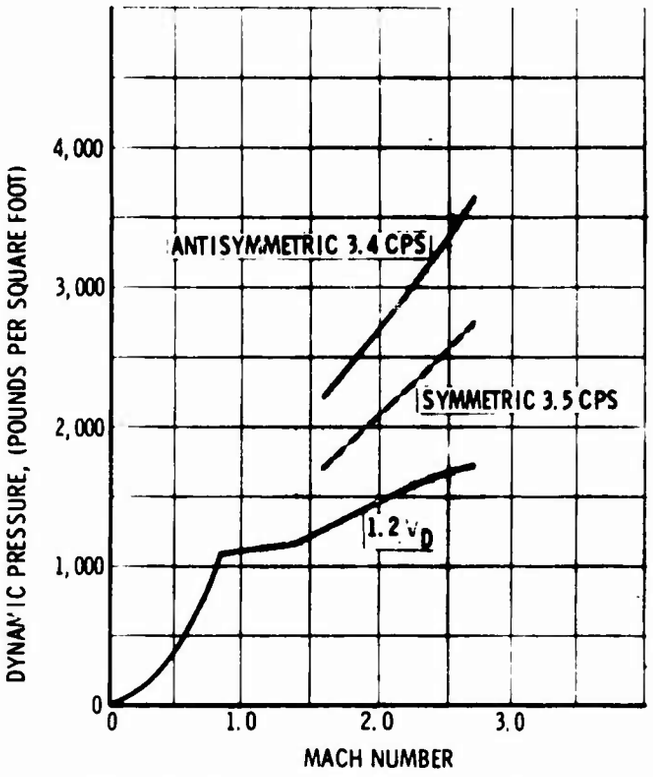

Figure 5-6. Supersonic Flutter Analysis Results, 72-Degree Wing Leading-Edge Sweep

the nominal configuration are summarized in Fig. 5-12. The wing, fuselage, and empennage surfaces were all dynamically scaled. Figures 5-13 through 5-16 show the construction of the model and the vibration test setup and wind tunnel installation. As shown, the subsonic model construction consisted of segmented aerodynamic shells attached to a single aluminum spar representing stiffness along the elastic axis of each component. The wing permitted sweep change in 5-deg increments from 22 to 72 deg with provision for simulating trailing-edge extension.

A shear attachment between the stabilizer and the fully swept wing was provided at 57-percent wing span to simulate wing-tail interconnect. (See Fig. 5-17.) Model variations in wing and stabilizer stiffnesses, fuel distributions, and nacelle chordwise positions were tested.

Figure 5-18 shows the variation of flutter speed of the empty wing with wing sweep. The flutter mode is predominantly outboard wing bending and

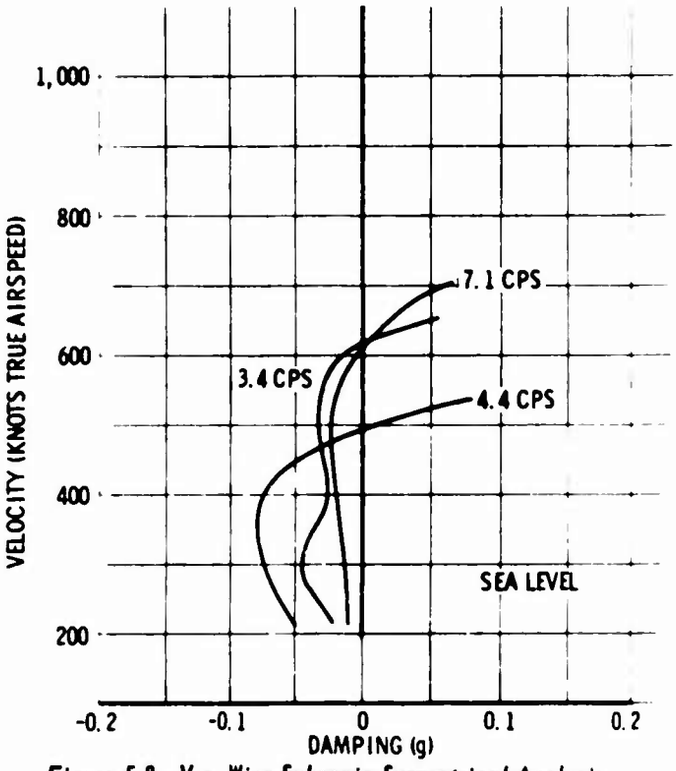

Figure 5-8. V-g, Wing Subsonic Symmetrical Analysis, 42-Degree Wing Leading-Edge Sweep

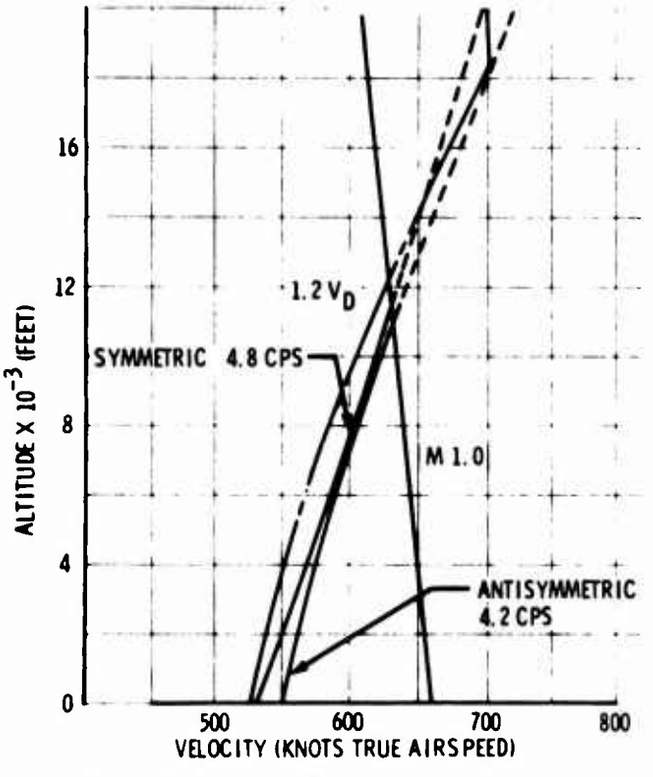

Figure 5-7. Subsonic Flutter Analysis Results, 42-Degree Wing Leading-Edge Sweep

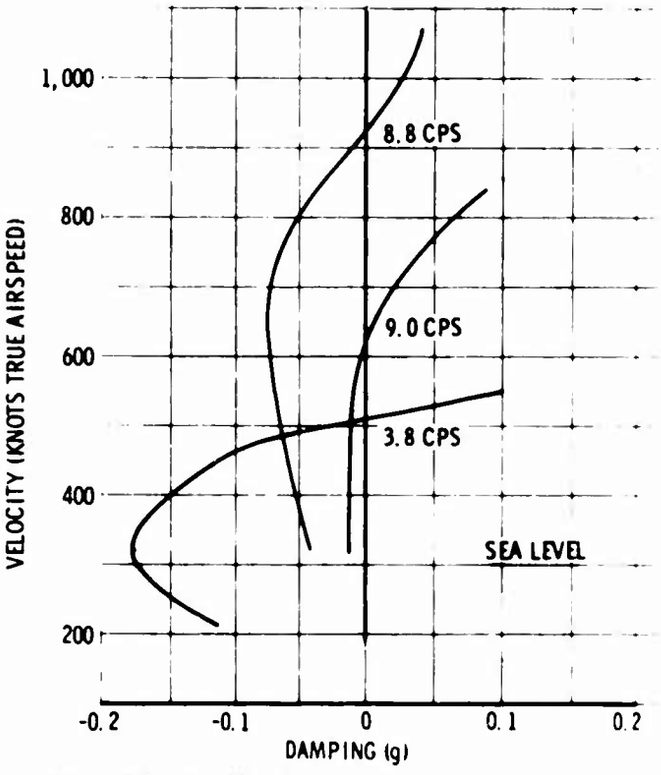

Figure 5-9. V-g, Wing Subsonic Antisymmetrical Analysis, 42-Degree Wing Leading-Edge Sweep

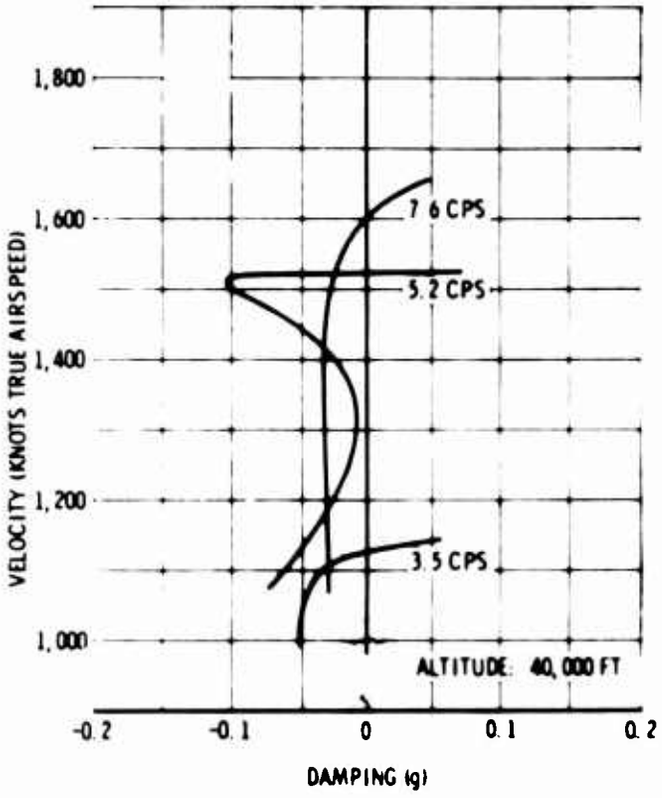

Figure 5-10. V-g, Wing Supersonic Symmetrical Analysis, 72-Degree Wing Leading-Edge Sweep

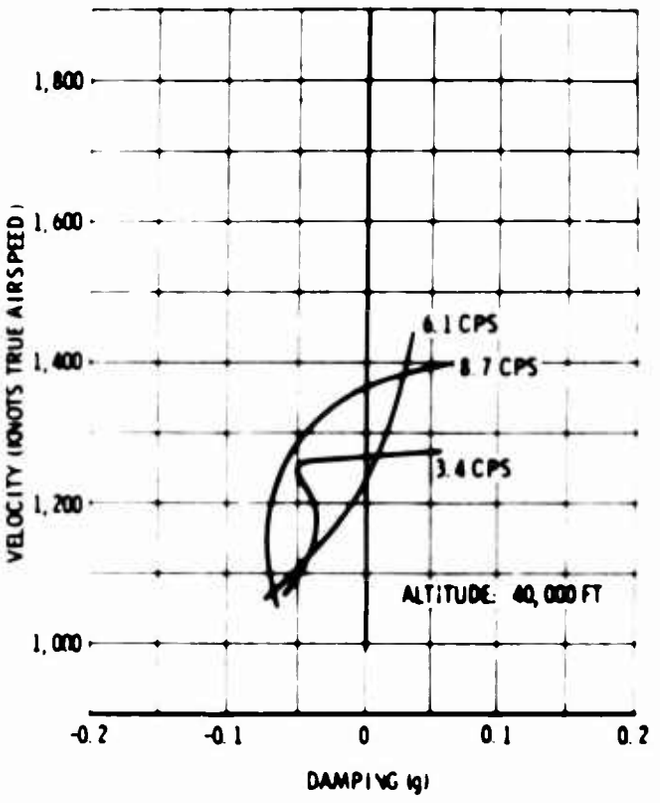

Figure 5-11. V-g, Wing Supersonic Antisymmetrical Analysis, 72-Degree Wing Leading-Edge Sweep

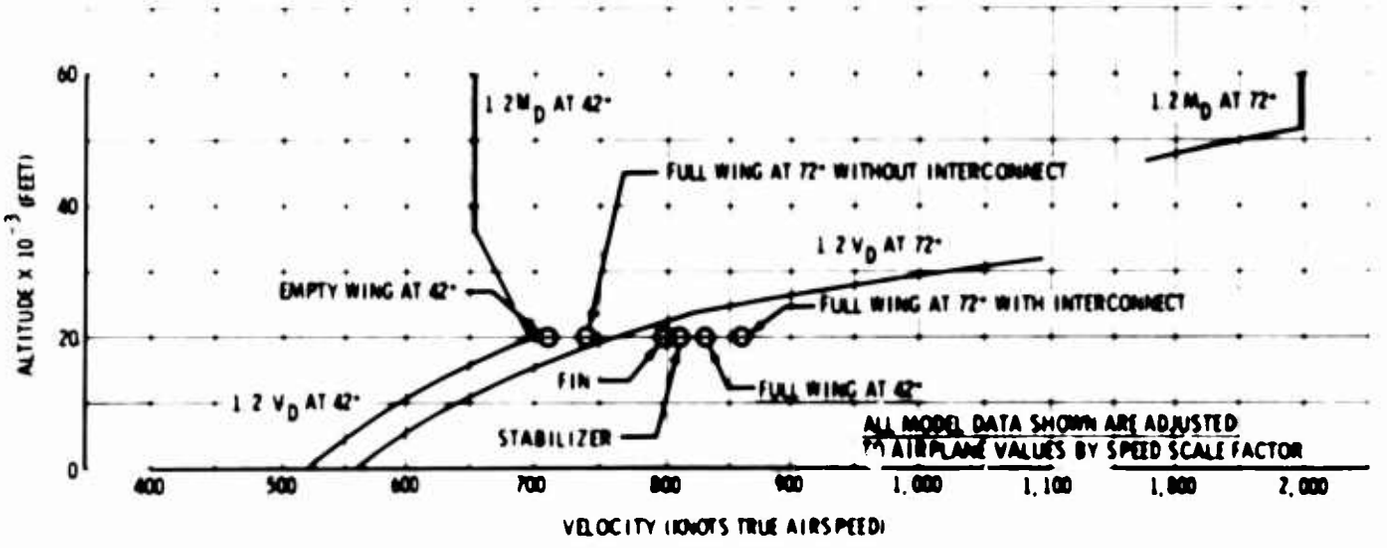

Figure 5-12 B-2707 Flutter Test Speeds, Subsonic Model

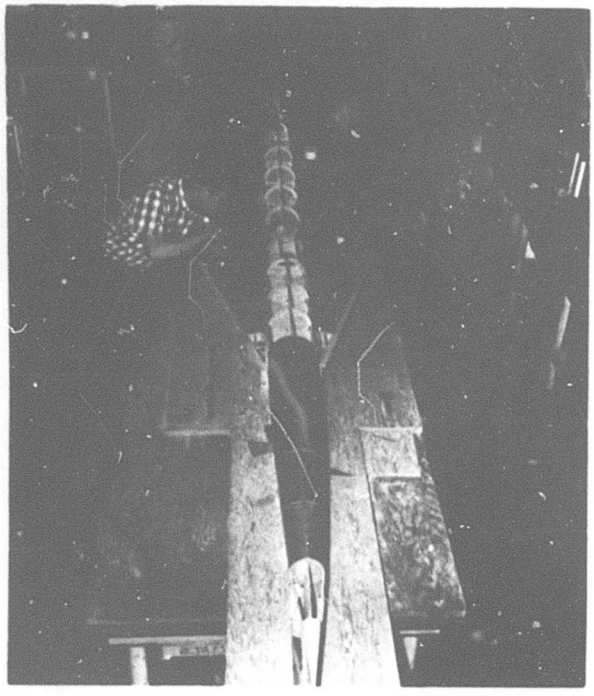

Figure 5-13. Subsonic Flutter Model Construction

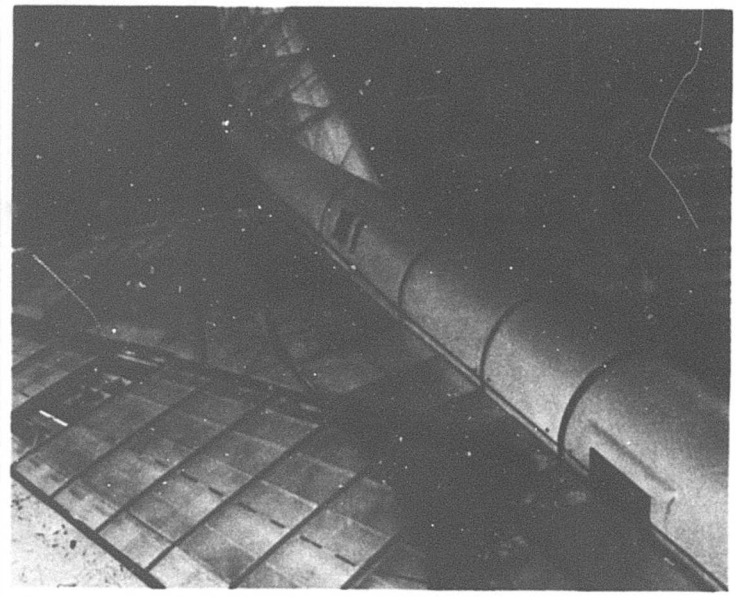

Figure 5-14. Subsonic Flutter Model, Wing-Empennage Assembly

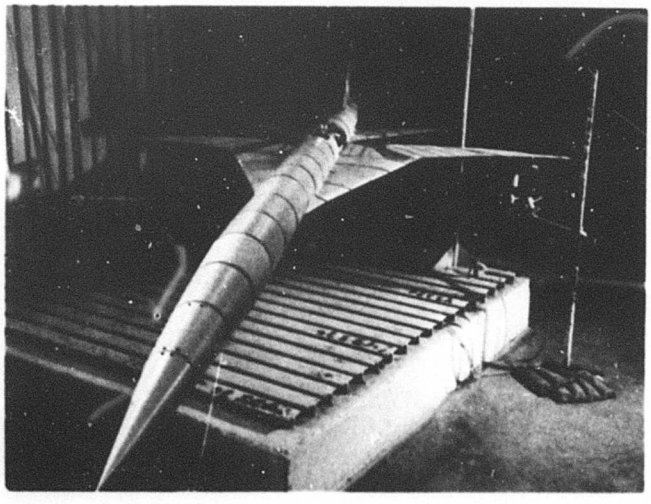

Figure 5-15. Vibration Test Setup

Figure 5-16. Subsonic Wind-Tunnel Test Installation

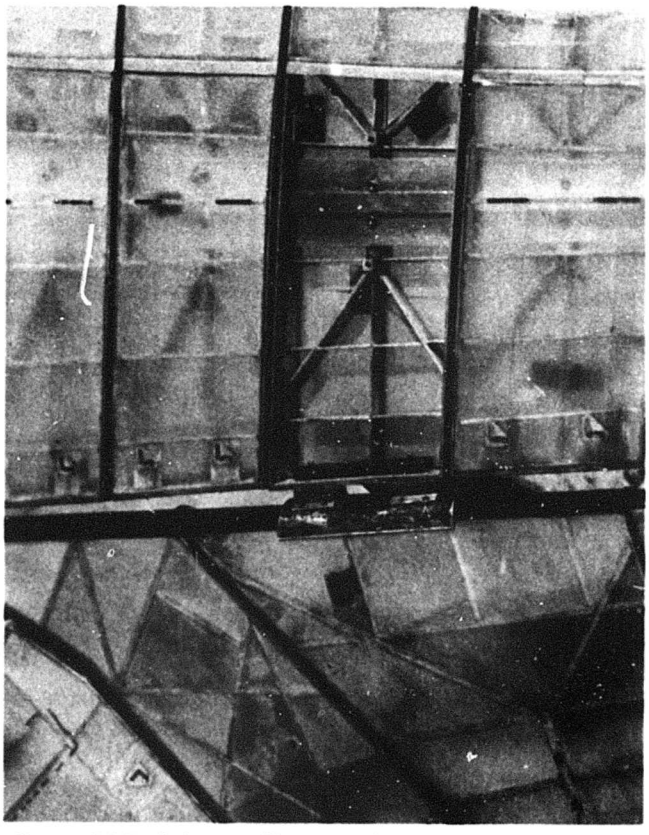

Figure 5-17. Subsonic Flutter Model, Wing-Stabilizer Interconnect

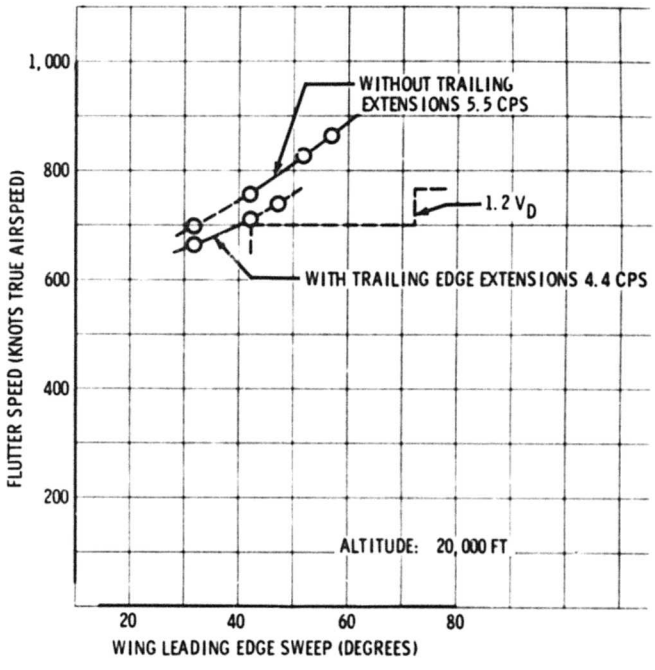

Figure 5-18. Wing Flutter Speeds, Empty

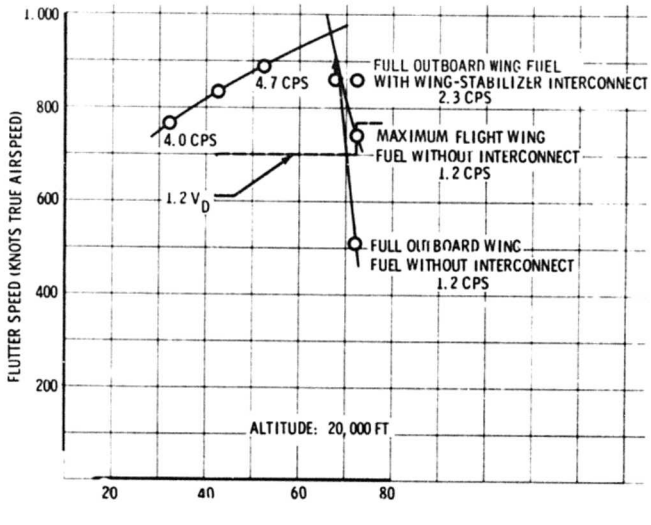

Figure 5-19. Wing Flutter Speeds, Full Outboard Wing

torsion. Trailing-edge extension with the wing in the forward sweep position lowers the flutter speed significantly; however, the 1.2 V_D boundary for flutter is maintained at the minimum clearance position of 42-deg sweep. The flutter frequency is approximately 4.4 cps with trailing edge extensions and 5.5 cps without extensions.

Figure 5-19 shows the variation of flutter speed with wing sweep for the full wing. For sweeps less than 72 deg, the flutter speeds are higher than those of the empty wing. The mode is still outboard wing bending and torsion with the frequency in the range of 4.0 to 4.7 cps. However, at 72-deg sweep, a coupling between wing and tail develops for the unlocked condition resulting in a low-frequency flutter mode (1.2 cps) with substantial reduction in speed to 510 kn true airspeed (TAS). Flutter speeds are improved markedly with the removal of a small amount of fuel from the tip region of the outboard wing, Fig. 5-20. Thus, for maximum wing fuel in flight for the 72-deg wing sweep position, unlocked, the flutter

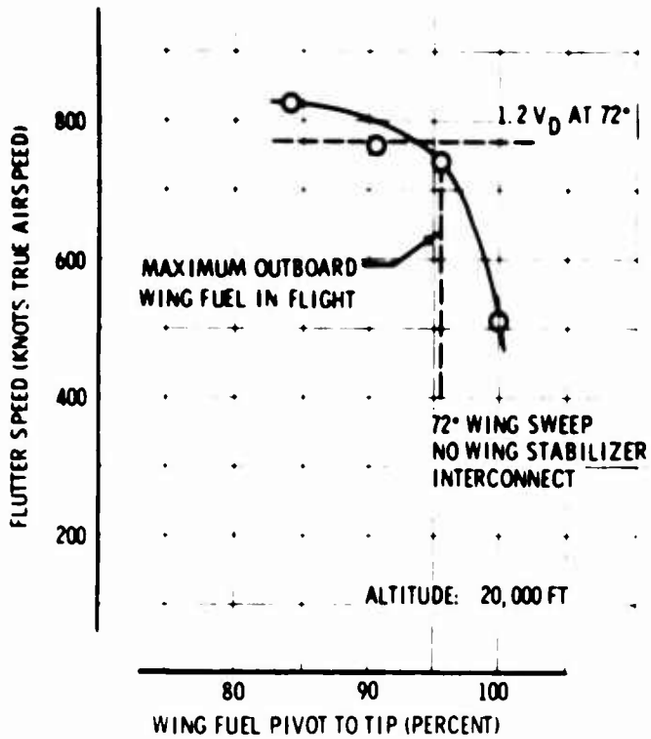

Figure 5-20. Effect of Outboard Wing Fuel on Flutter Speed

speed is increased to 740 kn TAS at 20,000 ft. Locking the wing and tail together effectively prevents the low-frequency coupling and results in a further increase in speed to 860 kn TAS at 20,000 ft for the full wing. (See Fig. 5-19.)

Figure 5-21 shows the effect of wing stiffness variation on flutter speeds. The outboard wing flutter speeds increase in conventional fashion with increased stiffness. The low-frequency flutter, however, shows a reversal of speed with stiffness, the nominal spar giving the lowest speed and indicating a frequency tuning characteristic of the mode.

The nominal horizontal tail and fin were tested to speeds well in excess of 1.2 V_D on the complete-airplane model without encountering flutter. The horizontal tail with 75 percent of nominal stiffness fluttered on the complete-airplane model at speeds scaling to 1.27 V_D or greater for both empty and full fuel conditions. The tail surfaces were tested separately on a cantilever support, and the results are reported in Pars. 5.2.2 and 5.2.3.

5.1.3 Transonic Tests

A full-span 0.05-scale transonic flutter model is

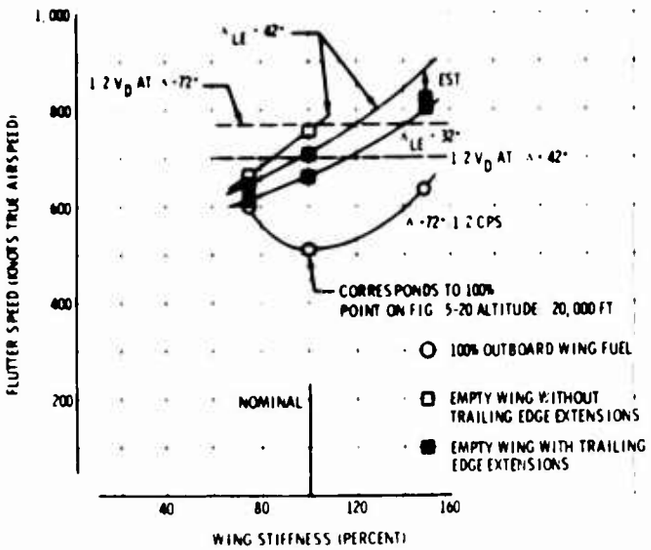

Figure 5-21. Effect of Wing Stiffness on Flutter Speed

being fabricated in preparation for flutter test in the NASA-Langley 16-ft Transonic Dynamics Tunnel beginning 26 September 1966. The test will be performed with two models: a rigid model to check the stability of the airplane configuration on the NASA-developed cable support system in the tunnel and a dynamically scaled flutter model, which will be tested at 42- and 72-deg wing sweep angles with zero fuel and payload. Figures 5-22 and 5-23 show construction of model components in the wind tunnel shop.

Additional flutter model testing and analysis is planned for Phase III to fully verify the preliminary findings discussed under Par. 5.1.

5.2 MAJOR COMPONENTS

The studies of this section are principally trend-oriented to evaluate off-nominal design variables and establish design sensitivities. This approach is taken to make efficient use of computer and wind-tunnel test time. Both analytical and wind-tunnel test parametric investigations of flutter are presented.

5.2.1 Wing Flutter

Semispan flutter studies of the wing have employed slender-beam theory to compute mode shapes. The nominal bending and torsional stiffness distributions are shown in Fig. 5-24. The vibration modes included first bending and torsion of the wing inboard of the pivot and three bending and two torsion modes of the outboard wing. The following aerodynamic theories were used:

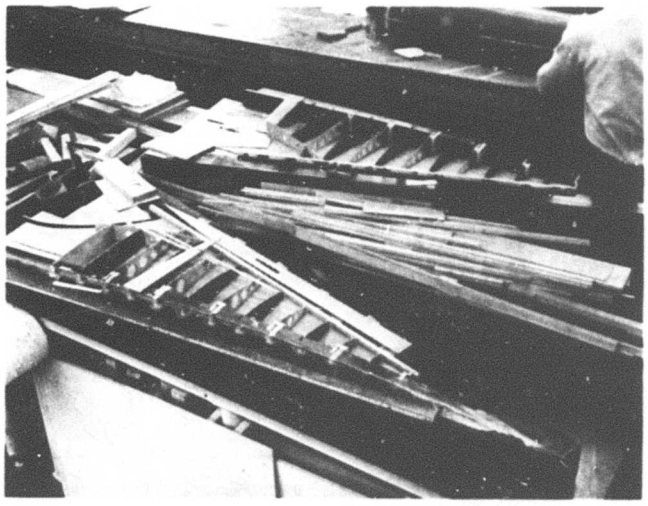

Figure 5-22. Transonic Flutter Model Strake Construction

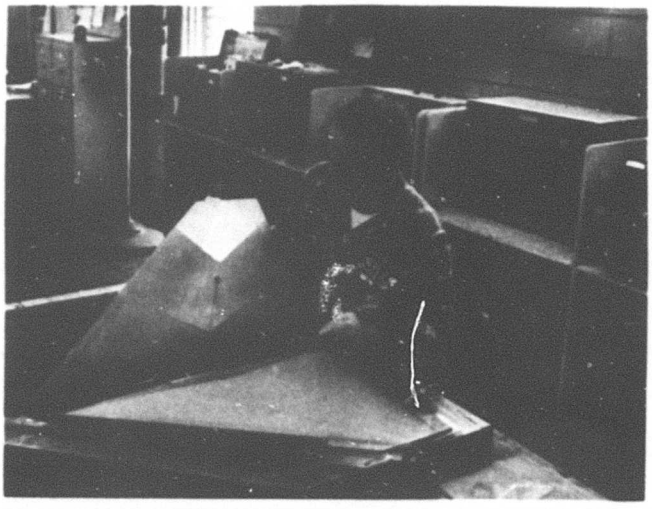

Figure 5-23. Transonic Flutter Model Vertical-Tail Skin Layup

Mach range	Leading-edge sweep angle (deg)	Theory	Reference No.
-	30 to 42	2-D incompressible and Mach correction factors	5-1
0 to 0.9	30 to 55	Subsonic Kernel-Function (Rho airforces)	5-3
1.4 to 2.0	55 to 72	Supersonic Kernel-Function "Mach Box"	5-4, 5-5

In Fig. 5-25, relative dynamic pressure (q) at flutter versus Mach number is presented in the subsonic regime for three sweep angles of the wing. The reference position is at 42-deg and the fuel condition is wing empty. The three-dimensional aerodynamic theory of Ref. 5-3, which accounts for compressibility effects, has been used in the analysis.

Figure 5-26 presents the effect of wing sweep on flutter speed of the empty wing at three altitudes. Comparing the aerodynamic theories of Refs. 5-1 and 5-3 for the sea-level case, the two-dimensional results are approximately 12 percent conservative on speed.

Wing stiffness effects on flutter speed of the empty wing are shown in Fig. 5-27. Results indicate increasing flutter speed with an increase in wing stiffness outboard of the pivot, but decreasing flutter speed with increase in inboard wing stiffness.

Results of a limited number of semispan empty wing tests (Fig. 5-28) conducted in the low-speed tunnel at Convair are presented in Fig. 5-29. The trend and magnitude of flutter speeds compare favorably with the results of semispan analysis using Ref. 5-3 aerodynamic theory.

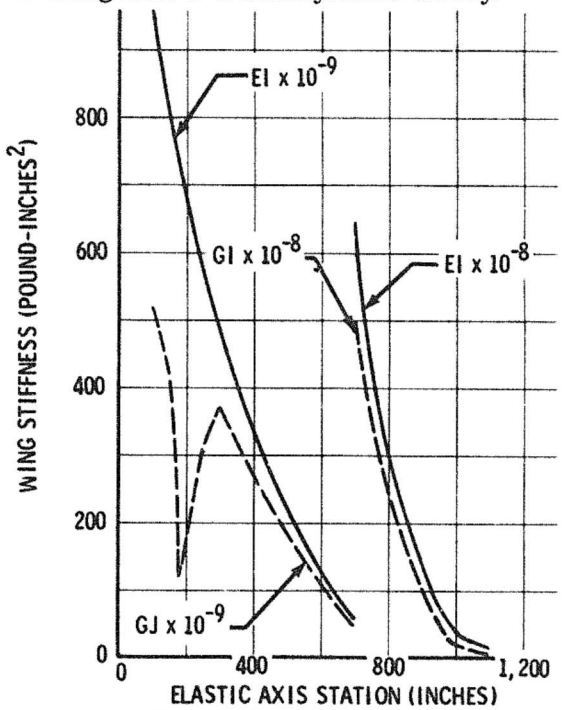

Figure 5-24. B-2707 Wing Stiffness

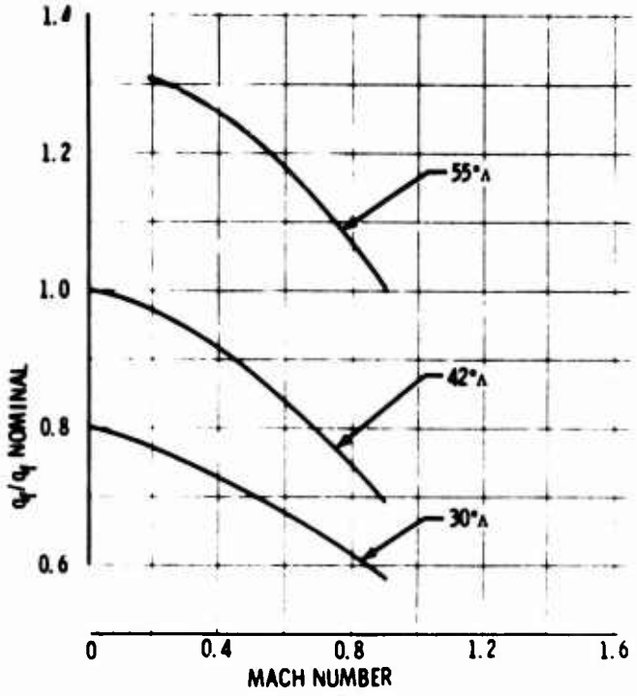

Figure 5-25. Effect of Mach Number on Wing Flutter Speed

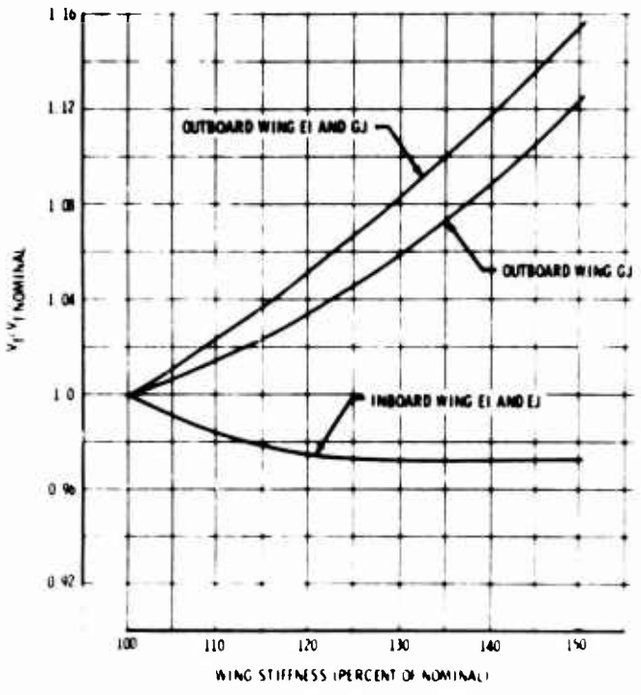

Figure 5-27. Effect of Wing Stiffness on Flutter Speed

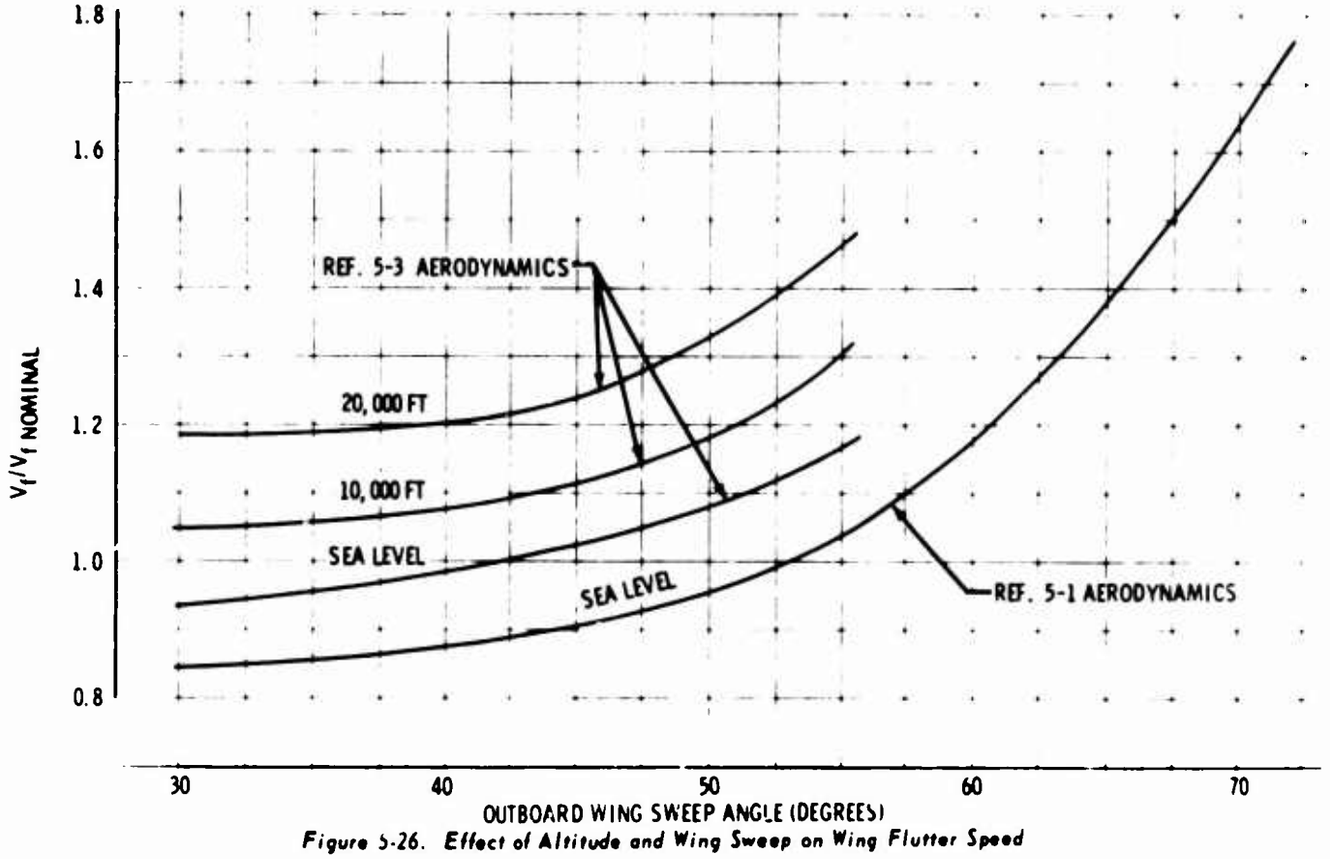

Figure 5-26. Effect of Altitude and Wing Sweep on Wing Flutter Speed

Supersonic wind-tunnel tests of semispan wings (Figs. 5-30 and 5-31) were conducted in the Boeing supersonic wind tunnel during November 1965 and April 1966. The models were fabricated of fiberglass using spar and rib construction and were injected into the tunnel. Results of the two tests, shown in Figs. 5-32 and 5-33, indicate substantial margins of safety for flutter. Note the rapid increase of flutter q with Mach number in the region of M 1.6 for both 60- and 72-deg sweep.

5.2.2 Horizontal Tail

Semispan parametric studies of the B-2707 horizontal tail were conducted using slender beam theory modified to allow inclusion of cranked elastic axis effects and included three bending and three torsional modes of the stabilizer. The aerodynamic theory of Ref. 5-3 was employed for the subsonic studies. The nominal bending and torsional stiffness distributions are shown in Fig. 5-34. Computed flutter speed for the B-2707 cantilevered stabilizer is 700 kn TAS at sea level, which substantially exceeds 1.2 V_D. The computed value compares favorably with the test speed of 800 kn TAS at 20,000 ft. (See Fig. 5-35.)

A comparison of the planform parameters for three horizontal tail configurations with mounted engines, for which flutter analyses have been made, is presented in Table 5-A, and the relative torsional stiffnesses are plotted in Fig. 5-36. Areas and lengths shown are based on a planform where the root chord is taken as a streamwise line at the point where the elastic axis meets the side of the fuselage, and the tip chord is taken as parallel to the stream at the point where the elastic axis cuts the actual swept tip.

Computed flutter speeds for the configurations listed in Table 5-A are shown in Fig. 5-37. Speeds for various positions of the outboard-engine center of gravity display a trend of decreasing flutter speed with aft movement of the center of gravity and indicate a beneficial effect from movement of the engine inboard, since the speed increase of the 467D and B-2707 configurations over the 467C cannot be accounted for by stiffness differences alone.

Subsonic wind-tunnel tests of semispan horizontal-tail models (Fig. 5-38) conducted in the Convair Tunnel in August 1966 produced the results shown in Fig. 5-35. The test speeds are in general agreement with analytical speeds for the B-2707, both exceeding the required flutter speed margin. However, trends of flutter speed with chordwise position of the outboard nacelle, as obtained from test and analysis, do not correspond. Analytical studies to investigate the trend discrepancy are in progress.

Subsonic flutter analyses of earlier horizontal tail configurations provided a comparison of analytical results with wind-tunnel test data for low-aspect-ratio surfaces. The results, shown in Table 5-B, indicate good agreement between test data and analysis using the aerodynamic theory of Ref. 5-3. Analysis employing Ref. 5-1 aerodynamics is seen to be very conservative.

Supersonic flutter tests to investigate aerodynamic coupling effects with the wing adjacent to the horizontal tail are scheduled for mid-September 1966. The horizontal-tail test configuration includes scaled flow-through nacelles, as shown by Fig. 5-39.

5.2.3 Vertical Tail

Flutter analyses of the vertical tail of the B-2707 were based on elastic axis representation of the cantilevered structure and included two bending and two torsional modes. The aerodynamic theory of Ref. 5-3 was used for subsonic studies and the Mach Box theory of Refs. 5-4 and 5-5 for supersonic analysis. Subsonic analyses were conducted on the proposal-configuration fin with 60-deg leading edge sweep as well as an earlier fin planform with 50-deg leading edge sweep. Supersonic flutter analysis was made only on the fin planform with 50-deg leading edge sweep. Results of analyses and supporting tests indicate that the B-2707 vertical tail configuration with 60-deg leading edge sweep provides adequate flutter speed margins.

The comparative stiffness distribution for the two fin configurations is shown in Fig. 5-40. Figure 5-41 presents results of flutter analyses in terms of altitude-airspeed boundary. A test data point scaled from the low-speed wind tunnel test of the 50-deg leading edge fin (Fig. 5-42) at the Convair 8- by 12-ft tunnel in August 1966, is plotted in Fig. 5-41 at the scaled altitude of 20,000 ft. The analysis is somewhat conservative when compared with test data. Data from supersonic tests

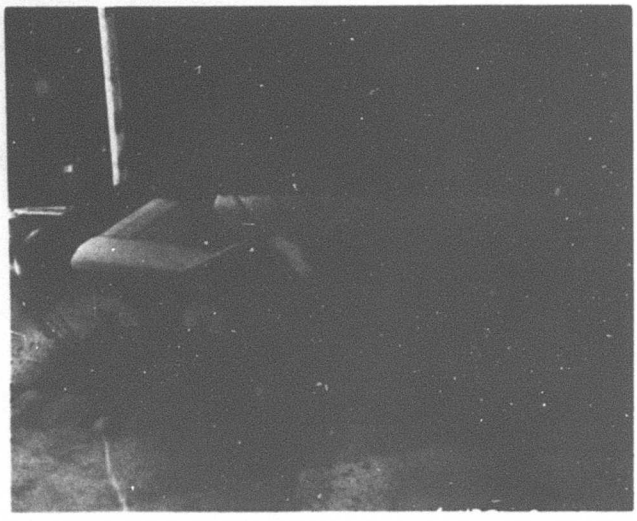

Figure 5-28. Semispan Subsonic Wing Model

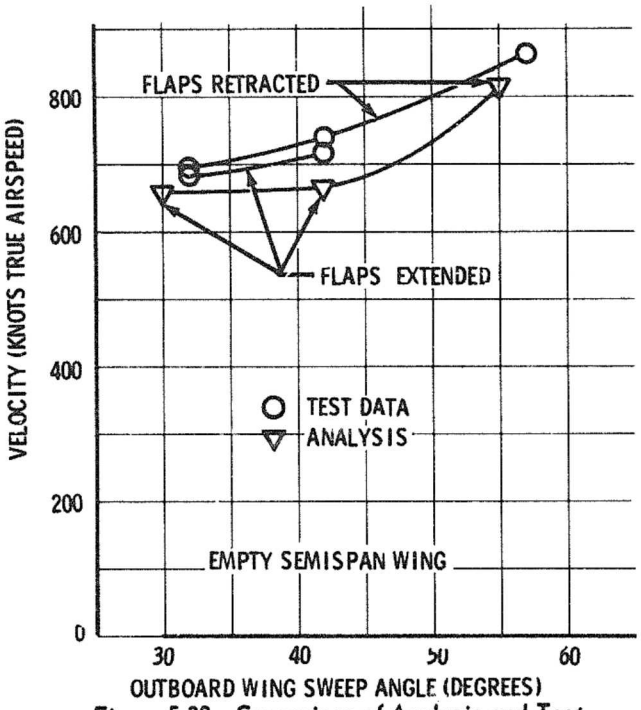

Figure 5-29. Comparison of Analysis and Test Flutter Speeds

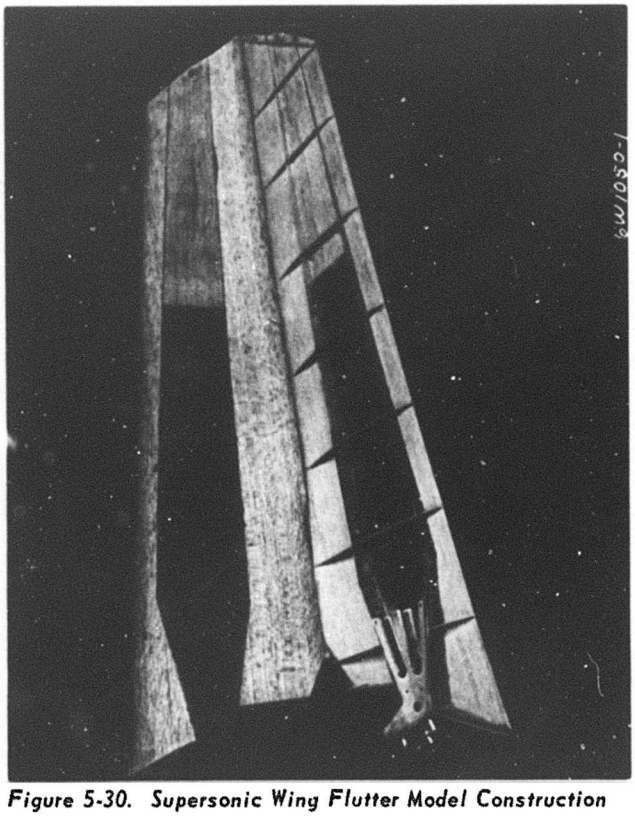

Figure 5-30. Supersonic Wing Flutter Model Construction

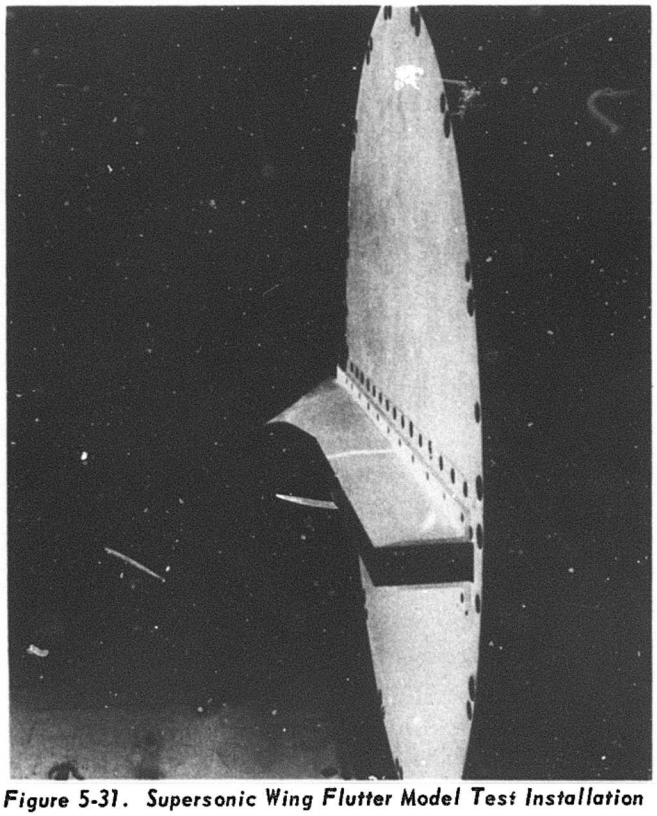

Figure 5-31. Supersonic Wing Flutter Model Test Installation

of 50-deg leading edge fins (Fig. 5-43), conducted during April and July 1966, are shown in Fig. 5-44. No flutter was encountered. The shaded portion of the plot indicates a dynamic pressure – Mach number region where an intermittent oscillation, confined to the outboard portion of the fin, appeared at dynamic pressures substantially higher than the 1.2 V_D boundary.

5.3 CONTROL SURFACES

Control surface flutter is prevented by the irreversible control system, which provides adequate frequency separation between the control surfaces and the primary surfaces. For example, the elevons have 10-cps rotational frequencies compared with the first torsional frequency, 5 cps, of the horizontal tail. The frequency requirements for the other control surfaces are established for the prevention of transonic buzz. All these frequencies meet or exceed the frequency-separation criterion specified in Military Specification MIL-A-8870.

The criterion that establishes the minimum frequency requirements for the prevention of transonic buzz is presented in Par. 2.3.1. Using this criterion, the required minimum rotational frequencies for the various control surfaces are:

Control surface	Minimum frequency (cps)
Lower rudder	5.02
Upper rudder	16.0
Inboard elevons	5.34
Elevators	8.9
Aileron	17.8
Flap	7.25 to 15.6
Wing spoilers	17.8 to 36.4

Design is proceeding to equal or exceed these minimum requirements.

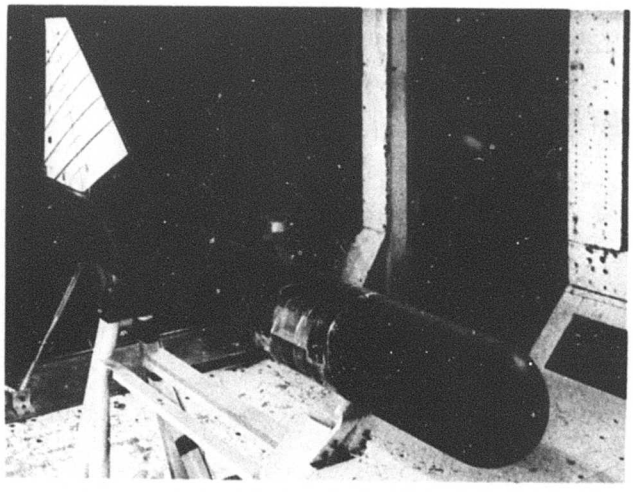

Figure 5-42. Subsonic Fin Flutter Model

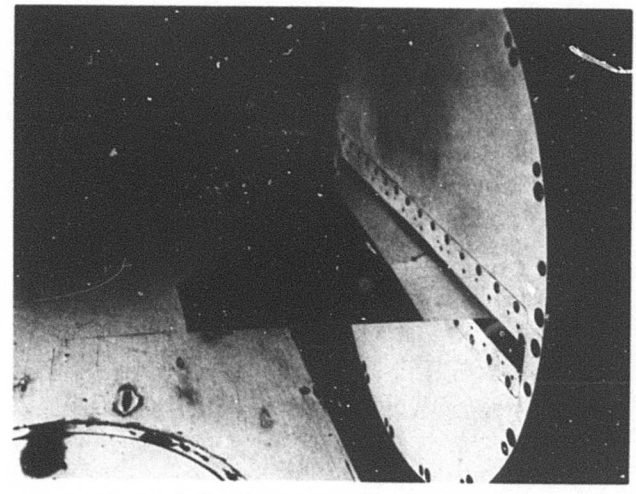

Figure 5-43. Supersonic Fin Flutter Model

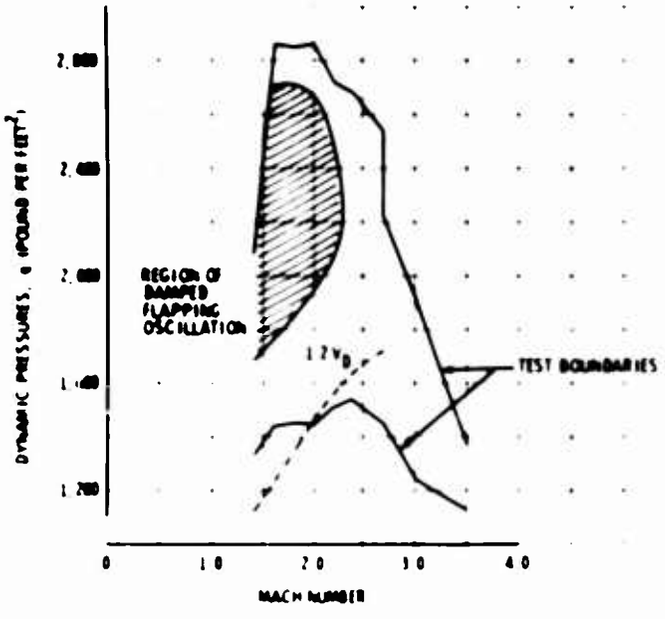

Figure 5-44. Supersonic Fin Test Data

A large-scale model with representative control surfaces will be tested in a transonic wind tunnel, such as the Ames 11-ft tunnel, to verify that the requirements are satisfactory. Provisions for varying the rotational spring rates of all surfaces will be incorporated into this model. Although the buzz phenomenon is not expected to occur on spoiler-type surfaces, these surfaces will be properly represented on the model, and free-floating tests will be conducted.

5.4 STABILITY AUGMENTATION SYSTEM

Preliminary study of electronic filtering as the optimum method for prevention of aeroelastic-feedback instabilities has established the feasibility of the concept. Reliance on hydraulic filtering, related to control system properties, is not proposed since servo and actuator frequency response is maintained flat to 5 cps to provide for adequate speed of response to control input and to ensure satisfactory phase relationships at the lower frequencies. Figure 3-81 shows representative modal frequencies for the first four vibration modes of 1.47, 2.25, 2.56, and 3.81 cps. Past experience has indicated that any method of attenuating elastic feedback potential must begin at just beyond the flying qualities frequencies and be well attenuated at the lowest elastic frequencies.

Preliminary study of electronic filtering characteristics required for pitch axis SAS design had an objective of providing satisfactory handling qualities without using scheduled feedback gains. This analysis resulted in a filter that had too much gain at high frequency when flexible mode coupling effects were considered. By grouping the flight conditions in wings-forward and wings-aft sets and designing a compensation filter for each set, the high-frequency gain is reduced considerably. This analysis is presented in the Development Data Document, D6A-10339-1.

Stability analysis is underway for the pitch axis of the SAS using digital techniques. The mathematical model has two rigid modes, five flexible modes, and the pitch axis SAS. Root locus diagrams showing the variation of pole zero location due to tolerances in the loop gain and loop phase are also presented in the Development Data Document. Expanded investigation of the required filter characteristics is planned for Phase III when both airframe stability derivatives and vibration modes are better defined. The goal of this study will be to derive filters that cut off the gain above the rigid-mode frequencies at a high rate so that the flexible-mode gain margins are satisfactory. Effects of sensor placement will also be studied.

Provisions for triple force summed servos and surface actuators ensure that a single failure does not impair system operation and that the second failure will be passive. Failure of electronic filtering elements is very remote due to the use of solid-state technology. Protection against such failures is provided by having at least three channels of electronics and sensors in each SAS axis. The output signals are passed through voting circuits before they are routed to the servos. The pitch and yaw axes are fail operational after two failures and fail passive on the third. The roll axis is fail-operational on the first failure and fail-passive on the second.

5.5 PANEL FLUTTER

Design criteria for the prevention of panel flutter have been applied to surface structure of the B-2707 for the most critical conditions of load factor, dynamic pressure, and Mach number. Requirements for the design of skin panels for the prevention of panel flutter are based on data from

Ref. 5-6 updated to reflect subsequent test data from numerous sources. (These composite data are somewhat more conservative than the parametric curve presented in Ref. 5-7). The composite criteria are used in conjunction with the critical portion of the flight profile (M 1.2 to M 1.8) and the required flutter margins (1.44 q_D) to determine design requirements for the unstressed, unpressurized, flat panels. These requirements are shown in Fig 5-45. Also shown for comparison are the most critical panels on the airplane.

The effects of environment (other than external airflow conditions) are considered separately. Figures 5-46 through 5-49 present data for adjusting the flat panel requirements to reflect the effects of pressure differential, compression loading, midplane tension stress, and curvature. These data are given in terms of the ratio of effective thickness to actual thickness; the effective thickness is then used in Fig. 5-45 to evaluate the panel. Elevated temperature is taken into account by reduction in the modulus of elasticity.

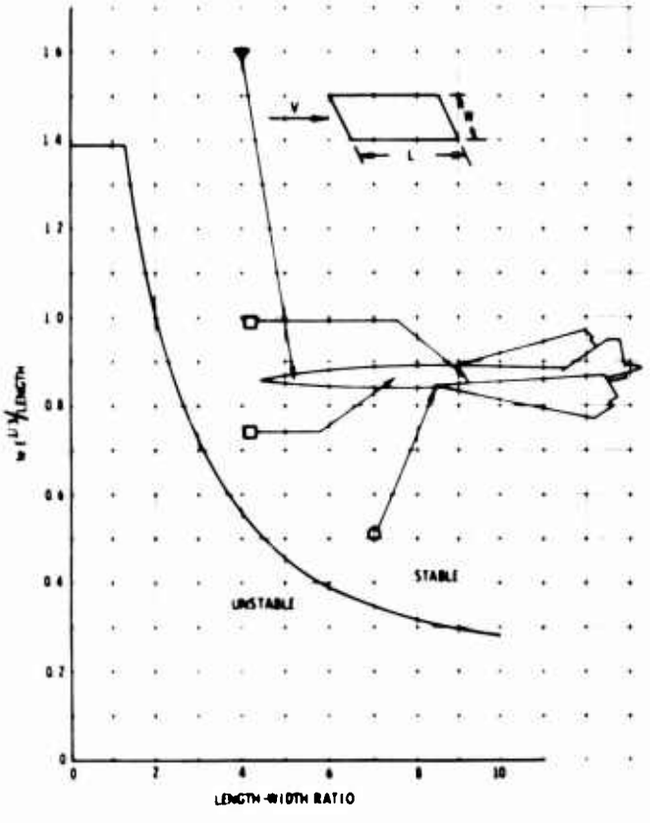

Figure 5-45. Panel Flutter Requirements

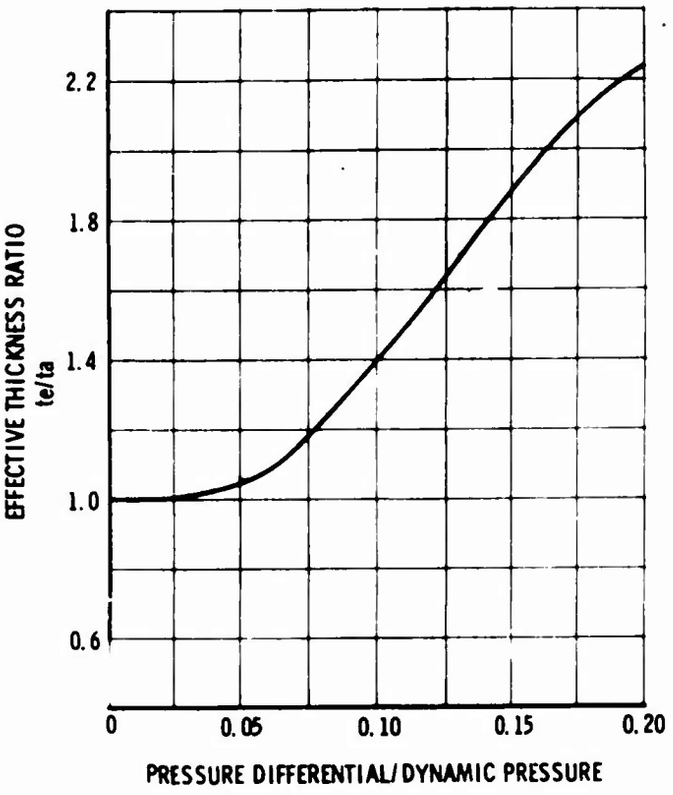

Figure 5-46. Effect of Pressure Differential

The effect of pressurization on effective thickness (Fig. 5-46) is based on test data presented in Ref. 5-6. The pressure differential used in the design of the panels is the minimum that is expected to occur during any operating condition throughout the critical Mach number range.

The effect of compressive loading in terms of critical buckling load on effective thickness (Fig. 5-47) is based on unpublished data obtained from tests conducted by Robert W. Hess of the NASA-Langley Research Center. The ratio of actual load to critical buckling load (N/N_{CR}) is the maximum that is expected to occur through the critical Mach number range.

The effect of tension loading on effective thickness, given by the equation in Fig. 5-48, is based on frequency equivalence (i.e. panels having similar geometric and frequency properties have been shown to exhibit the same flutter dynamic pressures). A panel of thickness t_a with midplane tension stress σ_x and σ_y has the same first natural frequency as a nonstressed panel of thickness t_e. The tension stresses used to establish the

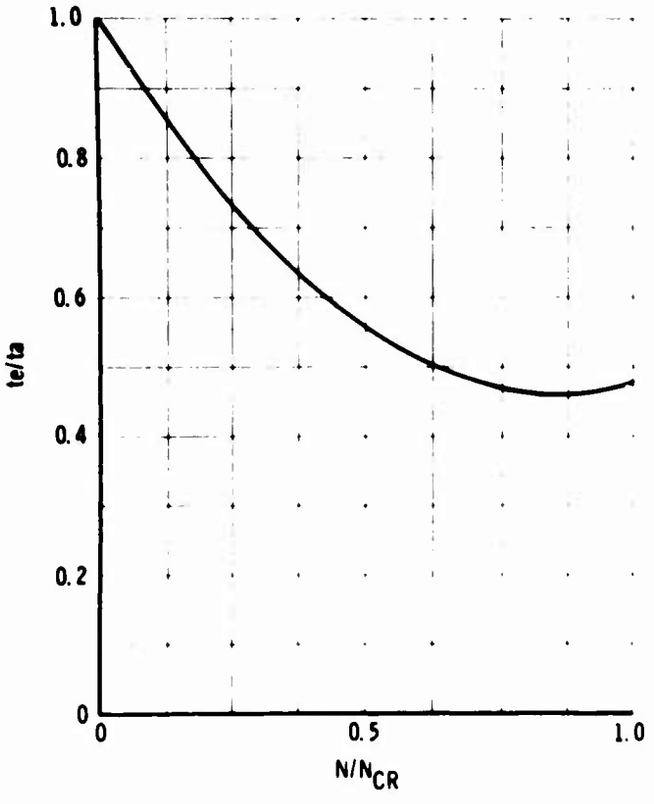

Figure 5-47. Effect of Compression Loading

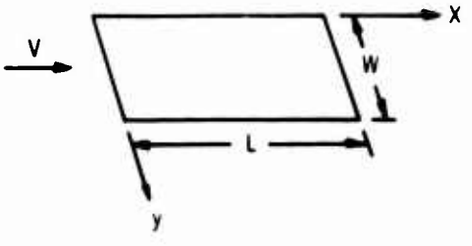

$$\frac{t_e}{t_a} = \left\{ 1 + \frac{12(1-\mu^2)}{\pi^2 E t^2_a} \frac{\left[\frac{\sigma_x}{W^2} + \frac{\sigma_y}{L^2}\right]}{\left[\frac{1}{W^2} + \frac{1}{L^2}\right]^2} \right\}^{1/3}$$

Figure 5-48. Effect of Tension Loading

$$\frac{t_e}{t_a} = \left\{ 1.0 + 0.0887 \frac{W^4}{r^2 t^2_a} \right\}^{1/3}$$

$$\frac{r}{t_a} \leq 3.11 E^{1/3}$$

Figure 5-49. Effect of Curvature

equivalent thicknesses are the minimums expected to occur through the critical Mach number range.

The effect of curvature on effective thickness is given by the equation in Fig. 5-49. Again, frequency equivalence is the basis of the equation. Frequency equivalence is used as a rough guide for $W/r \leq \pi/4$. For larger values of W/r, it is required that $t/r \geq 0.322\left(\frac{1}{E}\right)^{1/3}$ as shown by Y. C. Fung in Ref. 5-8.

As the design progresses, any panels that appear to be marginal will be analyzed in detail using stiffness and aerodynamic computer programs that have been developed by the Company.

5.6 FULL-SCALE TESTS

5.6.1 Ground Vibration Test

A comprehensive vibration test program will be conducted on the first prototype airplane as a final experimental verification of vibration modes and frequencies employed in theoretical analysis and measured on wind-tunnel flutter models. In some cases, preliminary vibration checks of full-scale components will be made in order to obtain the earliest verification of basic data. Ground vibration test of the prototype airplane will be performed on the airplane before rollout

For preliminary component tests, special jigs will be constructed to provide required boundary conditions for each surface. In the case of the complete airplane, support will be provided through the main and nose gear with air and oil removed from the struts and with wheel axles supported by special trunnions attached to the hangar floor. Vibration test configurations will be established on the basis of results of model and analytical flutter investigations. Airplane modes will be compared with those from the model and analyses for comparable boundary conditions and differences accounted for in repeat analyses and model testing.

All control surfaces will be locked except during tests involving the control systems. When control surfaces are vibrated, the supporting structure will be appropriately supported to effectively lock out the structure.

Multiple electromagnetic shakers will be employed to provide excitation of natural modes. Response measurements from accelerometers located on the airplane will be recorded on magnetic tape. Visual display will provide an on-the-spot evaluation of resonant conditions. Computer programs will be utilized that permit conversion of taped readout to plotted mode shapes for the resonant conditions within 24 hr.

Shaker locations and phasing will be chosen to provide excitation of the airplane and all major components in all significant modes. Excitation will be provided with continuous frequency variation from 0 cps to a selected maximum. Response will be recorded at small frequency intervals and at all resonant peaks in the selected range.

5.6.2 Flight Flutter

A flight flutter test program will be conducted to demonstrate the flutter safety of the airplane. The test program will evaluate and demonstrate the flutter stability boundaries for all flight conditions up to the design dive speed. Stability will be established using the criterion that the minimum acceptable coefficient of damping be equal to or greater than 3 percent for all pertinent modes. Preliminary flight flutter clearance speeds will be established during the first 100-hr flight test program to facilitate early testing for other critical programs. The final clearance will be established early in the test period following the initial 100-hr test program.

The technique used to evaluate the damping characteristics is to measure the response (including rate of decay) due to various types of excitation. The response of the airplane will be measured by vibration pickups (accelerometers and vibrometers) at a sufficient number of points on the primary structure, control surfaces, control systems, and skin panels to accurately define the mode shapes and associated frequencies, phasing, and damping. About 60 pickup locations are required to measure the response. The frequency response range that will be explored is 0 to 20 cps except for the skin panels in which it will be 50 to 500 cps.

The following methods of structural excitation are being considered:

a. Control-surface impulse by pilot

b. Surface-mounted rocket charges

c. Surface-mounted eccentric inertia shakers

d. Oscillating external aerodynamic vane

e. Oscillation of control surfaces by the control actuation system

The selection of the method or combination of methods will be made after the airplane response studies are completed.

The flutter stability characteristics will be evaluated for each condition by exciting the airplane using one or more of these methods, measuring the response, and determining the damping. The response will be monitored at a ground control station where telemetered data will be automatically reduced and plotted. When adequate damping has been established, the airplane will be cleared to proceed to the next condition. In this manner the airplane will be cleared throughout the operating speed range for all critical combinations of minimum altitude and maximum Mach number, and the minimum altitude at which maximum dynamic pressure can be obtained for each design wing sweep position.

BLANK PAGE

6.0 VIBRATION

The B-2707 configuration was analyzed for sonic and mechanical forcing environments and the attendant structural vibration. Aerodynamic boundary-layer noise is the design environment for the cab area and forward electronics bay. Engine-generated noise is the design environment for most of the rest of the airplane. Areas such as wheel wells and engine nacelles are treated as local structural environments and are analyzed separately.

The vibration environment and test requirements for B-2707 equipment have been established. The equipment vibration test specification (Ref. 6-1) was released and is applicable for Phase III use.

Vibration environments compare favorably with Boeing 707 transport environments.

6.1 METHODS OF ANALYSIS

The primary forcing function for airplane environmental vibration is the external sound field composed of contributions from aerodynamic boundary-layer noise and engine noise. The effects on equipment located near mechanical vibration sources, such as rotating equipment, is studied.

The general approach to vibration design employs the use of data on vibration response of structure to the various forcing functions obtained from company-sponsored research (Ref. 6-2). These data are backed up by a theoretical analysis of the structural environment in the application of the data to the B-2707 airplane.

The environments from the various sources are compiled on a frequency spectra basis along with expected total times at these conditions. These environments are added on a damage basis by a method outlined in Ref. 6-3 to obtain a single design environment at a relatively long service time.

This same principle is then used to effect a time compression for the purpose of obtaining a test environment at a reasonably short test time (about 5 hr). The resultant test amplitudes have been increased over the design environment as outlined in Ref. 6-3.

6.1.1 Sonically Induced Vibration

The major contribution to airplane vibration comes from dynamic response of the structure to the external noise field. Maximum vibration levels in the forward fuselage result from turbulent boundary-layer-induced aerodynamic noise and in the remainder of the airplane from takeoff engine noise levels and thrust reverser application.

The dynamic response of the structure is a function of the external sound pressure, structural joint acceptance, and the effective mass of the structure in the various modes of vibration.

The sonic design environments are shown in Figs. 6-1 and 6-2 for the two engine configurations being proposed (Ref. 6-4). Reductions are included for proposed sound suppression (Refs. 6-5 and 6-6).

The structural joint acceptance (a coupling term between structural wave length and acoustic wave length) and the effective mass are combined to form a vibro-acoustic mobility term. This mobility term or transfer function is used in conjunction with the sound environment and structural surface density to produce the vibratory acceleration design environment.

The response of a panel to an incident sound field is of the form

$$A_n^2(f) = \left[P^2(f)\right]\left[J_n(f)\right]^2\left[\left|Y_n(f)\right|\right]^2 \qquad \text{(Ref. 6-7)}$$

where:

$A_n^2(f)$ = acceleration power spectral density (APSD) (g^2/ cps)

$P^2(f)$ = pressure spectral density of random noise (psi^2 cps)

$J_n(f)$ = joint acceptance of nth mode

$Y_n(f)$ = absolute value of average acceleration mobility of the panel

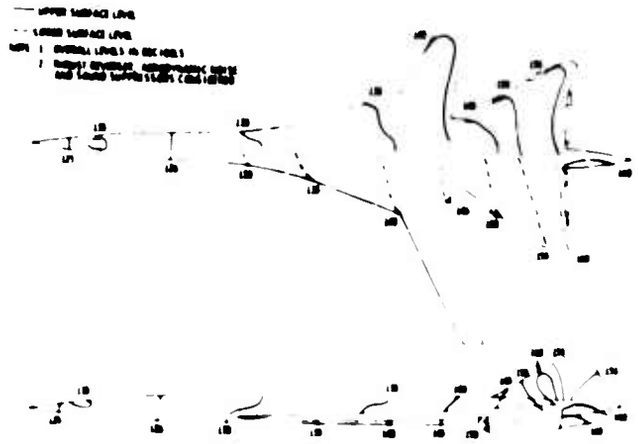

Figure 6-1. External Design Sound Levels, GE Engines

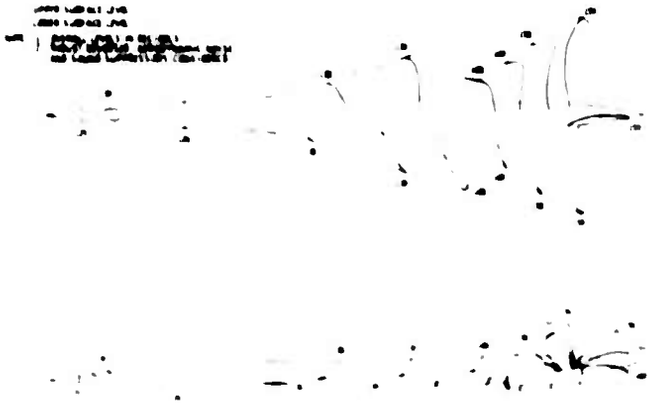

Figure 6-2 External Design Sound Levels, P&WA Engines

The acceleration mobility is given by

$$Y_n(f) = \left[\frac{1}{m^2 \overline{\alpha^2}(x,y)} \left(\frac{f^4}{(f_n^2 - f^2)^2 + (f_n f Q)^2}\right)\right]^{1/2}$$

where

m = surface weight density of panel (psi)

$\overline{\alpha^2}(x,y)$ = mean square mode shape

f_n = natural frequency of nth mode

Q = dynamic amplification factor

The mean square mode shape for a simple supported panel is $\overline{\alpha^2}(x,y) = 1/4$. The joint acceptance of a simply supported panel is $J_{1,1} = 4/\pi^2$. Combining these equations and setting $f = f_n$, the space average response is

$$A^2(f) = \frac{P^2(f)}{m^2}\left(\frac{64}{\pi^4} Q^2\right)$$

The vibro-acoustic transfer function or mobility used for vibration prediction is about 80 percent of mechanical transmissibility or Q and may be expressed as

$$\text{Vibro-acoustic mobility} = \frac{A^2(f)\, m^2}{P^2(f)} = \left(\frac{8}{\pi^2} Q\right)^2$$

In decibel form, 10 log mobility = 10 log $[A^2(f)\, m^2]$ - PSL = 10 log Q^2 - 172.4 where PSL is the pressure spectrum level, db (re 0.0002 dynes/cm^2) per cps.

This development can be applied to large sections of structure as well as panels. A graph of the actual design value used for vibration prediction is shown in Fig. 6-3. The curve is based on panel and cylinder test data from Refs. 6-2 and 6-8 altered to B-2707 construction and grazing incidence. The resultant design environment for the wing is shown in Fig. 6-4.

6.1.2 Mechanically Induced Vibration

Mechanically induced vibration from rotating equipment is investigated on an individual basis. Where structural fatigue or passenger comfort is affected, tuned vibration isolators will be specified, using out-of-balance limits and operating speeds of the equipment as design parameters. The resultant transmitted vibration will be within acceptable limits for equipment support fatigue life and passenger comfort tolerances.

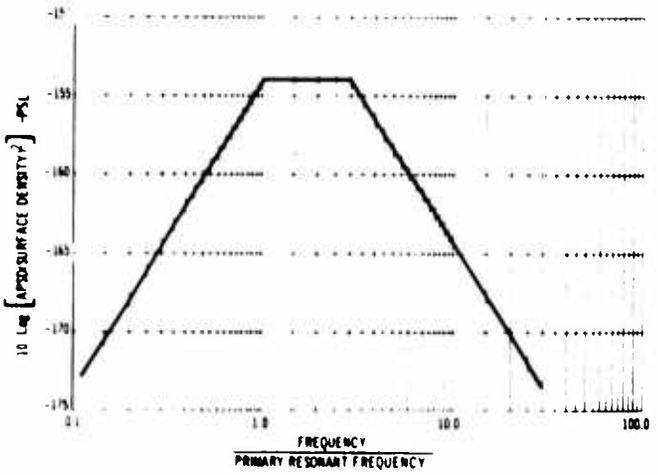

Figure 6-3. Vibro-Acoustic Mobility Function

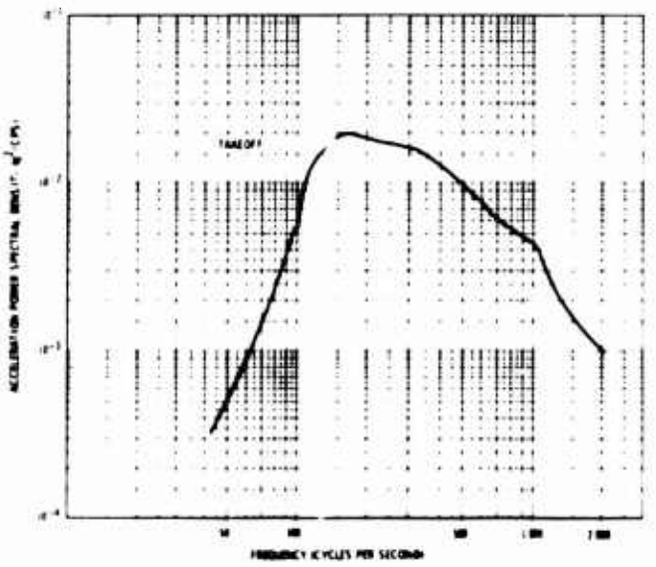

Figure 6-4. Vibration Environment, Wing-Mounted Equipment

The engines are to be designed to a vibration tolerance of 5 mils double amplitude. In view of the short transmitted load path from the inboard engine to the fuselage, vibration isolation is specified in the interest of minimizing annoyance due to rotor vibration. The support frequencies will be well below the operating rpm range of the engines, resulting in attenuation of operating vibration.

Vibration levels recorded in Boeing subsonic jet engines have been scaled to the B-2707 engine vibration environment.

6.2 DESIGN

When analysis or past experience shows that a particular piece of equipment is susceptible to vibration damage, vibration isolators may be specified to maintain transmitted vibration to safe levels. Vibration isolators will also be employed at the mounting points of rotating equipment in order to keep structural excitation minimized. Equipment support vibration load factors will be provided for stress design.

6.3 EQUIPMENT TEST PROGRAM

An equipment vibration test program will be initiated to provide adequate reliability of equipment. The test specification will employ predictions from Par. 6.1, which have been altered to provide ease of testing for random vibration. A sinusoidal testing option may be employed where equipment design permits. All qualification testing will be preceded by sinusoidal sweeps for resonance identification. The equipment vibration test specification (Ref. 6-1) will be followed.

When an item of equipment has passed equivalent testing from other airplane test requirements, it may be exempted from additional testing for B-2707 certification.

6.3.1 Random Testing

Random vibration testing will be the preferred testing technique, since it more closely simulates the airplane environment. For equipment in which simultaneous interaction of several resonances would produce malfunction, this test method may uncover problems in the development stage, whereas sinusoidal testing may not.

Testing is performed at slightly elevated levels to compress test times for economic reasons. A typical vibration test requirement is shown in Fig. 6-5.

6.3.2 Sinusoidal Testing

When an equipment item is shown by analysis to contain no internal resonance coupling problems and does not contain vacuum tubes or other sensitive components, sinusoidal testing will be permitted on a selective basis. The preliminary resonance scan may be used to specify a substitute sinusoidal test on the basis of equal peak response for both tests.

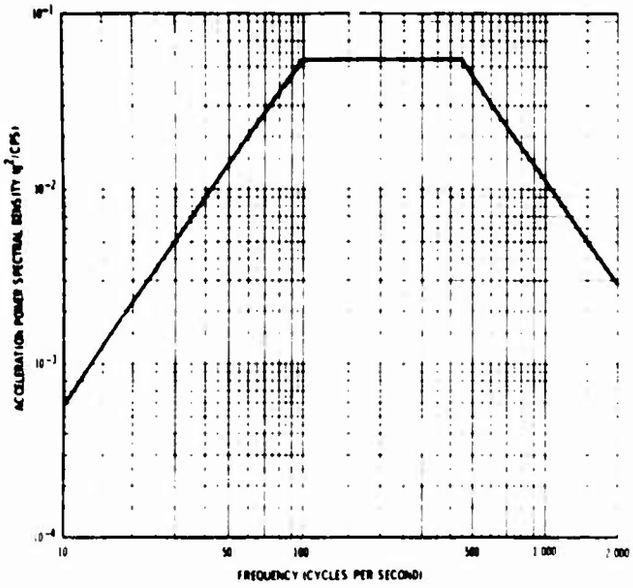

Figure 6-5. Vibration Test, Wing-Mounted Equipment

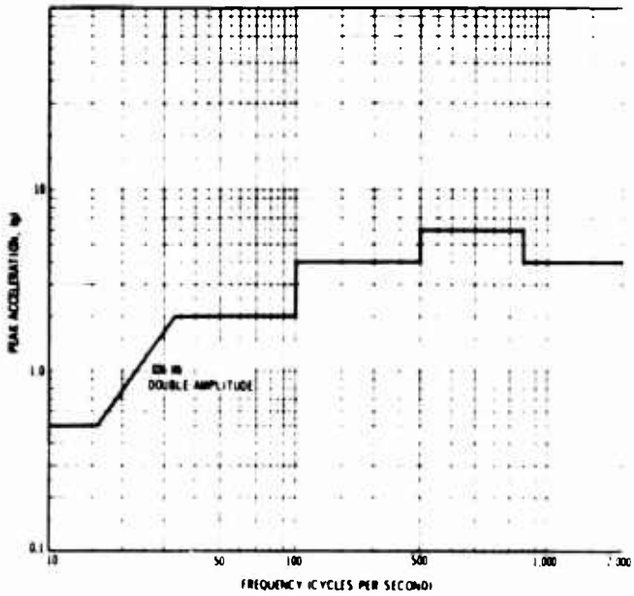

Figure 6-6. Typical Sinusoidal Test, Wing-Mounted Equipment

A typical substitute sinusoidal test is shown in Fig. 6-6 assuming several package resonances with a resonant amplification factor of 10.

6.3.3 Special Considerations

Because the sonic forcing environment impinging on the external surface of the airplane is effectively a force environment (sound pressure times wetted area), the resultant acceleration is a function of the effective mass of the structure. The external structure is very light in weight and therefore has a low mechanical impedance. When a heavy equipment is located on secondary structure, the mechanical impedance mismatch results in a radically reduced acceleration environment at the heavy equipment. This fact was verified on test structure (Ref. 6-8) as well as analytically. Therefore, reduced test levels will be used for equipment exceeding 50 lb in weight.

6.4 VERIFICATION AND PLANNING

The airplane vibration environment will be verified by the ground vibration survey with engines running, conducted on the prototype during Phase III. One purpose of this test will be to confirm the predicted relationship between take-off sound field and airplane internal vibration response. The internal vibration measurements will reveal any deficiencies that might exist in the equipment in time for changes in equipment or supports in prototype airplanes.

The external sound field will be measured to establish a structural transfer function to evaluate changes in vibration environment for possible future engine changes.

Test-stand engine operation will yield data on engine vibration and sonic environment and will be useful as support information. Vibration predictions will be updated during Phase III as improved information on sonic levels and structural definition becomes available.

The flight measurement program will be carried out using instrumentation installed from previous ground tests. Nominal flight missions will be chosen from the flight test plan for recording data.

A major effort toward project support will be made during Phase III to assist design personnel in equipment specification preparation and design for vibration control.

ILLUSTRATIONS

ILLUSTRATIONS (Continued)

ILLUSTRATIONS (Continued)

ILLUSTRATIONS (Continued)

ILLUSTRATIONS (Concluded)

TABLES